

Ultrafast electronic, vibrational and conformational relaxation dynamics of heme model compounds and proteins in various environments using femtosecond pump-probe spectroscopy

By

CHINJU GOVIND M. V.

10CC14A39003

A thesis submitted to the
Academy of Scientific and Innovative Research
for the award of the degree of
DOCTOR OF PHILOSOPHY
in
SCIENCE

Under the supervision of
Dr. V. KARUNAKARAN



**CSIR-National Institute for Interdisciplinary
Science and Technology (CSIR-NIIST),
Thiruvananthapuram - 695 019**



Academy of Scientific and Innovative Research
AcSIR Headquarters, CSIR-HRDC campus
Sector 19, Kamla Nehru Nagar,
Ghaziabad, U.P. - 201 002, India

August 2020



राष्ट्रीय अंतरविषयी विज्ञान तथा प्रौद्योगिकी संस्थान

रसायन विज्ञान तथा प्रौद्योगिकी प्रभाग (सीएसटीडी)

वैज्ञानिक तथा औद्योगिक अनुसंधान परिषद

इंडस्ट्रियल इस्टेट पी.ओ., तिरुवनंतपुरम, भारत 695 019

NATIONAL INSTITUTE FOR INTERDISCIPLINARY SCIENCE & TECHNOLOGY

Photosciences and Photonic Section, Chemical Sciences and Technology Division

Council of Scientific and Industrial Research

Industrial Estate P.O., Thiruvananthapuram, INDIA 695 019

डॉ. वी. करुणाकरण

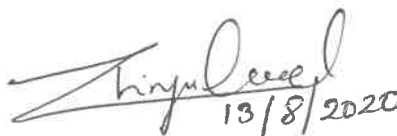
प्रधान वैज्ञानिक


Dr. V. Karunakaran

Principal Scientist

CERTIFICATE

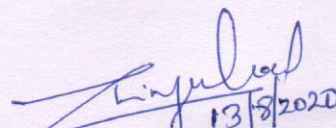
This is to certify that the work incorporated in this Ph.D. thesis entitled, “*Ultrafast Electronic, Vibrational and Conformational Relaxation Dynamics of Heme Model Compounds and Proteins in Various Environments Using Femtosecond Pump-Probe Spectroscopy*”, submitted by Mrs. Chinju Govind M. V. to the Academy of Scientific and Innovative Research (AcSIR) in fulfillment of the requirements for the award of the Degree of *Doctor of Philosophy in Science*, embodies original research work carried-out by the student. We, further certify that this work has not been submitted to any other University or Institution in part or full for the award of any degree or diploma. Research materials obtained from other sources and used in this research work has been duly acknowledged in the thesis. Images, illustrations, figures, tables etc., used in the thesis from other sources, have also been duly cited and acknowledged.


Chinju Govind M. V. 13/8/2020


Dr. V. Karunakaran 13/8/2020
(Thesis Supervisor)

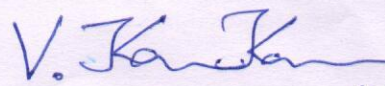
STATEMENTS OF ACADEMIC INTEGRITY

I Chinju Govind M. V., a Ph.D. student of the Academy of Scientific and Innovative Research (AcSIR) with Registration No. 10CC14A39003 hereby undertake that, the thesis entitled “**Ultrafast Electronic, Vibrational and Conformational Relaxation Dynamics of Heme Model Compounds and Proteins in Various Environments Using Femtosecond Pump-Probe Spectroscopy**” has been prepared by me and that the document reports original work carried out by me and is free of any plagiarism in compliance with the UGC Regulations on “*Promotion of Academic Integrity and Prevention of Plagiarism in Higher Educational Institutions (2018)*” and the CSIR Guidelines for “*Ethics in Research and in Governance (2020)*”.


Chinju Govind M. V.

August 13th, 2020
Thiruvananthapuram

It is hereby certified that the work done by the student, under my/our supervision, is plagiarism-free in accordance with the UGC Regulations on “*Promotion of Academic Integrity and Prevention of Plagiarism in Higher Educational Institutions (2018)*” and the CSIR Guidelines for “*Ethics in Research and in Governance (2020)*”.

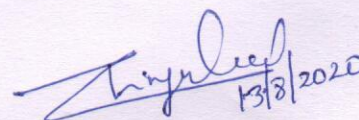

Dr. V. Karunakaran 13/8/2020

August 13th, 2020
Thiruvananthapuram

DECLARATION

I, Chinju Govind M. V., bearing AcSIR Registration No. 10CC14A39003 declare: that my thesis entitled, "Ultrafast Electronic, Vibrational and Conformational Relaxation Dynamics of Heme Model Compounds and Proteins in Various Environments Using Femtosecond Pump-Probe Spectroscopy" is plagiarism free in accordance with the UGC Regulations on "*Promotion of Academic Integrity and Prevention of Plagiarism in Higher Educational Institutions (2018)*" and the CSIR Guidelines for "*Ethics in Research and in Governance (2020)*".

I would be solely held responsible if any plagiarised content in my thesis is detected, which is violative of the UGC regulations 2018.



Chinju Govind M. V.

August 13th, 2020

Thiruvananthapuram

ACKNOWLEDGEMENTS

I have great pleasure in expressing my deep sense of gratitude to Dr. V. Karunakaran, my thesis supervisor, for suggesting the research problem and for his constant guidance, support, motivation and encouragement, leading to the successful completion of this work.

I thank Dr. A. Ajayaghosh, Director CSIR-National Institute for Interdisciplinary Science and Technology (CSIR-NIIST), Thiruvananthapuram for his constant support and inspiration and for providing the necessary facilities for carrying out this work.

I thank Dr. Suresh Das (former Director) and Dr. Gangan Pratap (former acting Director) of CSIR-NIIST, Thiruvananthapuram, for providing the necessary facilities for carrying out this work.

My sincere thanks to

➤ *Dr. K. G. Raghu, Dr. K. N. Narayanan Unni and Dr. Vijayakumar C. Nair, Doctoral Advisory Committee (DAC) members and the whole AcSIR faculty for the successful completion of course work.*

➤ *Dr. C. H. Suresh, Dr. Luxmi Varma, and Dr. Mangalam S. Nair present and former AcSIR co-ordinators.*

➤ *Dr. K. R. Gopidas, Dr. Biswapriya Deb, Dr. Joshy Joseph, Dr. K. Yoosuf, Dr. Suraj Soman, Dr. Ishitha Neogi, Dr. Adarsh Ashok, scientists of the Photosciences and Photonics Section, Chemical Sciences and Technology Division (CSTD), for their help and support.*

➤ *Dr. J. D. Sudha, Principal Technical Officer, Chemical Sciences and Technology Division (CSTD) for all her support and motivation.*

➤ *Mr. C. K. Chandrakanth, Mr. Kiran J. S., Mr. Robert Philip, and Mr. Kiran Mohan, for general help.*

➤ *Mr. Peer Mohamed, Mr. Vivek, Ms. Shilpa for the successful completion of CSIR-800 project.*

➤ *Dr. Anjali Soman, Mr. Rajeev for general help.*

➤ *Mr. Guruprasad M. S., Ms. Sumitha Paul, Mrs. Tessy T. D., Mr. Hasim Fayiz, Ms. Megha Paul, Ms. Ranimol and Mrs. Afeefah, present and former group members.*

➤ *M. Sc. project students Ms. Simi Thomas for her hardwork and support and other students. Mrs. Athira M., Ms. Jesna Das, Ms. Ranu Dhale, Ms. Tessy Thampy and Ms. Chithra for their hardwork.*

- *Dr. Vinila, Dr. Jyothi, Dr. Jayanthi, Dr. Jagatheesh, Mrs. Daisy, Mr. Thejus and Mr. Rajeev, MSc classmates.*
- *All my teachers and friends for their care and support.*
- *My parents for their endless caring, love, and support.*
- *University Grand Commission (UGC) for the fellowship.*

I am deeply grateful to my brother Sayooj and my husband Kiran for their love, understanding and care. And above all, I thank Almighty for all his blessing.

Chinju Govind M. V.

TABLE OF CONTENTS

Certificate		i
Statements of academic integrity		ii
Declaration		iii
Acknowledgement		iv
Table of contents		vi
List of abbreviations		x
Preface		xiv
CHAPTER 1	An Overview on Ultrafast Dynamics of Heme and Heme Proteins	1–31
1.1	Abstract	1
1.2	Introduction	2
1.3	Heme Model Compounds	2
1.4	Biological Significance of Heme Proteins	5
1.5	Myoglobin	6
1.5.1	Structure of Myoglobin	6
1.5.2	Unfolding of Myoglobin	7
1.5.3	Functions of Myoglobin	8
1.6	Cytochrome c	8
1.6.1	Structure of Cytochrome c	9
1.6.2	Oxidation States of Cytochrome c	9
1.6.3	Unfolding of Cytochrome c	10
1.6.4	Functions of Cytochrome c	12
1.7	Ultrafast Dynamics of Heme Proteins	14
1.7.1	Vibrational Relaxation Dynamics	17
1.7.2	Involvement of Intermediate Excited Electronic State	19
1.8	Objective of the Thesis	21
1.9	References	23
CHAPTER 2	Experimental Methods and Instrumentation	33-47
2.1	Ultrafast Spectroscopy	33
2.1.1	Generation and Amplification of Ultrashort Pulses	34
2.1.2	Temporal and Spectral Resolution	35

2.1.3	Femtosecond Pump-Probe Transient Absorption Spectroscopy	36
2.1.4	Chirp Compensation	40
2.1.5	Singular Value Decomposition	41
2.1.6	Analysis of Femtosecond Transient Absorption Spectra	42
2.1.6.1	Global Analysis	42
2.1.6.2	Target Analysis	43
2.2	Time Correlated Single Photon Counting	44
2.3	Circular Dichroism Spectroscopy	44
2.4	Fluorescence Spectroscopy	45
2.5	Dynamic Light Scattering	45
2.6	UV-Visible Electronic Absorption Spectroscopy	45
2.7	References	46
CHAPTER 3	Ultrafast Heme Relaxation Dynamics of Model Compounds: Via Multiple Electronic Spin States and Vibrational Cooling	49-82
3.1	Abstract	49
3.2	Introduction	50
3.3	Results and Discussions	56
3.3.1	Steady State Absorption Spectra	56
3.3.2	Femtosecond Transient Absorption Spectra	58
3.3.3	Analysis of Transient Absorption Spectra	65
3.3.3.1	Signature of Vibrational Cooling Dynamics	66
3.3.3.2	Involvement of Multiple Electronic Spin States.	71
3.3.3.3	Effect of Axial Ligands, Peripheral Substituents, and Solvents	75
3.4	Conclusion	76
3.5	Materials and Methods	77
3.6	References	78

CHAPTER 4	Ultrafast Relaxation Dynamics of Heme in Liposomes: Influence of Charge of Phospholipids on the Partial Unfolding Dynamics of Cytochrome c	83-124
4.1	Abstract	83
4.2	Introduction	84
4.2.1	Apoptosis	84
4.2.2	Phospholipids	85
4.3	Results and Discussions	91
4.3.1	Size Distribution of Liposomes	91
4.3.2	Stationary Absorption Spectra	93
4.3.3	Fluorescence Spectra	94
4.3.4	Circular Dichroic Spectra	95
4.3.5	Femtosecond Time-Resolved Excited State Relaxation Dynamics	97
4.3.5.1	Analysis of Transient Absorption Spectra	105
4.3.5.2	Effect of Excitation Wavelength	109
4.3.5.3	Effect of Ionic Strength	115
4.4	Conclusion	118
4.5	Materials and Methods	119
4.6	References	120
CHAPTER 5	Interaction Dynamics of Hematin with Antimalarial Drugs: An Ultrafast Investigation	125-161
5.1	Abstract	125
5.2	Introduction	126
5.2.1	Antimalarial Drugs	128
5.2.2	Hematin Dimers	129
5.2.3	Interaction of Antimalarial Drugs with Heme	131
5.3	Results and Discussion	134
5.3.1	Stationary Absorption Spectra	134
5.3.2	Fluorescence Spectra	136
5.3.3	Femtosecond Transient Absorption Spectra	138
5.3.3.1	Analysis of Transient Absorption Spectra	142
5.3.3.2	Signature of Vibrational Cooling Dynamics	149
5.3.3.3	Involvement of Multiple Electronic Spin States	149

5.3.3.4	Dynamics at Different pH	153
5.4	Conclusions	155
5.5	Materials and Methods	156
5.6	References	157
Abstract of the Thesis		163
List of Publications		165
Papers Presented at Conferences		166
Attachment of the Photocopy of Publications		

List of Abbreviations

Å	Angstrom
AFM	Atomic force microscopy
Arg	Arginine
Asn	Asparagine
ATP	Adenosine tri phosphate
Br	Bromine
°C	Degree Celsius
C	Cysteine
CaF ₂	Calcium fluoride
CCO	Cytochrome c oxidase
CD	Circular dichroism
CL	Cardiolipin
Cl	Chlorine
CO	Carbon monoxide
CPA	Chirped pulse amplification
CQ	Chloroquine
CT	Charge transfer
Cyt c	Cytochrome c
DAS	Decay associated spectra
DFG	Difference frequency generation
DFT	Density functional theory
DLS	Dynamic light scattering
DMSO	Dimethyl sulfoxide
DNA	Deoxyribonucleic acid
EPR	Electron paramagnetic resonance
ESA	Excited state absorption
ET	Electron transfer
et al.	Et alii/alia
ETC	Electron transport chain
Fe	Iron
FRET	Fluorescence resonance energy transfer
fs	Femtosecond

FSRS	Femtosecond stimulated Raman spectroscopy
FTAS	Femtosecond time-resolved transient absorption spectra
FWHM	Full width at half maximum
GdHCl	Guanidine hydrochloride
GSB	Ground state bleach
GUV	Giant unilamellar vesicles
GVD	Group velocity dispersion
H ₂ O	Water
H ₂ O ₂	Hydrogen peroxide
Hb	Hemoglobin
HEPES	(4-(2-hydroxyethyl)-1-piperazineethanesulfonic acid)
His	Histidine
HOMO	Highest occupied molecular orbital
HS	High spin
Hz	Hertz
IC	Internal conversion
IR	Infrared
IRF	Instrument response function
IVR	Intramolecular vibrational energy redistribution
K	Kelvin
kDa	Kilo Dalton
Kpi	Potassium phosphate buffer
K _{sv}	Quenching constant
LMCT	Ligand to metal charge transfer
LUV	Large unilamellar vesicles
Lys	Lysine
M	Molar
Mb	Myoglobin
MeOH	Methanol
Met	Methionine
MFQ	Mefloquine
MHz	Mega Hertz
mJ	Milli Joule

MLCT	Metal to ligand charge transfer
mm	Millimeter
mM	Millimolar
mW	Milliwatt
n	Refractive index
Na	Sodium
NaCl	Sodium chloride
Ngb	Neuroglobin
nJ	Nano Joule
nm	Nanometer
NMR	Nuclear magnetic resonance
NO	Nitrous oxide
OD	Optical density
PBS	Phosphate buffer
PDB	Protein data bank
pH	Hydrogen ion concentration at logarithmic scale
ps	Picosecond
QN	Quinine
RBC	Red blood cells
ROS	Reactive oxygen species
S	Spin
S	Singlet
SDS	Sodium dodecyl sulphate
SE	Stimulated emission
SUV	Small uni-lamellar vesicles
SVD	Singular value decomposition
T	Triplet
t	Time
TAS	Transient absorption spectra
TCSPC	Time Correlated Single Photon Counting
TOPAS	Travelling optical parametric amplification system
TPPCl	Tetraphenyl porphyrin chloride
Trp	Tryptophan

UV	Ultraviolet
VC	Vibrational cooling
VR	Vibrational relaxation
ΔA	Change in absorbance
Δf	Dipolar solvation
λ	Wavelength
λ_{exctn}	Excitation wavelength
μM	Micrometer
τ	Lifetime

PREFACE

The understanding of the excited state relaxation dynamics is important to describe the biological function of heme proteins. Heme proteins, for example, cytochrome c (**Cyt c**) has various biological functions including electron transfer from cytochrome c reductase to cytochrome c oxidase, energy transfer in mitochondrial transport chain reaction, catalysis of redox reactions such as oxidation of cardiolipin, and triggering of cell apoptosis. The electronic, vibrational and conformational changes of the protein due to redistribution of the excess energy generated by biological functions play an important role. These can be triggered optically by ultrafast laser and accompanying electronic, vibrational, and conformational relaxation dynamics in the heme group and the surrounding protein can be investigated.

Chapter 1 gives an overview of biological functions and ultrafast dynamics of heme model compounds and heme proteins. The details of the instrumentation and analysis of femtosecond transient absorption spectra are discussed in **Chapter 2**.

The prosthetic group of heme proteins, iron metalloporphyrins serve as a model system to understand its biological functions. Hence the ultrafast excited state relaxation dynamics of various heme model compounds (**Hemin-Cl**, **Hemin-Br** and **Hemin-meso**) and met-myoglobin (**met-Mb**) have been investigated in **Chapter 3** with the aim of understanding the influence of the axial ligands, peripheral substituents and the solvents on the excited state relaxation dynamics of the heme. Transient absorption spectra of the model compounds are systematically measured using femtosecond pump-probe spectroscopy upon excitation at 380 nm. An excited state deactivation pathway of the model compounds comprising different electronic spin states of iron is proposed along with the vibrational cooling processes based on the spectral evolution and the data analysis. This study revealed that the involvement of multiple iron spin states in the electronic relaxation dynamics of heme model compounds and **met-Mb** is an inherent feature of the heme *b* type¹.

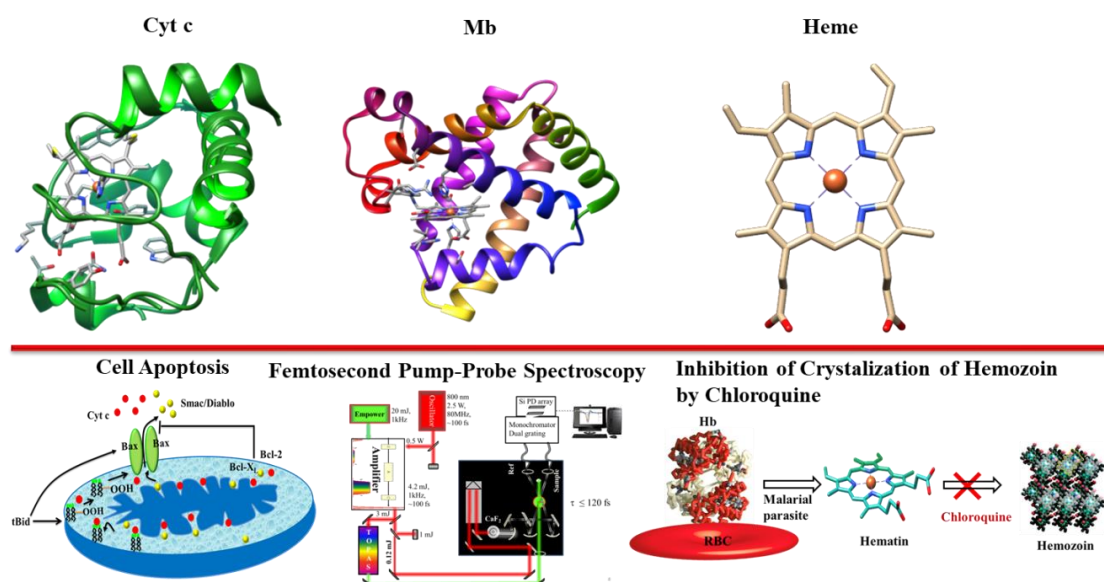
Cytochrome c (**Cyt c**) is an important heme protein used as a model system for electron transfer proteins and folding-unfolding studies. The interaction dynamics of **Cyt c** with various phospholipids having different charges [**CL**: 2–, **POPG**: 1– and **POPC**: 0] are discussed in **Chapter 4** to understand the electronic, vibrational, and conformational changes of the protein in its partially unfolded state. The various degrees of partial unfolding in **Cyt c** in the presence of liposomes are studied with absorption, fluorescence, CD spectra and femtosecond time resolved pump-probe spectroscopy. The decrease of efficiency of fluorescence resonance energy transfer (FRET) from tryptophan (Trp) to heme upon an increase of the partial unfolding of the proteins by liposomes revealed the Trp as a marker amino acid to reflect the dynamics of partial unfolding of the protein. In addition, the refolding of the protein after the addition of NaCl indicated the electrostatic interaction between **Cyt c** and liposomes rather than the hydrophobic interaction².

Malaria is a serious life threatening disease to human health. The malaria parasite digests host hemoglobin (**Hb**) and produces free heme which further crystallizes to insoluble hemozoin. Most of the antimalarial drugs inhibit the crystallization of heme to hemozoin. The exact mechanism of interaction of antimalarial drugs with heme is remaining elusive. In **Chapter 5**, we discuss the interaction dynamics between the **Hematin** and antimalarial drugs chloroquine (**CQ**) and mefloquine (**MFQ**) in pH 5.5 and 7.0 using steady–state and time–resolved absorption and emission spectroscopy. We observed the formation of a ground state complex of **Hematin** with **CQ** and **MFQ**. The excited state relaxation pathway of **Hematin** in the presence of drugs comprises both multiple electronic spin states and vibrational relaxation process. **Hematin–CQ** complex was more stabilized than **Hematin** by non-covalent interactions and thereby preventing the formation of hemozoin³. This study will help in developing new antimalarial drugs to overcome the parasite resistance.

References

1. Govind, C.; Karunakaran, V. Ultrafast Relaxation Dynamics of Photoexcited Heme Model Compounds: Observation of Multiple Electronic Spin States and Vibrational Cooling. *J. Phys. Chem. B* **2017**.
2. Govind, C.; Paul, M.; Karunakaran, V. Ultrafast Heme Relaxation Dynamics Probing the Unfolded States of Cytochrome c Induced by Liposomes: Effect of Charge of Phospholipids. *J. Phys. Chem. B* **2020**, *124* (14), 2769-2777.
3. Govind, C.; Paul, M.; Karunakaran, V. U Interaction Dynamics of Hematin with Antimalarial Drugs: An Ultrafast Investigation (To be submitted).

An Overview on Ultrafast Dynamics of Heme and Heme Proteins



1.1 Abstract

Heme proteins are very large class of metalloprotein containing heme (Protoporphyrin IX) as the prosthetic group. Heme proteins carry out various functions originating from the flexibility of the heme group and the diversity of interactions with protein backbone. Understanding the dynamics of a protein is important for describing its functionality. The chemistry behind all these processes occurs on a large range of timescales. It can be optically triggered using a short light pulse and the associated electronic as well as vibrational relaxation dynamics of the heme group and the surrounding protein can be studied. Optical methods are often used to understand the global protein conformational dynamics triggered by localized excess of vibrational energy for heme proteins, ligand photolysis and energy dissipation and redistribution. In

this chapter, an overview of heme and heme proteins and their ultrafast dynamics are discussed.

1.2 Introduction

The important building block of life, proteins have a unique structure and functions. Heme proteins are very large class of metallo–protein containing heme (Fe Protoporphyrin IX) as the metal cofactor, and considered to be the ubiquitous active centres for these heme proteins. The chemical structure of heme is shown in **Figure 1.1**. Heme proteins have various functions such as electron transfer¹, ligand sensing² and transport³, metal ion storage⁴ and substrate oxidation.⁵ Moreover, these proteins are involved in other biological functions such as apoptosis or programmed cell death⁶, steroid biosynthesis⁷ and aerobic respiration.⁸ The respiratory proteins such as myoglobin (**Mb**) and hemoglobin (**Hb**) serve as oxygen storage and transport agents respectively. Cytochrome b, c and p450 function as electron transfer agents and mono-oxygenases. This variety of functions originates from the flexibility of the heme group and the diversity of interactions with protein frameworks that produce different heme environments. There has been a large amount of research for the last half century about understanding of the various functions of heme proteins.

1.3 Heme Model Compounds

Heme model compounds are single porphyrin complex designed to be similar to the prosthetic heme group found in heme proteins. Model compounds are used as a building block to understand the dynamics of the heme proteins.⁹ The porphyrin molecule of the heme is a heterocyclic macrocycle having four pyrroline units interconnected through methine bridges and their α -carbon atoms. The porphyrin can coordinate hydrogen or metal cations in its center by four indole nitrogen atoms to perform a

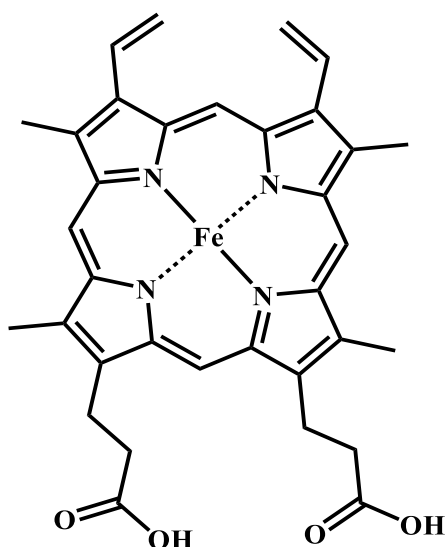


Figure 1.1 The chemical structure of heme.

variety of different functions that exploit the oxidation state, electronic structure, and axial ligation of the metal centre.¹⁰ The conjugated tetrapyrrole rings are strongly absorbing chromophores with electronic transitions in the visible and ultraviolet regions of the electromagnetic radiation. The most apparent example is the chlorophyll and bacteriochlorophyll which act as primary photoreceptor in Photosynthesis.¹¹ Natural and synthetic metalloporphyrins found applications in medical therapeutics, energy conversion, optoelectronic thin films, photodynamic therapy and molecular electronics.¹²⁻¹⁵ Most of these applications involve electronic dynamics, including population of electronically excited states. However, some applications exploit the axial ligation of the central metal atom. The porphyrins can readily complex with many metal atoms such as iron (Fe), zinc, copper, magnesium, cobalt, and nickel.^{9, 16} Iron metallo-porphyrins are of the highest biological significance, as it is the active site of heme proteins present throughout the living systems. The dynamics of cyclic metallo-tetrapyrroles are mainly controlled by electronic relaxation dynamics including internal conversion (IC) and intersystem crossing (ISC). It was reported that the excited state evolution of model porphyrins follows an initial charge transfer (CT) mechanism occurring on

sub-picosecond to nanosecond time scales. The heme reactivity can be tuned by the number and nature of axial ligands to Fe¹⁷, the accessibility of the heme to exogenous ligands, the distribution of polar and charged groups around the heme¹⁰, and the heme-binding site and of the protein. Depending upon the nature of peripheral substituent on the porphyrin macrocycle the heme group can be varied. Six possible coordination sites are available for the iron atom. The four nitrogen of the porphyrin ring bind to the iron, leaving the other two positions of the iron available for bonding to the protein and a divalent atom.¹⁸ There are different kinds of biologically important heme such as heme *a*, heme *b*, heme *c* etc. The chemical structures of heme *a*, heme *b* and heme *c* are shown in **Figure 1.2**.

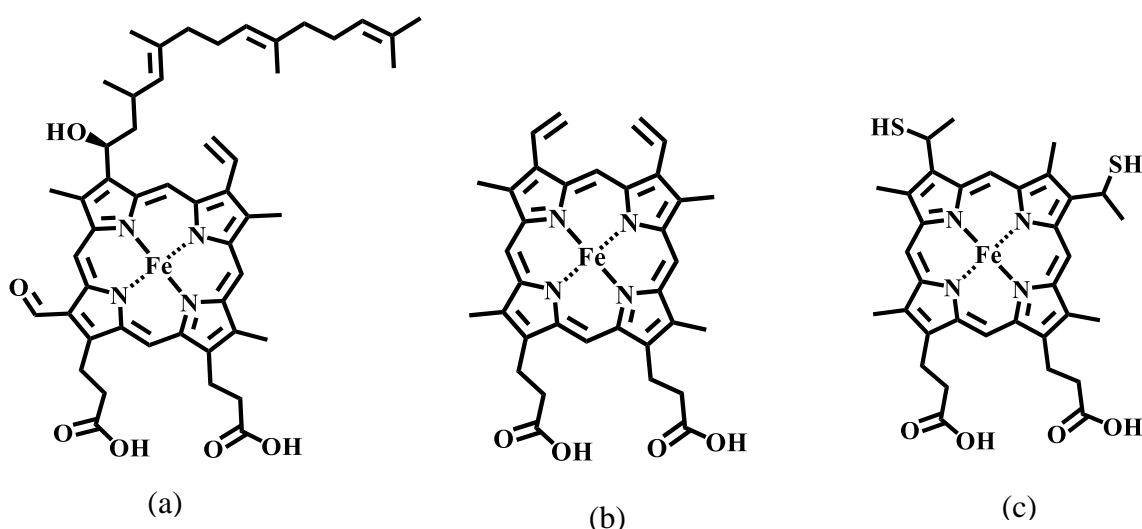


Figure 1.2 Chemical structures of Heme *a* (a), Heme *b* (b) and Heme *c* (c).

Heme *b*, is one of the most common heme cofactors, consisting of four methyl, two vinyl, and two propionate groups as peripheral substituents.¹⁹ The metal porphyrin is generally bound within the protein matrix or heme pocket through Fe–ligand coordination and non-covalent interactions. The structure of heme *b* was synthetically confirmed by Hans Fischer.²⁰ The heme framework has an asymmetric structure about the α,γ -meso axis due to the linkage of the two methyl (1- and 3-positions) and two vinyl groups

(2- and 4-positions) of the β -pyrrole rings. Several important heme proteins such as **Mb**, **Hb**, horseradish peroxidase (HRP), cytochrome p450 and cytochrome b5 have heme *b* in the heme pocket. Generally, the removal of heme cofactor from native protein under acidic conditions yields the corresponding colorless apoprotein and addition of heme *b* into an apoprotein give the reconstituted heme protein.²¹

Heme *c* is formed from heme *b* through covalent attachment to the protein backbone in which the heme *b* vinyl groups are replaced by thioether linkage.²² There is a striking difference in the redox potential between heme *b* and heme *c*. The potentials range from –130 to +390 mV vs standard hydrogen electrode (SHE) for heme *b*, whereas it ranges –400 to +400 mV for heme *c*.²³⁻²⁴ The difference in the potential is suggested to be the more exposure of heme *c* to solvent than heme *b*.²⁵

In heme *a*, formyl group is attached at ring position 8 and ring position 2 is occupied by a hydroxyethylfarnesyl group, an isoprenoid chain of the iron tetrapyrrole heme.²⁶ Heme *a* is connected to the apoprotein via a coordinate bond between the heme iron and a conserved amino acid side chain.²⁷ Compared to heme *b*, heme *a* is more hydrophobic and electron-withdrawing in nature.¹⁹ Heme *a* is found only in terminal oxidases such as mammalian cytochrome *c* oxidase (CCO) which is responsible for preserving the energy of dioxygen reduction by pumping protons into the inner mitochondrial space.²⁸ In addition, other less common heme existing in nature are heme *d*²⁹, heme *dI*³⁰, heme P460³¹, siroheme³², and chlorocruoroheme and etc.³³

1.4 Biological Significance of Heme Proteins

Heme proteins have been used as a model systems to structural biology, protein folding, and to the treatment of sickle cell anaemia.³⁴ The special attention to heme

proteins started after the pioneering research on the determination of **Mb** and **Hb** structure.³⁵⁻³⁶ Currently most of the research is focused on the understanding of how the biological function relates to the protein structure.³⁷⁻³⁹ Another important area in protein research is the design of new proteins with heme cofactor and related ligands.⁴⁰⁻⁴¹ Heme proteins show non-linear optical properties, electron transfer properties, and they are used as smart materials which respond to changes in ionic strength, pH, and redox potential.⁴²⁻⁴⁶ The understanding of the heme group and its binding sites in proteins is very important in the designing of new heme proteins with precise structural and functional properties, and it is only possible by the systematic study of available heme cofactor and heme proteins.

1.5 Myoglobin

Mb is a small molecular weight (16.7 kDa) heme *b* protein; consist of a single polypeptide chain of 154 amino acids with one oxygen binding site. **Mb** is mainly present in the muscle tissues of vertebrates. The heme iron can exist in the +2 (reduced) or +3 (oxidized) states. **Mb** binds oxygen in its reduced form. When oxygen binds to the iron atom, it partially pulls back to the plane of the porphyrin ring. **Mb** can also bind alternate ligands such as CO, nitrite, and azide molecules. For example, CO binds strongly to **Mb** ($K_q > 10^7 \text{ M}^{-1}$)⁴⁷ just as it does to **Hb**, which forms carboxy-**Mb**.⁴⁸

1.5.1 Structure of Myoglobin

The crystal structure of **Mb** was solved by John Kendrew in 1958.³⁵ The tertiary structure of **Mb** is composed of eight α helices joined by short non helical regions (**Figure 1.3**). The helices give a rigid structural framework for the heme pocket. The heme consists of a protoporphyrin that surrounds an iron atom which is ligated to four nitrogens of the protoporphyrin. The fifth coordination of iron atom is satisfied by a histidine (His) which makes the heme in the hydrophobic pocket. The sixth ligation

position will be available for the binding of oxygen. **Mb** contains two intrinsic tryptophan (Trp) in the seventh and fourteen positions.

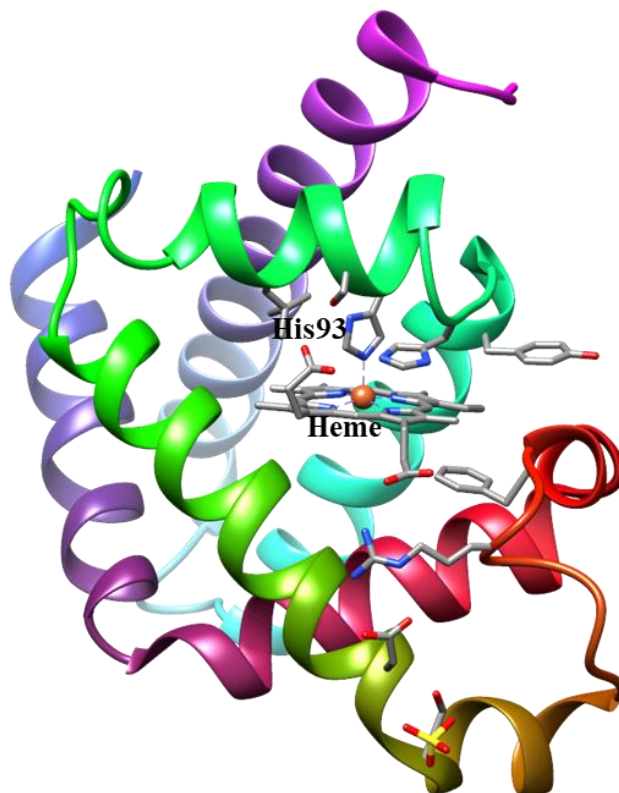


Figure 1.3 X- ray crystal structure of sperm whale **Mb** obtained from PDB: 1MBD.⁴⁹

1.5.2 Unfolding of Myoglobin

Studies on unfolding and folding of **Mb** have focused mainly on characterizing the structures and stabilities of the apoglobin states without heme. After the removal of heme, sperm whale apo-**Mb** has been shown to lose a substantial amount of secondary structure. Further addition of chemical denaturants such as urea, acid, or guanidinium hydrochloride (GdHCl) or heat or lead to complete loss of both secondary and tertiary structure. Balestrieri et al.⁵⁰ first proposed the presence of a folding intermediate for apo-**Mb**.

1.5.3 Functions of Myoglobin

a) Oxygen storage

Mb is an important O₂ storage protein in muscles. The **Mb** content is very large in highly oxidative muscle fibers. **Mb** does not have subunits to produce cooperative binding as it consists of a single polypeptide chain. The major functions of **Mb** are to store oxygen in muscles to use during heavy exercise and enhance diffusion by carrying the oxygen through the cytosol. By binding O₂, **Mb** provides a second diffusive pathway for O₂ through the cytosol.

b) P_{O2} buffering

Mb serves as a buffer of intracellular P_{O2} in different species such as the human, rodent and bovine models. When muscle activity increases, **Mb** buffer O₂ concentrations and as a result, the intracellular concentration of O₂ remains relatively constant and homogeneous despite dramatic activity-induced increases in O₂ flux from capillary to mitochondria.⁵¹

1.6 Cytochrome c

Cytochrome c (**Cyt c**), is a small (~12.4 kDa) heme *c* protein mediating the electron transfer from **Cyt c** reductase to **Cyt c** oxidase.⁵² It is a highly water soluble heme protein and loosely associated with the inner mitochondrial membrane. It is an essential protein of the electron transport chain and is capable of changing the oxidation state. Research on **Cyt c** is still of great interest to biophysicists and biochemists owing to its multi-functionality. It serves as an electron carrier between major membrane proteins in the inner membrane of the mitochondria⁵³, as a scavenger for H₂O₂ and as an initiator for mitochondrial apoptosis.⁵⁴ The protein has also been utilized as a model system for protein folding studies.⁵⁵⁻⁵⁶ Moreover it is observed that in the early stages of apoptosis^{6,57}, **Cyt c** acts as a catalyst for peroxidation of anionic phospholipid, cardiolipin (**CL**).⁵⁸⁻⁵⁹

1.6.1 Structure of Cytochrome *c*

Ferric **Cyt c** (oxidised form) was one of the first proteins characterized completely by X-ray crystallography.⁶⁰⁻⁶¹ It is a globular protein (diameter of 34 Å) with single polypeptide chain containing 104 amino acid residues (**Figure 1.4**).^{60, 62} **Cyt c** has a net charge of +8 in neutral pH⁶³⁻⁶⁴ and having isoelectric point ranging from 10.0 - 10.5. It contains of nineteen positively charged lysine (K), two positively charged arginine (Arg), and 12 acidic residues (aspartic or glutamic acids). The secondary structure of **Cyt c** consists of three major and two minor helical elements (~45% helix), a very short two-stranded anti-parallel β-sheet, two type III β-turns (~8%) and four type II β-turns (~14%).⁶¹ The Fe atom is coordinated to a proximal His18 ligand and distal methionine (Met80) ligands in the native form. The Fe atom serves as an electron acceptor and donor in the inner mitochondrial membrane. In *c* type cytochromes, the two vinyl substituents of the porphyrin form thioether bonds via Cys14 and Cys17. The heme group of **Cyt c** is not planar, and undergoes an out-of-plane ruffling due to the covalent attachment to the heme as well as the axial ligands linked with the iron atom.^{22, 65,66-67} The electron transfer rate between the heme and redox partners was observed to be altered with modification in the magnitude of the heme ruffling.⁶⁸ The non-planar heme is buried in the hydrophobic pocket of the polypeptide chain. The functional properties of the heme are related to the interaction of the heme with the protein matrix.

1.6.2 Oxidation States of Cytochrome *c*

Cyt c exists in both oxidised and reduced forms. Major conformational differences were not observed between the fully folded oxidized and reduced states of **Cyt c** in the vicinity of propionic group in the side chain.⁶⁹ The protein interior was less solvent accessible due to some hydrogen bonding changes upon reduction of the heme.

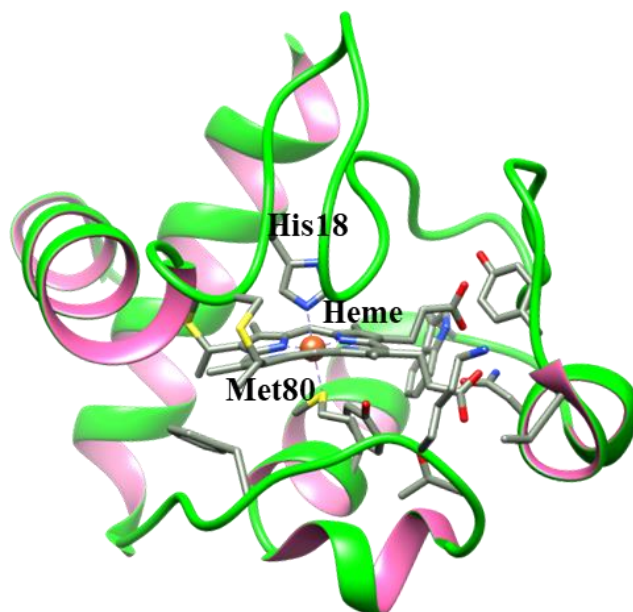


Figure 1.4 Crystal structure of horse heart ferric **Cyt c** from PDB: 1HRC.⁷⁰

The reduced **Cyt c** is more stable than the oxidised **Cyt c** at high temperature (~100°C) and acidic and alkaline pH due to a weaker Fe–Met80 bond in the oxidized state.⁷¹

1.6.3 Unfolding of Cytochrome c

The mechanisms of **Cyt c** unfolding and folding have been a subject of deep research and debate in the scientific community over several years and it has been considered as an ideal model for protein folding and unfolding studies.⁷² Different spectroscopic methods, such as UV–Vis, fluorescence, NMR, IR, and CD has been used to investigate the folding and unfolding process of **Cyt c**. **Cyt c** can be unfolded reversibly so that it can refold back without degradation of the protein as the prosthetic heme group remains intact as the protein unfolds due to the covalent linkages between the heme and the protein group. Different conditions causing the unfolding in **Cyt c** are given below.

a) Denaturing Agents

Chemicals can be used as unfolding agents to unfold the polypeptide chain, leading the protein to adopt a disordered structure. **Cyt c** unfolds reversibly in the presence of GdHCl (6 M) and urea (8 M). Both of these denaturants destabilize the proteins through

different mechanisms, even though the results are structurally similar. Urea form hydrogen bonds to the peptide NH group and CO groups, whereas GdHCl acts by a mechanism other than the formation of a hydrogen bond⁷³. Under slight denaturing conditions, the proximal His18 remains bound to the heme iron and distal Met80 dissociates. Immediately, Met80 will be replaced by other nearby residues, and form a denatured protein with a disordered tertiary structure and native-like secondary structure⁷⁴. In the presence of strong denaturing agent with high concentration, the Met80 ligand was replaced by histidine (His26, His33 or His39) forming a high spin Fe atom⁷⁵.

b) **Acidic and Alkaline pH.**

In 1941, Theorell and Åkenson demonstrated that ferric **Cyt c** changed its conformations depending on pH.⁶³ Dolpner et al.⁷⁶ proposed five different states populated between pH 1 and 12 are represented as states I–V based on resonance Raman studies, which differ with respect to the axial ligands of the heme iron and shown in the **Figure 1.5**. The native state is represented as state III and states IV and V are populated under alkaline conditions. Subscripts a and b indicate different isomers. The neutral form (III) with pK_a 8.7 and 8.9 undergoes two conformational transitions with similar to those of IV_a and IV_b in the medium alkaline pH. In the states IV_a and IV_b, Met80 is replaced with Lys73 and Lys79. Another state V_a and V_b exist in the high alkaline pH range with pK_a of 10.5 and 11. In these states strong ligands are formed that can displace Lys73 and Lys79 from the sixth coordination position of the heme iron. Generally, strong field ligands such as hydroxide or alkoxide ions occupy the sixth axial coordination site in the states V_a and V_b.

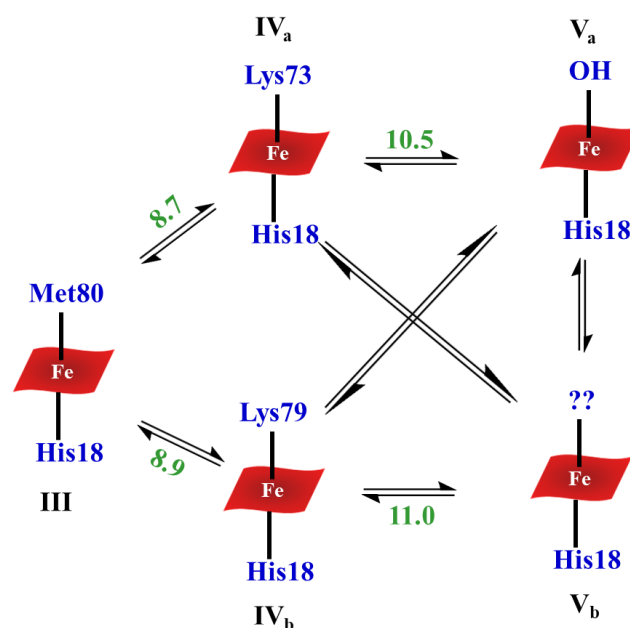


Figure 1.5 Conformational equilibrium of **Cyt c** in the pH range 7.0 and 12.0. The Figure is reproduced from Ref. 59.

c) Temperature

The thermal stability of **Cyt c** is highly depended on the stability of the Fe–Met80 linkage. Thermal unfolding starts around 40 °C in neutral pH in the case of oxidized **Cyt c**. As the temperature increases to more than 50 °C, thermal unfolding starts leading to a decrease in the redox potential, and the replacement of Met80 from the axial coordination.⁷⁷ Hagarman et al.⁷⁸ reported the existence of a low-spin heme iron at temperature above 50 °C. Temperatures above 75°C, the protein existed in the unfolded state. For reduced **Cyt c** the initial unfolding starts at temperatures above 100 °C.⁷⁹

1.6.4 Functions of Cytochrome c

The multi-functional heme protein, **Cyt c** is involved in both the life and death process happening in the cell. Various functions of **Cyt c** are charted in **Figure. 1.6**. It plays a major role in the energy production process. It is also participating in the process of programmed cell death called apoptosis.⁸⁰ Additional functions of **Cyt c**, includes the peroxidase function.⁸¹⁻⁸² The investigation of the exact pathways that operate these

regulatory mechanisms and their effects are important for targeting various diseases such as congestive heart failure, neurodegenerative diseases and cancer. Different functions of **Cyt c** are discussed below in detail.

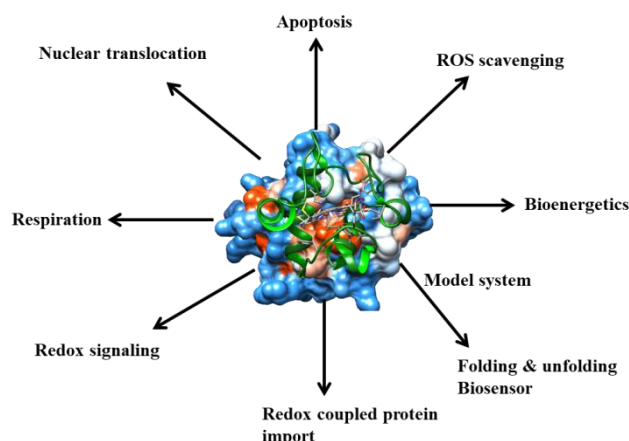


Figure 1.6 Various functions of **Cyt c**.

1. Oxidative Phosphorylation

ATP generates through oxidative phosphorylation (OxPhos) in the inner mitochondrial membrane and with ATP synthase and the electron transport chain (ETC).⁸³ ATP synthase utilizes the mitochondrial membrane potential by for the synthesis of ATP.⁸⁴ **Cyt c** functions as a single electron carrier in the final step of the ETC, from the bc1 complex to CCO. Since four electron transfers are necessary to reduce an oxygen molecule to water and hence four times reduced **Cyt c** transfers an electron to CCO.⁸⁵⁻⁸⁶

2. Free Radical Scavenger of ROS

Reactive oxygen species (ROS) are highly reactive species generated in the mitochondria and it can damage DNA and other compounds within the cell. In the inner-mitochondrion space, free **Cyt c** can able to remove the unpaired electron from superoxide and regenerating O₂. Hence **Cyt c** can act as a free radical scavenger in the mitochondria.⁸⁷ Similarly in both the reduced and oxidized states, **Cyt c** has also been shown to function as a hydrogen peroxide scavenger.⁸⁸

3. Cellular Apoptosis

Apoptosis is an essential process which eliminates unwanted cells and is vital for embryonic development, immune defence and homeostasis. Over the last few years, more research have been focused on the role of **Cyt c** in apoptosis. Apoptosis plays a significant role in diverse physiological processes especially fetal cells and in adult tissues.⁸⁹⁻⁹⁰ Different diseases such as cancers, and neurodegenerative disorders are reported to be caused by the deregulation of apoptosis. The mechanism of apoptosis is complicated and is mainly implemented by cysteine proteases known as caspases. In the mammalian cells the main caspase activation pathway was initiated by the protein **Cyt c**.^{7,91} During the process, different types of apoptotic stimuli induce the release of **Cyt c** to the cytoplasm from mitochondria causing various biochemical reactions which activate the caspase action and lead to cell death.^{92,93} During the initial stage of apoptosis, the stimulated ROS can oxidise **CL** and induce the liberation of **Cyt c** from inner mitochondrial membrane. The release of different proteins such as adenylate kinase-2 (AK-2), SmacDIABLO, and **Cyt c** present in the inter membrane space have been observed during the early stages of apoptotic cell death. The release of **Cyt c** from mitochondria is therefore considered as a key initial step in apoptosis.⁸ In the outer mitochondrial membrane two proteins, Bax and Bak (Bcl-2 family) are associated with a voltage-dependent anion channel component of the permeability transition pores, allows **Cyt c** release from the inner mitochondrial membrane into the cytoplasm.⁹

1.7 Ultrafast Dynamics of Heme Proteins

Electronic, vibrational and conformational changes and local structural changes in proteins resulting from long-distance interactions are characteristics of protein functions. Real time visualization of such processes was possible only after the invention of femtosecond laser spectroscopy.⁹⁴ Triggering and probing systems, in which light is

physiologically used, such as photosynthetic and retinal pigment-protein complexes, are ideally suited for optical techniques. Whereas the dynamics of heme proteins can be triggered by using the optically active porphyrin cofactor. Moreover, the amino acid residues also allow the study of the protein dynamics.⁹⁵ The pioneering studies on ultrafast processes occurring in heme proteins were initially performed on the mammalian ‘model’ oxygen storage protein **Mb** and oxygen transport protein **Hb**.⁹⁶ An overview on ultrafast studies of **Mb** and **Cyt c** are discussed below.

In addition to O₂, **Hb** and **Mb** can reversibly bind CO and NO. In the bound state the iron atom is in the plane of the porphyrin macrocycle and has a low spin ($S = 0$) state. Whereas the Fe atom will be displaced from the plane of the porphyrin by $\sim 0.3 \text{ \AA}$ towards the proximal histidine ligand in the unligated state and has high spin ($S = 2$) state. This ligand can be photolysed on the ultrafast time scale which then recombines at a later time to reform the bound heme. Even though these heme proteins are not directly involved in any photochemical transformations, the biological function of **Hb** and **Mb** can be optically triggered using a short light pulse and the associated structural changes in the heme group as well as the surrounding protein can be studied by creating a situation similar to oxygen uptake and release. In order to briefly explain the events associated with the photolysis in heme proteins, part of the light energy will be consumed in breaking the iron to ligand bond and the energy in excess of that required for photolysis is shared between the unligated heme and ligand. The events following photolysis include ligand escape, electronic and vibrational relaxation (VR) of the unligated heme, out of plane motion of Fe atom, and spin state change, ligand rebinding and the associated protein structural and conformational relaxation. The usefulness of the transient spectral changes occurring as a result of these events in elucidating the protein structure function relationships has led to an enormous amount of theoretical and experimental studies of these heme proteins. The

early protein dynamics following photo-dissociation of **Mb** have been studied using time-resolved femtosecond spectroscopy, and observed that the deoxy species was formed within 350 fs.⁹⁷ The relaxation was occurred by heme-CO dissociation on multiple time scales and was non-exponential and heterogeneous and change of spin state occurred, accompanied by motion of the iron atom out of the porphyrin plane. Henry et al.⁹⁸ observed that the quantum yield of photo-dissociation in **Mb** was close to 1 for CO. Whereas photo-dissociation of NO and O₂ gave a quantum yield of ~0.5 and 0.3 respectively.⁹⁹ From femtosecond infrared polarization studies, it was observed that the heme bound CO was oriented near perpendicular to the porphyrin plane in **Mb**.¹⁰⁰ The dissociated NO was observed to have a high chance to rebind to the heme as NO is more reactive than CO towards the heme. The rebinding kinetics of NO have been broadly used to probe the dynamic properties of the heme in **Mb**. Recently Kim and Lim observed three distinct conformations of dissociated NO by using time-resolved infrared spectroscopic study.¹⁰¹

The first femtosecond time-resolved absorption study of the dynamics of **Cyt c** and cytochrome b5 was by Traylor and co-workers.¹⁰² They compared the dynamics of ferrous cytochrome b5 with **Cyt c** and observed the formation of 5c species due to ligand dissociation and it was recombined within ~7 ps. They interpreted the dissociated ligand as histidine. Later in 2000, Champion's group¹⁰³ proposed that it was the methionine residue that was dissociated from **Cyt c** (quantum yield ~1), and rebound in ~6 ps. Whereas photo-dissociation was not occurred in ferric **Cyt c**. A multiphasic rebinding kinetics of CO (10¹–10⁴ ps) was observed from ultrafast investigation by Vos et al.¹⁰⁴ and proposed that it was extremely sensitive to the local heme environment. Thus CO rebinding in **Cyt c** is similar to NO rebinding to **Mb**. In the past decades, a huge number of ultrafast spectroscopy experiments have been reported on heme proteins. Even then the heme

electronic and vibrational dynamics are not fully understood. Mainly two models have been suggested by various groups in the ultrafast relaxation dynamics of heme.

1.7.1 Vibrational Relaxation Dynamics

In femtosecond experiments the absorption of a photon will cause a significant increase in temperature in a system because of the excess energy. The flow of vibrational energy is a fundamental physical process that is not well understood. The excess energy in the molecular system can be redistributed intramolecularly to other vibrational modes within the molecule (IVR) or it can decay rapidly towards equilibrium by transferring energy into the solvent.¹⁰⁵ The first molecular dynamics simulation of molecular cooling for **Mb** and **Cyt c** in vacuo was carried by Henry et al.¹⁰⁶ in 1986. A non-exponential decay of the vibrational temperature with about 50% loss was occurred within 1–4 ps. Kholodenko et al.¹⁰⁷ reported an electronic relaxation processes of deoxy **Mb** upon Soret band excitation, involving two time constants, one was less than 100 fs and another of a few 100 fs. They did not observe any electronic relaxation components after ~ 600 fs, which was contrary to the work carried out by Petrich et al.¹⁰⁸ and Franzen et al.¹⁰⁹ The ground state VR was shown to be bi-exponential involving a faster component with higher amplitude (1.5 to 4 ps) and a slower component with lower amplitude (~ 15 ps) component. The vibrational dynamics of heme proteins have been studied in detail by various techniques such as time-resolved anti-Stokes resonance Raman scattering¹¹⁰, transient absorption, IR and transient grating studies.¹¹¹ Chergui et al.¹¹² reported early photodynamic of ferric and ferrous horse heart **Cyt c** using UV-visible ultrafast time-gated emission and transient absorption spectroscopy. The proposed photo-cycle is given in **Figure 1.7**. From the S₂ state around 86% of the molecules undergoes IC to the

anti-bonding d_z^2 metal orbital through channel A (110–150 fs) by inducing ligand photo-dissociation in the ferrous form.

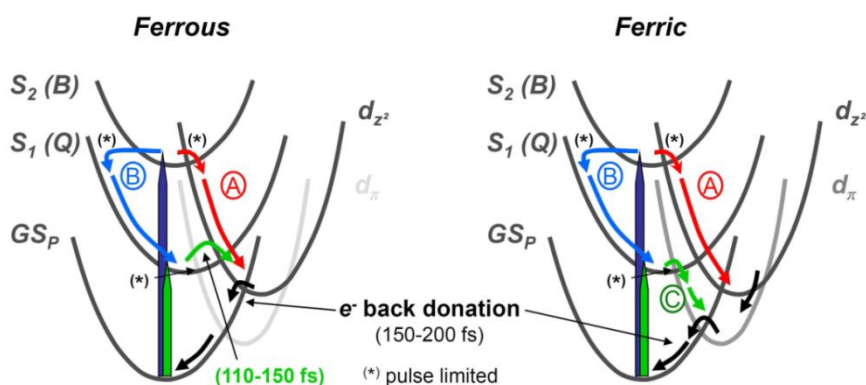


Figure 1.7 The relaxation pathways of ferrous and ferric **Cyt c**. Channels A and B correspond to the branching that occur in ferrous **Cyt c** under Soret or δ band excitation. In the ferric form, since the d_{xy} orbital is half filled, IC to d_{xy} (channel C) is allowed and more efficient than the 100–150 fs IC to d_z^2 (end of channel B). Figure is copied from Ref. 112.

Then the configuration was recovered back by back electron transfer from the d_z^2 orbital or from another d state. The remaining 14% underwent IC to the Q band through channel B and reached the anti-bonding metal state through a energetically less favourable crossing point, causing a delayed photo-dissociation. The full occupancy of this state prevented the favourable path to d_{xy} through channel C. In the ferric form, the most favourable relaxation pathway was through partially occupied d_{π} orbital, permitting a faster de-excitation without cleavage of the bond. The first electron end up on the d_z^2 orbital and after 150–200 fs, the system reached to the same state, responsible for the excited state absorption (ESA). Very recently in 2020, Ferrante et al.¹¹³ investigated ultrafast evolution of two proteins, **Cyt c** and Neuroglobin (Ngb) using femtosecond stimulated Raman spectroscopy (FSRS). Based on the response of the system, detailed properties of energy redistribution and atomic motions were discussed for different delay time and Raman pump resonances. The proposed scheme for energy flow for both the proteins is shown in **Figure 1.8**. The system decayed to the vibrationally hot photo-dissociated state of Ngb (blue area) and **Cyt c** (red

area) with a time scale of < 50 fs, in which the axial ligands His (for Ngb) and Met (for Cyt c) was detached from the heme. In that situation a structural relaxation and cooling process were observed. The first ν_4 hot band observed in Ngb testified the population of vibrational excited states. The last step was the recovery of the ground state within 5–9 ps with rebinding of the ligands.

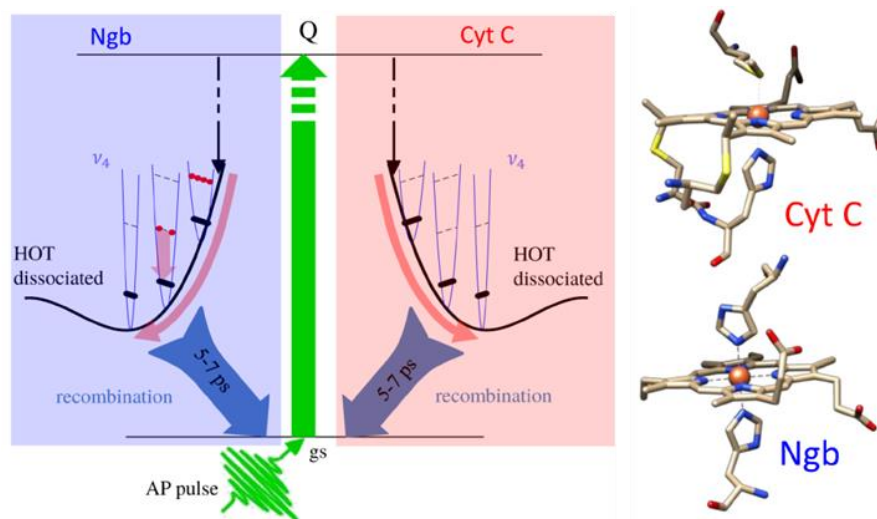


Figure 1.8 Summary of the energy flow in Ngb and Cyt c obtained from FSRs transient spectra. The Figure is copied from Ref.113.

1.7.2 Involvement of Intermediate Excited Electronic State

A detailed description of the electronic dynamics of the heme proteins ligated with diatomic ligands CO, NO and O₂ as well as that of a protoheme ligated with CO and NO was given by Petrich et al.¹⁰⁸ in 1988. Photolysis was reported to occur upon photo-excitation in the Q-band for Hb in less than 50 fs leading to the formation of two intermediate electronic states **HbI*** and **HbII*** each having a lifetime of 300 fs and 2.5 ps (3.2 ps in case of deoxy **Mb**) respectively (**Figure 1.9** a). Later Franzen et al.¹⁰⁹ proposed an intermediate electronic state decay model by a sequential relaxation pathway

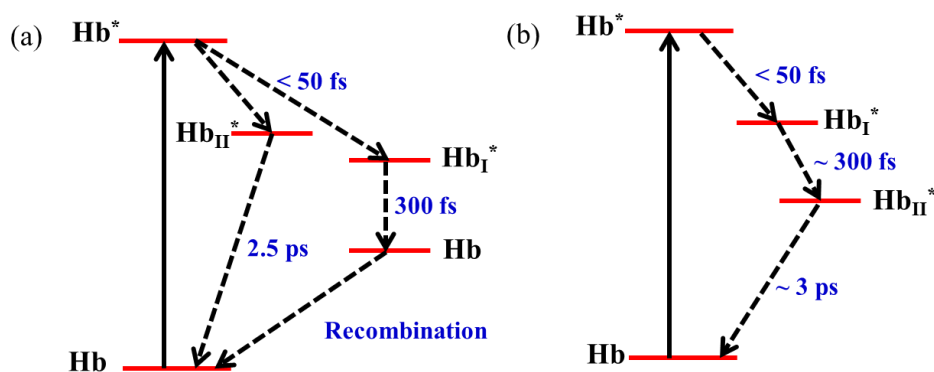


Figure 1.9 Intermediate excited electronic state decay models proposed by Petrich et al. (a) and Franzen et al. (b) representing the electronic relaxation dynamics of both ligated and unligated heme proteins as well Fe PPIX.

as shown in **Figure 1.9** b ($Q1-Hb_I^*-Hb_{II}^*-Hb$) through the same intermediate electronic states. Again, both the ligated and unligated heme proteins were studied following electronic excitation in the Q-band. The intermediate electronic state Hb_I^* was proposed to form via ultrafast iron-to-porphyrin ring CT and then Hb_{II}^* due to porphyrin ring-to-iron back CT process. In 2014 Chergui et al.¹¹⁴ reported an early relaxation dynamics of met-**Mb** using combined ultrafast broadband fluorescence and transient absorption spectroscopy. A strong evidence for an electronic character in the early relaxation of **Mb** was observed besides identifying a branching in the usual cases. The photo cycle for the relaxation dynamics of **Mb** are shown in **Figure 1.10**. The ultrafast ET from the porphyrin to the iron d-states was followed by a back electron transfer on a 400–500 fs time scale from Mb_I^* . Around ~57% of the excited population was relaxed directly to the ground state whereas the remaining leads to the population of electronically excited states of Fe atom consisting of different spin. In Mb_{III}^* ($S = 1/2$), four electrons occupy the d_π orbitals representing low-spin ferrous met-**Mb**. The relaxation towards the high-spin ground state proceeds through a quartet state Mb_{II}^* via an intermediate $S = 3/2$ electronic excited state.

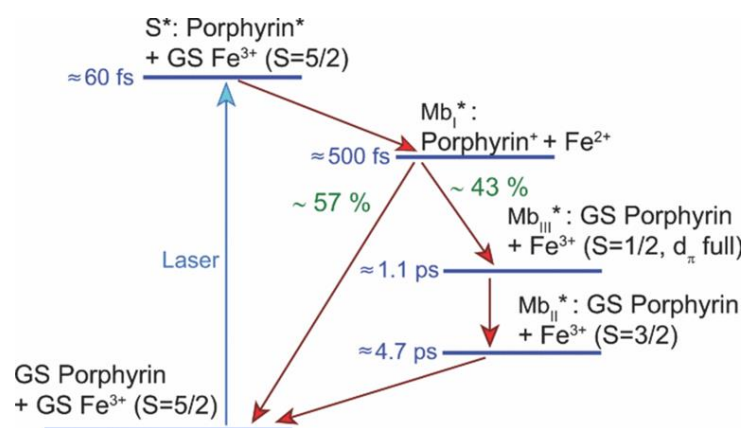


Figure 1.10 Proposed photocycle for the relaxation of photoexcited met-Mb. The Figure is copied from Ref. 114.

1.8 Objectives of the Thesis

The understanding of the excited state relaxation dynamics is important to describe the biological function of heme proteins. Heme proteins, for example **Cyt c** has various biological functions including electron transfer from cytochrome c reductase to cytochrome c oxidase, energy transfer in mitochondrial transport chain reaction, catalysis of redox reactions such as oxidation of **CL** triggering of cell apoptosis and also model system for studying the unfolding dynamics of proteins. The electronic, vibrational and conformational changes of the protein due to redistribution of the excess energy generated by biological functions play important role. These can be triggered optically by ultrafast laser and accompanying electronic, vibrational and conformational relaxation dynamics in the heme group and the surrounding protein can be investigated. Despite several years of active research by various groups, the heme electronic dynamics has not been understood completely. The main focus of the thesis is to investigate the ultrafast electronic, vibrational and conformational relaxation dynamics of heme model compounds, heme proteins with lipids and hematin with antimalarial drugs using femtosecond pump-probe spectroscopy to understand the correlation between the excited state relaxation dynamics and biological functions of the protein.

Hence, the ultrafast excited state relaxation dynamics of various heme model compounds and met-**Mb** have been investigated in Chapter 3 with the aim of understanding the influence of the axial ligands, peripheral substituents and the solvents on the excited state relaxation dynamics of the heme.

Cyt c catalyzes the peroxidation of **CL** in the early stage of apoptosis and undergoes conformational changes leading to the partial unfolding of the protein. The various degrees of partial unfolding in **Cyt c** in the presence of liposomes are studied with absorption, fluorescence, CD spectroscopy and femtosecond time resolved pump-probe spectroscopy in Chapter 4 to understand the interaction dynamics of **Cyt c** with different liposomes.

During the intra-erythrocytic stage of the malaria parasite's lifecycle, it digests host erythrocyte **Hb**, producing free **Hematin**. The heme, toxic to the parasite, is converted into hemozoin by crystallization. The antimalarial drug is used to prevent the crystallization by binding with **Hematin**. Hence, the understanding of the underlying mechanism of the interaction dynamics between the **Hematin** and antimalarial drugs will enable the design of new antimalarial drugs (Chapter 5).

1.9 References

1. Gray, H. B.; Winkler, J. R., *Annu. Rev. Biochem.* **1996**, *65* (1), 537-561.
2. Rodgers, K. R., *Curr. Opin. Chem. Biol.* **1999**, *3* (2), 158-167.
3. Reichlin, M., *Science* **1972**, *178* (4058), 296-296.
4. Harrison, P.; Huehns, E. R., *Nature* **1979**, *279* (5713), 476-477.
5. Brooks, G. T., *Pesticide Science* **1998**, *52* (4), 409-409.
6. Hengartner, M. O., *Nature* **2000**, *407* (6805), 770-776.
7. Privalle, C. T.; Crivello, J. F.; Jefcoate, C. R., *Proc. Natl. Acad. Sci. U S A.* **1983**, *80* (3), 702-706.
8. Yoshikawa, S., *Adv. Protein. Chem.* **2002**, *60*, 341-395.
9. Ha-Thi, M.-H.; Shafizadeh, N.; Poisson, L.; Soep, B., *Phy. Chem. Chem. Phys.* **2010**, *12* (45), 14985-14993.
10. Kumble, R.; Palese, S.; Lin, V. S. Y.; Therien, M. J.; Hochstrasser, R. M., *J. Am. Chem. Soc.* **1998**, *120* (44), 11489-11498.
11. Dietzek, B.; Kiefer, W.; Hermann, G.; Popp, J.; Schmitt, M., *J. Phys. Chem. B* **2006**, *110* (9), 4399-4406.
12. Rury, A. S.; Goodrich, L. E.; Galinato, M. G. I.; Lehnert, N.; Sension, R. J., *J. Phys. Chem. A* **2012**, *116* (32), 8321-8333.
13. Jahan, M.; Bao, Q.; Loh, K. P., *J. Am. Chem. Soc.* **2012**, *134* (15), 6707-6713.
14. Lee, D. H.; Lee, W. J.; Lee, W. J.; Kim, S. O.; Kim, Y. H., *Phys. Rev. Lett.* **2011**, *106* (17), 175502.
15. El-Nahass, M. M.; El-Deeb, A. F.; Metwally, H. S.; Hassanien, A. M., *Eur. Phys. J. Appl. Phys.* **2010**, *52* (1), 10403.
16. Tripathy, U.; Kowalska, D.; Liu, X.; Velate, S.; Steer, R. P., *J. Phys. Chem. A* **2008**, *112* (26), 5824-5833.

-
17. Cao, W.; Ye, X.; Georgiev, G. Y.; Berezhna, S.; Sjodin, T.; Demidov, A. A.; Wang, W.; Sage, J. T.; Champion, P. M., *Biochemistry* **2004**, *43* (22), 7017-7027.
 18. Gouterman, M.; Wagnière, G. H.; Snyder, L. C., *J. Mol. Spectr.* **1963**, *11* (1), 108-127.
 19. Reedy, C. J.; Gibney, B. R., *Chem. Rev.* **2004**, *104* (2), 617-650.
 20. Fischer, H.; Orth, H., *Die Chemie des Pyrrols*. Akademische Verlagsgesellschaft: Leipzig, **1934**.
 21. Hayashi, T., Generation of Functionalized Biomolecules using Hemoprotein Matrices with Small Protein Cavities for Incorporation of Cofactors. In *Coordination Chemistry in Protein Cages*, Hoboken : Wiley: **2013**; 87-110.
 22. Moore, G. R.; Pettigrew, G. W., *Cytochromes c: Evolutionary, Structural and Physicochemical Aspects*. Springer Berlin Heidelberg: Berlin, Heidelberg, **1990**; 161-227.
 23. Reedy, C. J.; Elvekrog, M. M.; Gibney, B. R., *Nucleic. Acids. Res.* **2008**, *36*, D307-313.
 24. Zheng, Z.; Gunner, M. R., *Proteins* **2009**, *75* (3), 719-734.
 25. Kleingardner, J. G.; Bren, K. L., *Acc. Chem. Res.* **2015**, *48* (7), 1845-1852.
 26. Mogi, T.; Saiki, K.; Anraku, Y., *Mol. Microbiol.* **1994**, *14* (3), 391-398.
 27. Caughey, W. S.; Smythe, G. A.; O'Keeffe, D. H.; Maskasky, J. E.; Smith, M. I., *J. Biol. Chem.* **1975**, *250* (19), 7602-7622.
 28. Shimokata, K.; Katayama, Y.; Murayama, H.; Suematsu, M.; Tsukihara, T.; Muramoto, K.; Aoyama, H.; Yoshikawa, S.; Shimada, H., *Proc. Natl. Acad. Sci. U.S.A* **2007**, *104* (10), 4200.

29. Vainshtein, B. K.; Melik-Adamyanyan, W. R.; Barynin, V. V.; Vagin, A. A.; Grebenko, A. I.; Borisov, V. V.; Bartels, K. S.; Fita, I.; Rossmann, M. G., *J. Mol. Biol.* **1986**, *188* (1), 49-61.
30. Williams, P. A.; Fülöp, V.; Garman, E. F.; Saunders, N. F. W.; Ferguson, S. J.; Hajdu, J., *Nature* **1997**, *389* (6649), 406-412.
31. Igarashi, N.; Moriyama, H.; Fujiwara, T.; Fukumori, Y.; Tanaka, N., *Nat. Struct. Mol. Biol.* **1997**, *4* (4), 276-284.
32. Crane, B. R.; Siegel, L. M.; Getzoff, E. D., *Science* **1995**, *270* (5233), 59-67.
33. Lemberg, R.; Falk, J. E., *Biochem. J.* **1951**, *49* (5), 674-683.
34. Pauling, L.; Itano, H. A.; Singer, S. J.; Wells, I. C., *Science* **1949**, *110* (2865), 543.
35. Kendrew, J. C.; Bodo, G.; Dintzis, H. M.; Parrish, R. G.; Wyckoff, H.; Phillips, D. C., *Nature* **1958**, *181* (4610), 662-666.
36. Perutz, M. F.; Rossmann, M. G.; Cullis, A. F.; Muirhead, H.; Will, G.; North, A. C., *Nature* **1960**, *185* (4711), 416-422.
37. Stevens, J. M.; Daltrop, O.; Allen, J. W. A.; Ferguson, S. J., *Acc. Chem. Res.* **2004**, *37* (12), 999-1007.
38. Anderson, J. L. R.; Chapman, S. K., *Dalton Trans.* **2005**, (1), 13-24.
39. Krieg, S.; Huche, F.; Diederichs, K.; Izadi-Pruneyre, N.; Lecroisey, A.; Wandersman, C.; Delepelaire, P.; Welte, W., *Proc. Natl. Acad. Sci. U S A* **2009**, *106* (4), 1045-1050.
40. Robertson, D. E.; Farid, R. S.; Moser, C. C.; Urbauer, J. L.; Mulholland, S. E.; Pidikiti, R.; Lear, J. D.; Wand, A. J.; DeGrado, W. F.; Dutton, P. L., *Nature* **1994**, *368* (6470), 425-432.
41. D'Souza, A.; Torres, J.; Bhattacharjya, S., *Commun. Chem.* **2018**, *1* (1), 78.

-
42. Huang, S. S.; Koder, R. L.; Lewis, M.; Wand, A. J.; Dutton, P. L., *Proc. Nat. Acad. Sci. U. S. A* **2004**, *101* (15), 5536.
 43. Ramanavicius, A.; Ramanaviciene, A., *Fuel Cells* **2009**, *9* (1), 25-36.
 44. Ye, S.; Strzalka, J. W.; Discher, B. M.; Noy, D.; Zheng, S.; Dutton, P. L.; Blasie, J. K., *Langmuir* **2004**, *20* (14), 5897-5904.
 45. Ueno, T.; Yokoi, N.; Unno, M.; Matsui, T.; Tokita, Y.; Yamada, M.; Ikeda-Saito, M.; Nakajima, H.; Watanabe, Y., *Proc. Nat. Acad. Sci. U. S. A* **2006**, *103* (25), 9416.
 46. Lehmann, A.; Saven, J. G., *Biotechnol. Prog.* **2008**, *24* (1), 74-79.
 47. Balasubramanian, S.; Lambright, D. G.; Simmons, J. H.; Gill, S. J.; Boxer, S. G., *Biochemistry* **1994**, *33* (27), 8355-8360.
 48. Ordway, G. A.; Garry, D. J., *J. Exp. Biol.* **2004**, *207* (Pt 20), 3441-3446.
 49. Phillips, S. E. V.; Schoenborn, B. P., *Nature* **1981**, *292* (5818), 81-82.
 50. Balestrieri, C.; Colonna, G.; Giovane, A.; Irace, G.; Servillo, L., *FEBS Lett* **1976**, *66* (1), 60-64.
 51. Hochachka, P. W., *Proc. Nat. Acad. Sci. U. S. A.* **1999**, *96* (22), 12233.
 52. Cox, M.; Nelson, D., *Lehninger Principles of Biochemistry*. Freeman, : New York., **2000**; Vol. 5.
 53. Adman, E. T., *Biochim. Biophys. Acta.* **1979**, *549* (2), 107-144.
 54. Belikova, N. A.; Vladimirov, Y. A.; Osipov, A. N.; Kapralov, A. A.; Tyurin, V. A.; Potapovich, M. V.; Basova, L. V.; Peterson, J.; Kurnikov, I. V.; Kagan, V. E., *Biochemistry* **2006**, *45* (15), 4998-5009.
 55. Englander, S. W.; Sosnick, T. R.; Mayne, L. C.; Shtilerman, M.; Qi, P. X.; Bai, Y., *Acc. Chem. Res* **1998**, *31* (11), 737-744.
 56. Winkler, J. R., *Curr. Opin. Chem. Biol.* **2004**, *8* (2), 169-174.

57. Balakrishnan, G.; Hu, Y.; Spiro, T. G., *J. Am. Chem. Soc.* **2012**, *134* (46), 19061-19069.
58. Ow, Y.-L. P.; Green, D. R.; Hao, Z.; Mak, T. W., *Nat. Rev. Mol. Cell. Biol* **2008**, *9* (7), 532-542.
59. Osman, C.; Voelker, D. R.; Langer, T., *J. Cell. Biol* **2011**, *192* (1), 7-16.
60. Dickerson, R. E.; Takano, T.; Eisenberg, D.; Kallai, O. B.; Samson, L.; Cooper, A.; Margoliash, E., *J. Biol. Chem.* **1971**, *246* (5), 1511-1535.
61. Dickerson, R. E., *J. Mol. Evol.* **1971**, *1* (1), 26-45.
62. Banci, L.; Bertini, I.; Gray, H. B.; Luchinat, C.; Reddig, T.; Rosato, A.; Turano, P., *Biochemistry* **1997**, *36* (32), 9867-9877.
63. Theorell, H.; Åkesson, Å., *J. Am. Chem. Soc.* **1941**, *63* (7), 1818-1820.
64. Van Gelder, B. F.; Slater, E. C., *Biochim. Biophys. Acta.* **1962**, *58* (3), 593-595.
65. Ma, J.-G.; Zhang, J.; Franco, R.; Jia, S.-L.; Moura, I.; Moura, J. J. G.; Kroneck, P. M. H.; Shelnutt, J. A., *Biochemistry* **1998**, *37* (36), 12431-12442.
66. Michel, L. V.; Ye, T.; Bowman, S. E.; Levin, B. D.; Hahn, M. A.; Russell, B. S.; Elliott, S. J.; Bren, K. L., *Biochemistry* **2007**, *46* (42), 11753-11760.
67. Liptak, M. D.; Wen, X.; Bren, K. L., *J. Am. Chem. Soc.* **2010**, *132* (28), 9753-9763.
68. Mao, J.; Hauser, K.; Gunner, M. R., *Biochemistry* **2003**, *42* (33), 9829-9840.
69. Takano, T.; Dickerson, R. E., *J. Mol. Biol.* **1981**, *153* (1), 95-115.
70. Bushnell, G. W.; Louie, G. V.; Brayer, G. D., *J. Mol. Biol.* **1990**, *214* (2), 585-595.
71. Filosa, A.; Wang, Y.; Ismail, A. A.; English, A. M., *Biochemistry* **2001**, *40* (28), 8256-8263.
72. Karunakaran, V., *ChemPhysChem* **2015**, *16* (18), 3974-3983.
73. Lim, W. K.; Rösgen, J.; Englander, S. W., *Proc. Natl. Acad. Sci. U S A.* **2009**, *106* (8), 2595-2600.

-
74. Babul, J.; Stellwagen, E., *Biopolymers* **1971**, *10* (11), 2359-2361.
 75. Colon, W.; Wakem, L. P.; Sherman, F.; Roder, H., *Biochemistry* **1997**, *36* (41), 12535-12541.
 76. Döpner, S.; Hildebrandt, P.; Rosell, F. I.; Mauk, A. G., *J. Am. Chem. Soc.* **1998**, *120* (44), 11246-11255.
 77. Taler, G.; Schejter, A.; Navon, G.; Vig, I.; Margoliash, E., *Biochemistry* **1995**, *34* (43), 14209-14212.
 78. Hagarman, A.; Duitch, L.; Schweitzer-Stenner, R., *Biochemistry* **2008**, *47* (36), 9667-9677.
 79. Varhac, R.; Antalík, M.; Bánó, M., *J. Biol. Inorg. Chem.* **2004**, *9* (1), 12-22.
 80. Orrenius, S.; Zhivotovsky, B., *Nat. Chem .Biol.* **2005**, *1* (4), 188-189.
 81. Kagan, V. E.; Borisenko, G. G.; Tyurina, Y. Y.; Tyurin, V. A.; Jiang, J.; Potapovich, A. I.; Kini, V.; Amoscato, A. A.; Fujii, Y., *Free. Radic. Biol. Med.* **2004**, *37* (12), 1963-1985.
 82. Kagan, V. E.; Tyurin, V. A.; Jiang, J.; Tyurina, Y. Y.; Ritov, V. B.; Amoscato, A. A.; Osipov, A. N.; Belikova, N. A.; Kapralov, A. A.; Kini, V.; Vlasova, I. I.; Zhao, Q.; Zou, M.; Di, P.; Svistunenko, D. A.; Kurnikov, I. V.; Borisenko, G. G., *Nat. Chem .Biol.* **2005**, *1* (4), 223-232.
 83. Huttemann, M.; Pecina, P.; Rainbolt, M.; Sanderson, T. H.; Kagan, V. E.; Samavati, L.; Doan, J. W.; Lee, I., *Mitochondrion* **2011**, *11* (3), 369-381.
 84. Stock, D.; Leslie, A. G. W.; Walker, J. E., *Science* **1999**, *286* (5445), 1700.
 85. Acin-Perez, R.; Bayona-Bafaluy, M. P.; Bueno, M.; Machicado, C.; Fernandez-Silva, P.; Perez-Martos, A.; Montoya, J.; Lopez-Perez, M. J.; Sancho, J.; Enriquez, J. A., *Hum. Mol. Genet.* **2003**, *12* (3), 329-339.

86. Villani, G.; Greco, M.; Papa, S.; Attardi, G., *Nat. Chem .Biol.* **1998**, 273 (48), 31829-31836.
87. Pereverzev, M. O.; Vygodina, T. V.; Konstantinov, A. A.; Skulachev, V. P., *Biochem. Soc. Transact.* **2003**, 31 (6), 1312-1315.
88. Wang, Z.-B.; Li, M.; Zhao, Y.; Xu, J.-X., *Protein. Peptide. Lett.* **2003**, 10 (3), 247-253.
89. Vladimirov, Y. A.; Proskurnina, E. V.; Alekseev, A. V., *Biochemistry (Moscow)* **2013**, 78 (10), 1086-1097.
90. Elmore, S., *J. Toxicol .Pathol* **2007**, 35 (4), 495-516.
91. Cai, J.; Yang, J.; Jones, D., *Biochim. et Biophys. Acta* **1998**, 1366 (1–2), 139-149.
92. Kagan, V. E.; Bayır, H. A.; Belikova, N. A.; Kapralov, O.; Tyurina, Y. Y.; Tyurin, V. A.; Jiang, J.; Stoyanovsky, D. A.; Wipf, P.; Kochanek, P. M.; Greenberger, J. S.; Pitt, B.; Shvedova, A. A.; Borisenko, G., *Free. Radic. Biol. Med.* **2009**, 46 (11), 1439-1453.
93. Alnemri, E. S.; Livingston, D. J.; Nicholson, D. W.; Salvesen, G.; Thornberry, N. A.; Wong, W. W.; Yuan, J., *Cell* **1996**, 87 (2), 171.
94. Shank, C. V., *Science* **1986**, 233 (4770), 1276-1280.
95. J L Martin, a.; Vos, M. H., *Ann. Rev. Biophys. Biomol. Struct.* **1992**, 21 (1), 199-222.
96. Vos, M. H.; Martin, J.-L., *Biochim. Biophys. Acta* **1999**, 1411 (1), 1-20.
97. Martin, J. L.; Migus, A.; Poyart, C.; Lecarpentier, Y.; Astier, R.; Antonetti, A., *Proc. Natl. Acad. Sci. U. S. A.* **1983**, 80 (1), 173-177.
98. Henry, E. R.; Sommer, J. H.; Hofrichter, J.; Eaton, W. A., *J. Mol. Biol.* **1983**, 166 (3), 443-451.

-
99. Ye, X.; Demidov, A.; Champion, P. M., *J. Am. Chem. Soc.* **2002**, *124* (20), 5914-5924.
 100. Kachalova, G. S.; Popov, A. N.; Bartunik, H. D., *Science* **1999**, *284* (5413), 473-476.
 101. Kim, S.; Lim, M., *J. Am. Chem. Soc.* **2005**, *127* (25), 8908-8909.
 102. Jongeward, K. A.; Magde, D.; Taube, D. J.; Traylor, T. G., *J. Biol. Chem.* **1988**, *263* (13), 6027-6030.
 103. Wang, W.; Ye, X.; Demidov, A. A.; Rosca, F.; Sjodin, T.; Cao, W.; Sheeran, M.; Champion, P. M., *J. Phys. Chem. B* **2000**, *104* (46), 10789-10801.
 104. Silkstone, G.; Jasaitis, A.; Wilson, M. T.; Vos, M. H., *J. Biol. Chem.* **2007**, *282* (3), 1638-1649.
 105. J C Owrutsky; D Raftery, a.; Hochstrasser, R. M., *Ann. Rev. Phys. Chem.* **1994**, *45* (1), 519-555.
 106. Henry, E. R.; Eaton, W. A.; Hochstrasser, R. M., *Proc. Nat. Acad. Sci. U. S. A.* **1986**, *83* (23), 8982-8986.
 107. Kholodenko, Y.; Volk, M.; Gooding, E.; Hochstrasser, R. M., *Chem. Phys.* **2000**, *259* (1), 71-87.
 108. Petrich, J. W.; Poyart, C.; Martin, J. L., *Biochemistry* **1988**, *27* (11), 4049-4060.
 109. Franzen, S.; Kiger, L.; Poyart, C.; Martin, J.-L., *Biophys. J.* **2001**, *80* (5), 2372-2385.
 110. Causgrove, T. P.; Dyer, R. B., *J. Phys. Chem.* **1996**, *100* (8), 3273-3277.
 111. Ogilvie, J. P.; Plazanet, M.; Dadusc, G.; Miller, R. J. D., *J. Phys. Chem. B* **2002**, *106* (40), 10460-10467.
 112. Bräm, O.; Consani, C.; Cannizzo, A.; Chergui, M., *J. Phys. Chem. B* **2011**, *115* (46), 13723-13730.

113. Ferrante, C.; Batignani, G.; Pontecorvo, E.; Montemiglio, L. C.; Vos, M. H.; Scopigno, T., *J. Am. Chem. Soc.* **2020**, *142* (5), 2285-2292.
114. Consani, C.; Auböck, G.; Bräm, O.; van Mourik, F.; Chergui, M., *J. Chem. Phys.* **2014**, *140* (2), 025103.

Experimental Methods and Instrumentation

The results described in this thesis have been obtained from various instrumental techniques. An introduction to ultrafast spectroscopy, principle and technical details of femtosecond pump-probe spectroscopy and instrumentation details of other spectroscopic technique are discussed in this chapter.

2.1 Ultrafast Spectroscopy

Ultrafast optical spectroscopy is a collective of various experimental techniques using ultra-short light pulses to study photo-induced dynamical processes in atoms, molecules, nano structures and solids.¹ Generally, the birth of ultrafast optical spectroscopy is ascribed to the development of high-speed photography by Eadweard Muybridge in 1878. He captured different phases of the motion of a horse on the Palo Alto racetrack by multiple cameras with fast shutters to resolve the instant when all four hooves of horse are lifted from the ground. Further the advancement in the time resolution of high speed photography lead to the development of shorter light flashes. In 1949, Norrish and Porter² used flash photolysis technique, having milli to microsecond duration combined with two electronically delayed light flashes to measure the long lived photochemical intermediates such as triplet states and aromatic free radicals. They have been awarded the Nobel Prize in Chemistry in 1967 for their contributions. Further, a revolution in the ultrafast spectroscopy was occurred in the 1980s after the discovery of colliding-pulse modelocked (CPM) dye laser, generating 100-fs pulses. Self mode-locking in Ti: sapphire-based lasers were discovered in 1990 and recently the pulse width of 10–20 fs pulses can be generated

To resolve a chemical reaction at the atomic scale, techniques with a temporal resolution shorter than a vibrational period are required. For the pioneering contribution on fundamental investigation of chemical reactions using femtosecond time-resolved techniques, Prof. Ahmed Zewail who is known as the “father of femtochemistry” was awarded the Nobel Prize in chemistry in 1999.³

2.1.1 Generation and Amplification of Ultrashort Pulses

In an ultrafast laser system, oscillators typically generate pulses with too low level energy. Ti:Sapphire based femtosecond lasers, has been used by most of the research laboratories as it possesses broad gain bandwidth, high thermal conductivity and high energy density and able to produce very short pulses. But the energy per pulses required for many applications are very low (nJ energy). Pulse energy can be amplified by the chirped pulse amplification (CPA) technique.⁴ This technique was introduced by Prof. Mourou and his co-workers in 1980. In 2018 they have been awarded the Nobel Prize in physics for their pioneering contribution for generation of ultra-short laser pulses. The principle of CPA technique is shown in the **Figure 1.11**. The pulses are chirped and temporally stretched to longer duration before passing through the amplifier by strongly dispersive element reducing the peak power. After the gain medium, a dispersive compressor removes the chirp from the low intensity optical pulse and temporally compresses it to have similar input pulse duration.

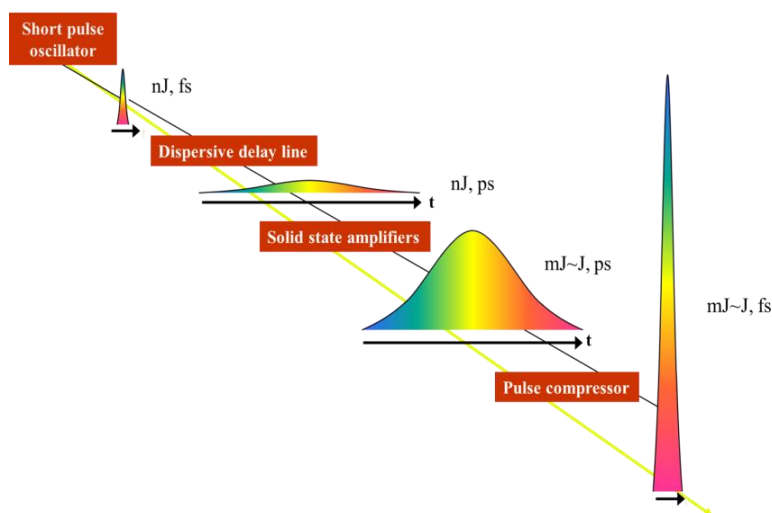


Figure 2.1 The principle of chirped pulse amplification. The femtosecond seed pulses are temporally stretched, amplified and compressed back to Fourier transform limited duration.

2.1.2 Temporal and Spectral Resolution

Generally, an optical spectrum gives information about the various energy levels of the molecule and different static and dynamic processes. The line width of an optical spectra is known as full width at half maximum (FWHM). The FWHM for various processes is not narrow. The vibrational transitions are overlapped with electronic transitions and short lifetime of the excited state will cause broad spectral width. Though ultra-short pulses can offer the desired temporal resolution, the large energy bandwidth limits the spectral resolution due to the Heisenberg uncertainty principle (**Figure 2.2**). The relation between the FWHM of the frequency bandwidth ($\Delta\nu$) and the time bandwidth (Δt) of the pulse is given by

$$\Delta\nu\Delta t \geq K \quad (1)$$

where K is a constant that depends on the shape of the pulse envelope.

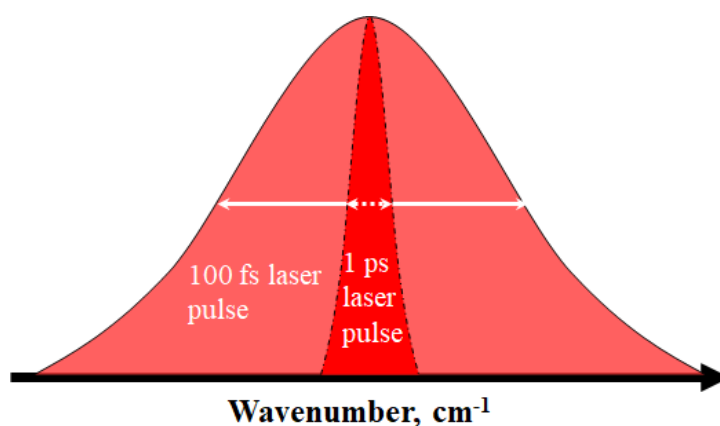


Figure 2.2 An ultrafast pulse with broad bandwidth (100 fs) and narrow bandwidth (1 ps).

2.1.3 Femtosecond Pump–Probe Transient Absorption Spectroscopy

Among the various ultrafast spectroscopic techniques, the pump–probe spectroscopy is a most widely used technique for recording molecular motion in a real time. The “pump–probe” technique⁵, uses two synchronized laser pulses, the excitation (pump) pulse triggering a photoinduced phenomenon, and a delayed probe pulse measuring a time dependent optical property of the sample, including absorption or transmittance.

Figure 2.3 shows the experimental set up of the femtosecond pump–probe spectroscopy used for this work. The oscillator is a Ti:sapphire laser (MaiTai HP, Spectra Physics, USA) centered at 800 nm having 80 MHz repetition rate with a pulse width of < 100 fs. The amplified laser was split into pump and probe pulses. The high energy beam, pump was used for exciting the sample by using TOPAS (Prime, Light Conversion).⁶ The other part of the amplified beam (200 mW) was focused on a CaF₂ (1 mm) plate to generate the white light continuum (340–1000 nm) which further split into sample and reference probe beams. The delay between the pump and probe pulses at the sample was controlled, by making one of the beams travel a fixed optical path and the second beam go through a motorized optical delay line.

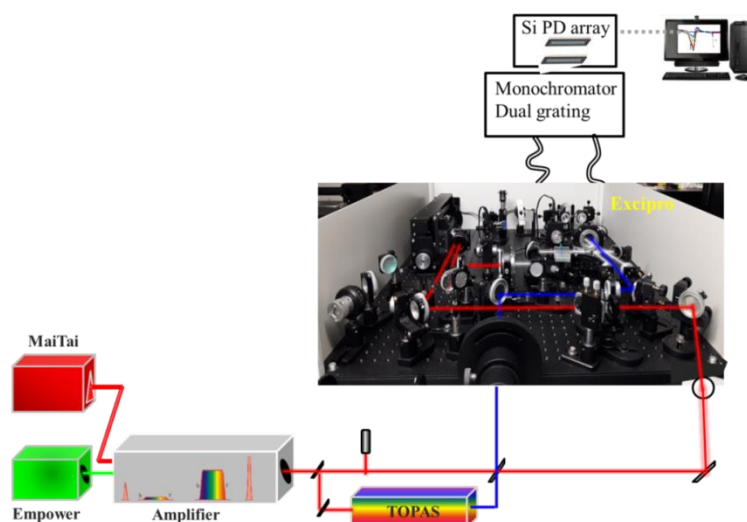


Figure 2.3 Experimental setup for femtosecond transient absorption spectroscopy.

The delay stage consists of a retro reflector mounted on a computer controlled linear translation stage with micrometer precision. Since the speed of light is finite and the two pulses are in synchrony, if the optical delay line is translated by the distance L then,

$$L = 1 \mu\text{m} \quad (2)$$

The optical path length difference between the two beams

$$= \frac{L}{c} \quad (3)$$

$$= \frac{(1 \times 10^{-6}) \text{ m}}{(2.998 \times 10^8) \text{ ms}^{-1}} \quad (4)$$

$$= 3.33 \times 10^{-15} \text{ s}$$

The sample cell having 0.4 mm path length was refreshed by rotating at a constant speed. After passing through the sample, the probe pulse dispersed in a mono-chromator and focused onto the detector. The pump-probe spectrophotometer (ExciPro) setup was purchased from CDP Systems Corp, Russia. Normally transient absorption spectra were obtained by averaging about 2000 excitation pulses for each spectral delay. Usually a pump beam in the UV-Vis wavelength region is passed through a chopper. A chopper wheel having half the frequency of repetition rate (500 Hz) of the laser in the pump beam blocks

every second excitation pulse to get subsequent pump-on and pump-off conditions in the sample according to:

$$\Delta OD = \log \left(\frac{I_{probe}}{I_{pump+probe}} \right) \quad (5)$$

To understand the kinetics of excited state processes, spectra are recorded at different time delay. Absorption of a pump pulse causes the excitation of molecule from ground state S_0 to first excited state S_1 as shown in **Figure 2.4** (a). The probe pulse may induce a transition between S_1 and a higher lying state S_2 . The different features observed in a typical transient absorption spectra are explained below.

1. Ground State Bleach

Generally, ground state bleach (GSB) is observed in the region where the molecule absorbs in the ground state. Only the ground state spectrum of the molecule will be recorded in the pump off condition. Whereas, when the pump-on case, a fraction of molecules is excited from the ground state and the population of molecules in the ground state is reduced. The reduction in population of ground state molecule results in lower absorbance of the white light probe through the photo-excited sample, so in the Eq. (4), $I_{pump+probe}$ will be higher than I_{probe} at the wavelength where the molecule absorbs in its ground state. Thus, the ratio $I_{probe}/I_{pump+probe}$ will be less than 1 and hence the change in absorbance (ΔA) will be negative. Therefore the GSB is usually plotted as a negative signal as shown in **Figure 2.4** (b).

2. Stimulated Emission

As GSB, stimulated emission (SE) is also observed as a negative signal. The spectral profile of stimulated emission will be roughly the same as the fluorescence profile and will be Stokes-shifted from the ground state absorption. During stimulated emission, a photon from the probe pulse will stimulate the emission of another photon having same

energy and in the same direction, so both photons will be detected. In the pump–on case, a fraction of molecules are present in the excited state that can relax to the ground state by SE of photons, and also, the absorbance is lower than in the case of pump–off. Therefore, $I_{\text{pump+probe}}$ will be higher than I_{probe} and the ratio $I_{\text{probe}}/I_{\text{pump+probe}}$ will be less than 1 resulting in a negative ΔA value for SE.

3. Excited State Absorption (ESA)

Upon excitation by the pump beam, the molecule will be excited to the higher energy states. The molecule undergoes an optically allowed transition to a higher excited state upon interaction with the probe pulse. Generally, the ESA appear as a positive signal. The $I_{\text{pump+probe}}$ condition has no contribution to wavelengths of ESA, therefore $I_{\text{pump+probe}}$ will be lower than I_{probe} and the ratio $I_{\text{probe}}/I_{\text{pump+probe}}$ will be greater than 1, giving a positive signal for ESA.⁷ Sometimes bands other than ESA can be observed in the FTAS due to photo–product absorption or due to absorption from a long–lived species.

4. Vibrational Energy Redistribution

The energy of electronic excitation is typically 100 times larger than k_{BT} . This excess vibrational energy is often deposits into Franck–Condon active modes⁷. During the relaxation of molecules, the excess of energy is redistributed within the molecule or to the solvent degrees of freedom. When the molecule distribute its energy among all other modes while keeping the molecule in the same electronic state is known as intramolecular vibrational energy redistribution (IVR).⁸ IVR will be completed within a few hundreds of femtosecond in the condensed phase. Concurrently, within less than 100 fs, the solute and its first solvation shell undergo an inertial response in polar solvents.⁹ The transfer of the excess energy from the thermally equilibrated solute particles that are still at a higher temperature to the surrounding solvent molecules is known as vibrational cooling

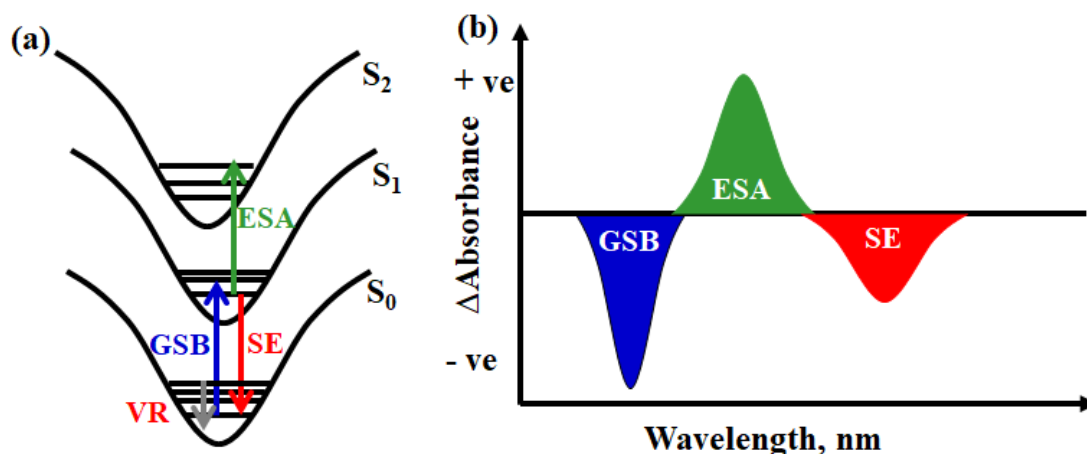


Figure 2.4 Different energy states along with their vibrational states (a) and different types of signals obtained in a femtosecond pump–probe transient absorption experiment (b).

(VC) or VR. VC can be otherwise defined as transport of heat from the thermalized intramolecular low–frequency modes to the solvent through vibrational coupling.⁸ Generally, VR of protein occurs in the range of picosecond.¹⁰

2.1.4 Chirp Compensation

During the measurement of transient absorption spectra, some unwanted signal or different types of potential artifacts, for example chirp can be generated with femtosecond time scale.¹³ The chirp of an optical pulse is understood as the time dependence of its instantaneous frequency. The white–light is chirped during generation of continuum, i.e., the red wavelengths are generated earlier in time than the blue wavelengths due to temporal distribution of the different Fourier components of the laser pulse.¹⁴ As the white–light continuum has inherent group velocity dispersion (GVD), when traveling through an optically dense substances such as cuvettes and lenses, the GVD in the white light will increase to picosecond range.^{14–15} A long temporal chirp may prevent the detection of the occurrence of fastest occurring physically relevant process in a spectral region. The reaction inducing pump pulse arrives at the sample at time t_0 , but the time of arrival of the probe

pulse is delayed for every wavelength. The wavelength–dependent chirp is modelled by polynomial function.⁶ The raw spectral data have to be corrected for the chirp in order to obtain the FTAS at a selected time delay. Usually for multichannel data acquisition chirp correction will be done after the experiment. All the transient absorption spectra obtained from the equipment is compensated for chirp of the white light by determining the time zero using coherent artifact observed in the solvent.¹⁶ By linear interpolation of the transient absorption spectral data along the time axis, the true spectral data will be reconstructed using the chirp correction function. The molecular dynamics are accessible only after the chirp correction in global fitting and target analysis.¹⁶

2.1.5 Singular Value Decomposition (SVD)

In SVD, the spectral informations are considered as a data matrix including the change in optical density delay time and wavelength. Thus, the continuous two dimensional function of the absorption change $\Delta A(\lambda, t)$ becomes a matrix (A_{ij}) , where the changes in absorbance at particular probe wavelengths λ_i form the columns and particular delay time t_j form the rows.¹⁷

$$\Delta A(\lambda_i, t_j) = (A_{ij}), \lambda_i (i = 1, M) \text{ and } t_j (j = 1, N) \quad (6)$$

The matrix A will be consisting of m probe wavelengths and n delay time. SVD is based on a theorem obtained from linear algebra defining that a rectangular matrix A can be broken down into the product of an orthogonal matrix U, a diagonal matrix S, and the transpose of an orthogonal matrix V:

$$A_{mn} = U_{mm} S_{mn} V_{nn}^T \quad (7)$$

where $U^T U = I$, $V^T V = I$;

The columns of orthogonal matrix, U consist of orthonormal eigenvectors of AA^T , V consist of orthonormal eigenvectors of $A^T A$. The diagonal matrix S contains the square roots of eigenvalues from U or V in descending order. Columns of U denote normalized

basic spectra, the rows of V^T contain their normalized dynamics, and diagonal S have the singular values $S_{kk} > 0$ arranged in a descending order. It is to be noted that SVD was performed for all the FTAS in this thesis before global analysis. It will help to find out the number of components before the global exponential fit.

2.1.6 Analysis of Femtosecond Transient Absorption Spectra

A time-resolved spectrum is a well-known example of two dimensional data. The first dimension is wavelength or wavenumber and the second dimension is time after the excitation. The IRF depends mainly on the pulse width of the laser and detector response. A detailed analysis of the time-resolved spectral data is essential to investigate the mechanisms of various biological processes. There are different advanced tools for the analysis of transient spectra such as Ultrafast toolbox¹⁸, MCRALS¹⁹ and TIMP/Glotaran.^{11,20} In this thesis we have used the R package TIMP and its graphical user interface of GLOTARAN for the global analysis. It allows to load and study the data in an cooperative way, set up and perform a TIMP analysis, and picturise the obtained results from a graphical interface²¹. The femtosecond transient absorption spectra (FTAS) can be analysed by global and target analysis methods.¹¹

2.1.6.1 Global Analysis

In global analysis the large amount of data will split into a small number of components and spectra. The first step in global analysis is the fitting of the data with a adequate number of exponential decays and their amplitudes without a prior knowledge about a detailed kinetic model.²² In global analysis method, where the data $S(t)$, is approximated by a discrete sum of exponentials function as shown in eq. 8

$$S(t, \lambda_{exc}, \lambda_i) = \sum_{j=1}^n A_j (\tau, \lambda_{exc}, \lambda_i) \exp(-t/\tau_j) \quad (8)$$

Where τ is the lifetime and A is the pre-exponential amplitude. The analysis results different spectra with the amplitudes associated with exponential decays, known as Decay

Associated Spectra (DAS).²³ It is associated with specific lifetime components obtained by data analysis, in which the amplitudes (A) for each component (τ) are plotted against an experimental variable λ_i . The DAS represents the kinetic information of the data in a compact form²⁴ in which each species decay independently after photo-excitation. In pump–probe spectroscopy if the IRF $i(t)$ is not negligible, the exponential decay has to be convolved with the IRF. IRF is often described by a Gaussian with the location (mean) μ and the full width at half maximum (FWHM) Δ as follows.

$$i(t) = \frac{1}{\tilde{\Delta}\sqrt{2\pi}} \exp(-\log(2) (2(t - \mu)/\Delta)^2) \quad (9)$$

where $\tilde{\Delta} = \frac{\Delta}{2\sqrt{\log(2)}}$

The convolution of the IRF by an exponential decay results in an expression facilitating the estimation of the IRF parameters μ and Δ .

$$c(t, k, \mu, \Delta) = \exp(-kt) \phi i(t) \quad (10)$$

$$= \frac{1}{2} \exp(-kt) \exp(k(\mu + \frac{k\tilde{\Delta}^2}{2})) \{1 + \operatorname{erf}(\frac{t - (\mu + k\tilde{\Delta}^2)}{\sqrt{2}\tilde{\Delta}})\} \quad (11)$$

where ϕ indicates the convolution.

2.1.6.2 Target Analysis

In target analysis, a specific kinetic model is tested with compartmental model.²³ Target analysis will provide the actual concentrations of each species or components. It consists of formulating a kinetic reaction scheme based on certain assumptions from previous knowledge. In target analysis, compartmental transitions are described by microscopic rate constants constituting the off diagonal elements of the matrix K. The total decay rates of each compartment is given in the diagonal elements of K. A vector $c(t)$ represents the concentrations of each compartment as

$$c(t) = [c_1(t) \cdots \cdots c_{n \text{ comp}}(t)]^T \quad (12)$$

A compartmental model having n_{comp} (compartments) is given by a differential equation as

$$\frac{d}{dt} c(t) = Kc(t) + j(t) \quad (13)$$

where the input vector $j(t) = i(t)[1 \ x_2 \ \dots \ x_{n_{\text{comp}}}]^T$ (14)

$i(t)$ represents the IRF and x_n represents extra input to compartment. An important parameter that emerges from target analysis is the species-associated spectrum (SAS), which physically represents the stationary spectra of the model compartments as if they were measured separately²⁵.

It is to be noted that the global analysis would be sufficient to analyse the transient absorption data when the model of relaxation dynamics is considered as either parallel or sequential. Whereas the target analysis should be used when both the parallel and sequential steps are proposed within the same model. In this thesis as the excited state relaxation dynamics were proposed as sequential model, we have used the global analysis only to analysis the femtosecond transient absorption data.

2.2 Time Correlated Single Photon Counting (TCSPC)

Time-resolved fluorescence spectra and lifetime decays were measured by using a picosecond single photon counting system (Horiba, DeltaFlex) employing 331 nm LED as excitation source and Picosecond Photon Detection modules (PPD-850) as a detector. The decay of the fluorescence intensity (I) with time (t) was fitted by single and double exponential function.

2.3 Circular Dichroism Spectroscopy

CD spectra were measured with JASCO 810 spectrometer, which was purged and cooled with gaseous nitrogen at room temperature. The samples were measured with a 1 cm quartz cell. The spectra were measured in the range from 300 to 750 nm with a scanning speed of 500 nm/min, a data pitch of 0.05 nm, a bandwidth of 5 nm, and a response time of

0.5 s. Three spectra were accumulated per sample at 25 °C. All spectra were solvent-corrected using Jasco spectral analysis program.

2.4 Fluorescence Spectroscopy

Steady-state fluorescence spectra were recorded with a FluoroLog-3 (Horiba) equipped with a 450W Xe arc lamp using 10 mm path-length quartz cuvettes. The samples were excited at the respective absorption maxima and an excitation and emission slit width at 2.0–3.0 nm were used.

2.5 Dynamic Light Scattering

The size distributions of liposomes having a concentration of 500 μM were measured using dynamic light scattering experiment. Particle radii were obtained from dynamic light scattering particle size analyzer (Zeta Nano-ZS, Ms. Malvern Instruments, UK). A 10 mm path-length quartz cuvette was used to collect the data at room temperature.

2.6 UV-Visible Electronic Absorption Spectroscopy

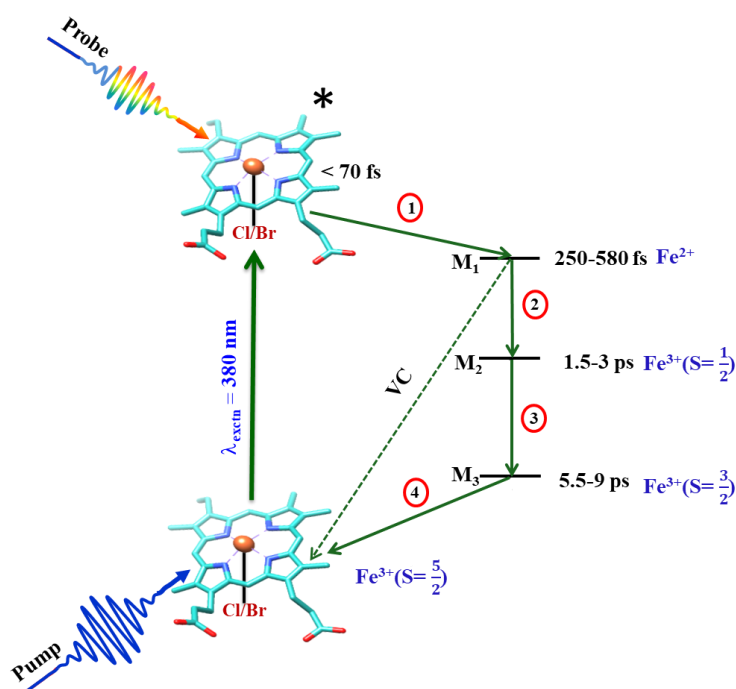
The absorption spectra were measured with a Shimadzu UV-2600 UV/Vis spectrophotometer coupled with Peltier thermostatic cell holders at various temperatures.

2.7 References

1. Maiuri, M.; Garavelli, M.; Cerullo, G., *J. Am. Chem. Soc.* **2020**, *142* (1), 3-15.
2. Norrish, R. G. W.; Porter, G., *Nature* **1949**, *164* (4172), 658-658.
3. Zewail, A. H., *J. Phys. Chem. A* **2000**, *104* (24), 5660-5694.
4. Strickland, D.; Mourou, G., *Opt. Comm.* **1985**, *55* (6), 447-449.
5. Abraham, H.; Lemoine, J., *CR Acad. Sci. Hebd Seances Acad. Sci. D* **1899**, *129*, 206-208.
6. Shen, Y. R., *J. Phys. Chem. C* **2012**, *116* (29), 15505-15509.
7. Ariese, F.; Roy, K.; Ravi Kumar, V.; Sudeeksha, H. C.; Kayal, S.; Umapathy, S., Time-Resolved Spectroscopy: Instrumentation and Applications. In *Encyclopedia of Analytical Chemistry*, R.A. Meyers (Ed.). : 2017; pp 1-55.
8. Rosspeintner, A.; Lang, B.; Vauthey, E., *Annu. Rev. Phys. Chem.* **2013**, *64* (1), 247-271.
9. Marcus, R. A., *Angew. Chem. Int. Ed.* **1993**, *32* (8), 1111-1121.
10. J L Martin, a.; Vos, M. H., *Ann. Rev. Biophys. Biomol. Struct.* **1992**, *21* (1), 199-222.
11. van Stokkum, I. H. M.; Larsen, D. S.; van Grondelle, R., *Biochim. Biophys. Acta* **2004**, *1657* (2), 82-104.
12. Kovalenko, S. A.; Dobryakov, A. L.; Ruthmann, J.; Ernsting, N. P., *Phys. Rev. A* **1999**, *59* (3), 2369-2384.
13. Devos, O.; Mouton, N.; Sliwa, M.; Ruckebusch, C., *Anal. Chim. Acta* **2011**, *705* (1-2), 64-71.
14. Berera, R.; van Grondelle, R.; Kennis, J. T. M., *Photosynth. Res.* **2009**, *101* (2), 105-118.

15. Lebedev, M. V.; Misochko, O. V.; Dekorsy, T.; Georgiev, N., *J. Exp. Theor. Phys.* **2005**, *100* (2), 272-282.
16. Megerle, U.; Pugliesi, I.; Schrieber, C.; Sailer, C. F.; Riedle, E., *Appl. Phys. B* **2009**, *96* (2), 215-231.
17. Satzger, H.; Zinth, W., *Chem. Phys.* **2003**, *295* (3), 287-295.
18. van Wilderen, L. J. G. W.; Lincoln, C. N.; van Thor, J. J., *PloS one* **2011**, *6* (3), e17373.
19. Jaumot, J.; Gargallo, R.; de Juan, A.; Tauler, R., *Chemom. Intell. Lab. Syst.* **2005**, *76* (1), 101-110.
20. Snellenburg, J. J.; Laptinok, S.; Seger, R.; Mullen, K. M.; van Stokkum, I. H. M., *J. Stat. Softw.* **2012**, *49* (3), 22.
21. Dedecker, P., *J. Chemometrics* **2014**, *28* (3), 137-138.
22. Knorr, F. J.; Harris, J. M., *Anal. Chem.* **1981**, *53* (2), 272-276.
23. Beechem, J. M.; Ameloot, M.; Brand, L., *Anal. Instrum.* **1985**, *14* (3-4), 379-402.
24. Slavov, C.; Hartmann, H.; Wachtveitl, J., *Anal. Chem.* **2015**, *87* (4), 2328-2336.
25. van Stokkum, I. H. M.; Jumper, C. C.; Snellenburg, J. J.; Scholes, G. D.; van Grondelle, R.; Malý, P., *J. Chem. Phys.* **2016**, *145* (17), 174201.

Ultrafast Heme Relaxation Dynamics of Model Compounds: Via Multiple Electronic Spin States and Vibrational Relaxation



3.1 Abstract

Hemin is an important heme model compound of heme proteins carrying out variable biological functions. Here, the excited-state relaxation dynamics of different heme model compounds in the ferric form are investigated by changing the axial ligand (Cl/Br), the peripheral substituent (vinyl/ethyl-meso), and the solvent (methanol/DMSO) systematically using femtosecond pump-probe spectroscopy upon excitation at 380 nm. The relaxation time constants of these model compounds are obtained by global analysis. Excited-state deactivation pathway of the model compounds comprising the decay of the porphyrin excited state (S^*) to ligand to metal charge transfer state (LMCT, τ_1), back electron transfer from metal to ligand (MLCT, τ_2), and relaxation to the ground state

through different electronic spin states of iron (τ_3 and τ_4) are proposed along with the vibrational cooling processes. This is based on the excited state absorption spectral evolution, similarities between the transient absorption spectra of the ferric form and steady-state absorption spectra of the low-spin ferrous form, and the data analysis. The observation of an increase of all the relaxation time constants in DMSO compared to the methanol reflects the stabilization of intermediate states involved in the electronic relaxation. The transient absorption spectra of met-myoglobin are also measured for comparison. Thus, the transient absorption spectra of these model compounds reveal the involvement of multiple iron spin states in the electronic relaxation dynamics, which could be an alternative pathway to the ground state besides the vibrational cooling processes and associated with the inherent features of the heme b type.

3.2 Introduction

Heme proteins possess a remarkable ability to actively involved in different types of biological functions through different chemical reactivity.¹⁻⁵ The prosthetic group, heme can be modified by several ways including changing the axial ligands⁶, electron-withdrawing or electron-donating peripheral substituents⁷, oxidation states of the iron atom, polar and non-polar groups around the heme⁸⁻¹⁰ and the conformation of the heme macrocycle (planar or non-planar)¹¹ to favour the different types of reactivity.⁵ Conformational distortions of the heme are related to the peripheral substituents of the macrocycle which in turn influence the ground and excited-state properties of the heme.¹²⁻¹⁵ The ultrafast excited-state relaxation dynamics of iron metalloporphyrins have been investigated extensively as they are serving as a model system for heme proteins.¹⁶⁻¹⁸ The transient absorption spectra of various heme model compounds and heme proteins were investigated to understand the underlying mechanism in the relaxation dynamics of

the heme.^{16, 18-21} Based on the experimental evidences, two distinct models comprising of the vibrationally excited (“hot”) electronic ground-state²¹⁻²⁵ and the multiple electronic intermediate excited-state are proposed.^{19-20, 26-27} Interestingly the heme model compounds are simplest, ubiquitous, possessing a rich diversity of chemical structures and reaction.²⁸⁻²⁹ The femtosecond time-resolved transient absorption spectra of ferric **Hemin** (Fe-Protoporphyrin IX-Cl) were investigated in solution and gaseous states^{18, 30}. Marcelli et al.¹⁸ reported that **Hemin** in the excited-state relaxed to the ground state by IC with the sub-picosecond time scale and subsequently, ground state was completely recovered through VC with a time constant of ~ 5.7 ps. Schematic representation of the relaxation pathways of **Hemin** upon excitation at the Soret band are shown in **Figure 3.1**.

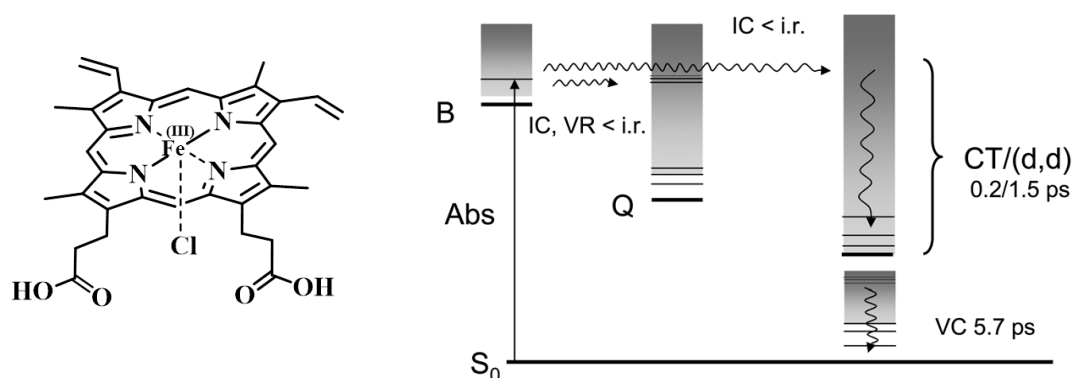


Figure 3.1 Chemical structure of **Hemin** and schematic representation of the energy relaxation dynamics of **Hemin** upon Soret band excitation. The Figure is copied from Ref. 18.

The vibrational levels of the Q_x , Q_y and B electronic states are represented by solid horizontal lines. The long wavy arrow corresponds to the internal conversion (IC) from B state to the metal states. The fastest time constant (0.2 ps) was attributed to the CT state. Since a back electron transfer from d to π orbital was possible, the 1.5 ps dynamics was assigned to the iron (d, d) state. The time constant for VC was observed to be 5.7 ps. The first report on the excited-state relaxation dynamics of **Hemin** in the gas phase was provided by Soep et al.³⁰ in 2010. They used femtosecond pump-probe spectroscopy

with 90 fs time resolution and found two exponential components including the ultrafast initial decay in the order of 50 fs attributed to the CT process from ligand to metal and a second relaxation time constant of 250 fs corresponding to the relaxation of this LMCT state to the ground state. Rury et al.³¹ studied the ultrafast dynamics of Fe(III) tetraphenylporphyrin chloride [Fe(III)TPPCl] in room temperature upon excitation at 400 and 520 nm to find the role of the spin configuration of the central metal atom in the relaxation of optically excited states. Upon, Soret band excitation the initially formed S_2 state was internally converted to the lower Q (π, π^*), manifold. The porphyrin excited singlet state relaxed into an LMCT state with a time scale of 0.4–0.6 ps. An MLCT transition from the Fe to the porphyrin happened on a time scale of 1.8–2.3 ps producing an excited 4T iron state (intermediate spin state). This state then relaxed to the ground state on a time scale of 13–19 ps (**Figure 3.2**).

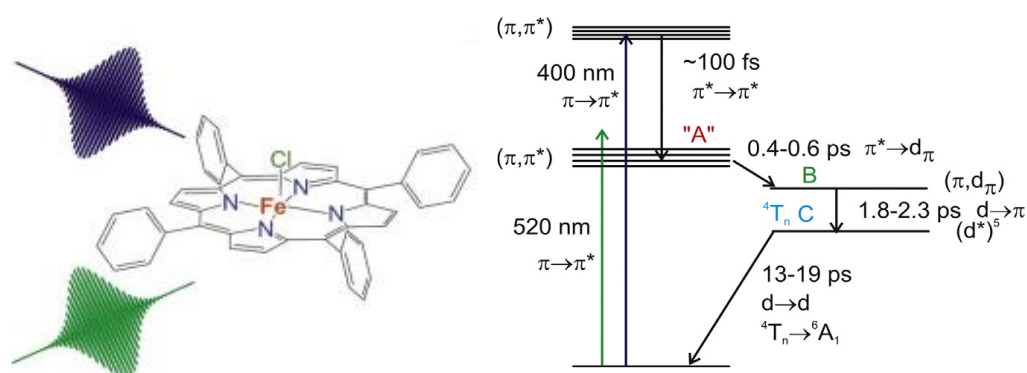


Figure 3.2 Structure of Fe(III)TPPCl and its proposed model for the electronic relaxation following excitation at 400 nm and 520 nm. The Figure is copied from the Ref. 31.

Humphrey et al.³² investigated the excited-state relaxation dynamics of Fe(III) tetrakis(4-hydroxyphenyl) porphyrins on a femto to nanosecond time scale in acetonitrile. The excited porphyrin relaxed back to the ground state in less than 30 ps in the solution state. Whereas in the electro-polymerized films the excited-state lifetime was increased to over

2.5 ns. They observed that the excitation was localized on a single porphyrin chromophore while the relaxation pathways differ in solution and solid-state. In the solid-state the increased relaxation lifetime was attributed to the changes in vibrational modes of the macrocycle induced by the steric strains. Because of the restriction of porphyrin macrocycle, ultrafast excited-state relaxation followed an alternate mechanism by creating CT state, other than through a (d, d*) state (**Figure 3.3**).

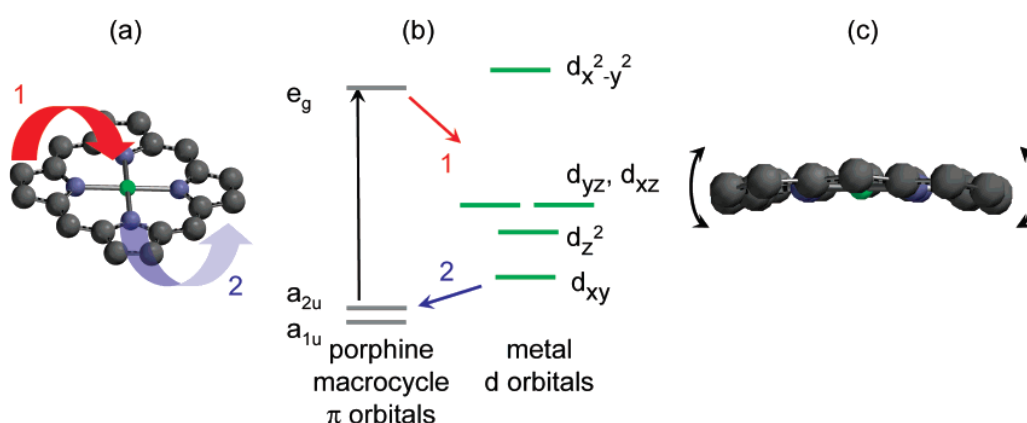


Figure 3.3 Illustration of two intramolecular CT steps (1 and 2), metal and macrocycle orbitals involved in CT (b) and macrocycle doming vibrational mode (c). The Figure is copied from Ref. 32.

In 2014, Atak et al.²⁶ reported the resonant inelastic X-ray scattering spectra at the iron L-edge of **Hemin** in dimethyl sulfoxide (DMSO). They observed that the effect of spin state on the molecular structure was more pronounced when chloride was included in the axial position. The bond angles in N–Fe–Cl was increased in the higher spin state structures as the Fe tends to be pulled away from the molecular ring plane. The singly occupied Fe d-orbital energy diagrams of the three different spin states and the corresponding molecular geometries of Fe(III) protoporphyrin IX with and without chloride ion are shown in **Figure 3.4**. Chergui et al.¹⁹ reported a spin state controlled early relaxation dynamics of **met-Mb** along with VC mechanism (**Figure 1.10**). Recently Scopigno et al.³³ proposed a mechanism in the early relaxation dynamics of deoxy-**Mb** and **Mb-CO** by the involvement of specific vibrational modes leading to the VC process using FSRS.

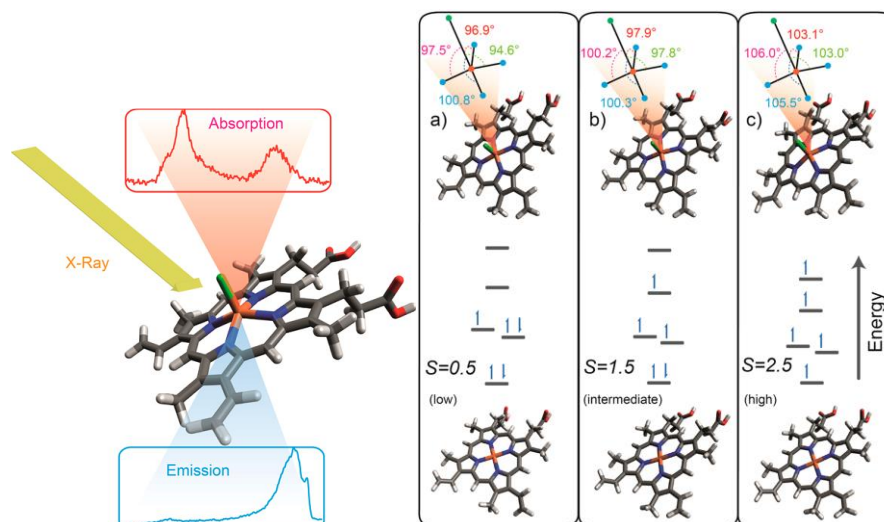


Figure 3.4 Simplified singly occupied iron d-orbital energy diagrams of the three different spin states and the molecular geometries of Fe(III) protoporphyrin IX with and without chloride ion at the top and the bottom, respectively. The Figure is copied from Ref. 26.

Spiro et al.³⁴ reported ultrafast CT and structural events in a novel Fe(II)porphyrazine (FePz) complex in aqueous solution using transient absorption spectroscopy, FSRS, and DFT. As shown in **Figure 3.5**, an excitation to the MLCT state followed a rapid relaxation with a time constant of 150 fs from the Franck–Condon region. Intersystem crossing to the d–d state occurred within 160 fs, which relaxed to the ground state within 4 ps. There have been a lot of studies on the spin state crossing of Fe porphyrin systems

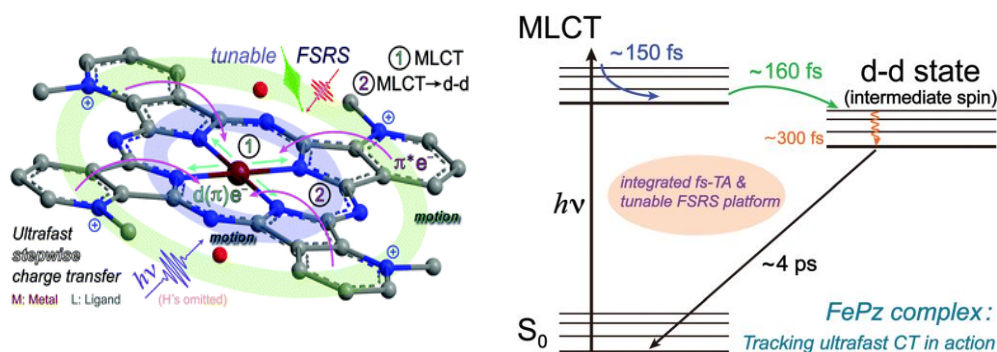


Figure 3.5 Chemical structure of Fe(II) porphyrazine compound and schematic representation of photoinduced charge flow inside the novel FePz complex in aqueous solution. The Figure is copied from Ref.34.

using different techniques other than time-resolved spectroscopy such as ^1H and ^{13}C NMR³⁵⁻³⁶, Mössbauer spectroscopy³⁷ and EPR.³⁸⁻³⁹ Despite the numerous studies on various heme dynamics comprising the spin cross over in Fe atom as well as VC pathways, the exact mechanisms of the relaxation dynamics are still under debate.

Herein, we report the influence of the axial ligands, peripheral substituents, and the solvents on the excited-state relaxation dynamics of various heme model compounds (**Hemin-Cl**, **Hemin-Br**, and **Hemin-meso**) using the femtosecond time-resolved pump–probe spectroscopy upon excitation at 380 nm in MeOH and DMSO. The structural difference in **Hemin-Cl** and **Hemin-Br** is the change in axial ligands and other peripheral substituents remains the same. Whereas in the case of **Hemin-meso**, vinyl groups are replaced with ethyl substituents. All of the heme model compounds are penta-coordinated and high spin ($S = 5/2$) in nature.⁴⁰ DMSO could mimic the aqueous environment of the biological system as it possesses a similar value of dipolar solvation [$\Delta f(\epsilon, n)$, 0.28] compared to the water (0.32).⁴¹⁻⁴² The dynamics were compared with **met-Mb**, which is an oxygen storage heme protein having heme b and high spin in nature.⁴³⁻⁴⁴ The chemical structures of various heme model compounds and **met-Mb** are shown in **Figure 3.6**.

The spectral and kinetic analysis of femtosecond time-resolved transient absorption spectra (FTAS) of heme model compounds revealed the involvement of multiple electronic spin states of Fe atom in the excited-state relaxation dynamics and also the ground state recovery by the VR.

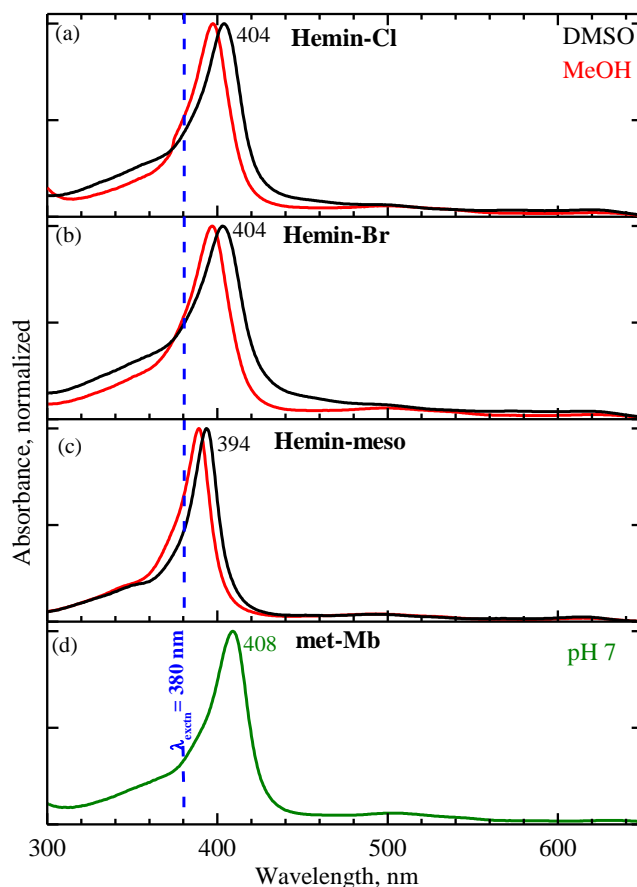


Figure 3.7 Stationary absorption spectra of **Hemin-Cl** (a), **Hemin-Br** (b), and **Hemin-meso** (c) in MeOH (red) and DMSO (black). The absorption spectrum of **met-Mb** (d) in 0.1 M Kpi buffer at pH 7 is also shown. The blue dotted line indicates the excitation wavelength ($\lambda_{\text{excitn}} = 380 \text{ nm}$) used for transient absorption measurements.

the replacement of the vinyl by ethyl group minimized the electron-withdrawing nature and conjugation of the peripheral substituents.⁴⁶ When compared to MeOH, all the model compounds showed red-shifted absorption maxima in DMSO (**Figure 3.7**). The absorption spectrum of **met-Mb** in 0.1 M Kpi buffer at pH 7 is also shown (**Figure 3.7** (d)). The temperature-dependent absorption spectra of all the heme model compounds (20 to 50 °C in MeOH with an increment of 10 °C) and **met-Mb** (20 to 60 °C at pH 7.0) were measured and shown in **Figure 3.8**. Generally, the temperature dependent absorption spectra of the heme model compounds and protein could relate the spectral shape of the FTAS. The differential absorption spectra (at temperature $\sim 40 \text{ }^\circ\text{C}$) show similar characteristic features of the transient absorption spectra at $\sim 1 \text{ ps}$ (*vide infra*).

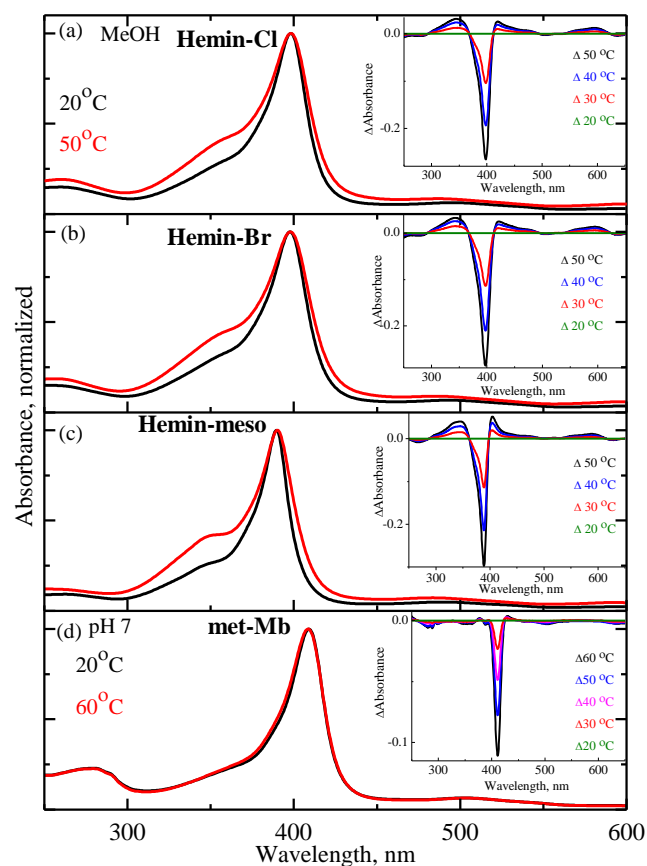


Figure 3.8 Normalized absorption spectra of heme model compounds in MeOH and **met-Mb** in 0.1 M Kpi buffer (pH 7) at different temperatures. Insets: Temperature-dependent differential absorption spectra, $\Delta A = A(T) - A(20)$ obtained relative to the spectrum at $T = 20^\circ\text{C}$.

It displays both positive and negative bands at around the Soret band region owing to the red-shift and broadening of absorption spectra at higher temperatures. In MeOH, the spectral bandwidth for all heme model compounds are broadening with an increase of temperature whereas no such spectral broadening is observed in the **met-Mb** until 60°C .⁴⁷ This reflects the weakening of the degree of coupling between heme vibronic transitions and low-frequency motions in the model compounds at high temperatures.⁴⁸

3.3.2 Femtosecond Transient Absorption Spectra

In order to record the FTAS, the absorbance of the samples was made to have between 0.4 and 0.6 at the pump wavelength in a 0.4 mm optical path length spinning

sample cell, equivalent to a concentration of 60-100 μM . The FTAS, $\Delta A(\lambda, t)$ of **Hemin-Cl** and **-Br** in MeOH were measured upon exciting at 380 nm (**Figure 3.9** and **3.10**).

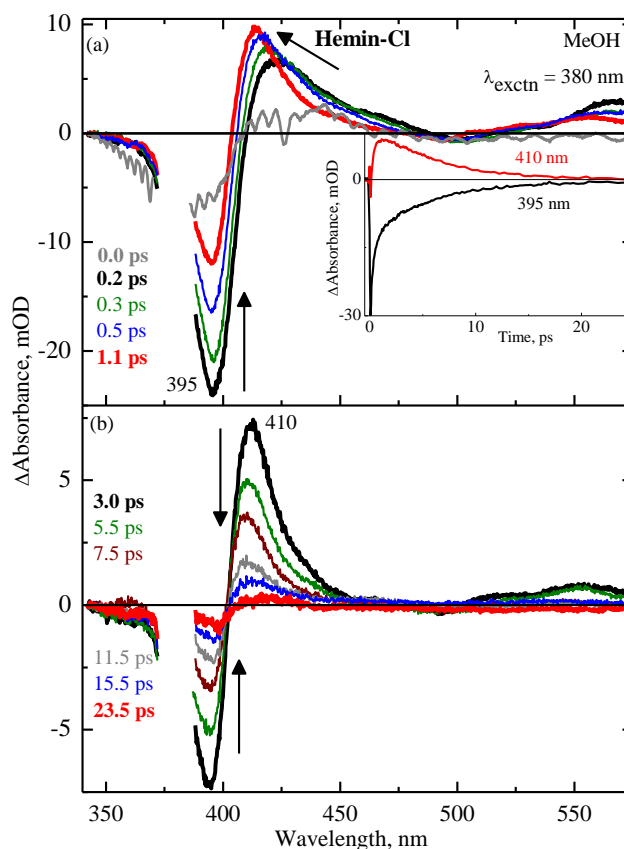


Figure 3.9 FTAS of **Hemin-Cl** in MeOH obtained upon excitation at 380 nm. The different time delays are given and the arrows indicate the spectral evolution. Inset: Transient decays of the ESA maximum and bleach maximum probed at the respective wavelengths.

In **Figure 3.9**, the panel a shows the spectral evolution of **Hemin-Cl** from 0.0 to 1.1 ps after the photo-excitation. The transient spectrum at 0.2 ps is dominated by a bleach band (~ 395 nm) owing to the depopulation of the ground state and an ESA at 410 to 470 nm and beyond 525 nm. When the delay time increased to 0.5 ps, the gradual decrease of the bleach band and increase of the ESA with a narrowing of spectral bandwidth and blue shifting are observed, which indicates the occurrence of the VC dynamics in the transient spectra. In panel b, when the delay time increased from 3.0 to 23.5 ps, the spectral intensity gradually decreases and recovered back to equilibrium at around ~ 23.5 ps. The spectral

evolution and shape of the transient spectra of **Hemin-Cl** in MeOH are consistent with literature.¹⁸ The kinetic traces of the ESA and bleach maxima are shown in the inset of **Figure 3.9**. The spectral pattern of **Hemin-Br** (**Figure 3.10**) in MeOH is similar to that of the **Hemin-Cl**. The spectral evolution of the **Hemin-Br** starting from 0.0 to 0.55 ps are shown in panel a of **Figure 3.10**. The spectrum at 0.1 ps is dominated by a bleach band (~396 nm) and the ESA bands (415 to 470 nm and beyond 525 nm). When the delay time is increased to 0.5 ps, the decrease of the bleach band along with an increase of ESA with the occurrence of signature of VC dynamics are observed. When the delay time increased from 1.35 to 28.35 ps, whole spectral intensity decreases and recovered back to the equilibrium within ~28.35 ps. To explore the effect of the excitation wavelength on the excited-state dynamics, the FTAS of **Hemin-Cl** and **-Br** in MeOH were also measured upon excitation at 530 nm (**Figure 3.11** and **3.12**). As in the case of 380 nm excitation, the decrease of the bleach band and an increase of ESA along with the signature of the VC dynamics are observed. To understand the effect of peripheral substituent on the excited-state relaxation dynamics, the FTAS of **Hemin-meso** were also measured in MeOH upon excitation at 380 nm (**Figure 3.13**). The spectral evolutions are similar to that of **Hemin-Cl**. The interaction of chromophore with solvent influences the excited-state relaxation dynamics of the heme. Therefore the FTAS of **Hemin-Cl**, **-Br**, and **-meso** were also measured upon excitation at 380 nm in DMSO (**Figure 3.14** to **3.16**). The pattern of spectral evolutions is similar in both DMSO and MeOH, whereas, the relaxation dynamics are observed to be more stabilized in DMSO. Markedly the presence of a long-lived species is observed in DMSO for all the heme model compounds attributed to the formation of photoproducts. The amount of the photoproduct component is negligible in MeOH whereas it is larger in DMSO. This indicates that, upon laser excitation, the model compounds are more susceptible to form photoproducts in DMSO than in MeOH. To correlate the excited-

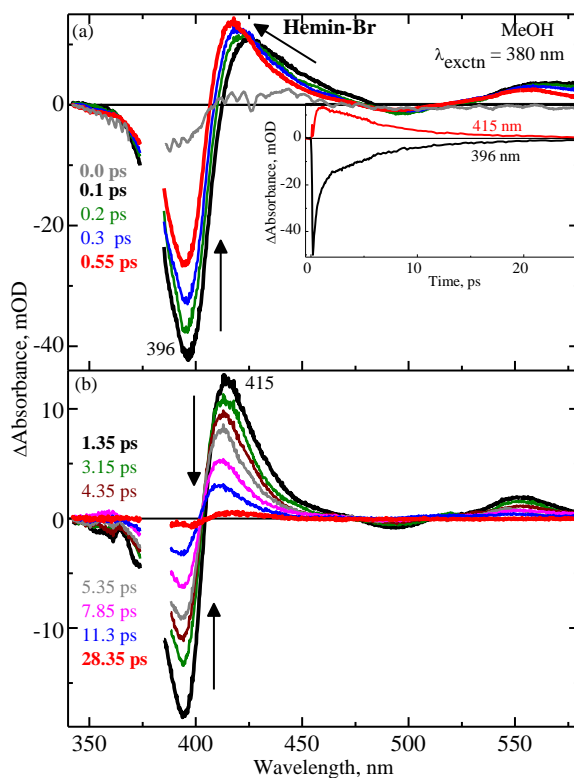


Figure 3.10 FTAS of **Hemin-Br** in MeOH obtained upon excitation at 380 nm. Inset: the transient decay of the ESA and bleach bands at the corresponding probe wavelength.

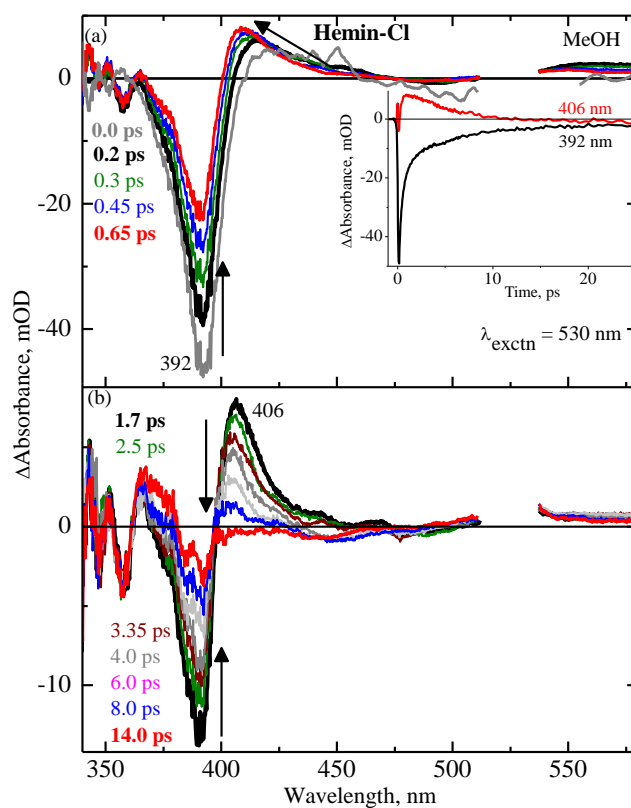


Figure 3.11 The FTAS of **Hemin-Cl** in MeOH obtained upon excitation at 530 nm.

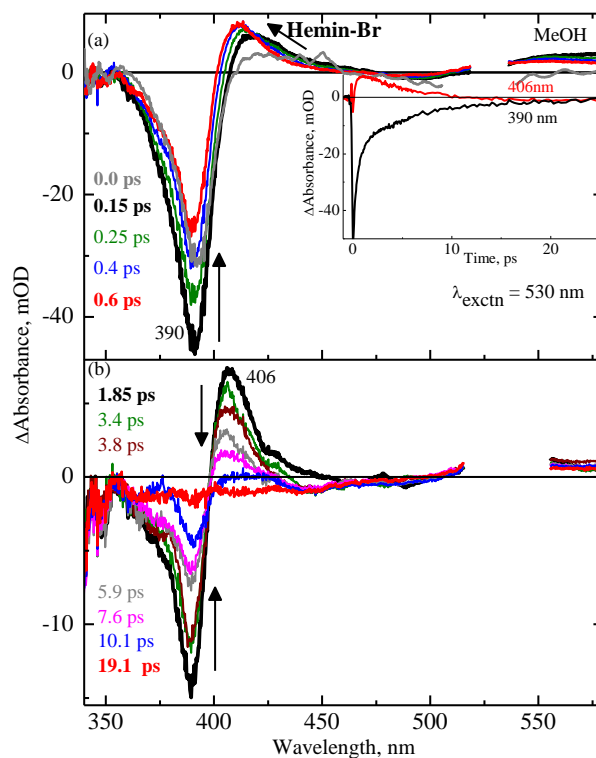


Figure 3.12 The FTAS of **Hemin-Br** in MeOH obtained upon excitation at 530 nm.

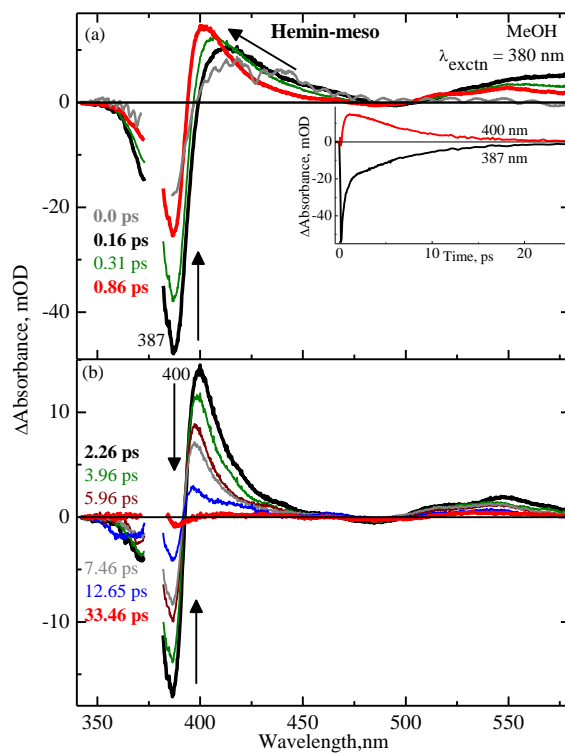


Figure 3.13 The FTAS of **Hemin-meso** in MeOH obtained upon excitation at 380 nm.

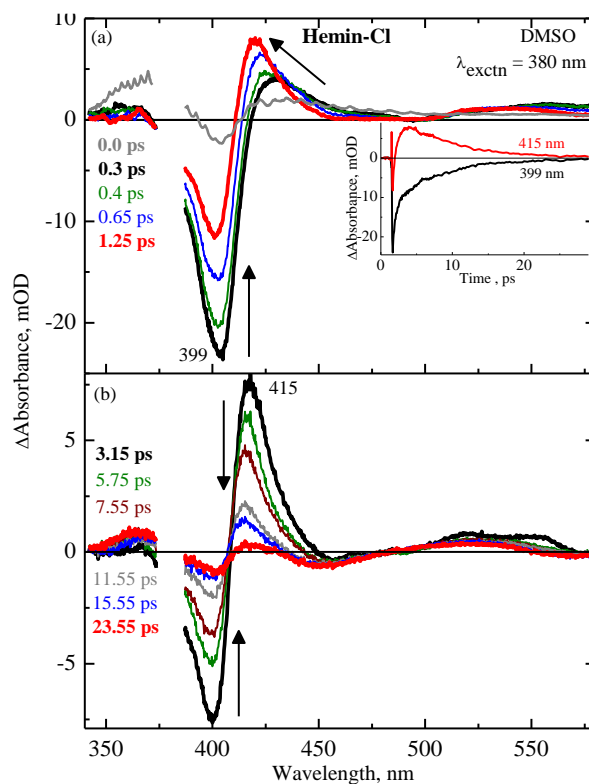


Figure 3.14 The FTAS of **Hemin-Cl** in DMSO obtained upon excitation at 380 nm.

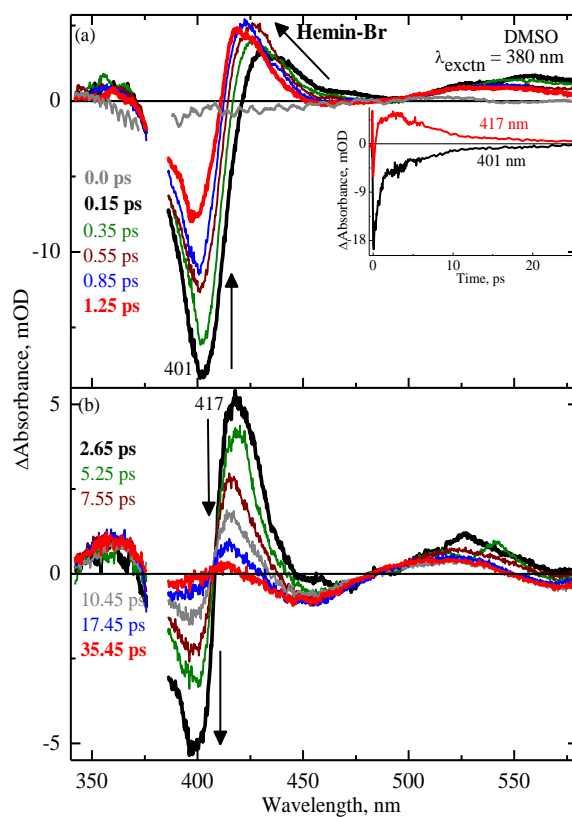


Figure 3.15 The FTAS of **Hemin-Br** in DMSO obtained upon excitation at 380 nm.

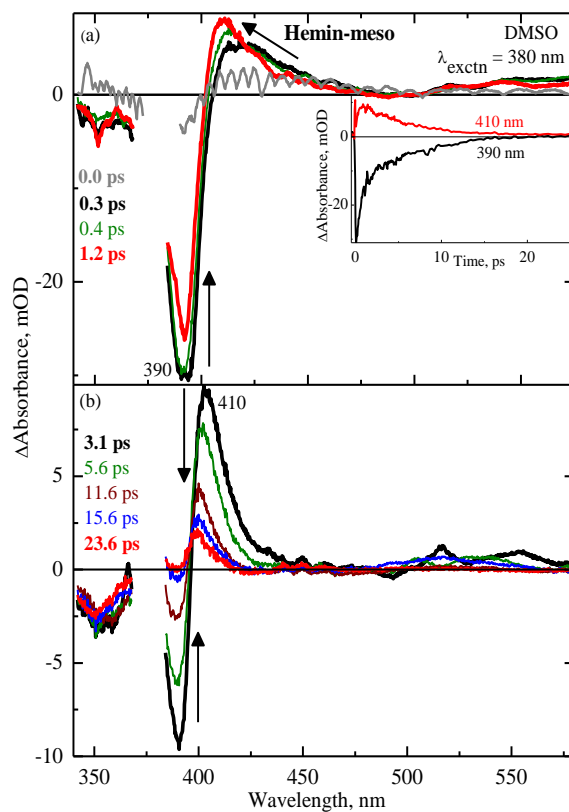


Figure 3.16 The FTAS of **Hemin-meso** in DMSO obtained upon excitation at 380 nm.

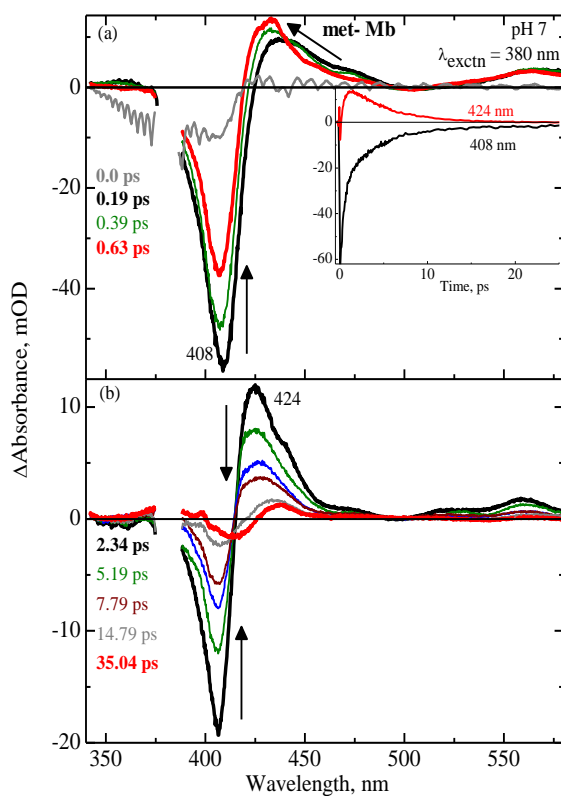


Figure 3.17 The FTAS of **met-Mb** in 0.1 M Kpi buffer at pH 7 obtained upon excitation at 380 nm.

state relaxation dynamics of the model compounds to heme protein, the FTAS of **met-Mb** at pH 7.0 were also measured upon excitation at 380 nm (**Figure 3.17**). The spectral evolution of the **met-Mb** at different delay times are similar to that of **Hemin-Cl** in MeOH and the spectral patterns and evolutions are consistent with the literature.¹⁹

3.3.3 Analysis of Transient Absorption Spectra

The analysis of FTAS of heme model compounds and **met-Mb** was performed with the R package TIMP and its graphical user interface of GLOTARAN⁴⁹⁻⁵⁰. All the transient absorption spectra obtained from the equipment is compensated for chirp of the white light by determining the time zero using coherent artifact observed in the solvent. SVD was performed before global analysis to estimate the number of kinetic parameter needed. Four exponential components were optimally fitted to the transient absorption data using sequential model to describe the excited-state relaxation dynamics of model compounds completely. The integrity of the sample is tested by measuring the absorption spectra of the sample before and after the experiments and found to be no significant changes in the absorption spectra.

The heat map of FTAS, time profile and exponential fit at maxima of GSB and ESA along with residual obtained from global sequential analysis of **Hemin-Cl** in MeOH and **met-Mb** are shown in **Figure 3.18** and **3.19**. The time constants obtained are shown in **Table 3.1**. The time constants obtained for **met-Mb** by global analysis are $\tau_1 \approx 70$ fs, $\tau_2 = 434 \pm 10$ fs, $\tau_3 = 1.09 \pm 0.06$ ps, and $\tau_4 = 4.34 \pm 0.07$ ps. These time constants are in accordance with previous literatures.^{19, 51} The DAS for the model compounds in MeOH and DMSO are shown in **Figure 3.20** and **3.21**. The DAS obtained for the excitation at 380 nm exhibit common features of FTAS.

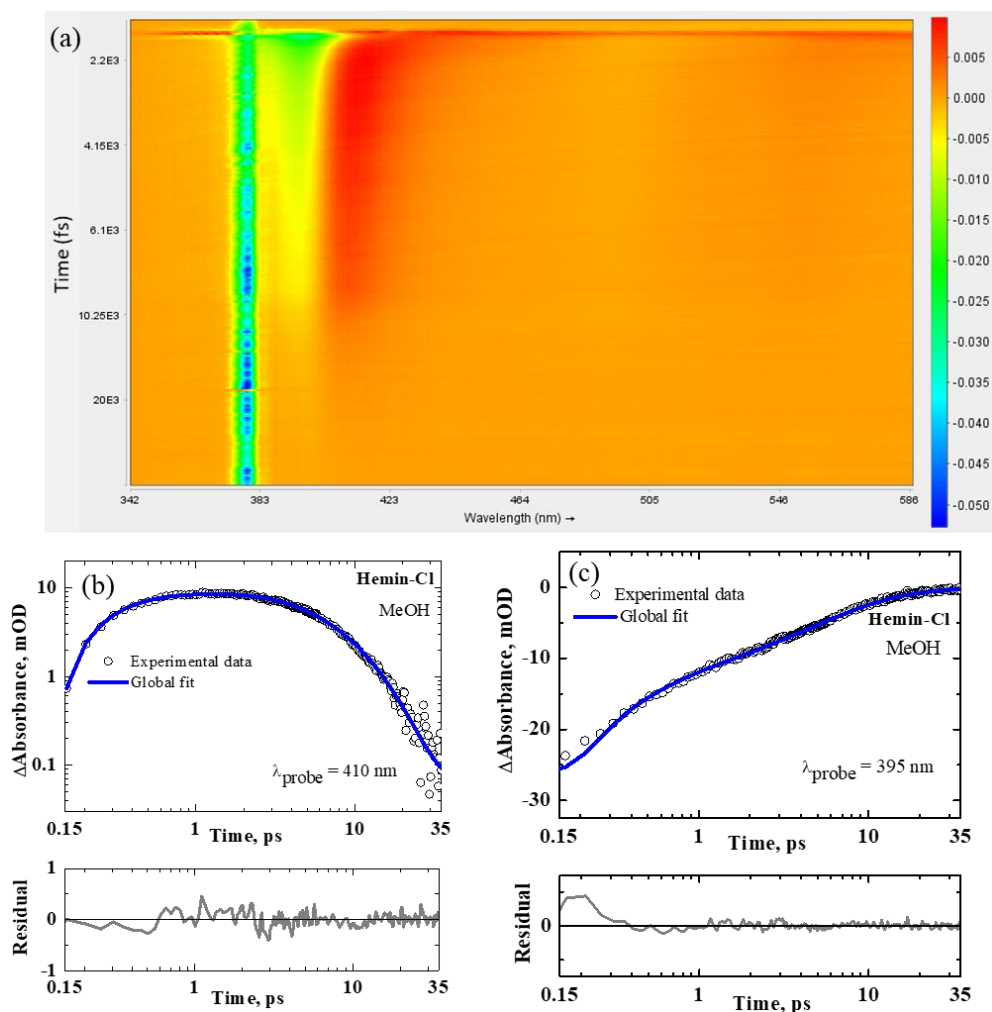


Figure 3.18 Heat map of FTAS of **Hemin-Cl** in MeOH as a function of time delay (vertical) and probe wavelength (horizontal) in 35 ps time window upon excitation at 380 nm. As indicated in the heat map, the zero level is coloured in yellowish red, red indicates positive signals (ESA) and green/blue denote negative signals (GSB) (a). The time profile at ESA maximum (b) and GSB maximum (c) (open circles) along with four-exponential fit curve obtained from global analysis (solid line) and residual data (ash coloured solid line, lower panel).

3.3.3.1 Signature of Vibrational Cooling Dynamics

The excited-state relaxation dynamics of heme model compounds, comprised of sequential steps of LMCT, iron d-d transition and significantly, the recovery of the ground state by VR.^{18, 30, 52} The transient absorption spectra (**Figures 3.9–3.16**) of various model compounds showed the occurrence of VC as the ESA spectra shifting toward the blue region along with narrowing of the spectral width with the increase of delay time in the picosecond range. Further, the amount of the ground state recovery occurring through

the back electron transfer (MLCT) was determined by the ratio between the area of the complete Soret band region of the static and transient absorption spectra, assuming that the

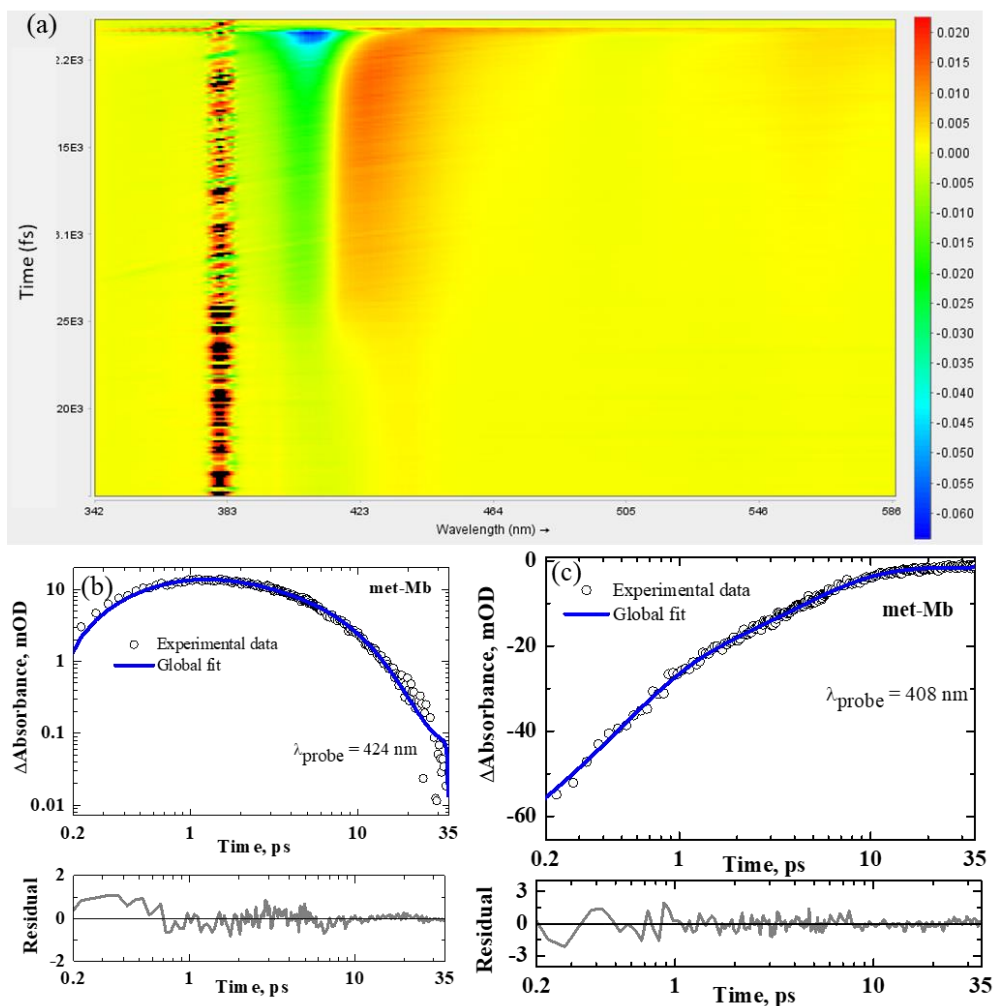


Figure 3.19 Heat map of FTAS of **met-Mb** as a function of time delay (vertical) and probe wavelength (horizontal) in 35 ps time window upon excitation at 380 nm. As indicated in the heat map, the zero level is coloured in yellowish red, red indicates positive signals (ESA) and green/blue denote negative signals (GSB) (a). The time profile at ESA maximum (b) and GSB maximum (c) (open circles) along with four-exponential fit curve obtained from global analysis (solid line) and residual data (ash coloured solid line, lower panel).

Table 3.1 The time constants obtained by global analysis for heme model compounds at 380 nm excitation.

Solvent	Hemin-Cl	Hemin-Br	Hemin-meso
MeOH	$\tau_1 = < 80$ fs	$\tau_1 = < 80$ fs	$\tau_1 = < 80$ fs
	$\tau_2 = 248 \pm 10$ fs	$\tau_2 = 274 \pm 10$ fs	$\tau_2 = 275 \pm 15$ fs
	$\tau_3 = 1.50 \pm 0.05$ ps	$\tau_3 = 1.82 \pm 0.05$ ps	$\tau_3 = 1.87 \pm 0.06$ ps
	$\tau_4 = 5.60 \pm 0.06$ ps	$\tau_4 = 5.98 \pm 0.05$ ps	$\tau_4 = 6.75 \pm 0.07$ ps
DMSO	$\tau_1 = < 80$ fs	$\tau_1 = < 80$ fs	$\tau_1 = < 80$ fs
	$\tau_2 = 296 \pm 10$ fs	$\tau_2 = 499 \pm 10$ fs	$\tau_2 = 580 \pm 20$ fs
	$\tau_3 = 2.02 \pm 0.05$ ps	$\tau_3 = 2.61 \pm 0.05$ ps	$\tau_3 = 2.95 \pm 0.06$ ps
	$\tau_4 = 6.58 \pm 0.06$ ps	$\tau_4 = 7.57 \pm 0.05$ ps	$\tau_4 = 9.22 \pm 0.08$ ps

transition strength of the transient state Soret band is same as that of the ground state (**Table 3.2**). It is observed that $\sim 52 \pm 5\%$ of excited molecules directly relax to the hot electronic ground state demonstrating the strong signature of VR in the excited-state dynamics.¹⁹ There are no significant changes are observed in the time constants obtained upon 530 nm excitation compared to 380 nm excitation. Whereas, the transient absorption spectra exhibited a red shift and broadening upon excitation at 380 nm compared to 530 nm (**Figure 3.22**). It could be due to the increase of local heme temperature⁵³ to ~ 880 K by excitation at 380 nm compared to excitation at 530 nm (~ 750 K). In addition, the direct ground state recovery for the 530 nm excitation is similar to that of the 380 nm excitation ($\sim 50 \pm 10\%$) revealing the independence of pump energy on VR.

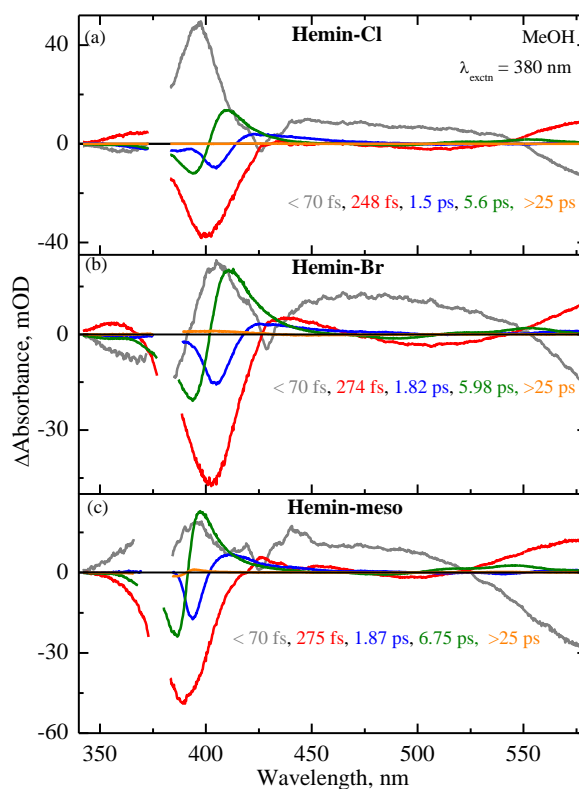


Figure 3.20 DAS of heme model compounds in MeOH obtained from global analysis upon exciting at 380 nm.

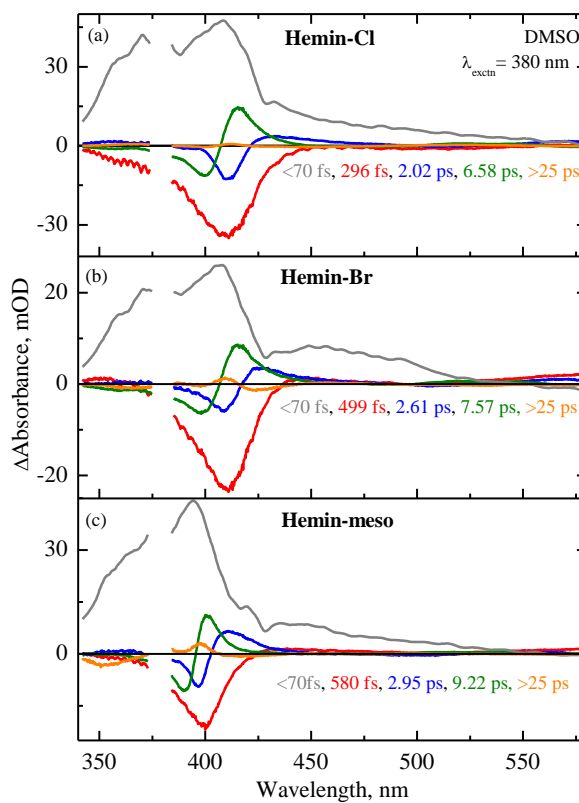


Figure 3.21 The DAS of heme model compounds in DMSO obtained from global analysis for 380 nm excitation.

Table 3.2 The calculation details for the ground state recovery for the different model compounds in MeOH and **met-Mb** in PBS buffer.

Compound	Ground-state absorption spectra		Transient absorption spectral time	Excited-state absorption spectra		Ratio of absolute area
	Wavelength range (nm)	Absolute area		Wavelength range (nm)	Absolute area	
met-Mb	365 – 493	37.277	440 fs	380 – 420	66.475	56.07%
Hemin-Cl	365 – 493	34.748	250 fs	360 – 409	66.313	52.40%
Hemin-Br	365 – 493	35.871	250 fs	360 – 409	62.690	57.21%
Hemin-meso	356 – 463	28.160	260 fs	356 – 396	51.950	54.20%

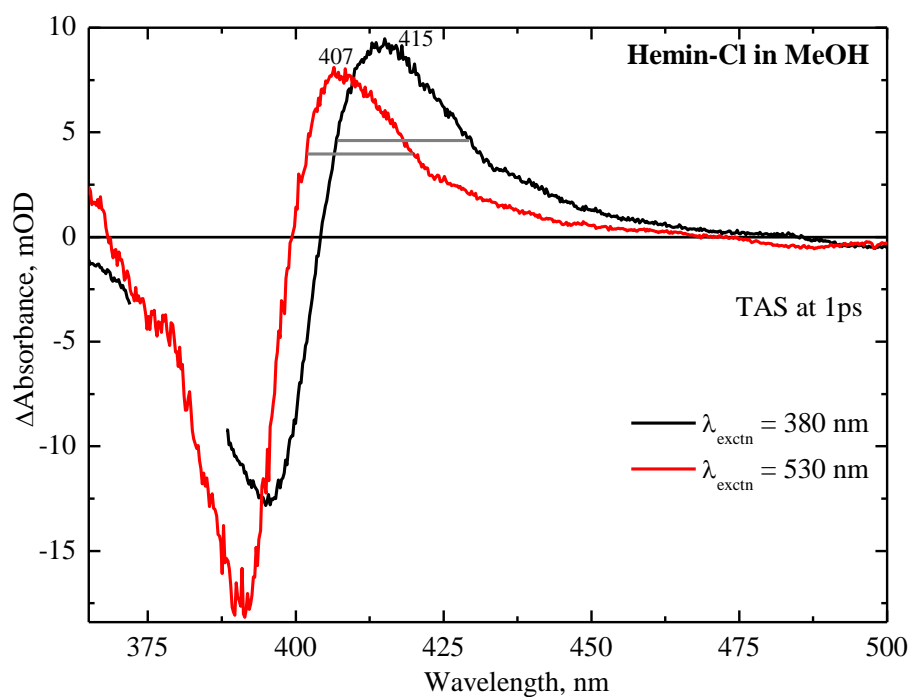


Figure 3.22 The transient absorption spectra of **Hemin-Cl** in MeOH at 1ps obtained by exciting at 380 (black) and 530 (red) nm is shown for comparison.

3.3.3.2 Involvement of Multiple Electronic Spin States.

The relaxation dynamics follows an alternative pathway by the involvement of multiple electronic spin state of the Fe atom in addition to the VR dynamics. A new peak appeared around at ~ 525 nm in the Q-band region of the FTAS of heme model compounds after ~ 300 fs (**Figure 3.23**). The resemblance of the FTAS of the Q-band region having doublet structure (peaks at ~ 525 and 560 nm) to the stationary absorption spectra of heme model compounds in the ferrous form (**Figure 3.24**) suggests the occurrence of a new electronic intermediate state in the fast relaxation process. There is no access to detect the transient formation of the peak around 525 nm upon excitation at 530 nm due to the experimental limitation (excitation laser scattering at 530 nm), which could support the involvement of different electronic spin states.

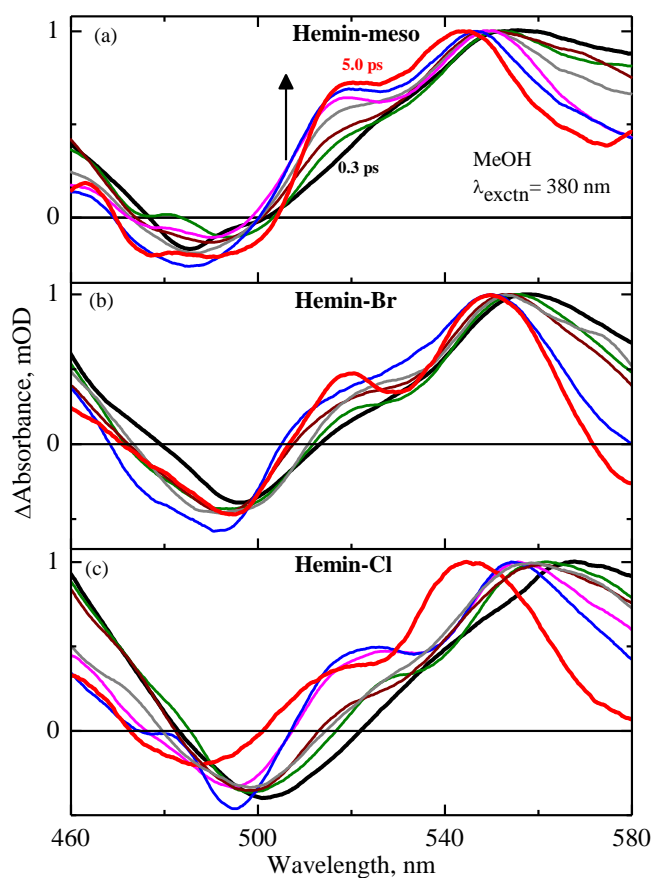


Figure 3.23 FTAS of heme model compounds in the Q band region upon excitation at 380 nm, normalized at the ESA maximum at around 560 nm to display the formation of peak around ~ 525 nm.

Hence, the involvement of multiple electronic spin states accompanied by the VC processes is proposed in the excited-state relaxation dynamics of various heme model compounds. Based on spectral evolution and literature^{18-19, 27, 30} the four time constants for the heme model compounds are discussed in detail.

$\tau_1 \sim \text{LMCT}$. The time constant τ_1 ($\sim <80$ fs) is within the IRF. Though the time constant of 70-80 fs is within the IRF of our femtosecond pump-probe spectroscopy (< 120 fs), it could be possible to deconvolute from the femtosecond transient absorption data by global analysis. As the fluorescence lifetimes of the metalloporphyrins are shorter^{18, 54} owing to the electron transfer from the porphyrin ring to the Fe atom, this lifetime could be attributed to the LMCT process. The appearance the broad peak around ~ 630 nm, due to the formation of a cation of porphyrin further support the LMCT transition in the FTAS of the model compounds (**Figure 3.25**).⁵⁵⁻⁵⁶

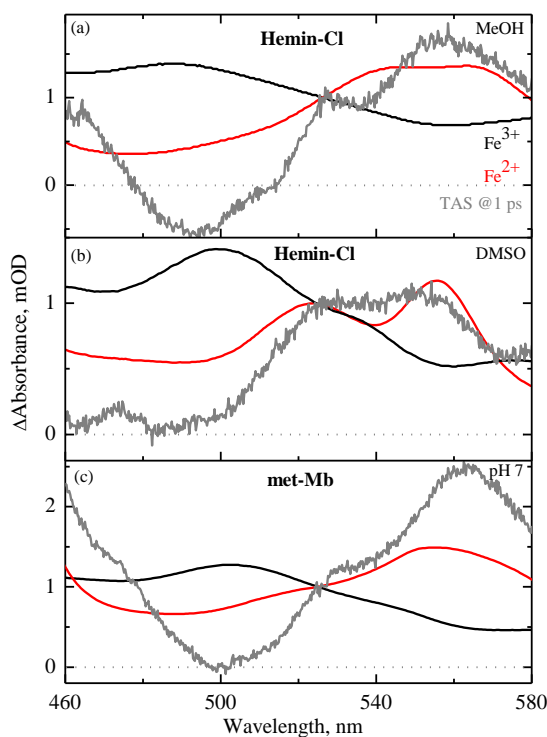


Figure 3.24 Stationary absorption spectra of ferric (black) and ferrous (red) **Hemin-Cl** in MeOH (a), DMSO (b) and **met-Mb** (c) at pH 7. FTAS (grey) at 1 ps are also shown for comparison. All the spectra are normalized at 525 nm.

However this time constant could also be attributed to the IC from $S_1 \leftarrow S_2$ state impeding the ultrafast LMCT transition.

$\tau_2 \sim \text{MLCT}$. The DAS of τ_2 is comparable to the singlet absorption spectra of the metalloporphyrins^{20, 57} and porphyrin cations^{56, 58} as it possess the ESA maxima between 430 and 470 nm and beyond 550 nm. Since the porphyrin cation formed by LMCT is much stable in the excited-state, electron can be transferred back from the metal orbital to the porphyrin HOMO.^{19, 59} Additionally, this time constant is much faster compared to the VC time constant ($\sim 3\text{--}8$ ps).⁶⁰⁻⁶¹ Franzen et al.²⁷ reported a similar time constant for the back electron transfer process in **Hb**. Therefore, the time constant obtained in the range of 248 to 580 fs could be assigned to the back electron transfer from the metal to porphyrin orbital.¹⁸

τ_3 and $\tau_4 \sim (S = 1/2 \text{ and } 3/2)$. There is an appearance of double peaks at ~ 525 and 560 in the Q-band region of transient absorption spectra after the 300 fs time delay for all the heme model compounds and **met-Mb**. The spectral resemblance between the FTAS of **Hemin-Cl** at 1 ps and the stationary absorption spectra of the low spin ferrous **Hemin-Cl** in MeOH and DMSO in the Q-band region are shown in **Figure 3.24**. Moreover, water ligated 6C ferric **met-Mb** and 6C ferrous **Mb** showed similar spectral features around the Q-band region of transient spectra at low temperature.⁶² Such similar observation could reflect the same electronic distribution on the heme-macrocycle, where Fe d_π orbitals are stabilized leading to the formation of low spin state. Thus, the time constant τ_3 is attributed to the state where the Fe is in the low spin state ($S = 1/2$) with four electrons in the d_π orbitals. The relaxation dynamics will be completed by passing through the intermediate quartet spin state ($S = 3/2$) to the high spin ground state ($S = 5/2$). Therefore, the time constant, τ_4 , is assigned to the intermediate spin state, where the Fe would have the spin state of ($S = 3/2$). It is to be noted that these assignments are in good agreement

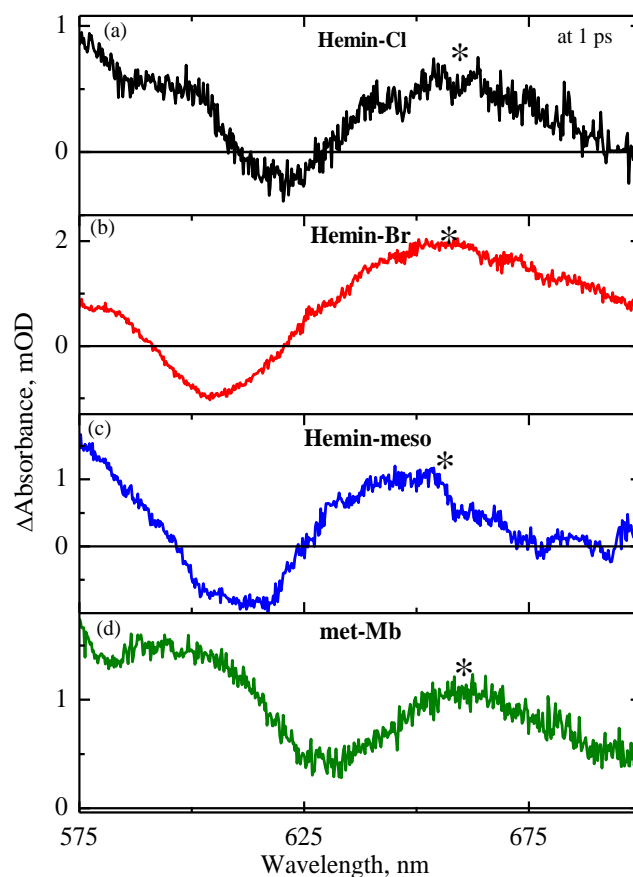
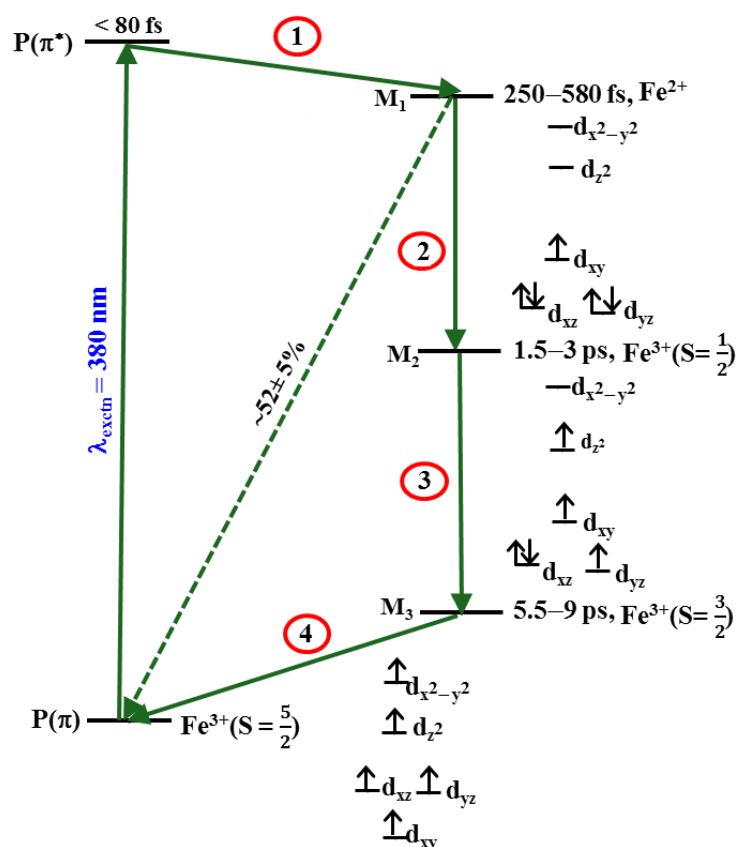


Figure 3.25 FTAS of model compounds and **met-Mb** measured at 1 ps after the photo-excitation. The asterisk denotes the absorption maximum of the porphyrin cation.

with the observation of the FTAS of **met-Mb** by Chergui et al.¹⁹, where the initial relaxation dynamics was found to have the involvement of different electronic spin state of the Fe atom. The presence of the electronically excited intermediate state in the relaxation dynamics has also been reported for the model compounds as well as proteins.⁶³⁻⁶⁴ However, the involvement of different electronic spin states can be further characterized by using the femtosecond X-ray absorption spectroscopy and FSRS with the time resolution of 50 fs.³³ Thus, the mechanism of excited-state relaxation dynamics of heme model compounds comprising different electronic spin states is proposed based on the spectral evolution, global analysis, and literature^{18-19, 30} and shown in **Scheme 3.1**



Scheme 3.1 Proposed mechanism for the excited-state relaxation dynamics of heme model compounds comprising different electronic spin states of iron atom.

3.3.3.3 Effect of Axial Ligands, Peripheral Substituents, and Solvents

The time constants obtained for **Hemin-Br**, **Hemin-meso** in MeOH and DMSO are compared to the **Hemin-Cl** in MeOH. No conclusion can be made from the shortest time constant, τ_1 , as it is within our IRF (< 120 fs).

Hemin-Br: The relaxation time constants of **Hemin-Br** are increased (particularly, τ_3 and τ_4) when compared to the **Hemin-Cl**. A weak field strength ligand ($\text{Cl} > \text{Br}$) could stabilize the energy level of both the d_z^2 and d_π orbitals by dropping an electron from the $d_x^2-y^2$ orbital to one of the lowest d_π orbitals⁶⁵⁻⁶⁷, leading to the intermediate or low spin states (**Scheme 3.1**).

Hemin-meso: When compared to **Hemin-Cl**, the relaxation time constants obtained for **Hemin-meso** are longer. The electron density at the iron center will be increased when

the vinyl group is replaced by the ethyl group in the case of **Hemin-meso** due to the lowering of the π conjugation in the periphery of the porphyrin ring. Furthermore, some significant changes including the basicity of amide nitrogen atoms, binding affinity of the ligand to a central metal and absence of the torsional conformers occur in the **Hemin-meso**.^{46, 48} All of these changes could lead to an increase of the time constants for the **Hemin-meso**.

DMSO: When compared to MeOH, systematic increases of all the relaxation time constants for all the compounds are observed in DMSO. It could be due to the increased interaction between oxygen atom in the DMSO with axial ligand leading to an alteration in the electron density of Fe atom in the porphyrin leading to the stabilization of the relaxation dynamics. However, the less efficient energy dissipation due to the higher viscosity of DMSO⁶⁸ leading to slower time constants may not be ruled out. Such stabilization of different electronic spin states, VC and CT dynamics with the increase of solvent viscosity and polarity were already observed in different metalloporphyrins.

3.4 Conclusion

In summary, the femtosecond time-resolved pump-probe spectroscopy was used to investigate the excited-state relaxation dynamics of the heme and to understand the effect of the axial ligand (Cl/Br), the peripheral substituent (vinyl/ethyl-meso), and solvent (MeOH/ DMSO). Overall, the FTAS of the heme model compounds reveal the evidence of the involvement of both vibrational relaxation and intermediate electronic spin states in the excited-state relaxation pathway. For example, the evolution of ESA spectra along with narrowing of the spectral bandwidth and shifting toward the blue region with an increase of the delay time indicate the occurrence of VC in the picosecond range. Concurrently the existence of multiple electronic spins states is observed by the

appearance of the new peak at ~ 525 nm after ~ 300 fs and lasting for ~ 8 ps, leading to the spectral similarities between the FTAS of the ferric and stationary absorption spectra of the low spin ferrous heme model compounds. The time constants proposed for the different electronic spin states can also be correlated with the various stages of the VC dynamics. The spectral and kinetic analysis of FTAS of **met-Mb** showed similar features to the heme model compounds. Therefore, the involvement of different electronic spin states could be an alternative pathway to the ground state along with the VR process in the deactivation pathway of photo-excited heme model compounds and correlated to be an inherent feature of the heme *b* type.

3.5 Materials and Methods

3.5.1 Sample Preparation: Hemin-Cl, Hemin-Br, and Hemin-meso and dehydrated **met-Mb** were purchased from Frontier Scientific and Sigma-Aldrich respectively and used without further purification. The ferrous compounds were prepared by the addition of sodium dithionite under the argon atmosphere.

In order to record the FTAS, the absorbance of the samples was made to have between 0.4 and 0.6 at the pump wavelength (380 nm) in a 0.4 mm optical path length spinning sample cell, equivalent to a concentration of 60–100 μM .

3.6 References

1. Poulos, T. L., *Chem. Rev.* **2014**, *114* (7), 3919-3962.
2. Kleingardner, J. G.; Bren, K. L., *Acc. Chem. Res.* **2015**, *48* (7), 1845-1852.
3. Vos, M. H., *Biochim. Biophys. Acta.* **2008**, *1777* (1), 15-31.
4. Girvan, H. M.; Munro, A. W., *J. Biol. Chem* **2013**, *288* (19), 13194-13203.
5. Kepp, K. P., *Coord. Chem. Rev.* **2017**, *344*, 363-374.
6. Dawson, J. H., *Science* **1988**, *240* (4851), 433.
7. Spiro, T. G.; Soldatova, A. V.; Balakrishnan, G., *Coord. Chem. Rev.* **2013**, *257* (2), 511-527.
8. Bowman, S. E. J.; Bren, K. L., *Nat. prod. rep.* **2008**, *25* (6), 1118-1130.
9. Schneider, S.; Marles-Wright, J.; Sharp, K. H.; Paoli, M., *Nat. Prod. Rep.* **2007**, *24* (3), 621-630.
10. Paoli, M.; Marles-Wright, J.; Smith, A., *DNA Cell Biol.* **2002**, *21* (4), 271-280.
11. A. Shelnutt, J.; Song, X.-Z.; Ma, J.-G.; Jia, S.-L.; Jentzen, W.; J. Medforth, C.; J. Medforth, C., *Chem. Soc. Rev.* **1998**, *27* (1), 31-42.
12. Osuka, A.; Maruyama, K.; Mataga, N.; Asahi, T.; Yamazaki, I.; Tamai, N., *J. Am. Chem. Soc.* **1990**, *112* (12), 4958-4959.
13. Banerji, N.; Bhosale, S. V.; Petkova, I.; Langford, S. J.; Vauthey, E., *Phys. Chem. Chem. Phys.* **2011**, *13* (3), 1019-1029.
14. Kumble, R.; Palese, S.; Lin, V. S. Y.; Therien, M. J.; Hochstrasser, R. M., *J. Am. Chem. Soc.* **1998**, *120* (44), 11489-11498.
15. Gentemann, S.; Medforth, C. J.; Forsyth, T. P.; Nurco, D. J.; Smith, K. M.; Fajer, J.; Holten, D., *J. Am. Chem. Soc.* **1994**, *116* (16), 7363-7368.
16. Challa, J. R.; Gunaratne, T. C.; Simpson, M. C., *J. Phy. Chem. B.* **2006**, *110* (40), 19956-19965.

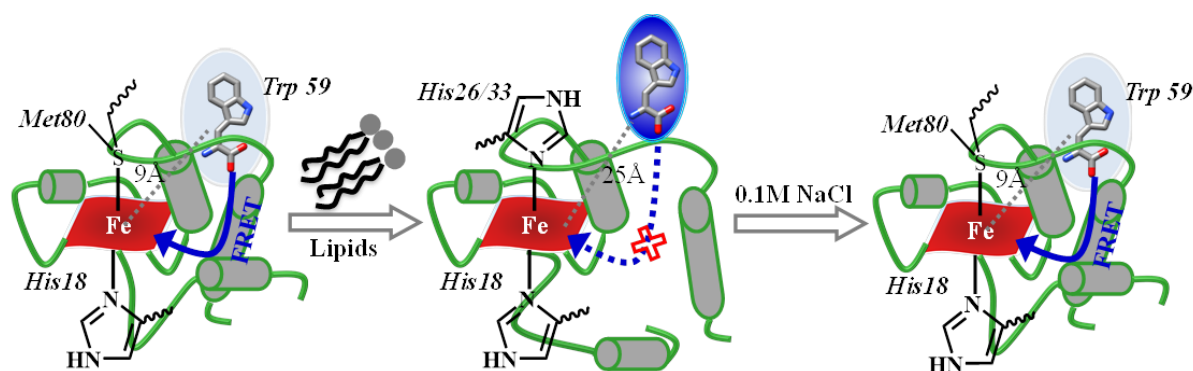
17. Rury, A. S.; Goodrich, L. E.; Galinato, M. G. I.; Lehnert, N.; Sension, R. J., *J. Phys. Chem. A* **2012**, *116* (32), 8321-8333.
18. Marcelli, A.; Jelovica Badovinac, I.; Orlic, N.; Salvi, P. R.; Gellini, C., *Photochem. Photobiol. Sci.* **2013**, *12* (2), 348-355.
19. Consani, C.; Auböck, G.; Bräm, O.; van Mourik, F.; Chergui, M., *J. Chem. Phys.* **2014**, *140* (2), 025103.
20. Rodriguez, J.; Kirmaier, C.; Holten, D., *J. Am. Chem. Soc.* **1989**, *111* (17), 6500-6506.
21. Ferrante, C.; Batignani, G.; Pontecorvo, E.; Montemiglio, L. C.; Vos, M. H.; Scopigno, T., *J. Am. Chem. Soc.* **2020**, *142* (5), 2285-2292.
22. Ye, X.; Demidov, A.; Rosca, F.; Wang, W.; Kumar, A.; Ionascu, D.; Zhu, L.; Barrick, D.; Wharton, D.; Champion, P. M., *J. Phys. Chem. A* **2003**, *107* (40), 8156-8165.
23. Yu, H. Z.; Baskin, J. S.; Steiger, B.; Wan, C. Z.; Anson, F. C.; Zewail, A. H., *Chem. Phys. Lett.* **1998**, *293* (1-2), 1-8.
24. Karunakaran, V., *ChemPhysChem* **2015**, *16* (18), 3974-3983.
25. Mizutani, Y.; Kitagawa, T., *Science* **1997**, *278* (5337), 443-446.
26. Atak, K.; Golnak, R.; Xiao, J.; Suljoti, E.; Pflüger, M.; Brandenburg, T.; Winter, B.; Aziz, E. F., *J. Phys. Chem. B* **2014**, *118* (33), 9938-9943.
27. Franzen, S.; Kiger, L.; Poyart, C.; Martin, J.-L., *Biophys. J.* **2001**, *80* (5), 2372-2385.
28. Petrich, J. W.; Poyart, C.; Martin, J. L., *Biochemistry* **1988**, *27* (11), 4049-4060.
29. Cornelius, P. A.; Steele, A. W.; Chernoff, D. A.; Hochstrasser, R. M., *Proc. Natl. Acad. Sci. U.S.A.* **1981**, *78* (12), 7526-7529.

30. Ha-Thi, M.-H.; Shafizadeh, N.; Poisson, L.; Soep, B., *Phy. Chem. Chem. Phys.* **2010**, *12* (45), 14985-14993.
31. Rury, A. S.; Goodrich, L. E.; Galinato, M. G. I.; Lehnert, N.; Sension, R. J., *J. Phys. Chem. A* **2012**, *116* (32), 8321-8333.
32. Humphrey, J. L.; Kuciauskas, D., *J. Phys. Chem. C* **2008**, *112* (5), 1700-1704.
33. Ferrante, C.; Pontecorvo, E.; Cerullo, G.; Vos, M. H.; Scopigno, T., *Nat. Chem.* **2016**, *8* (12), 1137-1143.
34. Tang, L.; Zhu, L.; Ener, M. E.; Gao, H.; Wang, Y.; Groves, J. T.; Spiro, T. G.; Fang, C., *Chem. Commun.* **2019**, *55* (90), 13606-13609.
35. Toney, G. E.; Gold, A.; Savrin, J.; Ter Haar, L. W.; Sangaiah, R.; Hatfield, W. E., *Inorg. Chem.* **1984**, *23* (25), 4350-4352.
36. Boersma, A. D.; Goff, H. M., *Inorg. Chem.* **1982**, *21* (2), 581-586.
37. Sahoo, D.; Quesne, M. G.; de Visser, S. P.; Rath, S. P., *Angew. Chem.* **2015**, *127* (16), 4878-4882.
38. Bertrand, P.; Theodule, F. X.; Gayda, J. P.; Mispelter, J.; Momenteau, M., *Chem. Phys. Lett.* **1983**, *102* (5), 442-445.
39. Shankar, S.; Peters, M.; Steinborn, K.; Krahwinkel, B.; Sönnichsen, F.; Grote, D.; Sander, W.; Lohmiller, T.; Rüdiger, O.; Herges, R., *Nat. Commun.* **2018**, *9*, 1–12.
40. Owens, J. W.; O'Connor, C. J., *Coord. Chem. Rev.* **1988**, *84*, 1-45.
41. Lakowicz, J. R., *Principles of Fluorescence Spectroscopy*. Springer: New York, **2006**.
42. Mataga, N.; Kaifu, Y.; Koizumi, M., *Bull. Chem. Soc. Jpn.* **1956**, *29* (4), 465-470.
43. Cao, W.; Christian, J. F.; Champion, P. M.; Rosca, F.; Sage, J. T., *Biochemistry* **2001**, *40* (19), 5728-5737.
44. Evans, S. V.; Brayer, G. D., *J. Biol. Chem.* **1988**, *263* (9), 4263-4268.

45. Boffi, A.; Das, T. K.; della Longa, S.; Spagnuolo, C.; Rousseau, D. L., *Biophys. J.* **1999**, *77* (2), 1143-1149.
46. Caughey, W. S.; Ibers, J. A., *J. Am. Chem. Soc.* **1977**, *99* (20), 6639-6645.
47. Chaijan, M.; Benjakul, S.; Visessanguan, W.; Faustman, C., *Food Chemistry* **2007**, *100* (1), 156-164.
48. Boffi, A.; Zamparelli, C.; Verzili, D.; Ilari, A.; Chiancone, E., *Arch. Biochem. Biophys.* **1997**, *340* (1), 43-51.
49. Snellenburg, J. J.; Laptanok, S.; Seger, R.; Mullen, K. M.; van Stokkum, I. H. M., *J. Stat. Softw.* **2012**, *49* (3), 22.
50. Mullen, K. M.; van Stokkum, I. H. M., *J. Stat. Softw.* **2007**, *18* (3), 46.
51. Ishizaka, S.; Wada, T.; Kitamura, N., *Photochem. Photobiol. Sci.* **2009**, *8* (4), 562-566.
52. Rodriguez, J.; Kirmaier, C.; Holten, D., *J. Chem. Phys.* **1991**, *94* (9), 6020-6029.
53. Henry, E. R.; Eaton, W. A.; Hochstrasser, R. M., *Proc. Nat. Acad. Sci. U. S. A.* **1986**, *83* (23), 8982-8986.
54. Berezin, M. Y.; Achilefu, S., *Chem. rev.* **2010**, *110* (5), 2641-2684.
55. Dolphin, D.; Felton, R. H., *Acc. Chem. Res.* **1974**, *7* (1), 26-32.
56. Fajer, J.; Borg, D. C.; Forman, A.; Dolphin, D.; Felton, R. H., *J. Am. Chem. Soc.* **1970**, *92* (11), 3451-3459.
57. Zhang, X.; Wasinger, E. C.; Muresan, A. Z.; Attenkofer, K.; Jennings, G.; Lindsey, J. S.; Chen, L. X., *J. Phys. Chem. A* **2007**, *111* (46), 11736-11742.
58. Chang, C. K.; Hanson, L. K.; Richardson, P. F.; Young, R.; Fajer, J., *Proc. Natl. Acad. Sci. USA* **1981**, *78* (5), 2652-2656.
59. Huszánk, R.; Lendvay, G.; Horváth, O., *J. Biol. Inorg. Chem.* **2007**, *12* (5), 681-690.

60. Zhang, Y.; Fujisaki, H.; Straub, J. E., *J. Chem. Phys.* **2009**, *130* (2), 025102.
61. Bu, L.; Straub, J. E., *J. Phys. Chem. B.* **2003**, *107* (44), 12339-12345.
62. Engler, N.; Ostermann, A.; Gassmann, A.; Lamb, D. C.; Prusakov, V. E.; Schott, J.; Schweitzer-Stenner, R.; Parak, F. G., *Biophys. J* **2000**, *78* (4), 2081-2092.
63. Helbing, J., *Chem. Phys.* **2012**, *396*, 17-22.
64. Lim, M.; Jackson, T. A.; Anfinrud, P. A., *J. Phys. Chem.* **1996**, *100* (29), 12043-12051.
65. Sakai, T.; Ohgo, Y.; Hoshino, A.; Ikeue, T.; Saitoh, T.; Takahashi, M.; Nakamura, M., *Inorg. Chem.* **2004**, *43* (16), 5034-5043.
66. Goff, H. M.; Shimomura, E. T.; Phillippi, M. A., *Inorg. Chem.* **1983**, *22* (1), 66-71.
67. Ikezaki, A.; Nakamura, M., *Inorg. Chem.* **2002**, *41* (10), 2761-2768.
68. Liu, J.-Y.; Fan, W.-H.; Han, K.-L.; Deng, W.-Q.; Xu, D.-L.; Lou, N.-Q., *J. Phys. Chem. A* **2003**, *107* (50), 10857-10861.

Ultrafast Heme Relaxation Dynamics Probing the Unfolded States of Cytochrome c Induced by Liposomes: Effect of Charge of Phospholipids



4.1 Abstract

The ubiquitous electron transfer heme protein, cytochrome *c* (**Cyt c**) catalyses the peroxidation of cardiolipin (**CL**) in the early stage of apoptosis, where **Cyt c** undergoes conformational changes leading to the partial unfolding of the protein. Here the interaction dynamics of **Cyt c** with liposomes having different charges [**CL**, -2 ; **POPG** (2-Oleoyl-1-palmitoyl-*sn*-glycero-3-phospho-*rac*-(1-glycerol) sodium salt), -1 ; and **POPC** (2-Oleoyl-1-palmitoyl-*sn*-glycero-3-phosphocholine), 0] leading to various degrees of partial unfolding is investigated with steady state optical spectroscopy and femtosecond time-resolved pump-probe spectroscopy. The signature of the partial unfolding of the protein was observed in the absorption, fluorescence, and CD spectra of **Cyt c**-liposome complexes with an increase of lipid/protein (*L/P*) ratio, and the protein was refolded by the addition of 0.1 M NaCl. The femtosecond transient absorption spectra of the complexes were measured by selectively exciting the heme and tryptophan (*Trp*) at 385 and 280 nm, respectively.

Though significant changes were not observed in the excited state relaxation dynamics of the heme in liposomes by exciting at 385 nm, the 280 nm excitation exhibited a systematic increase of the excited state relaxation dynamics leading to the increase of lifetime of Trp and global conformational relaxation dynamics with the increase of anionic charge of the lipids. This reveals the decrease of efficiency of fluorescence resonance energy transfer from Trp to heme due to the increase of distance between them upon increase of partial unfolding of the proteins by liposomes. Such observation exhibits the Trp as a marker amino acid to reflect the dynamics of partial unfolding of the protein rising from the change in the tertiary structure and axial ligand interaction of the heme proteins in liposomes. The relaxation dynamics of the complexes in the presence of salt are similar to that of the native protein, reflecting that the refolding of the protein and the interactions are dominated by electrostatic interaction rather than the hydrophobic interaction.

4.2 Introduction

Cyt c, is an important electron transfer heme protein and loosely associated with the inner mitochondrial membrane.¹⁻² It was observed that **Cyt c** could act as an initiator for mitochondrial apoptosis (programmed cell death).³⁻⁵ In the early stages of apoptosis, **Cyt c** acts as a catalyst for peroxidation of anionic phospholipid, **CL**.⁶⁻⁷ About 20% of total membrane lipids consists of **CL**, having a unique structure with four fatty acid tails and a head group.⁸ At physiological pH, **Cyt c** possesses an overall charge of +8 enabling its interaction with negatively charged molecules of the phospholipids.⁹

4.2.1 Apoptosis

Apoptosis is a process involved in the development and elimination of damaged cells, and maintenance of cellular process.^{10,5} Apoptosis plays an important role in diverse physiological processes especially fetal cells and in adult tissues.¹¹⁻¹³ Different diseases such as cancers, immune, and neurodegenerative disorders are reported to be caused by

the deregulation of apoptosis.⁶ The mechanism of apoptosis is complicated. Apoptosis is mainly implemented by cysteine proteases known as caspases. Major caspase activation pathway is initiated by **Cyt c** in mammalian cells.^{7,14-15} During the process, different types of apoptotic stimuli induce the release of **Cyt c** from mitochondria to cytoplasm, causing a series of biochemical reactions activating the caspase action leading to cell death.^{16-17,18} A schematic diagram representing the **Cyt c** liberation from inner mitochondrial membrane is shown in **Figure 4.1**. During the initial stage of apoptosis, the ROS can oxidize the **CL** and induce the liberation of **Cyt c** from inner mitochondrial membrane. The release of different proteins such as adenylate kinase-2 (AK-2), SmacDIABLO, alongwith **Cyt c** present in the inter membrane space have been observed during the early stages of apoptotic cell death. In the outer mitochondrial membrane two **BCL-2** family proteins, Bax and Bak are associated with a voltage-dependent anion channel component of the permeability transition (PT) pores allow the release of **Cyt c** from the inter-membrane space of the mitochondria into the cytoplasm.⁹ The release of **Cyt c** from mitochondria is therefore considered as a key initial step in the apoptotic process.⁸

4.2.2 Phospholipids

Phospholipids are present in all biological membranes and contain either a glycerol group or a long-chain unsaturated amino alcohol. Most of the phospholipids have a diglyceride, phosphate group and a simple organic molecule such as choline.⁷ The head is hydrophilic in nature comprising negatively charged phosphate group and glycerol. The hydrophobic tail contains long fatty hydrocarbon chains (**Figure 4.2**).¹⁸ Generally the fatty acid hydrocarbon chain is un-branched and possesses cis double bonds. Mammalian cell membranes contain thousands of various phospholipids having different fatty acyl chains.¹⁹ In mammalian cell membranes, about 40–50% of total phospholipids are

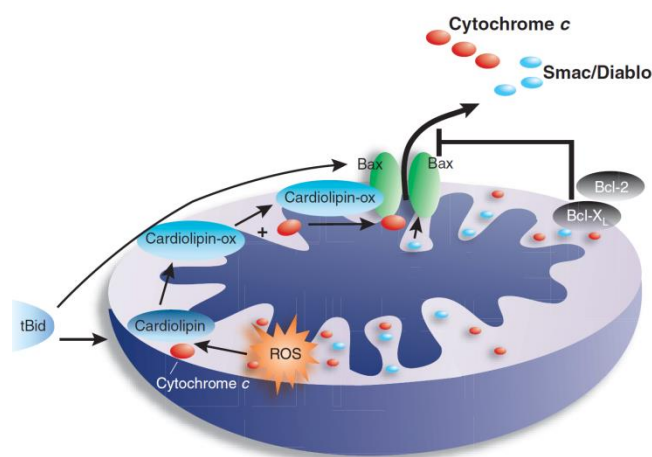


Figure 4.1 The liberation of **Cyt c** from the inner mitochondrial membrane. The Figure is copied from Ref. 16.

constituted by phosphatidyl-choline (PC) and phosphatidyl-ethanolamine (PE). Around 10% of total phospholipids consist of phosphatidyl-serine (PS) and **CL**. **CL** is a mitochondria specific diphosphatidyl glycerol, synthesized and located on the mitochondrial inner membrane.^{9, 20} **Cyt c** can undergo structural transitions including axial ligand exchange²¹⁻²², and change in the iron spin state in the presence of liposomes.²³ Different modes of interaction were proposed from various groups based on the experimental results.^{5, 24-27} **Figure 4.3** shows structural transitions happening in **Cyt c** upon electrostatic interaction with **CL**. Preliminary structural changes in **Cyt c** involve the breaking of the hydrogen bond between His26 and Pro44 and conversion of some of the loop and adjacent regions to β sheets.²⁸ Dissociation of the Fe–Met80 bond is another important structural change occurring in **Cyt c** upon interaction with liposomes. Later, breakup of inter helical contacts between N- and C-terminal helices takes place along with unfolding of the protein.²⁹ Interactions of the C-terminal helix with the membrane could lead to the formation of membrane pores.³⁰ The interaction dynamics of **Cyt c** with different liposomes have been carried out using various spectroscopies including NMR, FRET, EPR, CD, absorption, resonance Raman, and flash photolysis.^{29, 31-35}

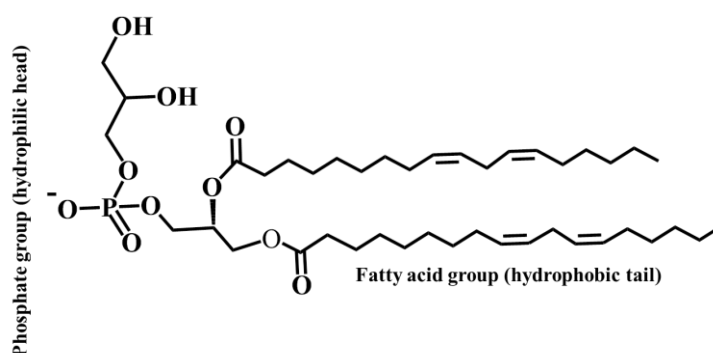


Figure 4.2 Chemical structure of a phospholipid containing polar and hydrophilic head and nonpolar hydrophobic tail.

Understanding of the interaction dynamics of **Cyt c** with liposomes is challenging, though the various mechanism including electrostatic and hydrophobic interactions and hydrogen bonding are proposed for the **Cyt c**–liposome interaction.³⁶ Mainly, two binding sites were proposed for the **Cyt c** liposome interactions, namely A and C sites. A site involves the electrostatic interaction via positively charged Lys72 and 73 and negatively charged phosphate group of lipids. However, the C site has the hydrophobic interaction through hydrogen bonding between Asn52 and protonated lipid phosphate group.³⁷⁻³⁸ A third binding L site was observed by the involvement of Lys22, Lys27, Lys87, and His33.³⁹ Different models are proposed for **Cyt c**-**CL** complex based on experimental data and molecular modelling optimizations.^{36,40} Initially it was proposed that one acyl chain of **CL** protruded into the protein interior through the hydrophobic channel located near to the Asn52 residue.⁴¹ This insertion was favoured by H-bonding between Asn52 and the protonated phosphate group of **CL**.²⁴ An alternative model affirms that the binding of **CL** to **Cyt c** occurs in the region of the Met80-containing loop, and that the acyl chain protrudes into the protein after anchoring of the phospholipid to the protein via electrostatic interactions between the deprotonated phosphate group of **CL** and the Lys72 residue⁴² (**Figure 4. 4**). The two acyl chains protrude in the vicinity of Asn52 and Met80. The proximal ligand of the heme Fe atom His18 and residues Lys72, Lys73, and Tyr74

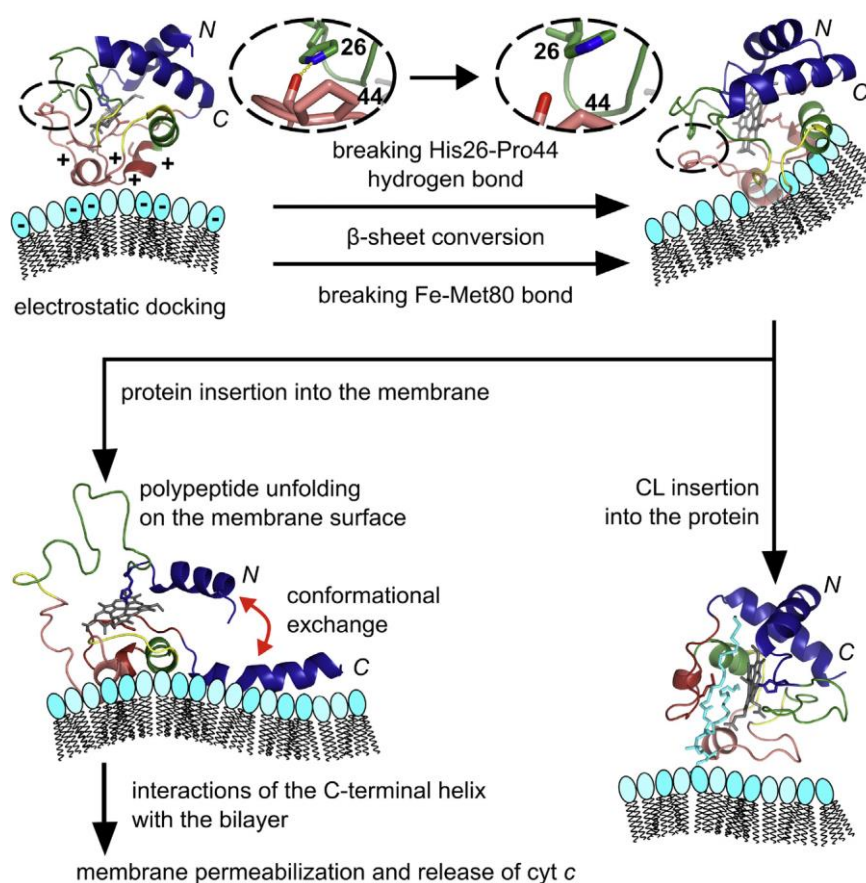


Figure 4.3 Different modes of **Cyt c**–CL interaction and the structural rearrangements of **Cyt c**. The Figure is copied from Ref. 28.

are also shown. Analysis of the emission maxima of dye-labelled **Cyt c** variants pointed to the hydrophobic environment of the labelling site at residue near to Arg91, however, it was not a deep insertion.⁵ Markedly, lipid-to-protein (L/P) ratio and the ionic strength strongly influenced the **Cyt c** and liposome interaction.^{8, 32, 43-44} The L/P ratio was associated with the lipid surface coverage by **Cyt c**.³² The heme group of **Cyt c** is highly sensitive to nature of axial ligand strength, spin state and conformational changes. Hence, Raman spectroscopy was widely used to study the **Cyt c** conformation under different conditions.^{32, 36, 45} **Cyt c** in aqueous solution possess the Raman marker bands at 1,372 (ν_4), 1,502 (ν_3), 1,584 (ν_2), and 1,635 cm^{-1} (ν_{10}). Upon binding with liposomes, a shift of all marker band frequencies was observed by Hildebrandt et al.³² and they proposed the existence of native (B1; His-Met coordination) and altered (B2) states of **Cyt c** in the

presence of DOPG liposome. The B2 state comprised a low-spin (B2[6CLS]), His-His-coordinated species, and two high-spin species (a penta-coordinated (B2[5cHS]) and a hexa-coordinated species (B2[6cHS])) in which a water molecule acted as the sixth ligand. The B2 species was predominated at high L/P ratios, whereas native B1 and His-His-coordinated B2[6CLS] coexisted at lower ratios. The CL content affect the Cyt c affinity to liposomes. Recently Stenner et al.³⁶ proposed, native-like, compact (C) and the “extended” (E) conformations of Cyt c which depended on the amount of CL, the L/P ratio and the electrostatic interactions, hydrogen bonds, and hydrophobic interactions at different ionic strength. Remarkably, most of the studies proposed a peripheral binding model of Cyt c with liposomes. The binding interaction of Cyt c–CL complex was studied by mutagenesis by substituting Lys72 and Lys73, with Asn³⁸ and CL-dependent peroxidase activity of Cyt c was cancelled upon mutagenesis, indicating the role of Lys72 and Lys73 in the interaction dynamics of Cyt c with CL. Cyt c persisted in an intermediate state in the presence of surfactant, sodium dodecyl sulphate (SDS), through unfolding of the protein by one step cooperative processes with an activation barrier of 16.8 kJ/mol.⁴⁶ Vos et al.³⁵ observed the multistep binding process of NO in ferric Cyt c–CL complex having a high value of escape fraction of NO and open nature of heme pocket in the complex using picosecond flash photolysis system.

Many spectroscopic techniques have been used to analyse the interaction of Cyt c with CL and observed the loosening and opening of the protein structure, unfolding of the protein, disruption of the axial ligand as well as the formation of membrane pores. Still there is no clear idea about the various degrees of unfolding of protein and the exact mechanism of interaction of Cyt c with liposomes. Hence the research has been focused on understanding the mechanism by which Cyt c binds to liposomes in the inner mitochondrial membrane as the interaction of phospholipids with Cyt c is a crucial step in

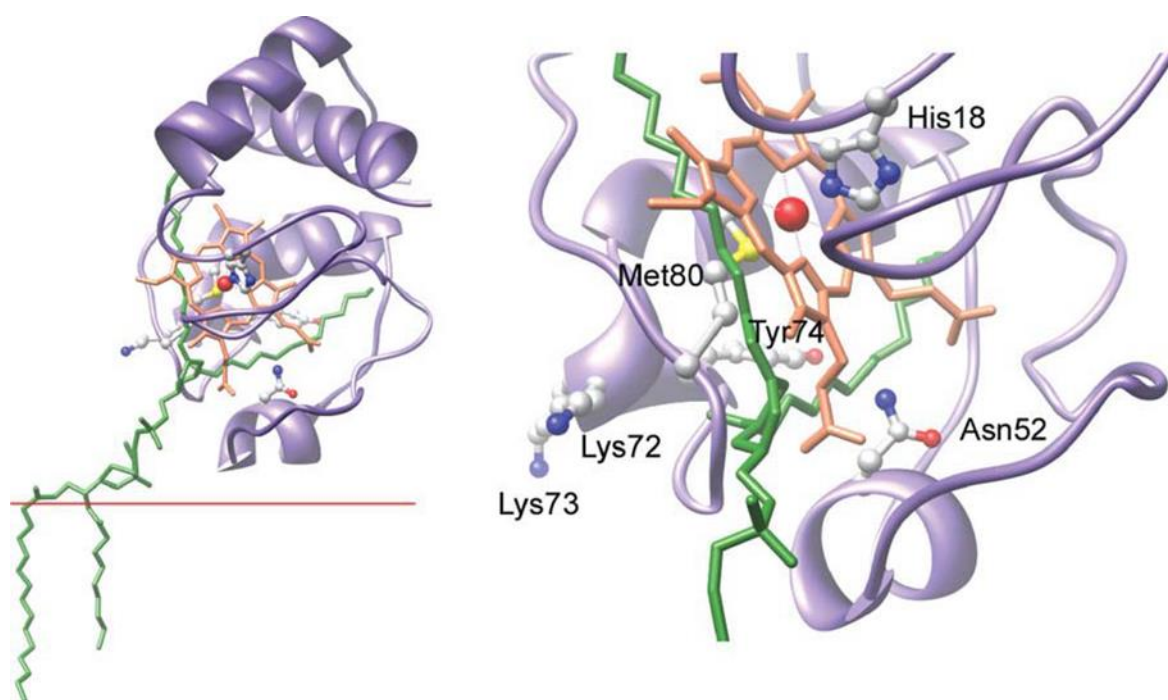


Figure 4.4 A molecular model for **Cyt c-CL** complex. The **CL** is shown as green, and the membrane plane is indicated by a red line (left panel). The enlarged view of the **Cyt c-CL** complex near to the heme (right panel). The Figure is copied from Ref. 41.

apoptosis. In this thesis, to understand the effect of the charges of phospholipids on the electronic, vibrational, and conformational relaxation dynamics of **Cyt c** upon complexation with liposomes with different charges, absorption, emission, CD, and femtosecond transient absorption spectra of the complexes were measured. **Cyt c** is systematically complexed with **CL**, **POPG**, and **POPC** having charges of -2 , -1 , and 0 , respectively. **CL** possesses four hydrophobic fatty acid tail and a hydrophilic phosphate head group with two negative charges. **POPG** is a phosphatidyl glycerol consist of single negative charge with two acyl chains. Whereas, **POPC** is a phosphatidylcholine and zwitterionic over a wide pH range as it possesses a quaternary ammonium group and a phosphate moiety.³⁵ The chemical structures of different phospholipids and crystal structure of **Cyt c** are shown in **Figure 4.5**. It is inferred that the transient absorption spectra obtained by excitation at 280 nm exhibited the excited state dynamics of Trp and changes of tertiary structure reflecting the conformational changes of the protein

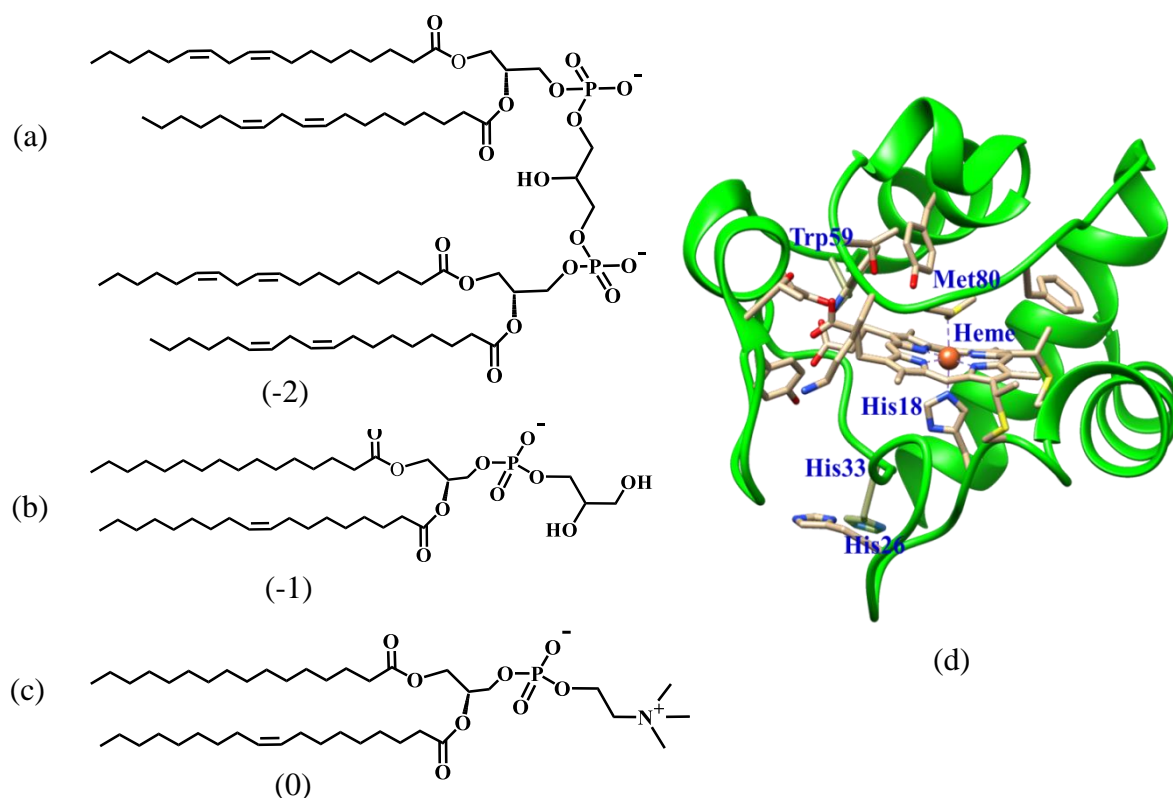


Figure 4.5 Chemical structures of **CL** (a), **POPG** (b) and **POPC** (c) and crystal structure of ferric **Cyt c** (d) from PDB: 1HRC.⁴⁷ The charge of the lipids is also shown.

during partial unfolding of **Cyt c** upon complexation with liposomes.²²

4.3. Results and Discussion

4.3.1 Size Distribution of Liposomes

The size distribution of liposome (500 μM) was obtained by dynamic light scattering (DLS) experiment. Liposomes having diameter between 20 and 100 nm are known as smaller unilamellar vesicles (SUV). Whereas, those with diameters in the range between 100 nm and micrometers are classified as large unilamellar vesicles (LUV) and giant unilamellar vesicles (GUV) are having diameters in the 1 μM range.⁴⁸⁻⁵⁰ Here the size distribution of **CL** and **POPG** (**Figure 4.6**) is between 20 and 200 nm, indicating unilamellar vesicle formation.⁴³ Homogeneous liposome distributions are more suitable for better interaction of **Cyt c** with liposomes.

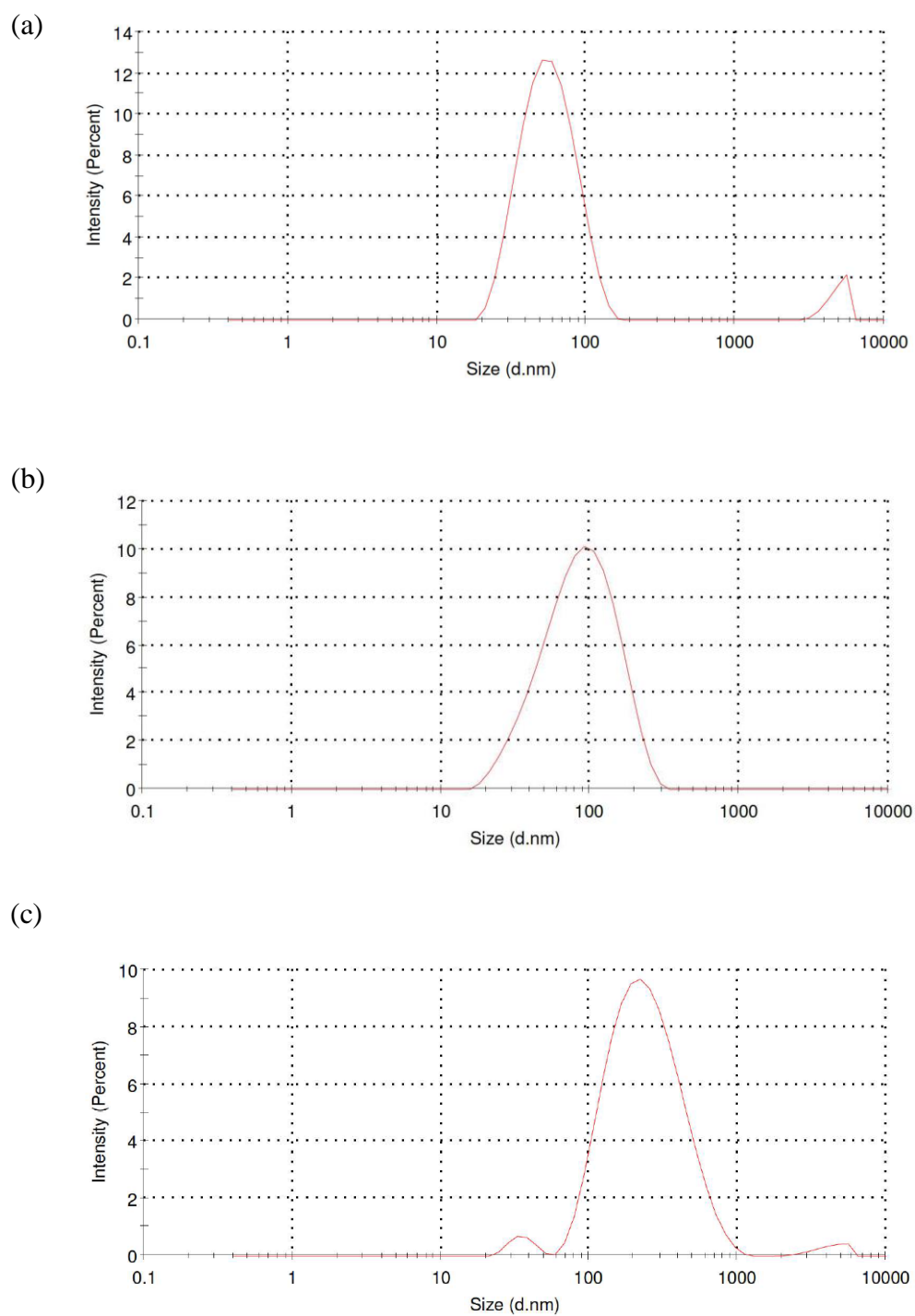


Figure 4.6 Size distribution of **CL** (a), **POPG** (b) and **POPC** (c) liposomes at a lipid concentration of 500 μM obtained from DLS experiment.

4.3.2 Stationary Absorption Spectra

The steady state absorption spectra of **Cyt c** and **Cyt c**-liposome complexes were measured at different L/P ratio (**Figure 4.7**). **Cyt c** in HEPES buffer showed a Soret absorption maximum at 409 nm along with a broad asymmetric Q band near 530 nm. Whereas the Soret band of **Cyt c-CL** and **-POPG** complexes is centered at 407 nm, slightly blue shifted from that of **Cyt c**. The enlarged view of CT band at 695 nm (normalized at 640 nm) is shown in the inset of **Figure 4.7**. A decrease of absorbance of band around 695 nm (MLCT band) is observed with increasing the L/P ratio, indicating

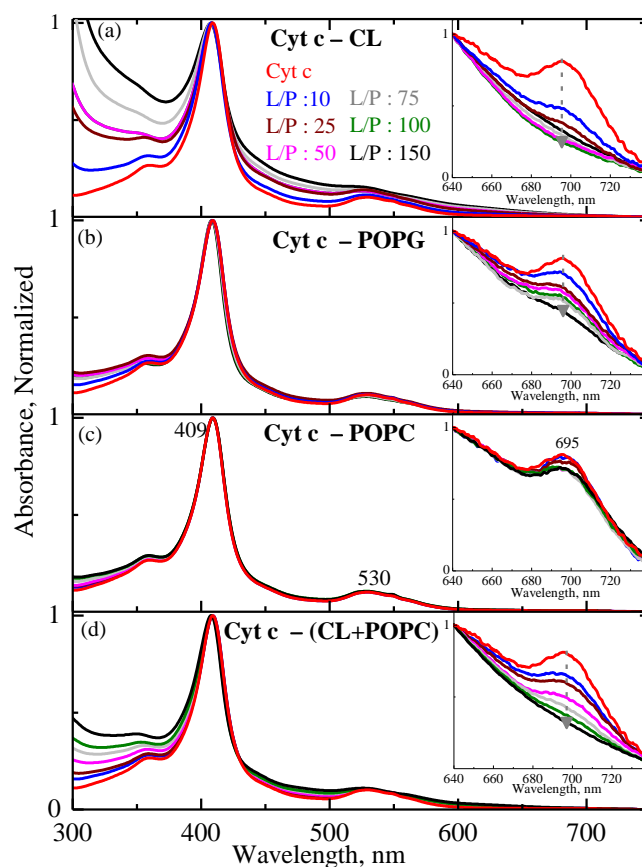


Figure 4.7 Ground state absorption spectra of **Cyt c-CL** (a), **Cyt c-POPG** (b), **Cyt c-POPC** (c) and **Cyt c-(CL+POPC)** (d) complexes with different L/P ratio at pH 7.4. Enlarged view of region near CT band at 695 nm is shown in the inset. The arrow depicts the decrease of absorbance of the CT band with increase of the L/P ratio.

the dissociation of the axial ligand Met80 from the heme.^{36, 51-53} Moreover, the appearance of a new peak at ~620 nm in the higher L/P ratio is observed due to the ferric high-spin (HS) formation.⁵⁴ **Cyt c-POPC** complex does not showed any significant changes in the absorption spectra as **POPC** is a neutral lipid. The complex of **Cyt c** with **CL** and **POPC** mixture (20:80 %) was also prepared to mimic the mitochondrial membrane. The absorption spectra of the **Cyt c-(CL+ POPC)** complex is similar to that of **Cyt c-CL**. Interestingly by the addition of 0.1 M NaCl, the CT band at 695 nm reappeared in the **Cyt c-liposome** complexes.

4.3.3 Fluorescence Spectra

The fluorescence spectra of **Cyt c-CL**, **-POPG**, **-POPC** and **-CL+ POPC** complexes having different L/P ratio were measured upon excitation at 290 nm in room temperature (**Figure 4.8**). A gradual increase of emission intensity at around 340 nm is observed for negatively charged **Cyt c-Liposome** complexes with increase of L/P ratio. The emission is attributed to Trp and it indicates the partial unfolding of **Cyt c**.⁵⁵⁻⁵⁶ The efficiency of fluorescence resonance energy transfer (FRET)⁵⁷ from Trp to heme will be decreased with increasing the concentration of liposomes due to the partial unfolding of the proteins in the presence of liposomes, the efficiency. The FRET efficiency is directly related to the donor-acceptor distance. Here the distance from Trp to heme will be increased from ~10 Å to 25 Å⁵⁸⁻⁵⁹ due to partial unfolding of **Cyt c** in the presence of liposomes. **Cyt c-CL**, **-POPG** and **-CL+POPC** complexes showed higher emission intensity with an increase of liposomes concentration, when compared to **POPC** liposomes. In addition, with increase of L/P ratio, a broad weak emission band at ~430 nm attributed to P band⁴³ was also observed. The fluorescence spectra of various **Cyt c-liposome** complexes were measured by the addition of 0.1 M NaCl to understand the significance of electrostatic interaction in **Cyt c-liposome** complexes. Insets of **Figure 4.8**

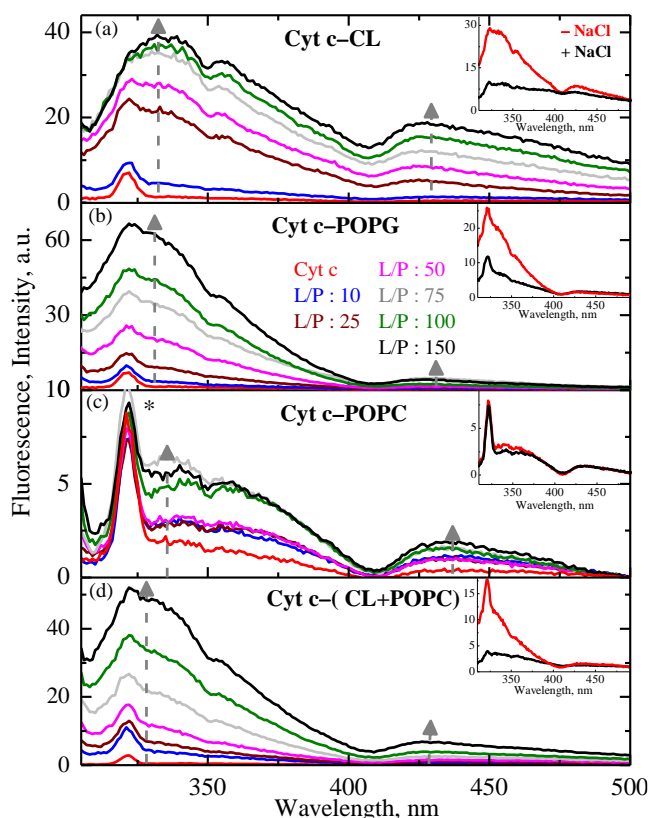


Figure 4.8 Fluorescence spectra of **Cyt c-CL** (a), **Cyt c-POPG** (b), **Cyt c-POPC** (c) and **Cyt c-(CL+POPC)** (d) complexes at different L/P ratio at pH 7.4 obtained upon excitation at 290 nm. Insets show the fluorescence spectra of complexes having L/P ratio of 50 with (black) and without NaCl (red). Asterisk (*) represents the characteristic O-H stretching frequency of water. The arrow indicates the increase of the fluorescence intensity with increase of the L/P ratio.

show the fluorescence spectra of **Cyt c**-liposome complexes having L/P ratio of 50 in 25 mM HEPES buffer with and without 0.1 M NaCl. In the presence of NaCl, the emission peak at ~340 nm, due to Trp is decreased for the **Cyt c**-liposome complexes when compared to the complexes in the absence of NaCl. The increased fluorescence intensity of **Cyt c** in the presence of negatively charged liposomes confirms the partial unfolding of the proteins indicating the changes of the tertiary structure.

4.3.4 Circular Dichroic Spectra

To understand the conformational and structural changes of **Cyt c** during the interaction with liposomes, the CD spectra of **Cyt c**-liposome complexes at different

L/P ratio were measured and shown in **Figure 4.9**. The CD spectrum of **Cyt c** exhibited a bisignate band, characteristic to the change of sign in the absorption maximum (~409 nm) caused by the variation of absorption of right- and left-circularly polarized light (Cotton effect) arising

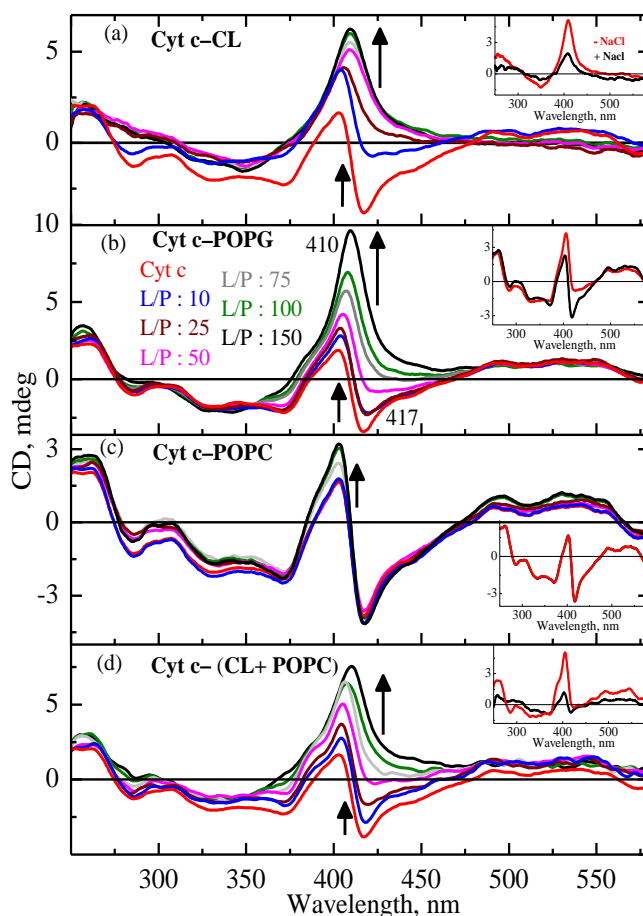


Figure 4.9 CD spectra of **Cyt c-CL** (a), **Cyt c-POPG** (b), **Cyt c-POPC** (c) and **Cyt c-(CL+POPC)** (d) complexes at different L/P ratio at pH 7.4. Insets show the CD spectra of the complex having L/P ratio of 50 with (black) and without 0.1 M NaCl (red).

from both electronic and vibronic perturbations of the heme.⁶⁰⁻⁶¹ Furthermore, **Cyt c** exhibited three negative bands at ~285, 330, and 371 nm. Weak positive band in the 450-520 nm region is attributed to CT transition between porphyrin and heme iron.⁵² The negative band at 417 nm is attributed to the presence of the sixth axial ligand, Met80.⁶² In

the **Cyt c**-**CL**, **-CL + POPC** and **-POPG** complexes, with an increase of L/P ratios, a gradual disappearance of the couplet replaced with a positive Cotton band was observed. This reflects a relaxation of the tertiary structure and axial ligand interactions of the heme in the protein. However the CD spectra of **Cyt c**-**POPC** complex does not showed any significant changes even at higher concentration [L/P:150] indicating the weak interaction of neutral POPC with **Cyt c**. Interestingly, the negative Cotton band at ~417 nm was reappeared upon addition of 0.1 M NaCl for **Cyt c**-**CL**, **-CL + POPG** and **-(CL+POPG)** complexes (insets of **Figure 4.9**). The decrease of Trp emission intensity in the fluorescence spectra and reappearance of Cotton band in the CD spectra in the presence of 0.1 M NaCl suggest the existence of electrostatic interaction between **Cyt c** and liposomes. In the presence of NaCl, the interaction of anionic phospholipids with Na⁺ ions will compete with the interaction of the lipids with the positive charge of the protein. Therefore, the partially unfolded protein refolded back to the native state.

4.3.5 Femtosecond Time-Resolved Excited State Relaxation Dynamics

The excited-state relaxation dynamics of the heme in **Cyt c**-liposome complexes were investigated using femtosecond time-resolved pump-probe spectroscopy. The pump wavelength was chosen to specifically excite the heme and Trp in **Cyt c** at 385 and 280 nm respectively. The FTAS of **Cyt c** upon excitation at 385 nm are shown in **Figure 4.10**. The spectral evolution of the **Cyt c** at different delay time after the photo-excitation starting from 170 to 820 fs and 2.32 to 10.27 ps are shown in panel a and b respectively. In the panel a, the earliest spectrum at 170 fs exhibited strong ground state bleach band at ~409 nm and an ESA at 375 and 420 nm. The decrease of bleach band and an increase of ESA with narrowing of spectral band-width along with shifting towards blue region were observed until ~2.0 ps. The intensity of both bleach and excited-state absorption decreases with an increase of the delay as shown in panel b and attained the equilibrium

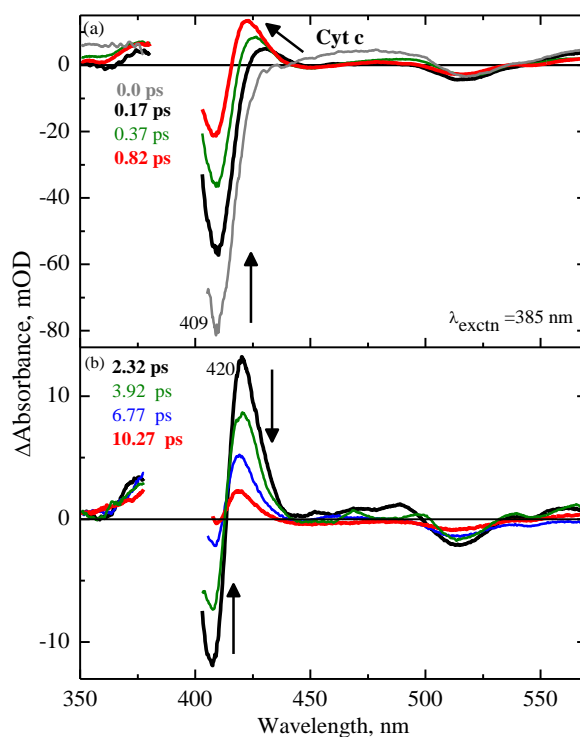


Figure 4.10 FTAS of Cyt c at pH 7.4 upon excitation at 385 nm. The different delay times are given and the arrows indicate the spectral evolution.

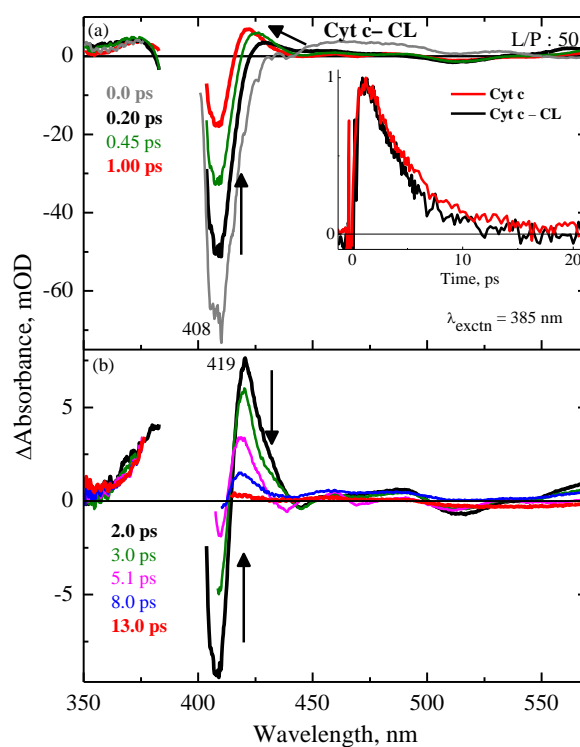


Figure 4.11 FTAS of Cyt c-CL complex having L/P ratio of 50 at pH 7.4 upon excitation at 385 nm. Inset shows the transient decay profile of Cyt c and Cyt c-CL complex probed at 419 nm.

within 20 ps. In **Figure 4.11**, the panel a and b depicts the spectral evolution of the **Cyt c–CL** complex at different delay time after the photo-excitation starting from 200 fs to 1.0 ps and 2.0 to 13.0 ps. The initial spectrum at 200 fs exhibited a strong bleach band at ~408 nm and an ESA at 375 and 419 nm (panel a). As the delay time increase, a decrease of bleach band (408 nm) and an increase of ESA (419 nm) accompanied by a narrowing of spectral band-width and shifting towards blue region were observed until ~2.0 ps. In the longer delay times, the intensity of both the bleach and ESA decreased and attained back to the equilibrium within 20 ps. The spectral features of FTAS of **Cyt c–CL** obtained by excitation at 385 nm are similar to that of native **Cyt c**. The transient decay profile of the **Cyt c–CL** complex and native **Cyt c** probed at 419 nm are similar to each other and found to be no significant changes in the dynamics (inset of **Figure 4.11**). The FTAS of **Cyt c–POPG** (**Figure 4.12**), **–CL+POPC** (**Figure 4.13**) and **–POPC** (**Figure 4.14**) obtained by exciting at 385 nm are similar to that of **Cyt c–CL**. Transient absorption spectra of **Cyt c–liposome** complexes were also measured upon excitation at 280 nm. The dynamics of Trp, heme and the tertiary structure of the protein in the partially unfolded form can be probed upon selective excitation at 280 nm. It is to be noted that heme will be excited indirectly through the FRET by the excitation of Trp at 280 nm. This will lead to the change in the Soret band bleach and heme electronic and vibrational relaxation processes. The femtosecond transient absorption spectra of **Cytc** upon exciting at 280 nm are shown in **Figure 4.15**. The spectral evolution of the **Cyt c** at different delay time after the photo-excitation starting from 200 fs to 1.1 ps and 2.5 to 30.2 ps are shown in panel a and b respectively. The earliest spectrum at 200 fs exhibited a strong ground state bleach band at ~408 nm and an ESA at 375 and 425 nm. The decrease of bleach band and an increase of ESA along with a narrowing of the spectral band-width and blue shifting were observed until ~2.2 ps. The intensity of both bleach

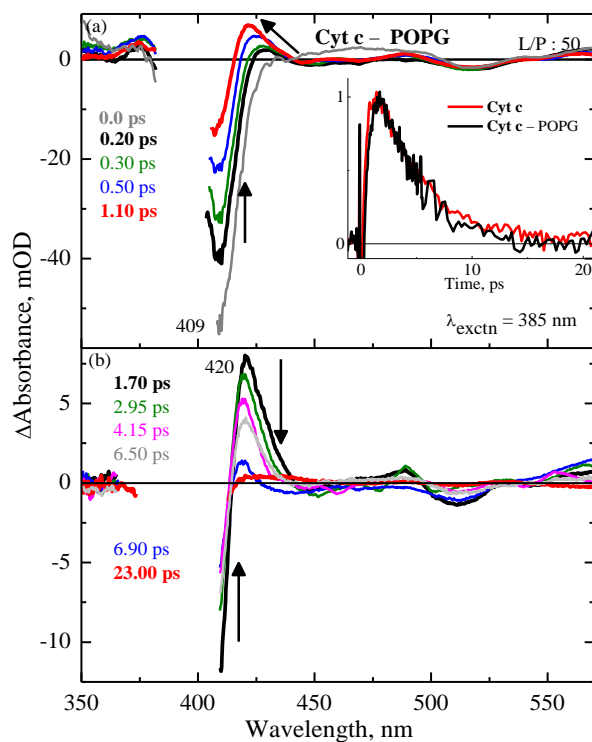


Figure 4.12 FTAS of Cyt c-POPG complex having L/P ratio of 50 upon excitation at 385 nm.

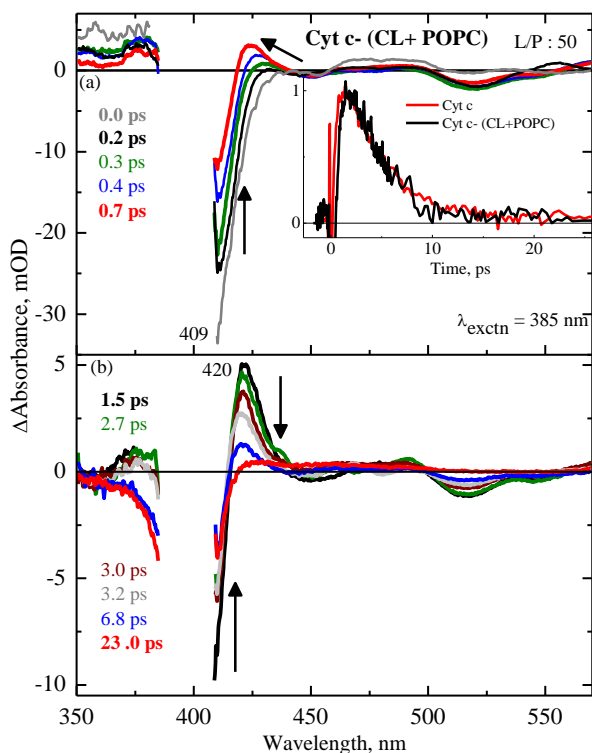


Figure 4.13 FTAS of Cyt c-(CL+POPC) complex having L/P ratio upon excitation at 385 nm.

and ESA decreased with an increase of the delay time. The FTAS of **Cyt c-CL**, **-POPG**, **-POPC** and **-CL+POPC** complexes obtained by exciting at 280 nm are shown in **Figure 4.16** and **4.17** and **Figure 4.18** and **4.19** respectively. The spectral shapes and evolutions are similar to that of **Cyt c**. When compared to the 385 nm excitation, both the bleach and the ESA do not attain the equilibrium within 20 ps. To understand the influence of electrostatic interaction in the excited state relaxation dynamics of protein-liposome complexes, FTAS of the complexes were measured in 0.1M NaCl. The FTAS of **Cyt c-POPG** and **Cyt c-POPC** complexes with 0.1 M NaCl are shown in **Figure 4.20** and **4.21** upon excitation at 280 nm. The transient decay of **Cyt c**-liposome complexes in the presence of 0.1M NaCl, are similar to that of the native **Cyt c** (**Figure 4.30**).

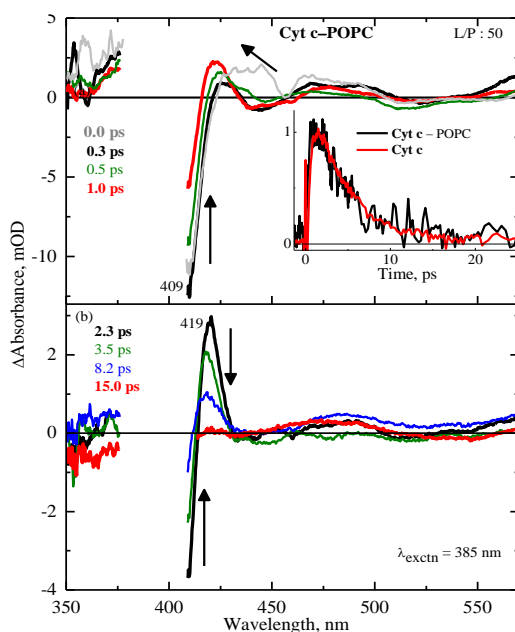


Figure 4.14 FTAS of **Cyt c-POPC** complex having L/P ratio of 50 upon excitation at 385 nm.

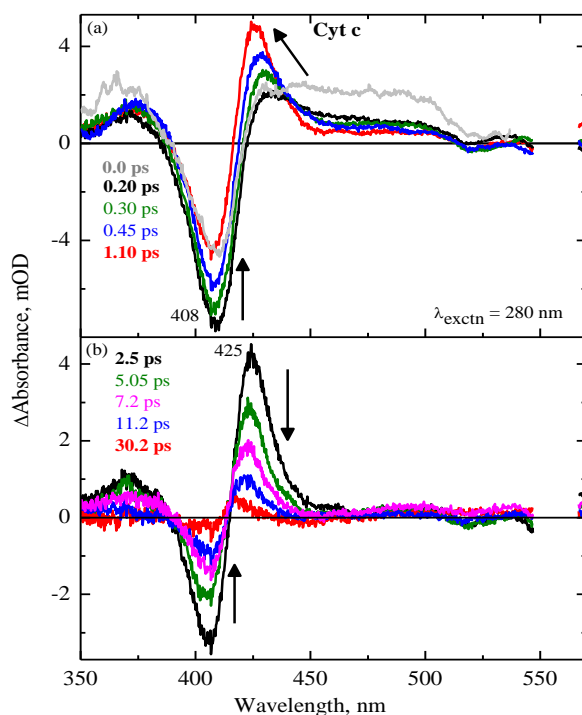


Figure 4.15 FTAS of Cyt c upon excitation at 280 nm. The different delay times are given and the arrows indicate the spectral evolution.

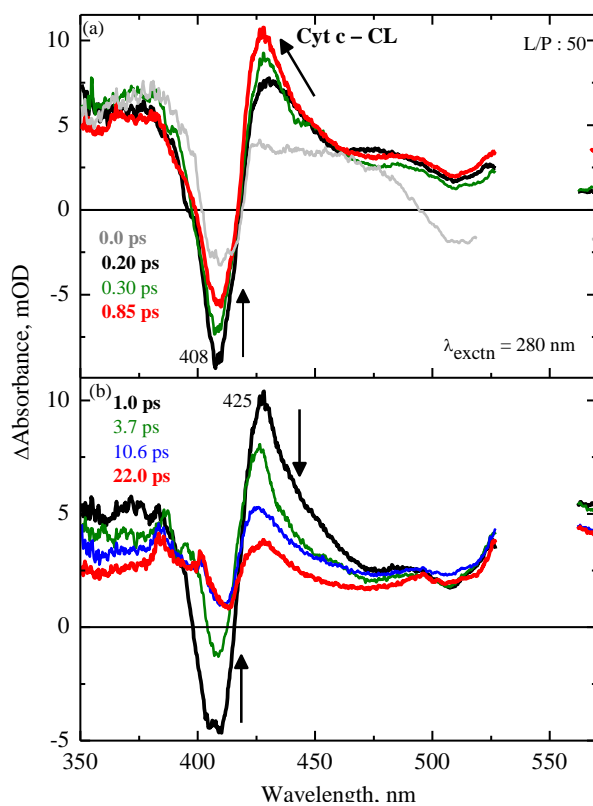


Figure 4.16 FTAS of Cyt c-CL complex having L/P ratio of 50 upon excitation at 280 nm. The different delay times are given and the arrows show the spectral evolution.

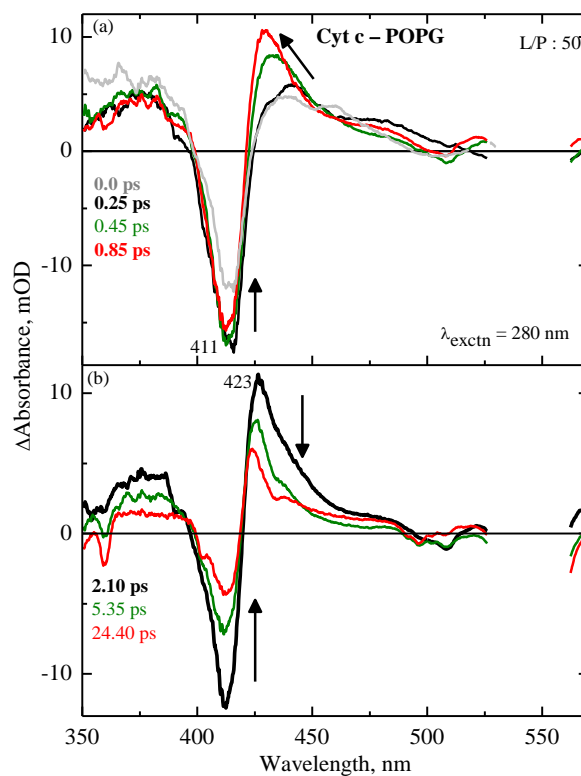


Figure 4.17 FTAS of Cyt c-POPG complex having L/P ratio of 50 upon excitation at 280 nm. The different delay times are given and the arrows show the spectral evolution.

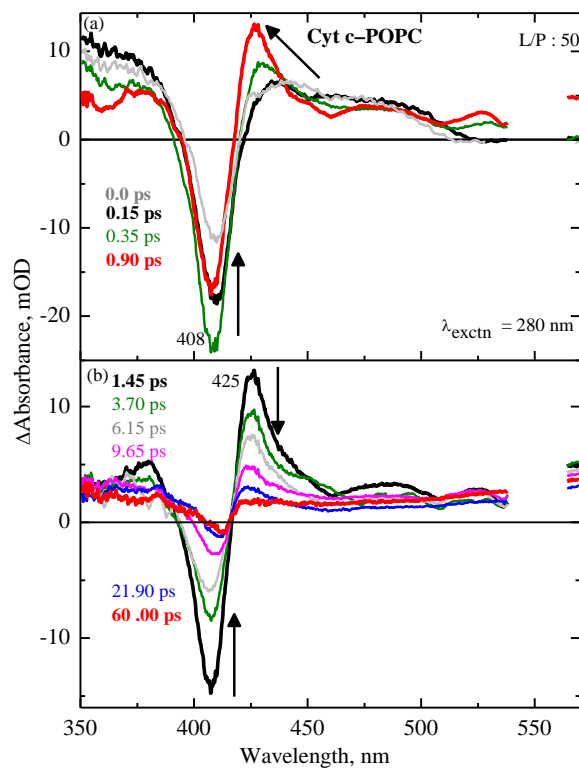


Figure 4.18 FTAS of Cyt c-POPC complex having L/P ratio of 50 upon excitation at 280 nm. The different delay times are given and the arrows show the spectral evolution.

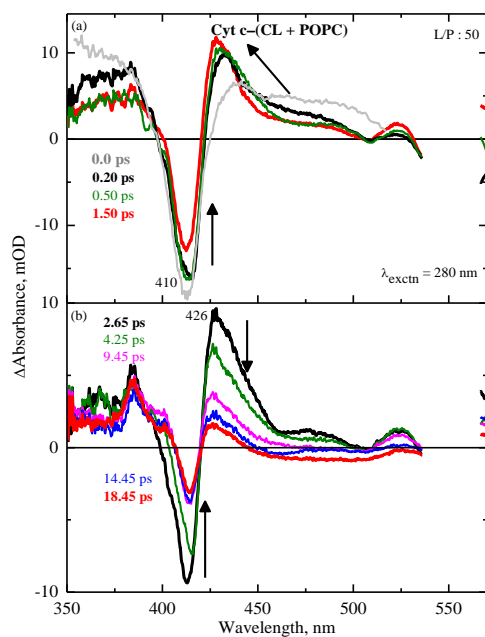


Figure 4.19 FTAS of Cyt c-(CL+POPC) complex having L/P ratio of 50 upon excitation at 280 nm. The different delay times are given and the arrows show the spectral evolution.

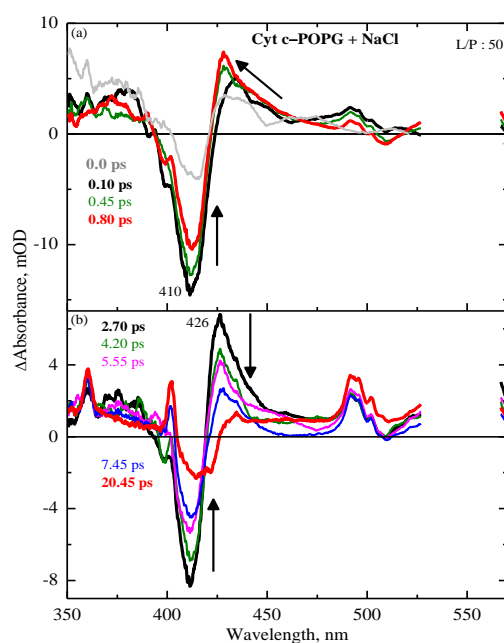


Figure 4.20 FTAS of Cyt c-POPG complex having L/P ratio of 50 with 0.1 M NaCl upon excitation at 280 nm. The different delay times are given and the arrows show the spectral evolution.

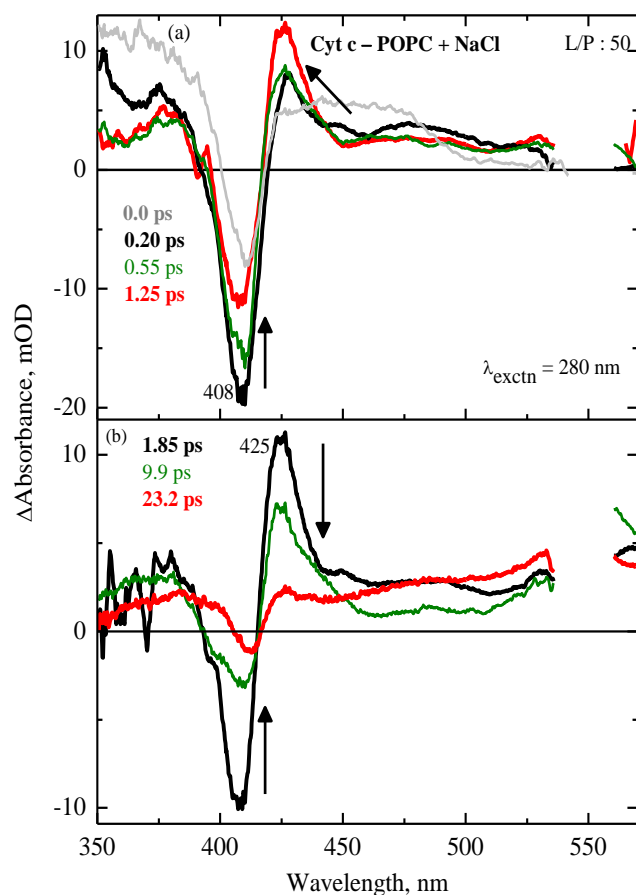


Figure 4.21 FTAS of **Cyt c-POPC** complex having L/P ratio of 50 with 0.1 M NaCl upon excitation at 280 nm. The different delay times are given and the arrows show the spectral evolution.

4.3.5.1 Analysis of Transient Absorption Spectra

FTAS of **Cyt c** and **Cyt c**-liposome complexes were analyzed by global analysis with a sequential decay model using the R package TIMP and its graphical user interface of GLOTARAN⁶³. A heat map with colour representation is chosen to clearly picture the whole spectral features. A comparative fit for the decay of ESA and GSB for **Cyt c** and **Cyt c-CL** complex upon excitation at 385 and 280 nm respectively is shown in **Figure 4.22** to **4.25** respectively. Four major time constants were obtained from the global exponential fit and the time constants are listed in **Table 4.1** and **4.2** for 385 and 280 nm excitation respectively. The corresponding DAS for these four time constants are given in **Figure 4.26**

and 4.27 for 385 and 280 nm excitation wavelengths, respectively. The DAS are similar to each other and exhibited both the ESA and ground state bleach band.

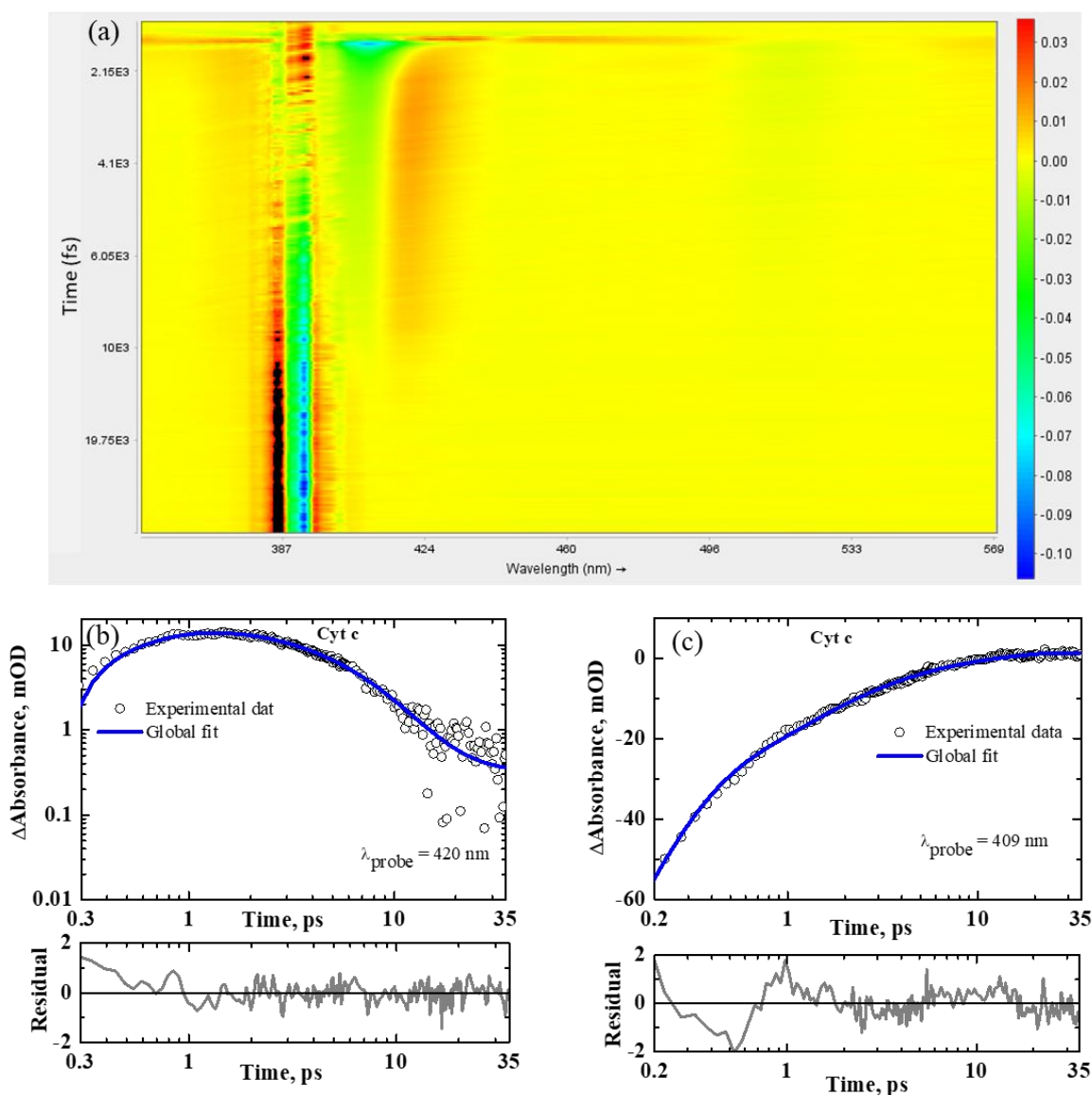


Figure 4.22 Heat map of the transient spectra (a) and time profile at ESA maximum (b) and GSB maxima (c) of **Cyt c** upon exciting at 385 nm. The open circles represent the experimental data and the solid line (blue) show the exponential fit and grey lines represents the residual obtained from global sequential analysis.

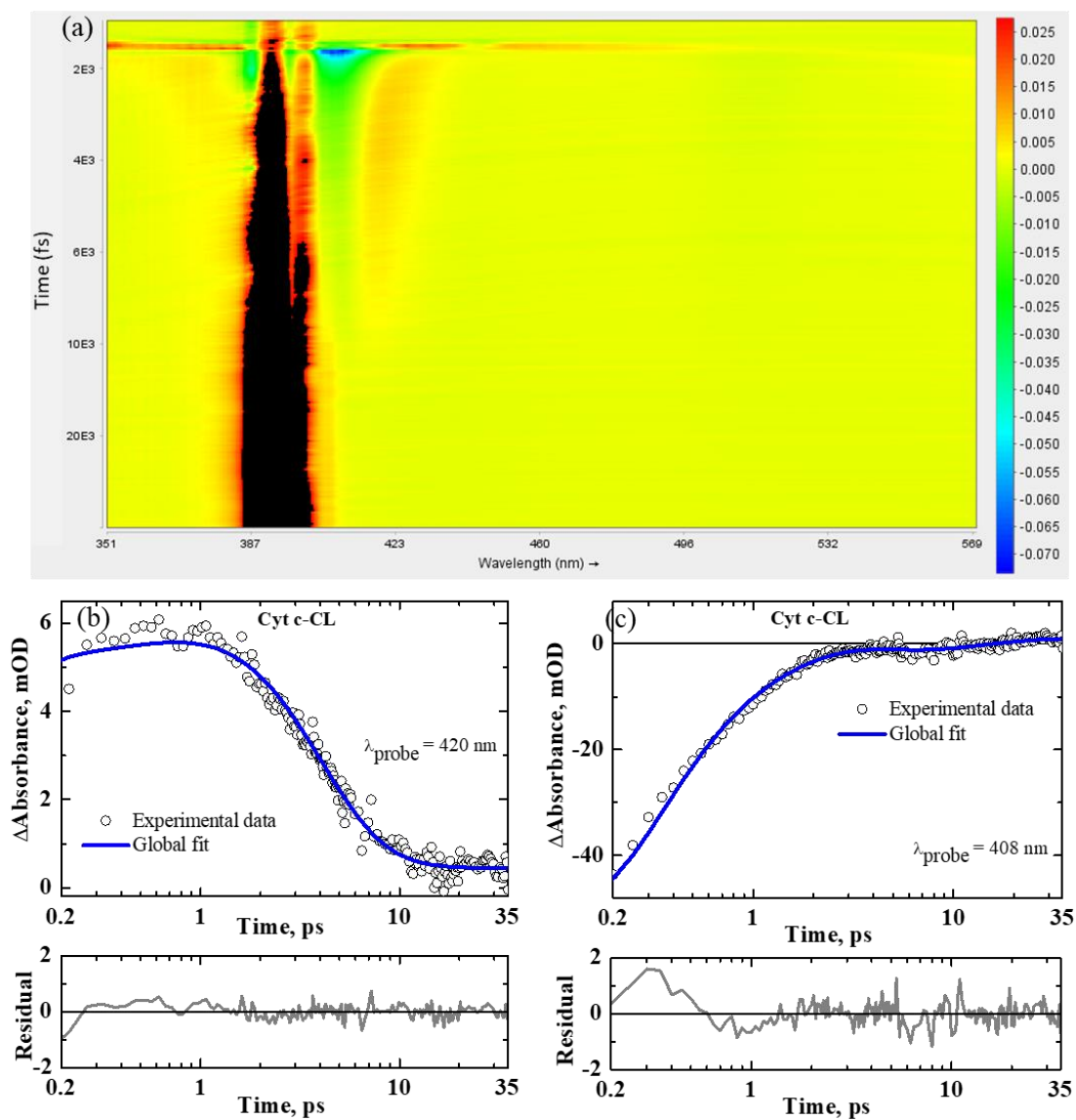


Figure 4.23 Heat map of the transient spectra (a) and time profile at ESA maximum (b) and GSB maxima (c) of **Cyt c-CL** upon exciting at 385 nm. The open circles represent the experimental data and the solid line (blue) show the exponential fit and grey lines represents the residual obtained from global sequential analysis.

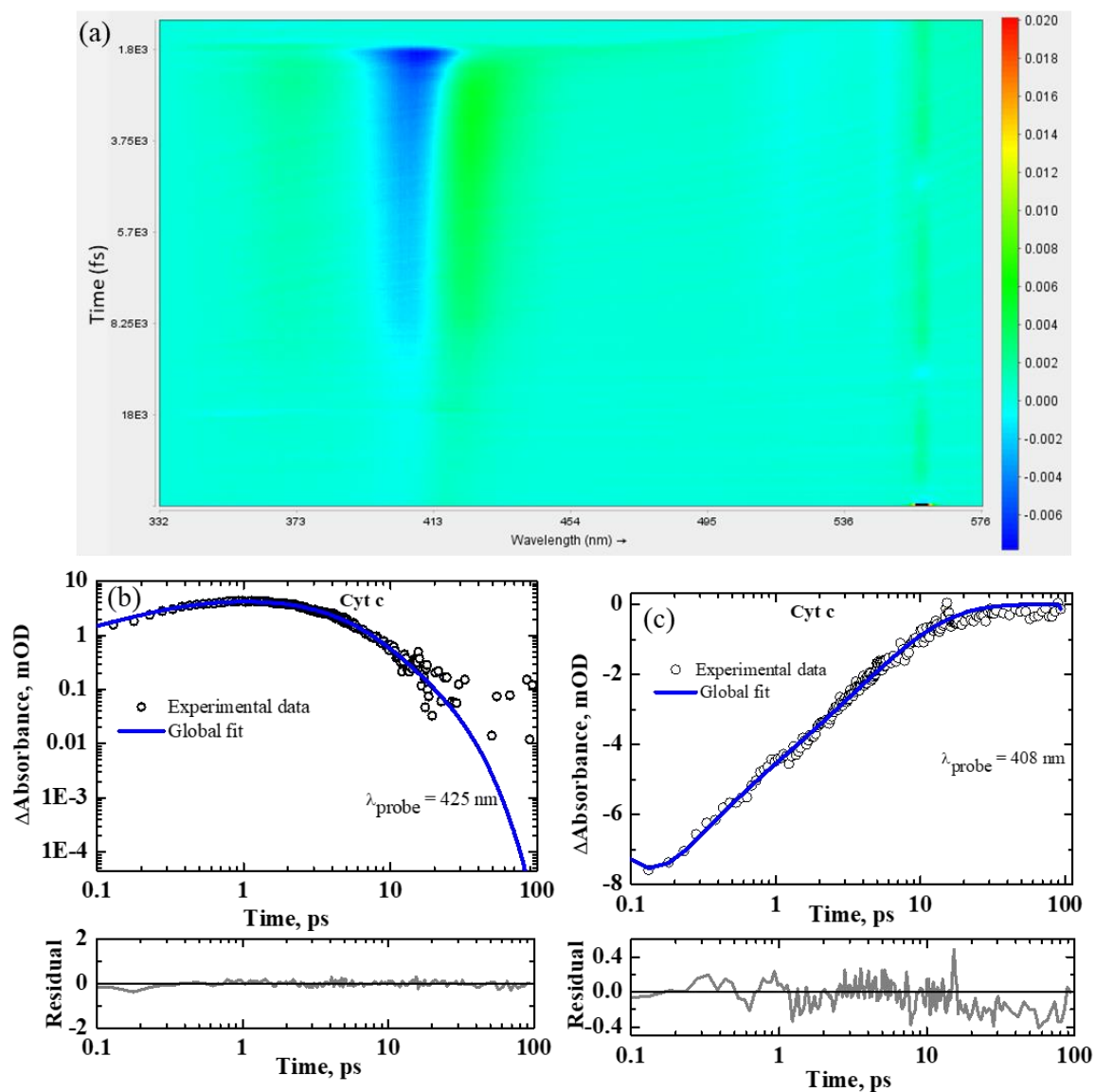


Figure 4.24 Heat map of the transient spectra (a) and time profile at ESA maximum (b) and GSB maxima (c) of **Cyt c** upon excitation at 280 nm. The open circles represent the experimental data and the solid line (blue) show the exponential fit and grey lines represents the residual obtained from global sequential analysis.

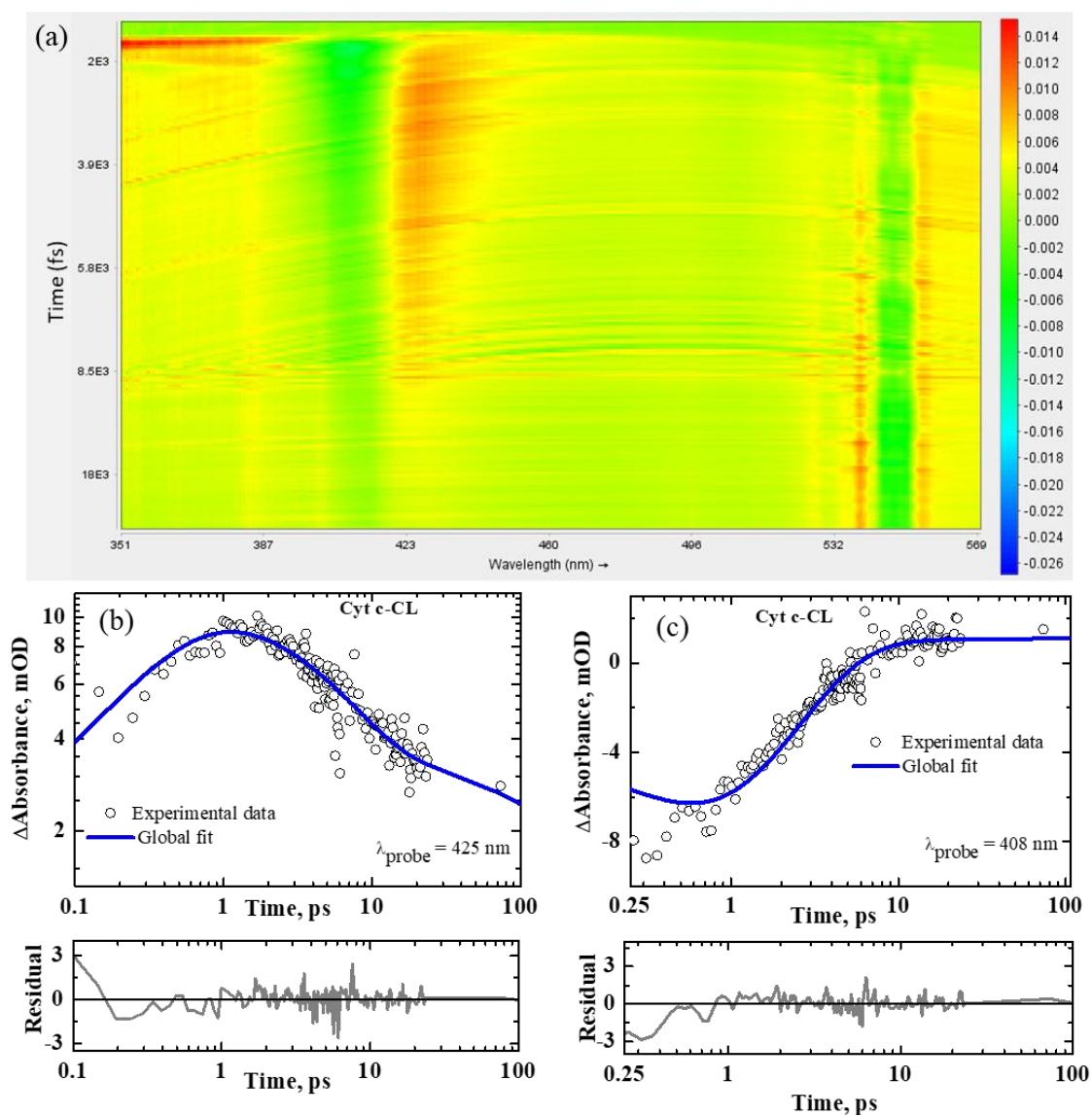


Figure 4.25 Heat map of the transient spectra (a) and time profile at ESA maximum (b) and GSB maxima (c) of **Cyt c-CL** upon excitation at 280 nm. The open circles represent the experimental data and the solid line (blue) show the exponential fit and grey lines represents the residual obtained from global sequential analysis.

4.3.5.2 Effect of Excitation Wavelength

Excitation at 385 nm: The time constants obtained from global analysis for the native ferric **Cyt c** at pH 7.4 are $\tau_1 = 148 \pm 50 \text{ fs}$, $\tau_2 = 666 \pm 100 \text{ fs}$, $\tau_3 = 3.72 \pm 0.30 \text{ ps}$ and $\tau_4 = 10.11 \pm 1.0 \text{ ps}$ and is consistent with the literatures.⁶⁴⁻⁶⁷ It was observed that in ferric **Cyt c**, the IC occurs within hundreds of femtoseconds.⁶⁵⁻⁶⁶ In the DAS, the τ_1 exhibited ESA and GSB at the corresponding absorption maximum. Therefore, the time constant τ_1 is

attributed to an excited-state decay of the heme to the ground state. Immediately after the IC, the heme in the hot ground state undergoes vibrational energy dissipation via multiple exponential pathways in the fast time scale. The shifting of the ESA towards the blue region with narrowing of the spectral band with increase of delay time confirmed the occurrence of the VC dynamics⁶⁸ with multiple exponential time constants in the transient spectra. Hence, the time constants τ_2 , τ_3 and τ_4 are attributed to the various degrees of VR dynamics of the heme in the ground-state. In the native **Cyt c** the fast and slow exponential components are due to the vibrational energy transfer via the coupling between heme and collective motions of the protein primarily through covalent bonds.⁶⁹ The excited-state relaxation dynamics of the heme in the liposomes upon excitation at 385 nm, did not exhibited any significant changes when compared to that of native **Cyt c**. It reflect an intact heme environment and it could be due to the replacement of Met80 by either His33 or His26^{32, 70} in the partially unfolded thermodynamic intermediate ground state. A Similar relaxation behaviour was reported for both the ferric and ferrous **Cyt c** with comparable vibrational relaxation time constants.⁶⁹

Table 4.1 Time constants obtained by global analysis for different **Cyt c**–liposome complexes having L/P ratio of 50 for 385 nm excitation.

Sample	Cyt c	Cyt c – CL	Cyt c – POPG	Cyt c – POPC	Cyt c – (CL+POPC)
	$\tau_1 = 0.14 \pm 0.05$ ps	$\tau_1 = 0.15 \pm 0.10$ ps	$\tau_1 = 0.14 \pm 0.10$ ps	$\tau_1 = 0.14 \pm 0.05$ ps	$\tau_1 = 0.14 \pm 0.10$ ps
	$\tau_2 = 0.66 \pm 0.10$ ps	$\tau_2 = 0.68 \pm 0.15$ ps	$\tau_2 = 0.67 \pm 0.50$ ps	$\tau_2 = 0.66 \pm 0.10$ ps	$\tau_2 = 0.67 \pm 0.15$ ps
	$\tau_3 = 3.72 \pm 0.30$ ps	$\tau_3 = 3.66 \pm 0.30$ ps	$\tau_3 = 3.52 \pm 0.20$ ps	$\tau_3 = 3.25 \pm 0.15$ ps	$\tau_2 = 3.43 \pm 0.10$ ps
	$\tau_4 = 10.11 \pm 1.00$ ps	$\tau_4 = 10.73 \pm 1.50$ ps	$\tau_4 = 10.55 \pm 2.00$ ps	$\tau_4 = 10.25 \pm 1.50$ ps	$\tau_3 = 10.34 \pm 1.10$ ps

Table 4.2 Time constants obtained by global analysis for **Cyt c**- liposome complex having L/P ratio of 50 for 280 nm excitation.

Sample	Cyt c	Cyt c – CL	Cyt c – POPG	Cyt c – POPC	Cyt c – (CL+POPC)
Absence of salt	$\tau_1 = 0.23 \pm 0.10$ ps	$\tau_1 = 0.38 \pm 0.15$ ps	$\tau_1 = 0.33 \pm 0.10$ ps	$\tau_1 = 0.29 \pm 0.10$ ps	$\tau_1 = 0.34 \pm 0.14$ ps
	$\tau_2 = 0.84 \pm 0.12$ ps	$\tau_2 = 2.35 \pm 0.50$ ps	$\tau_2 = 1.95 \pm 0.50$ ps	$\tau_2 = 0.98 \pm 0.10$ ps	$\tau_2 = 2.01 \pm 0.10$ ps
	$\tau_3 = 3.16 \pm 0.50$ ps	$\tau_3 = 5.49 \pm 0.20$ ps	$\tau_3 = 5.01 \pm 0.30$ ps	$\tau_3 = 3.91 \pm 0.15$ ps	$\tau_3 = 5.09 \pm 0.15$ ps
	$\tau_4 = 8.30 \pm 1.20$ ps	$\tau_4 = 26.50 \pm 1.10$ ps	$\tau_4 = 21.58 \pm 1.20$ ps	$\tau_4 = 14.00 \pm 1.50$ ps	$\tau_4 = 22.50 \pm 1.50$ ps
Presence of salt	$\tau_1 = 0.21 \pm 0.10$ ps	$\tau_1 = 0.22 \pm 0.15$ ps	$\tau_1 = 0.28 \pm 0.14$ ps	$\tau_1 = 0.28 \pm 0.15$ ps	$\tau_1 = 0.20 \pm 0.13$ ps
	$\tau_2 = 0.80 \pm 0.13$ ps	$\tau_2 = 0.83 \pm 0.15$ ps	$\tau_2 = 0.87 \pm 0.13$ ps	$\tau_2 = 0.90 \pm 0.14$ ps	$\tau_2 = 0.80 \pm 0.14$ ps
	$\tau_3 = 3.20 \pm 0.50$ ps	$\tau_3 = 3.00 \pm 0.50$ ps	$\tau_3 = 3.07 \pm 0.20$ ps	$\tau_3 = 3.85 \pm 0.20$ ps	$\tau_3 = 3.2 \pm 0.50$ ps
	$\tau_4 = 8.50 \pm 1.20$ ps	$\tau_4 = 8.90 \pm 1.20$ ps	$\tau_4 = 8.79 \pm 1.20$ ps	$\tau_4 = 13.65 \pm 1.10$ ps	$\tau_4 = 8.6 \pm 2.00$ ps

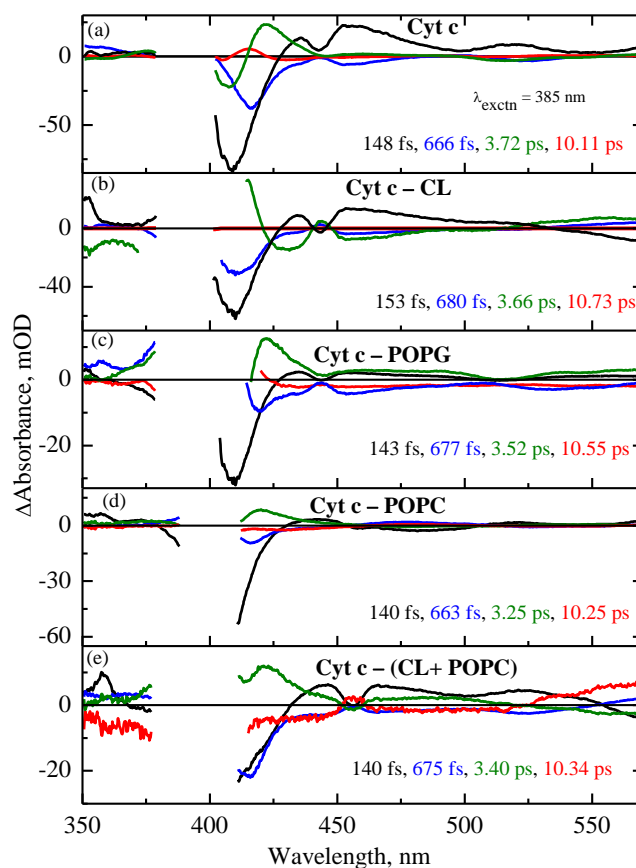


Figure 4.26 DAS of **Cyt c** and **Cyt c**-liposome complexes obtained from global analysis upon excitation at 385 nm.

Excitation at 280 nm: The dynamics of Trp, heme and tertiary structures associated with the partially unfolded form of the protein in the liposome was probed by the selective excitation of Trp at 280 nm. The time constants of **Cyt c** obtained from global analysis upon excitation at 280 nm are $\tau_1 = 230 \pm 100$ fs, $\tau_2 = 840 \pm 120$ fs, $\tau_3 = 3.16 \pm 0.5$ ps, and $\tau_4 = 8.50 \pm 1.2$ ps. The time constant τ_1 is ascribed to the excited state decay of heme, similar to the case of 385 nm excitation. It was observed that the fluorescence intensity of the native protein is efficiently quenched by the FRET from the excited Trp to the porphyrin ring of the heme group.⁷¹⁻⁷² The time constant of τ_2 is attributed to the excited-state lifetime of Trp.⁶⁷ The τ_3 and τ_4 are assigned to the VR time constants. The increase of the rate of IC (τ_1) of the heme in **CL** and **POPG** complexes reflected the slower electronic decay of the heme in the liposomes (**Table 4.2**).

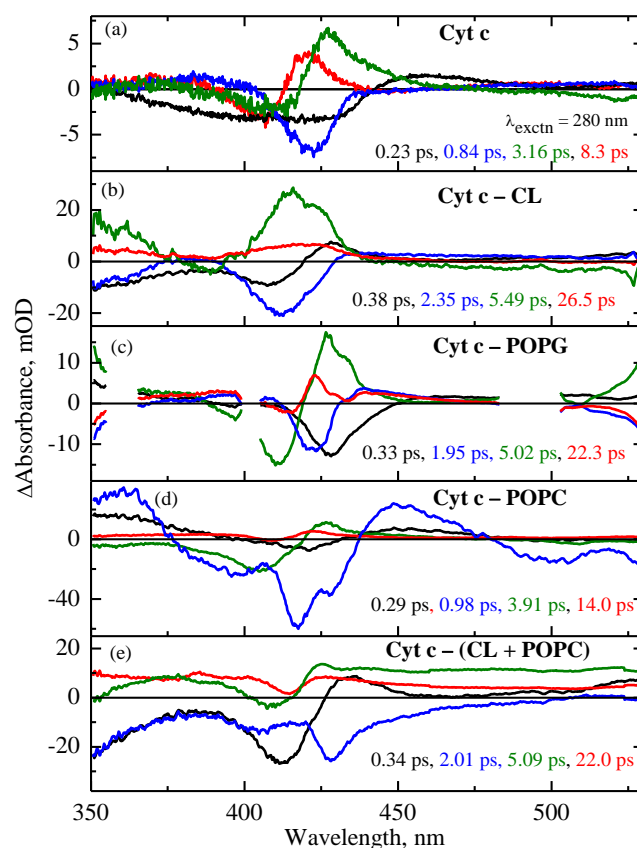


Figure 4.27 DAS of **Cyt c** and **Cyt c**-liposome complexes obtained from global analysis upon excitation at 280 nm.

A systematic increase of the time constant, τ_2 for **Cyt c**-**POPC** (0.98 ps), **-POPG** (1.95 ps), **-(CL+ POPC)** (2.01 ps) and **-CL** (2.35 ps) complexes with an increase of anionic charges of the liposomes were observed when compared to native **Cyt c**. This reveals a regular extent of the partial unfolding of **Cyt c** leading to an increased distance between Trp and heme reducing the FRET from Trp to heme. The time constant τ_3 was also increased in **Cyt c**-liposome complexes when compared to the native **Cyt c**. Remarkably, with an increase of anionic charges in the liposomes, a long-lived component τ_4 was observed for **Cyt c**-**POPG**, **-(CL+POPC)** and **-CL** complexes reflecting the global conformational change related to the tertiary structure by unfolding of **Cyt c** induced by liposomes. It is to be noted that, when compared to the completely unfolded protein by the addition of 4 M GdHCl^{64} , the time constant τ_4 obtained for **Cyt c**-liposome complexes is

shorter reflecting that the **Cyt c** in the liposome complexes is partially unfolded and conformational structures remain in an intermediate state between completely unfolded and native folded states.

In order to shed more light on the FRET process occurring from Trp to heme, the FTAS of **Cyt c-CL** complex at different L/P ratio have been measured upon excitation at 280 nm with different L/P ratio. The comparison of the magnitude of the heme bleach ($\lambda_{\text{probe}} = 409 \text{ nm}$) with an increase of L/P ratio is compared and shown in **Figure 4.28**. A systematic decrease of the magnitude of the heme bleach is observed upon increasing the L/P ratio when compared to the native **Cyt c**. This reveals the occurrence of various degrees of unfolding of **Cyt c** leading to an increased distance between heme and Trp. The time constants obtained for **Cyt c-CL** complexes with various L/P ratios are shown in **Table 4.3**. Compared to the native protein, the excited-state lifetime of Trp, τ_2 (~840 fs) is increased to ~ 4.48 ps for the **Cyt c-CL** complex having the L/P ratio of 75. This confirms the decrease of efficiency of FRET as the distance between Trp and heme increased from ~10 to 25 Å⁵⁸⁻⁵⁹ with increase of partial unfolding of the proteins in the presence of liposomes. The correlation between the increases of fluorescence intensity with increase of lifetime of Trp of various **Cyt c**-liposome complexes having L/P ratio of 50 is shown in **Figure 4.29**. An increase of the degree of unfolding of **Cyt c** is observed upon increase of anionic charge of the phospholipids,

4.3.5.3 Effect of Ionic Strength

The FTAS of **Cyt c**-liposome complexes were measured upon excitation at 280 nm by adding 0.1 M NaCl to understand the effect of ionic strength on the unfolding dynamics of the protein, The transient kinetic profiles of **Cyt c** and **Cyt c**-liposome complexes probed at the ESA maximum (425 nm) are shown in **Figure 4.30** with and without 0.1 M NaCl. The time constants obtained upon excitation at 280 nm for different

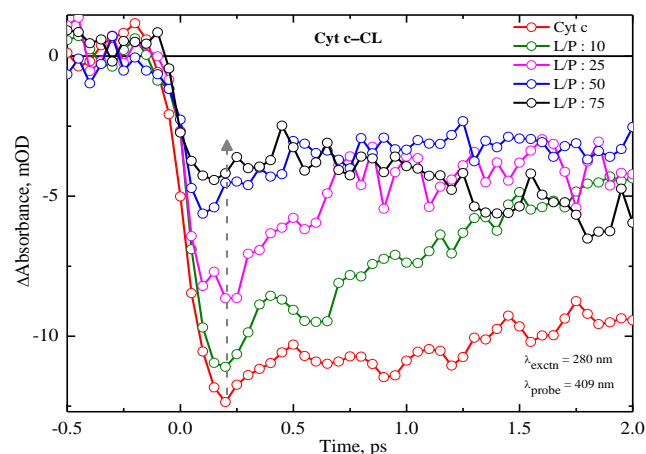


Figure 4.28 Femtosecond transient absorption decay of **Cyt c-CL** complexes with different L/P ratio probed at 409 nm by excitation at 280 nm.

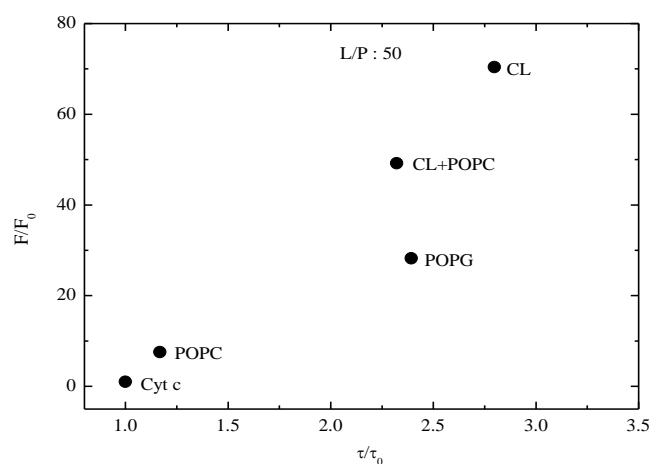


Figure 4.29 Correlation between the fluorescence intensity and lifetime of Trp for all the complexes having L/P ratio of 50.

Cyt c-liposome complexes in the presence of NaCl are also given in **Table 4.2**. In the presence of 0.1 M NaCl the dynamics are recovered back and similar to that of native **Cyt c** (**Figure 4.30**) reflecting the refolding of the partially unfolded **Cyt c** in the **Cyt c-CL**, **Cyt c-(CL+POPC)** and **Cyt c-POPG** complexes in the presence of NaCl. In addition it reveals that the charges of the phosphate group of lipids are essential in the **Cyt c**-liposome interaction and confirming the existence of electrostatic nature of interaction between **Cyt c** and negatively charged liposomes. However in the case of **Cyt c-POPC** complex, the dynamics are not changed by adding NaCl indicating the presence of weak hydrophobic interaction between **Cyt c** and **POPC**.

Table 4.3 Time constants obtained by global analysis using for Cyt c- CL complex having different L/P ratio upon excitation at 280 nm.

Cyt c (L/P :0)	Cyt c-CL (L/P :10)	Cyt c-CL (L/P :25)	Cyt c-CL (L/P :50)	Cyt c-CL (L/P :75)
$\tau_1 = 0.23$ ps	$\tau_1 = 0.27$ ps	$\tau_1 = 0.31$ ps	$\tau_1 = 0.38$ ps	$\tau_1 = 0.40$ ps
$\tau_2 = 0.84$ ps	$\tau_2 = 0.90$ ps	$\tau_2 = 1.77$ ps	$\tau_2 = 2.35$ ps	$\tau_2 = 4.48$ ps
$\tau_3 = 3.16$ ps	$\tau_3 = 3.94$ ps	$\tau_3 = 4.89$ ps	$\tau_3 = 5.49$ ps	$\tau_3 = 8.25$ ps
$\tau_4 = 8.30$ ps	$\tau_4 = 10.02$ ps	$\tau_4 = 18.23$ ps	$\tau_4 = 26.50$ ps	$\tau_4 = 30.00$ ps

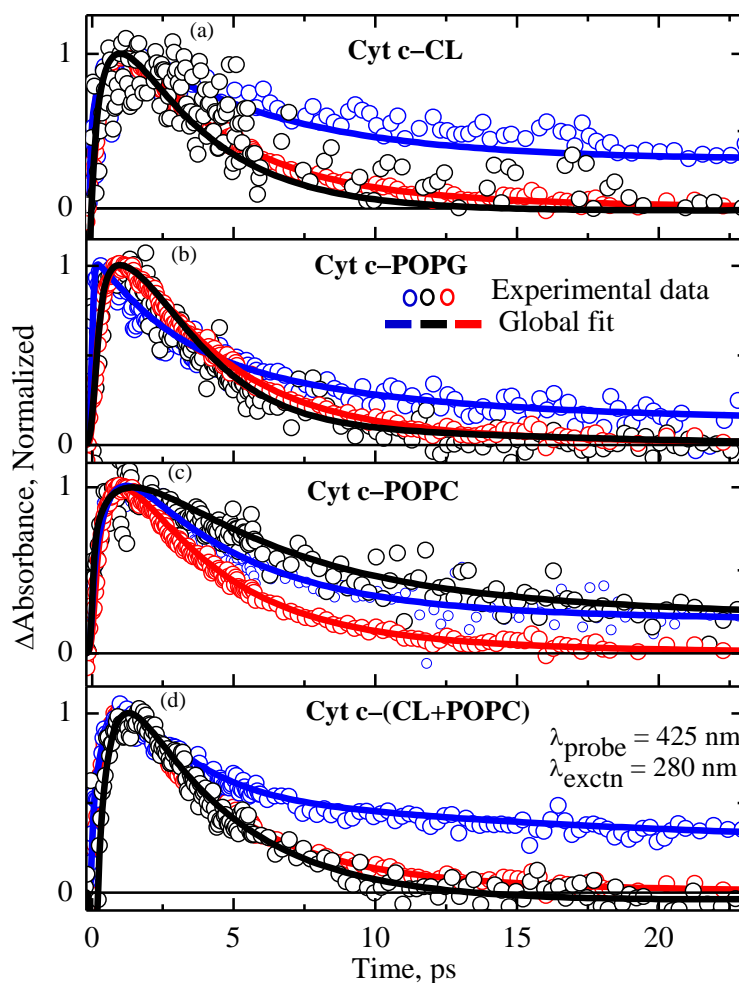


Figure 4.30 Comparison of time profile of **Cyt c** with **Cyt c-CL** (a), **Cyt c-POPG** (b), **Cyt c-POPC** (c) and **Cyt c-(CL+POPC)** (d) complexes having L/P ratio of 50 with and without 0.1 M NaCl in 25 mM HEPES buffer at pH 7.4 probed at 425 nm. Open circle depicts the experimental data and solid line represents the four-exponential fit obtained from global analysis with sequential model.

4.4 Conclusion

The interaction dynamics between the heme protein, **Cyt c** and various liposomes were investigated with steady state and time resolved optical spectroscopy by systematically increasing the anionic charge in the liposome. The excited state relaxation dynamics of heme in liposomes upon excitation at 385 nm were found to be similar to the native form reflecting that the heme environment is stabilized by the exchange of Met80 with other ligands (His33/26)^{32, 70}. The FTAS of the complexes obtained upon excitation at

280 nm, where Trp is selectively excited, showed an increase of excited state relaxation dynamics due to decrease of efficient FRET with increase of anionic charge of the lipid. Trp acted as an important probe to understand the dynamics of partial unfolding associated with the change in the axial ligand interaction and tertiary structure of **Cyt c** in liposomes. It is observed that the extent of partial unfolding mainly depends on the charges of the lipids and the refolding of the protein in the presence of 0.1 M NaCl suggests the importance of electrostatic interaction between **Cyt c** and liposomes.

4.5 Materials and Methods

Sample Preparation: Horse heart **Cyt c** was obtained from Sigma Aldrich. In order to completely remove any ferrous form present in the protein solution, potassium ferricyanide was added to the sample and was then passed through a Sephadex G-25 column to remove any remaining oxidizing agents and impurities. **POPG**, **POPC** and bovine heart **CL** and 4-(2-hydroxyethyl)-1-piperazineethanesulfonic acid (HEPES) were purchased from Sigma Aldrich and used without further purification. The lipids were dissolved in a 2:1 chloroform/methanol mixture. The solvent was removed by drying under the nitrogen atmosphere until a uniform thin, dry lipid film was formed. The film was kept in a vacuum desiccator overnight. The lipid film was then rehydrated with 25 mM HEPES buffer (pH 7.4) to obtain the desired concentration. The solution was then sonicated in an ice bath for two hours. The solution was centrifuged for 45 minutes at 13,000 rpm to remove all the impurities. The supernatant was then allowed to stabilize overnight. Different **Cyt c**–liposome mixtures were prepared by varying the concentration of liposome.

4.6 References

1. Kleingardner, J. G.; Bren, K. L., *Acc. Chem. Res.* **2015**, *48* (7), 1845-1852.
2. Bowman, S. E. J.; Bren, K. L., *Nat. prod. rep.* **2008**, *25* (6), 1118-1130.
3. Muenzner, J.; Toffey, J. R.; Hong, Y.; Pletneva, E. V., *J. Phys. Chem. B* **2013**, *117* (42), 12878-12886.
4. Kapetanaki, S. M.; Silkstone, G.; Husu, I.; Liebl, U.; Wilson, M. T.; Vos, M. H., *Biochemistry* **2009**, *48* (7), 1613-1619.
5. Hong, Y.; Muenzner, J.; Grimm, S. K.; Pletneva, E. V., *J. Am. Chem. Soc* **2012**, *134* (45), 18713-18723.
6. Ow, Y.-L. P.; Green, D. R.; Hao, Z.; Mak, T. W., *Nat. Rev. Mol. Cell. Biol* **2008**, *9* (7), 532-542.
7. Osman, C.; Voelker, D. R.; Langer, T., *J. Cell. Biol* **2011**, *192* (1), 7-16.
8. Belikova, N. A.; Tyurina, Y. Y.; Borisenko, G.; Tyurin, V.; Samhan Arias, A. K.; Yanamala, N.; Furtmüller, P. G.; Klein-Seetharaman, J.; Obinger, C.; Kagan, V. E., *J. Am. Chem. Soc* **2009**, *131* (32), 11288-11289.
9. Chen, D.; Zhang, X.-Y.; Shi, Y., *Biochem. J.* **2006**, *398* (2), 169-176.
10. Basova, L. V.; Kurnikov, I. V.; Wang, L.; Ritov, V. B.; Belikova, N. A.; Vlasova, I. I.; Pacheco, A. A.; Winnica, D. E.; Peterson, J.; Bayir, H.; Waldeck, D. H.; Kagan, V. E., *Biochemistry* **2007**, *46* (11), 3423-3434.
11. Elmore, S., *J. Toxicol. Pathol* **2007**, *35* (4), 495-516.
12. Vladimirov, Y. A.; Proskurnina, E. V.; Alekseev, A. V., *Biochemistry (Moscow)* **2013**, *78* (10), 1086-1097.
13. Elmore, S., *Toxicologic pathology* **2007**, *35* (4), 495-516.
14. Cai, J.; Yang, J.; Jones, D., *Biochim. et Biophys. Acta* **1998**, *1366* (1-2), 139-149.
15. Jiang, X.; Wang, X., *Annu. Rev. Biochem.* **2004**, *73*, 87-106.

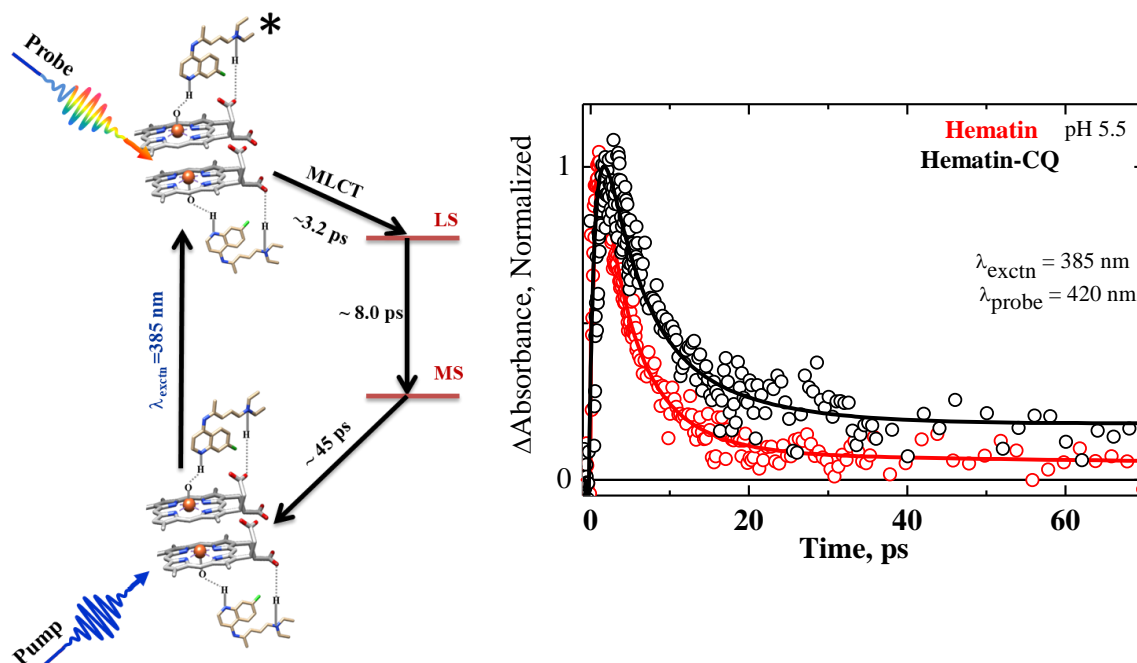
16. Orrenius, S.; Zhivotovsky, B., *Nat. Chem Biol.* **2005**, *1* (4), 188-189.
17. Kagan, V. E.; Bayir, H. A.; Belikova, N. A.; Kapralov, O.; Tyurina, Y. Y.; Tyurin, V. A.; Jiang, J.; Stoyanovsky, D. A.; Wipf, P.; Kochanek, P. M.; Greenberger, J. S.; Pitt, B.; Shvedova, A. A.; Borisenko, G., *Free Rad. Biol. Med.* **2009**, *46* (11), 1439-1453.
18. Zinser, E.; Sperka-Gottlieb, C. D.; Fasch, E. V.; Kohlwein, S. D.; Paltauf, F.; Daum, G., *J. Bacteriol.* **1991**, *173* (6), 2026-2034.
19. Chaurio, R.; Janko, C.; Muñoz, L.; Frey, B.; Herrmann, M.; Gaipf, U., *Molecules* **2009**, *14* (12), 4892.
20. Schlame, M.; Rua, D.; Greenberg, M. L., *Prog. Lipid Res.* **2000**, *39* (3), 257-288.
21. Pandiscia, L. A.; Schweitzer-Stenner, R., *J. Phys. Chem. B* **2015**, *119* (40), 12846-12859.
22. Govind, C.; Paul, M.; Karunakaran, V., *J. Phys. Chem. B* **2020**, *124* (14), 2769-2777.
23. Nantes, I. L.; Zucchi, M. R.; Nascimento, O. R.; Faljoni-Alario, A., *J. Biol. Chem.* **2001**, *276* (1), 153-158.
24. Rytömaa, M.; Kinnunen, P. K. J., *J. Biol. Chem.* **1995**, *270* (7), 3197-3202.
25. Tuominen, E. K. J.; Wallace, C. J. A.; Kinnunen, P. K. J., *J. Biol. Chem.* **2002**, *277* (11), 8822-8826.
26. Sinibaldi, F.; Howes, B. D.; Piro, M. C.; Polticelli, F.; Bombelli, C.; Ferri, T.; Coletta, M.; Smulevich, G.; Santucci, R., *J. Biol. Inorg. Chem* **2010**, *15* (5), 689-700.
27. Hanske, J.; Toffey, J. R.; Morenz, A. M.; Bonilla, A. J.; Schiavoni, K. H.; Pletneva, E. V., *Proc. Nat. Acad. Sci.* **2012**, *109* (1), 125-130.

28. Balakrishnan, G.; Hu, Y.; Spiro, T. G., *J. Am. Chem. Soc.* **2012**, *134* (46), 19061-19069.
29. Muenzner, J.; Pletneva, E. V., *Chem. Phys. Lipids* **2014**, *179*, 57-63.
30. Bergstrom, C. L.; Beales, P. A.; Lv, Y.; Vanderlick, T. K.; Groves, J. T., *Proc. Nat. Acad. Sci.* **2013**, *110* (16), 6269-6274.
31. Milazzo, L.; Tognaccini, L.; Howes, B. D.; Sinibaldi, F.; Piro, M. C.; Fittipaldi, M.; Baratto, M. C.; Pogni, R.; Santucci, R.; Smulevich, G., *Biochemistry* **2017**, *56* (13), 1887-1898.
32. Oellerich, S.; Lecomte, S.; Paternostre, M.; Heimburg, T.; Hildebrandt, P., *J. Phys. Chem. B* **2004**, *108* (12), 3871-3878.
33. Heimburg, T.; Marsh, D., *Biophys. J.* **1995**, *68* (2), 536-546.
34. Salamon, Z.; Tollin, G., *Biophys. J.* **1996**, *71* (2), 848-857.
35. Silkstone, G.; Kapetanaki, S. M.; Husu, I.; Vos, M. H.; Wilson, M. T., *Biochemistry* **2012**, *51* (34), 6760-6766.
36. Schweitzer-Stenner, R., *Biophysical reviews* **2018**, *10* (4), 1151-1185.
37. Rytömaa, M.; Kinnunen, P. K., *J. Biol. Chem.* **1994**, *269* (3), 1770-1774.
38. Sinibaldi, F.; Milazzo, L.; Howes, B. D.; Piro, M. C.; Fiorucci, L.; Polticelli, F.; Ascenzi, P.; Coletta, M.; Smulevich, G.; Santucci, R., *J. Biol. Inorg. Chem.* **2017**, *22* (1), 19-29.
39. Kawai, C.; Prado, F. M.; Nunes, G. L. C.; Di Mascio, P.; Carmona-Ribeiro, A. M.; Nantes, I. L., *J. Biol. Chem* **2005**, *280* (41), 34709-34717.
40. Lin, Y.-W.; Wang, J., *J. Inorg. Biochem* **2013**, *129*, 162-171.
41. Ascenzi, P.; Polticelli, F.; Marino, M.; Santucci, R.; Coletta, M., *IUBMB Life* **2011**, *63* (3), 160-165.
42. Kalanxhi, E.; Wallace, Carmichael J. A., *Biochem. J.* **2007**, *407* (2), 179-187.

43. Pandiscia, L. A.; Schweitzer-Stenner, R., *J. Phys. Chem. B* **2015**, *119* (4), 1334-1349.
44. McClelland, L. J.; Steele, H. B. B.; Whitby, F. G.; Mou, T.-C.; Holley, D.; Ross, J. B. A.; Sprang, S. R.; Bowler, B. E., *J. Am. Chem. Soc* **2016**, *138* (51), 16770-16778.
45. Oellerich, S.; Wackerbarth, H.; Hildebrandt, P., *J. Phys. Chem. B* **2002**, *106* (25), 6566-6580.
46. Das, T. K.; Mazumdar, S.; Mitra, S., *Euro. J. Biochem* **1998**, *254* (3), 662-670.
47. Bushnell, G. W.; Louie, G. V.; Brayer, G. D., *J. Mol. Biol.* **1990**, *214* (2), 585-595.
48. Lin, C.-M.; Li, C.-S.; Sheng, Y.-J.; Wu, D. T.; Tsao, H.-K., *Langmuir* **2012**, *28* (1), 689-700.
49. Tortorella, D.; Ulbrandt, N. D.; London, E., *Biochemistry* **1993**, *32* (35), 9181-9188.
50. Schön, P.; García-Sáez, A. J.; Malovrh, P.; Bacia, K.; Anderluh, G.; Schwille, P., *Biophys. J.* **2008**, *95* (2), 691-698.
51. Schejter, A.; George, P., *Biochemistry* **1964**, *3* (8), 1045-1049.
52. Mugnol, K. C. U.; Ando, R. A.; Nagayasu, R. Y.; Faljoni-Alario, A.; Brochsztain, S.; Santos, P. S.; Nascimento, O. R.; Nantes, I. L., *Biophys J* **2008**, *94* (10), 4066-4077.
53. Belikova, N. A.; Vladimirov, Y. A.; Osipov, A. N.; Kapralov, A. A.; Tyurin, V. A.; Potapovich, M. V.; Basova, L. V.; Peterson, J.; Kurnikov, I. V.; Kagan, V. E., *Biochemistry* **2006**, *45* (15), 4998-5009.
54. Babul, J.; Stellwagen, E., *Biochemistry* **1972**, *11* (7), 1195-1200.
55. Pandiscia, L. A.; Schweitzer-Stenner, R., *Chem. Comm* **2014**, *50* (28), 3674-3676.
56. Sanghera, N.; Pinheiro, T. J., *Protein Sci.* **2000**, *9* (6), 1194-1202.
57. Bräm, O.; Consani, C.; Cannizzo, A.; Chergui, M., *J. Phys. Chem. B* **2011**, *115* (46), 13723-13730.

58. Lee, J. C.; Engman, K. C.; Tezcan, F. A.; Gray, H. B.; Winkler, J. R., *Proc. Nat. Acad. Sci. U. S. A* **2002**, *99* (23), 14778.
59. Tsong, T. Y., *J. of Biol. Chem.* **1974**, *249* (6), 1988-1990.
60. Myer, Y. P., *Biochemistry* **1968**, *7* (2), 765-776.
61. Dragomir, I.; Hagarman, A.; Wallace, C.; Schweitzer-Stenner, R., *Biophys J* **2007**, *92* (3), 989-998.
62. Santucci, R.; Ascoli, F., *J. Inorg. Biochem.* **1997**, *68* (3), 211-214.
63. Snellenburg, J. J.; Laptinok, S.; Seger, R.; Mullen, K. M.; van Stokkum, I. H. M., *J. Stat. Softw.* **2012**, *49* (3), 22.
64. Karunakaran, V., *ChemPhysChem* **2015**, *16* (18), 3974-3983.
65. Negrerie, M.; Cianetti, S.; Vos, M. H.; Martin, J.-L.; Kruglik, S. G., *J. Phys. Chem. B.* **2006**, *110* (25), 12766-12781.
66. Zang, C.; Stevens, J. A.; Link, J. J.; Guo, L.; Wang, L.; Zhong, D., *J. Am. Chem. Soc.* **2009**, *131* (8), 2846-2852.
67. Consani, C.; Bräm, O.; van Mourik, F.; Cannizzo, A.; Chergui, M., *Chem. Phys.* **2012**, *396*, 108-115.
68. Ye, X.; Demidov, A.; Rosca, F.; Wang, W.; Kumar, A.; Ionascu, D.; Zhu, L.; Barrick, D.; Wharton, D.; Champion, P. M., *J. Phys. Chem. A.* **2003**, *107* (40), 8156-8165.
69. Bu, L.; Straub, J. E., *J. Phys. Chem. B.* **2003**, *107* (44), 12339-12345.
70. Colon, W.; Wakem, L. P.; Sherman, F.; Roder, H., *Biochemistry* **1997**, *36* (41), 12535-12541.
71. Fisher, W. R.; Taniuchi, H.; Anfinsen, C. B., *J. Biol. Chem.* **1973**, *248* (9), 3188-3195.
72. Dickerson, R. E.; Takano, T.; Eisenberg, D.; Kallai, O. B.; Samson, L.; Cooper, A.; Margoliash, E., *J. Biol. Chem.* **1971**, *246* (5), 1511-1535.

Interaction Dynamics of Hematin with Antimalarial Drugs: An Ultrafast Investigation



5.1 Abstract

The malaria parasite digests host erythrocyte **Hb** and produce free heme during the intra-erythrocytic stage of its lifecycle. As free heme is toxic to the parasite, it will be converted into hemozoin by crystallization. The antimalarial drug is used to prevent the crystallization by binding with heme. Recently the scientific community is actively exploring the efficacy of the antimalarial drug, hydroxyl chloroquine for the treatment of COVID-19, caused by a novel coronavirus, SARS-CoV-2. As the malaria parasite, the viral protein attacks the **Hb** and degrades the protein into heme and amino acids. Hence

the understanding of the underlying mechanism of the interaction dynamics between the heme and antimalarial drugs are important for the design of new drugs for malaria as well as COVID-19. Here the interaction dynamics between the **Hematin** and antimalarial drugs including chloroquine (**CQ**) and mefloquine (**MFQ**) have been investigated in pH 5.5 and 7.0 using steady-state and time-resolved absorption and emission spectroscopy. The observation of quenching of fluorescence and no significant changes in the fluorescence lifetime of **CQ** with increasing concentration of **Hematin** indicates the formation of a ground-state complex. The transient absorption spectra of the complex showed the formation of radical cation of porphyrin at ~640 nm and signature of formation of low spin state of iron during ~ 450 fs. It is inferred that the relaxation pathway to the ground state comprises predominantly the involvement of multiple electronic spin states rather than the vibrational relaxation process based on spectral signature and global analysis. The longer relaxation dynamics of the complex compared to the **Hematin** reveals the stabilization of the complex by non-covalent interaction between the **Hematin** and drug leading to prevent the formation of hemozoin.

5.2 Introduction

Malaria¹ is one of the most deadliest disease caused by the infection of *Plasmodium* species and spread by female anopheles mosquitos. There are six species of the genus *Plasmodium* infecting human and among which *Plasmodium falciparum*¹ caused most of the malaria death and severe disease. According to the World Health Organization, it infects over 200 million people and caused 430,000 deaths worldwide in 2017.² During the blood stage of the malaria infection, the *Plasmodium* species utilizes **Hb** as its main nutrient source. The complex life cycle³ of malaria parasite in the human is shown in **Figure 5.1**. It undergoes two development stages where it reproduces sexually in mosquitoes and asexually in vertebrates. During the blood meal, an infected mosquito injects sporozoites

into the host blood. Then the sporozoites travel to the liver of the host, where it enters into liver cells or hepatocytes.

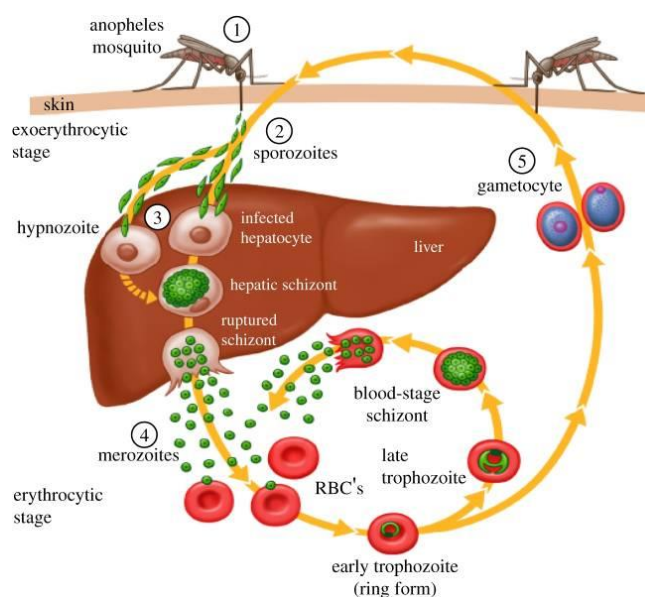


Figure 5.1 Life cycle of the malaria parasite showing the various stages in human body. The Figure is copied from Ref. 1.

The parasites then release merozoites into the blood stream and begin asexual reproduction in red blood cells (RBC). During this stage, the parasites digest a large amount of the host's **Hb** for the amino acids⁴ leading to an excess of free heme, ferroprotoporphyrin (Fe(II)PPIX), which is toxic to the parasite.⁵ The parasites oxidize the Fe(II)PPIX to Fe(III)PPIX undergoing dimerization and crystallization leading to form an insoluble by-product known as hemozoin or malarial pigment.⁶⁻⁷ It undergoes multiplication in the RBC and conversion into the sexual stages⁸ and infects mosquitoes to begin the cycle again.

A variety of spectroscopy has been used to characterize the structure of hemozoin and believed to be a coordination polymer.⁹⁻¹³ Pagola et al.⁷ determined the crystal structure of hemozoin consisting of **Hematin** dimers, where propionate group of each heme unit coordinated to the iron center of an adjacent heme moiety and the second propionate group coordinated to the propionic acid side chain of the heme in another

dimer through hydrogen bonding (**Figure 5.2**). Various crystallographic and spectroscopic analysis indicated that the crystal structure of hemozoin is similar to that of a synthetic bio-mineral, β -**Hematin**.¹⁴ In β -**Hematin**, the propionate side chain of one **Hematin** coordinated to the iron center of the other and form **Hematin** dimer.¹⁵ Though the structure of hemozoin is known, the mechanism of its formation remains unclear.^{13, 16-17} The molecular structure of β -**Hematin** was resolved at the single atom level⁷ in which Fe atom exists in a ferric high spin state.¹⁵

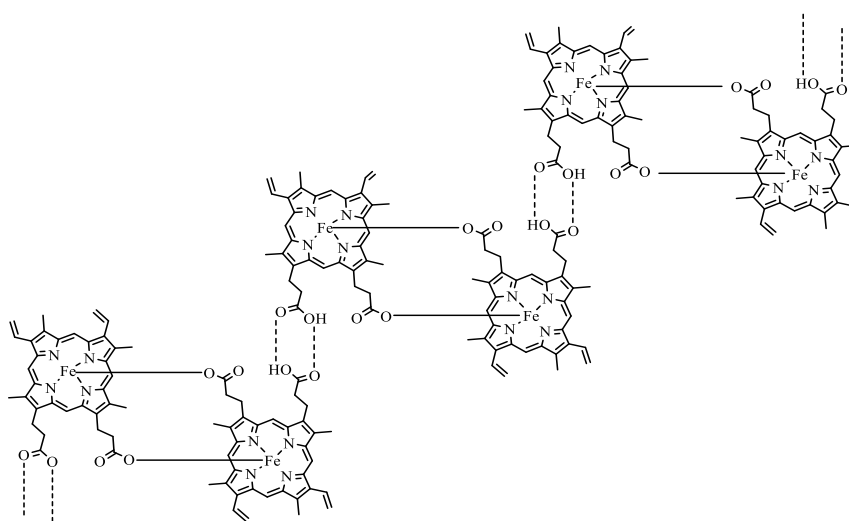


Figure 5.2 Chemical structure of hemozoin solved from powder X-ray diffraction. Figure is reproduced from Ref. 7.

5.2.1 Antimalarial Drugs

The treatment of malaria was difficult for several centuries until quinine (QN) had been isolated. It was obtained from the tree bark by purification and was used as an effective drug against malaria.¹⁸ Later QN was replaced by **CQ** (**Figure 5.3**) as it has similar structure and lower toxicity.¹⁹ Subsequently based on the QN structure various antimalarial drugs such as primaquine, mefloquine, etc. were discovered (**Figure 5.3**).²⁰ **CQ** and amodiaquine are 4-aminoquinolines based drugs. The main action of these drugs occurs inside the parasite lysosome and inhibit the parasite enzyme heme polymerase and

thus protects the host's heme from being converted to hemozoin.²¹ Primaquine is a derivative of 8-aminoquinoline and the mechanism of primaquine's antimalarial activity is not clear. It is believed that its antimalarial activity is due to interference with the parasite's DNA structure and the disruption of parasite's mitochondrial membranes and causing oxidative damage to the cell by the generation of ROS.²² Mefloquine (**MFQ**) is an arylaminoalcohol based antimalarial drug developed during 1970s and having blood schizonticidal properties.²³

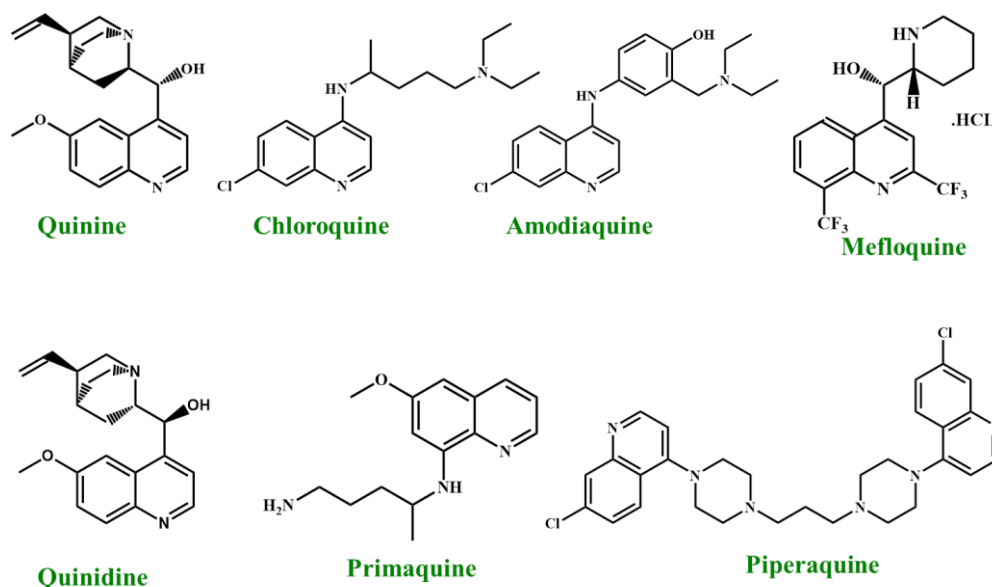


Figure 5.3 Chemical structures of common quinoline antimalarial drugs.

5.2.2 Hematin Dimers

In 1947, Clarke and Shack observed that heme exhibited complex behaviour in aqueous solution.²⁴ Further, in 1970, the spectrophotometric study on aqueous solutions of Fe(III)PPIX by Brown, Dean, and Jones showed marked changes in the Soret band with increase of concentration. Upon increase of concentration the broadening of Soret band was observed and assigned to the formation of aggregation called as a μ -oxo dimer.²⁵⁻²⁷ Later, in 1975, O'Keeffe et al.²⁸ synthesized and isolated μ -oxo dimers and

characterized by ^1H NMR, and UV–Vis absorption spectroscopy. In μ -oxo dimers, there is a linkage between Fe(III) and oxygen. The chemical structure of **Hematin** μ -oxo dimer is shown in **Figure 5.4 III**. In 2009, Egan et al.²⁹ reported that the UV–Vis absorption spectrum of **Hematin** in 40% (v/v) aqueous DMSO at pH 10 closely resembles the μ -oxo dimer reported by O’Keeffe et al.²⁸ Whereas, in aqueous MeOH at pH 10, the UV–Vis spectrum was different from that in aqueous DMSO and showed similarity to that of π - π dimer (**Figure 5.4 II**) in which two heme units with the $\text{H}_2\text{O}/\text{OH}$ axial ligands directed outward.³⁰

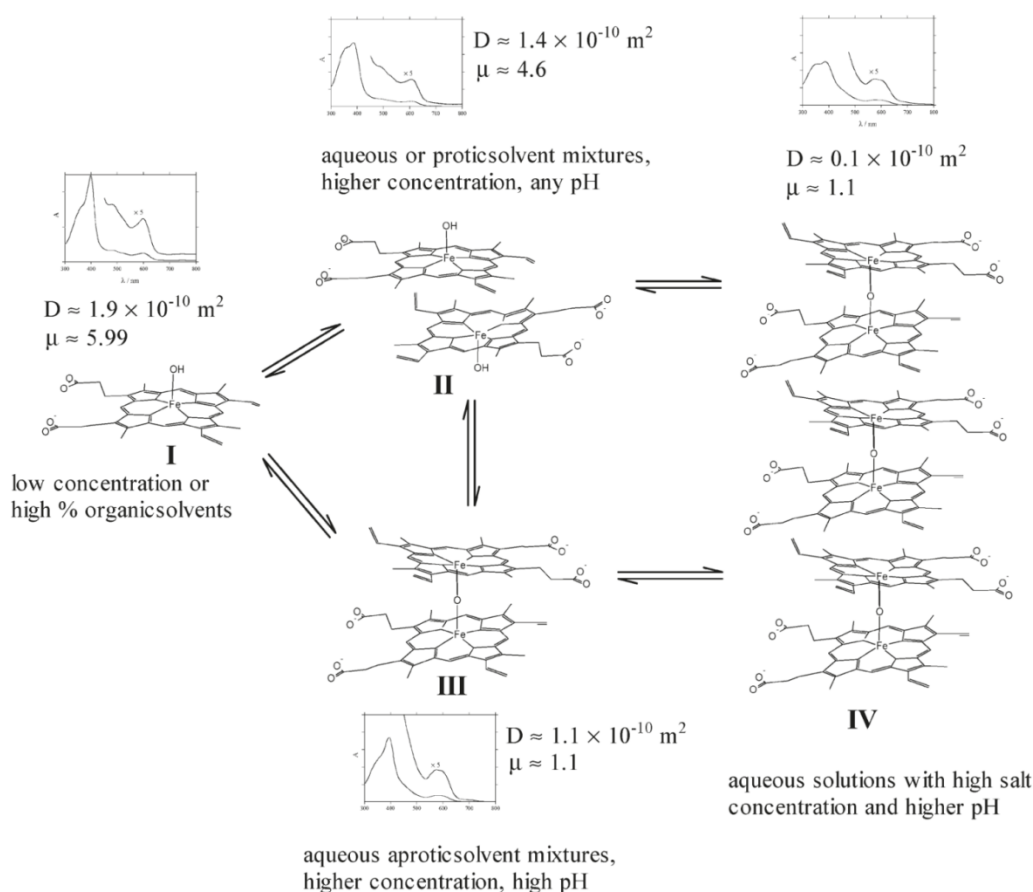


Figure 5.4 Different forms of **Hematin** in aqueous and mixed aqueous solution along with characteristic UV–Vis absorption spectra, diffusion coefficients and magnetic moments. Figure is copied from Ref. 29.

Thus the π - π dimer will not form higher aggregates in aqueous solution.²⁶ In the high salt concentrations, large numbers of aggregates of the μ -oxo dimers (**Figure 5.4 IV**) were formed.^{27, 29}

5.2.3 Interaction of Antimalarial Drugs with Hematin

The antimalarial activity of several types of drugs including **CQ** is based on the inhibition of crystallization of **Hematin** to hemozoin.³¹⁻³³ It was observed that 4-aminoquinoline moiety of **CQ** and related antimalarial drugs are important in forming complex with free heme.³⁴⁻³⁵ The complex formation between **CQ** and **Hematin**, was first reported by Cohen et al.³⁶ in 1960. UV-Vis³⁷, NMR³⁸, Mössbauer spectroscopy³⁹ and equilibrium dialysis experiments provided substantial evidence for the formation of complex between **CQ** and **Hematin**. NMR spectroscopy was used as a major tool for investigating the binding interaction quinoline drugs such as **CQ**, **QN** and **QD** with both Fe(III)PPIX and Fe(III) uroporphyrin.^{38, 40-41} NMR spectra of quinoline antimalarials were strongly affected in the presence of paramagnetic Fe(III)PPIX and resulted paramagnetic shifts in the NMR spectra.⁴¹ Fitch⁴² and co-workers reported the equilibrium constant for Fe(III)PPIX-**CQ** interaction for the first time using equilibrium dialysis and obtained an association constant of 8.5 and a **CQ**:Fe(III)PPIX ratio of 1:2. Villiers et al.⁴³ provided the crystal structure of Fe(III)PPIX with an antimalarial halofantrine for the first time and observed that the hydroxyl group of the drug was coordinated to the Fe(III) center of the heme monomer. Whereas the phenanthrene group of the drug interacted with the porphyrin through π -stacking and propionate group of heme formed hydrogen bonding with protonated nitrogen of the drug. In 2017, Vekilov et al.⁴⁴ investigated the interaction of five antimalarial drugs **QN**, **CQ**, pyronaridine (**PY**), amodiaquine (**AQ**), **MFQ**, and artemisinin (**ART**) with **Hematin** crystal using time-resolved in situ atomic force microscopy (AFM) to understand the **Hematin** growth inhibition by the drugs.

They observed that the drugs specifically interact with the growing edge of the β -**Hematin** crystals through three distinct modes of action namely step pinning, kink blocking, and step bunch induction. The reduction of nucleation of new layers (J_{2D}) and velocity of advancing steps (v) with increasing drug concentration (**Figure 5.5**) suggested that the drugs inhibit 2D nucleation of new layers and step motion by a step-pinning mechanism.

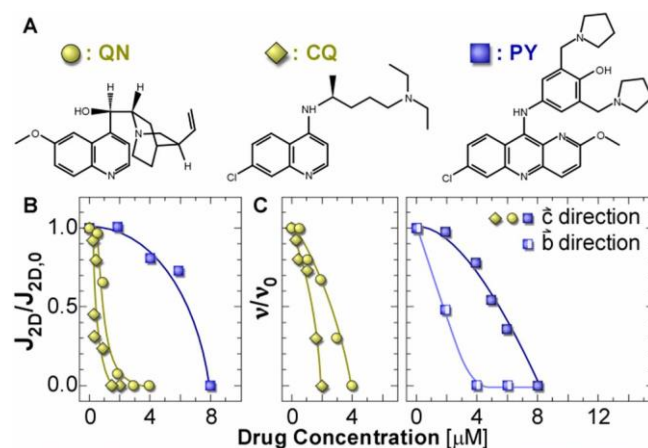


Figure 5.5 The structures of QN, CQ, and PY (A). A decrease in the J_{2D} relative to that in the absence of any drug, $J_{2D,0}$, with increasing drug concentration (B) and a decrease in step velocity relative to that in the absence of any drug, with increasing drug concentration (C). The Figure is copied from Ref. 44.

In 2010 Crespo et al.⁴⁵ proposed that **Hematin** forms a cofacial sandwich complex with **CQ** in 2:1 ratio by preventing crystallization of hemozoin. Recently, Cheng et al.⁴⁶ used femtosecond pump-probe transient absorption microscopy to selectively image β -**Hematin** in RBC. They quantitatively analyzed the amount of hemozoin at different infection stages in RBCs by single-shot transient absorption imaging. They found that β -**Hematin** exhibited significantly higher transient absorption intensity than RBC (**Figure 5.6** (c)). Upon selective excitation at 520 nm, the β -**Hematin** showed distinctively slower decay dynamics than RBC as shown in **Figure 5.6**. Hence, the transient decay could help as a spectroscopic signature to distinguish the β -**Hematin**

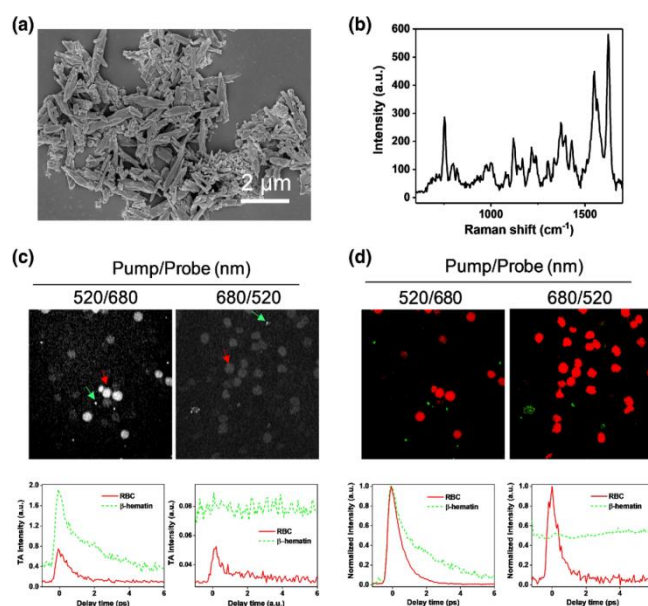


Figure 5.6 SEM image of the synthesized β -Hematin (a) and Raman spectrum of β -Hematin at laser wavelength of 785 nm (b). Time-resolved pump-probe images of β -Hematin and RBC mixture at pump wavelength 520 and 680 nm (c). β -Hematin is artificially coloured green and RBCs in red. The kinetics of both β -Hematin and RBC are also shown. The Figure is copied from Ref. 46.

from RBCs. Another approach for imaging the heme in live cells is based on the fact that heme enhances the FRET process of the fluorophores.⁴⁷⁻⁴⁸ The resistance of malaria parasites to the multidrug demands a great need for the design of novel, inexpensive and effective antimalarial drugs. Importantly, the viral protein of SARS-CoV-2 which is spreading the respiratory disease COVID-19, attacks the **Hb** similar to the malaria parasite. Hence the understanding of the underlying mechanism of the interaction dynamics between the heme and antimalarial drugs is important for the design of new drugs for malaria as well as COVID-19.

Here the interaction dynamics between the **Hematin** (Figure 5.7) and antimalarial drugs **CQ** and **MFQ** (Figure 5.3) have been investigated in pH 5.5 and 7.0 using steady-state and time-resolved absorption and emission spectroscopy. The observation of quenching of fluorescence and no significant changes in the fluorescence lifetime of **CQ**

with increasing concentration of **Hematin** indicated the formation of a ground state complex. The transient absorption spectra of the complex showed the formation of radical cation of porphyrin at ~640 nm and formation of low spin state of iron atom in the excited-state. The relaxation pathway to the ground state comprised predominantly the

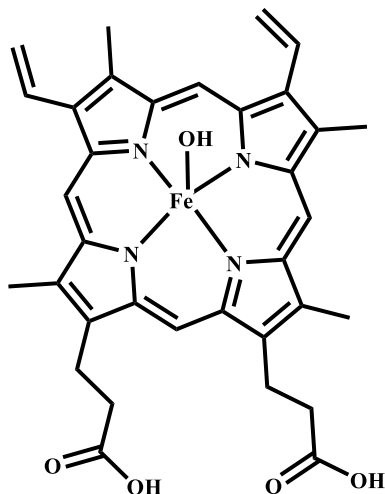


Figure 5.7 Chemical structure of **Hematin**.

involvement of multiple electronic spin states rather than the vibrational relaxation process. The longer relaxation dynamics of the complex compared to the **Hematin** reveals the stabilization of the complex by non-covalent interaction between the **Hematin** and drug leading to prevent the formation of hemozoin. These basic insights could help to develop antimalarial drugs that can overcome the parasite resistance.

5.3 Results and Discussion

5.3.1 Stationary Absorption Spectra

The steady-state absorption spectra of **Hematin** and **Hematin-CQ** complex having a ratio of 2:1 were measured at pH 5.5 and pH 7.0 and shown in **Figure 5.8**. **Hematin** exhibited an absorption maximum at around 390 nm with a shoulder around 358 nm where the degeneracy of Soret absorption band is broken by excitonic coupling in the ground state by the formation of the π - π dimer of **Hematin** with H₂O/OH as the axial

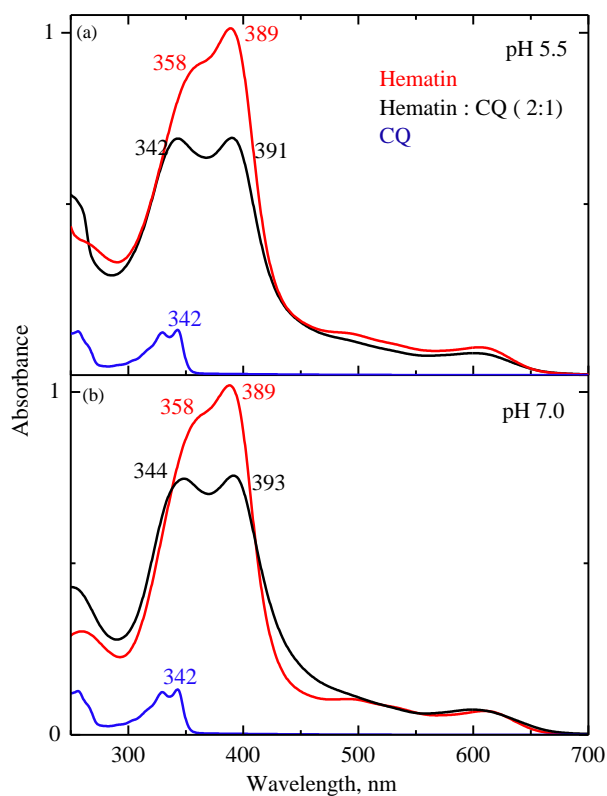


Figure 5.8 Steady-state absorption spectra of **Hematin–CQ** complex (2:1) at pH 5.5 (a) and pH 7.0 (b) at room temperature. Absorption spectra of **Hematin** (red), **CQ** (blue) are also shown.

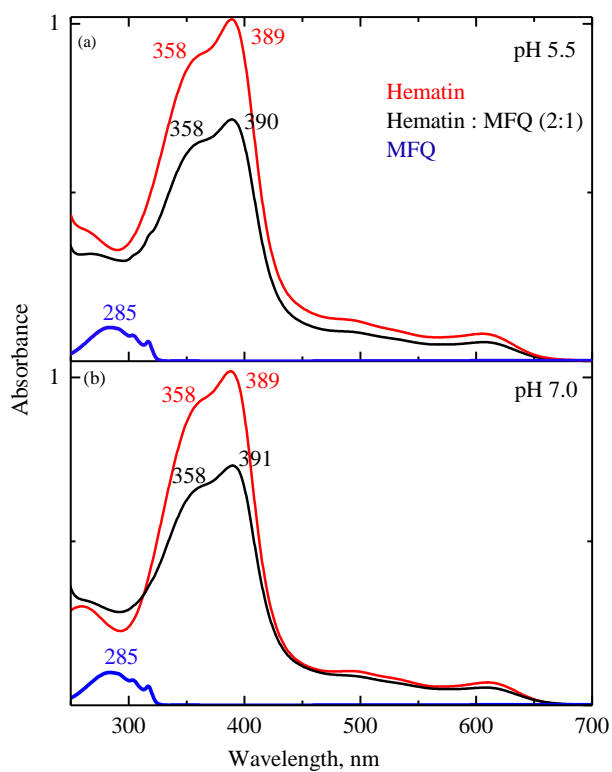


Figure 5.9 Steady-state absorption spectra of **Hematin–MFQ** complex (2:1) at pH 5.5 (a) and pH 7.0 (b) at room temperature. Absorption spectra of **Hematin** (red) and **MFQ** (blue) are also shown.

ligand.²⁹ It showed a characteristic CT absorption band at ~ 610 nm similar to that of **Mb** and **Hb** having the Fe atom in high spin state. Upon addition of **CQ**, the decrease of absorbance, shifting of maximum to 391 (393) nm in pH 5.5 (7.0), and appearance of a peak at around 340 nm due to **CQ** revealed the formation of a ground state complex. The absorption spectra of **Hematin** was also measured upon addition of **MFQ** at pH 5.5 and 7.0 exhibiting the decrease of absorbance and shifting of maximum to 390 (391) nm in pH 5.5 (7.0) (**Figure 5.9**).

5.3.2 Fluorescence Spectra

It is known that **Hematin** is non-emissive either from the B and Q states or from the CT state as the fluorescence lifetimes of the metalloporphyrins are shorter due to the electron transfer from the porphyrin macrocyclic ring to the metal iron atom. The fluorescence spectra of **CQ** were measured upon addition of **Hematin**. The fluorescence intensity of **CQ** in pH 5.5 is lesser compared to that of pH 7 for a particular concentration as the fluorescence quantum yields of **CQ** vary with pH.⁴⁹⁻⁵⁰ The systematic decrease of fluorescence intensity of **CQ** was observed with increase of concentration of **Hematin** in both the pH (**Figure 5.10**).

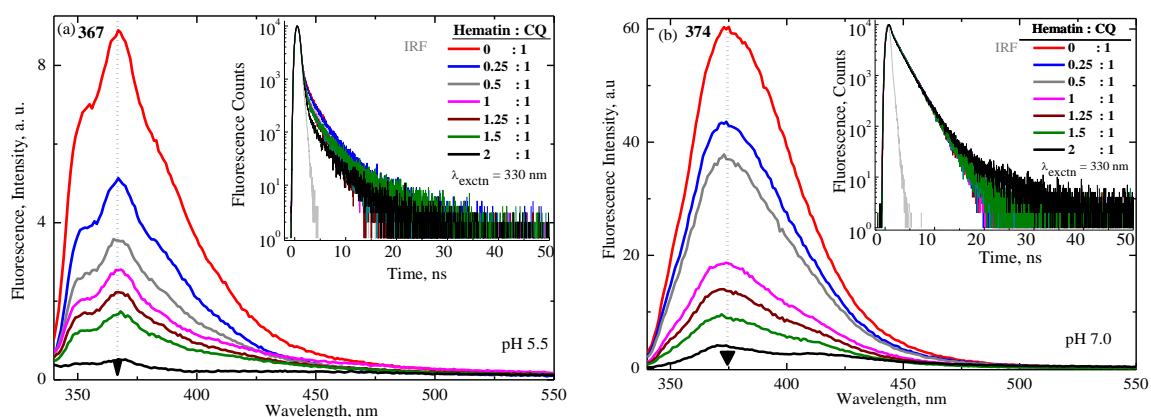


Figure 5.10 Fluorescence spectra of **Hematin–CQ** at pH 5.5 (a), and pH 7.0 (b) at room temperature. Inset: fluorescence kinetic profiles upon exciting at 330 nm.

Stern–Volmer plot (**Figure 5.11**) of fluorescence quenching of **CQ** with increase of concentration of **Hematin** shows a nonlinear behaviour (positive deviation) suggesting the existence of more than one heme binding site per drug molecule.⁵¹ K_{SV} is the Stern–Volmer quenching constant obtained from the equation $F_0/F = 1 + K_{SV} \times [\text{Hematin}]$ and found to be 3.00×10^5 and $1.82 \times 10^6 \text{ M}^{-1}$ at pH 5.5 and 7.0 respectively.

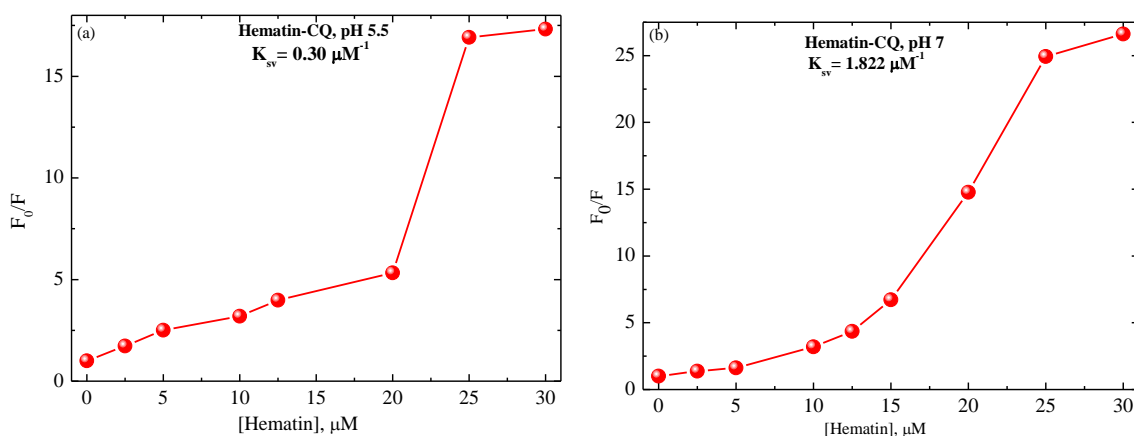


Figure 5.11 Stern–Volmer plot of quenching of fluorescence of **CQ** by **Hematin** at pH 5.5 (a) and 7.0 (b).

The fluorescence lifetime of **CQ** and **Hematin–CQ** complexes were measured upon excitation at 330 nm using a nanosecond LED source. The fluorescence kinetic profile of **Hematin–CQ** complex at pH 5.5 and 7.0 probed at the emission maxima are shown in the inset of **Figure 5.10**. The fluorescence lifetime of **CQ** alone at pH 7.0 were found to be $\tau_1 = 0.07 \text{ ns}$ (20.63%), $\tau_2 = 2.45 \text{ ns}$ (79.37%), attributed to the bi–protonated and mono–protonated species.⁵² Whereas at pH 5.5, it showed single exponential time constant of 0.08 ns consistent with the literature.⁵³ Upon addition of **Hematin**, no significant changes in the fluorescence lifetime of **CQ** were observed. The decrease of fluorescence intensity without change in the fluorescence lifetime upon addition of **Hematin** indicates the occurrence of static quenching by the formation of a ground state complex between **Hematin** and **CQ**. Since the fluorescence quantum yield of **MFQ**.

(0.017)⁵⁰ is lower than the **CQ** (0.17)⁴⁹, the quenching of fluorescence intensity of **MFQ** upon addition of **Hematin** was difficult to observe.

5.3.3 Femtosecond Transient Absorption Spectra

The femtosecond time-resolved transient absorption spectra $\Delta A(\lambda, t)$ of **Hematin** at pH 5.5 and 7.0 upon excitation at 385 nm were measured and shown in **Figure 5.12** and **5.13**. The panel a of **Figure 5.12** depicts the spectral evolution of the **Hematin** at various time delays after the photo-excitation starting from 0 to 1.0 ps. The spectrum at 0.2 ps is dominated by a bleach band at ~ 390 nm due to the depopulation of the ground state, which is not seen clearly due to the scattering of laser excitation, and an ESA at 415 to 570 nm.

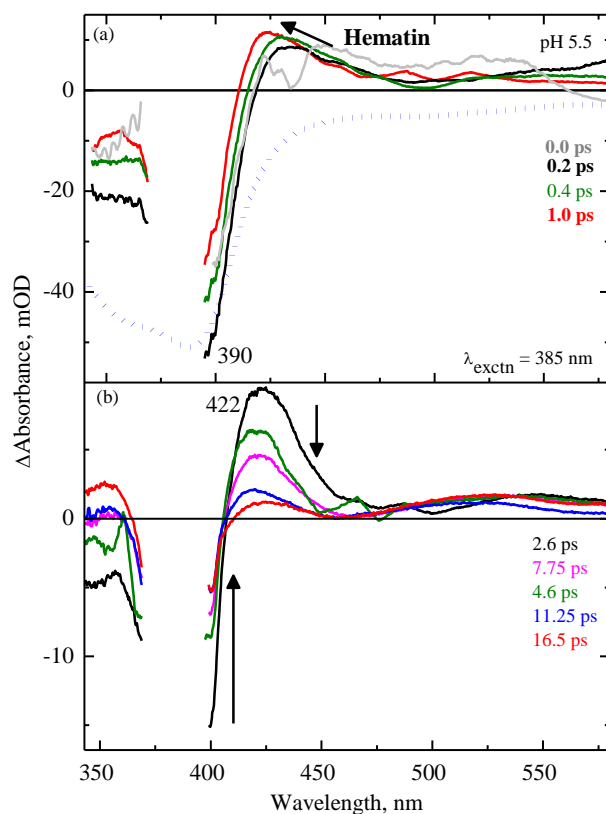


Figure 5.12 FTAS of **Hematin** at pH 5.5 obtained upon excitation at 385 nm. The different delay times are given and the arrows show the spectral evolution. The steady-state absorption spectrum is also shown (dotted blue line).

In the shorter time scales, when the delay time is increased to 1.0 ps, the decrease of the bleach band and an increase of ESA along with a narrowing of spectral bandwidth and

shifting toward blue region are observed indicating the occurrence vibrational cooling process in the **Hematin** during relaxation dynamics. In panel b, when the delay time increased from 2.6 to 16.5 ps, the overall spectral intensity is decreased. In the case of pH 7.0 (**Figure 5.13**), the spectral features of FTAS of the **Hematin** is similar to that of at pH 5.5. The FTAS of the **Hematin** upon complexation with **CQ** and **MFQ** (2:1) at pH 5.5 and 7.0 were measured by exciting at 385 nm and shown in **Figure 5.13** to **5.17**. It is observed that the spectral evolution of the complexes at both pH are identical to that of **Hematin**. However the excited–state relaxation dynamics of **Hematin** are longer upon complexation with **CQ** compared to **MFQ**.

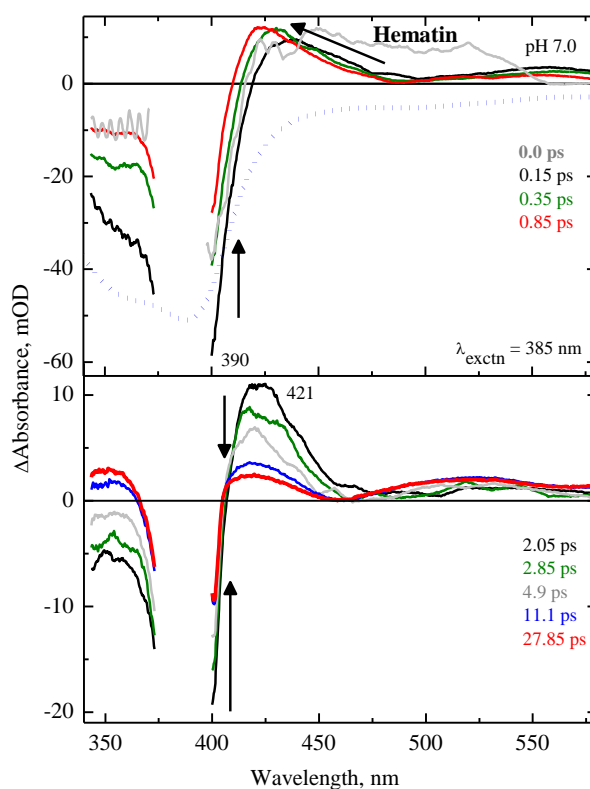


Figure 5.13 FTAS of **Hematin** at pH 7.0 obtained upon excitation at 385 nm. The steady–state absorption spectrum is also shown (dotted blue line).

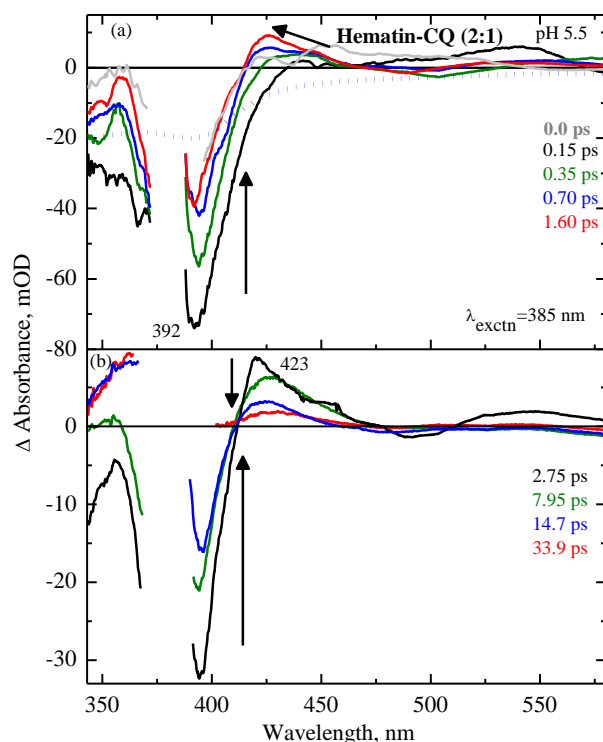


Figure 5.14 FTAS spectra of **Hematin–CQ** complex at pH 5.5 obtained upon excitation at 385 nm. The steady–state absorption spectrum is also shown (dotted blue line).

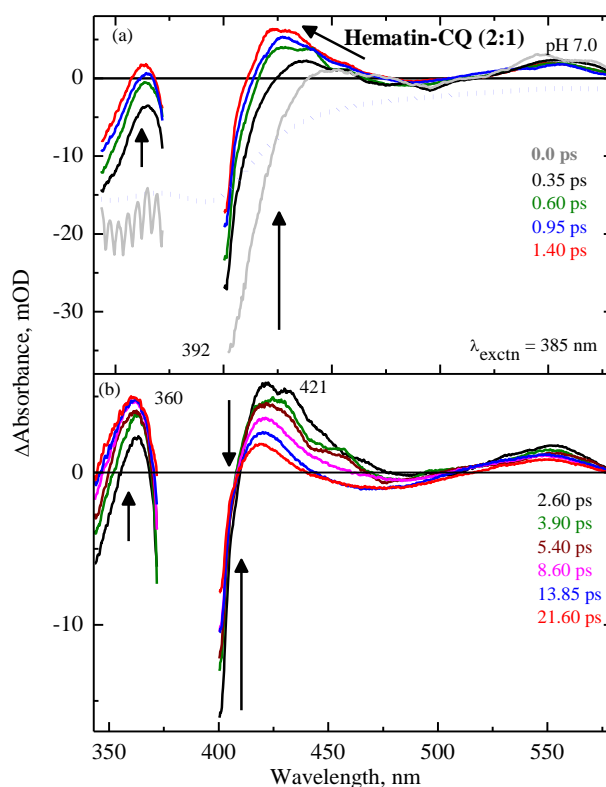


Figure 5.15 FTAS of **Hematin–CQ** complex at pH 7.0 obtained upon excitation at 385 nm. The steady–state absorption spectrum is also shown (dotted blue line).

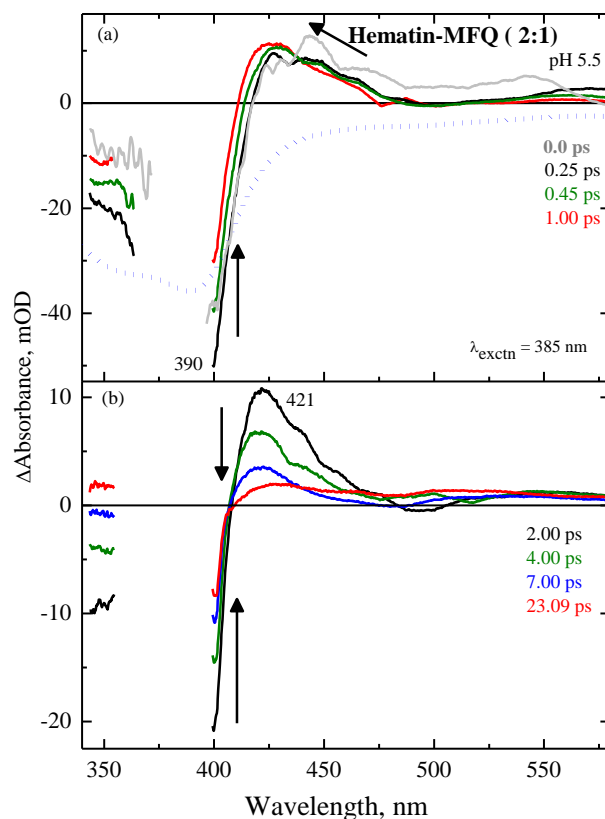


Figure 5.16 FTAS of Hematin–MFQ complex at pH 5.5 obtained upon excitation at 385 nm. The stationary absorption spectrum is also shown (dotted blue line)

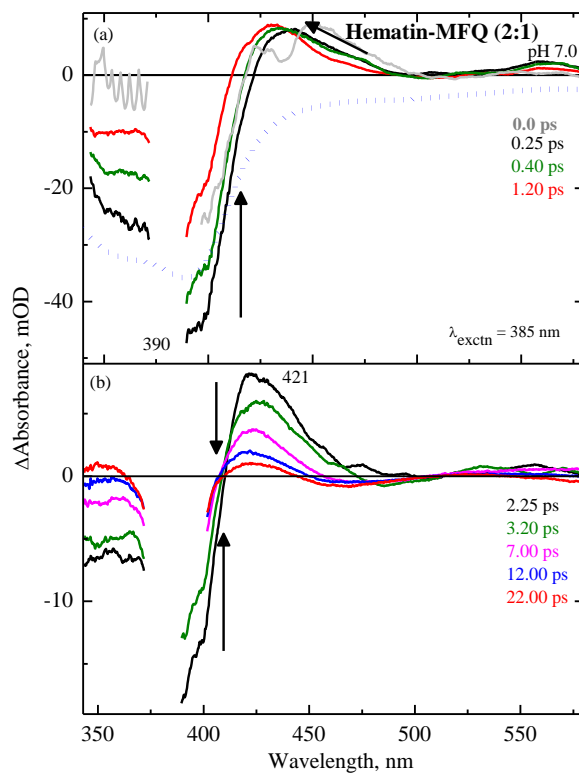


Figure 5.17 FTAS of Hematin–MFQ complex at pH 7.0 obtained upon excitation at 385 nm. The steady–state absorption spectrum is also shown (dotted blue line)

5.3.3.1 Analysis of Femtosecond Transient Absorption Spectra

The analysis of FTAS of **Hematin** and **Hematin**–drug complexes was performed with the R package TIMP and its graphical user interface of GLOTARAN⁵⁴ with sequential model. All the FTAS is compensated for chirp of the white light by determining the time zero using coherent artifact observed in the solvent. In order to estimate the number of kinetic parameters, SVD was performed before global analysis. Four exponential components were optimally obtained for **Hematin** and **Hematin**–drug complexes for both pH and the time constants are shown in **Table 5.1**. The heat map of FTAS, time profile and exponential fit at maxima of GSB and ESA along with residual obtained from global sequential analysis of **Hematin** and **Hematin-CQ** complex at pH 5.5 and pH 7.0 are shown in **Figure 5.18** to **5.21**. The DAS of the corresponding time constants are shown in **Figure 5.22** and **5.23** and it displayed the common features of transient absorption spectra. It is observed from the **Table 5.1** that all the time constants of **Hematin-CQ** complex at pH 5.5 are longer than that of the complex at pH 7.0 which is longer than that of the **Hematin** alone. Whereas the time constants of **Hematin-MFQ** are similar to that of **Hematin**. The time profile of **Hematin**, **Hematin-CQ** and **Hematin-MFQ** complex at pH 5.5 and 7.0 probed at the ESA maximum (420 nm) along with global fit are shown in **Figure 5.24** and **5.25** for comparison.

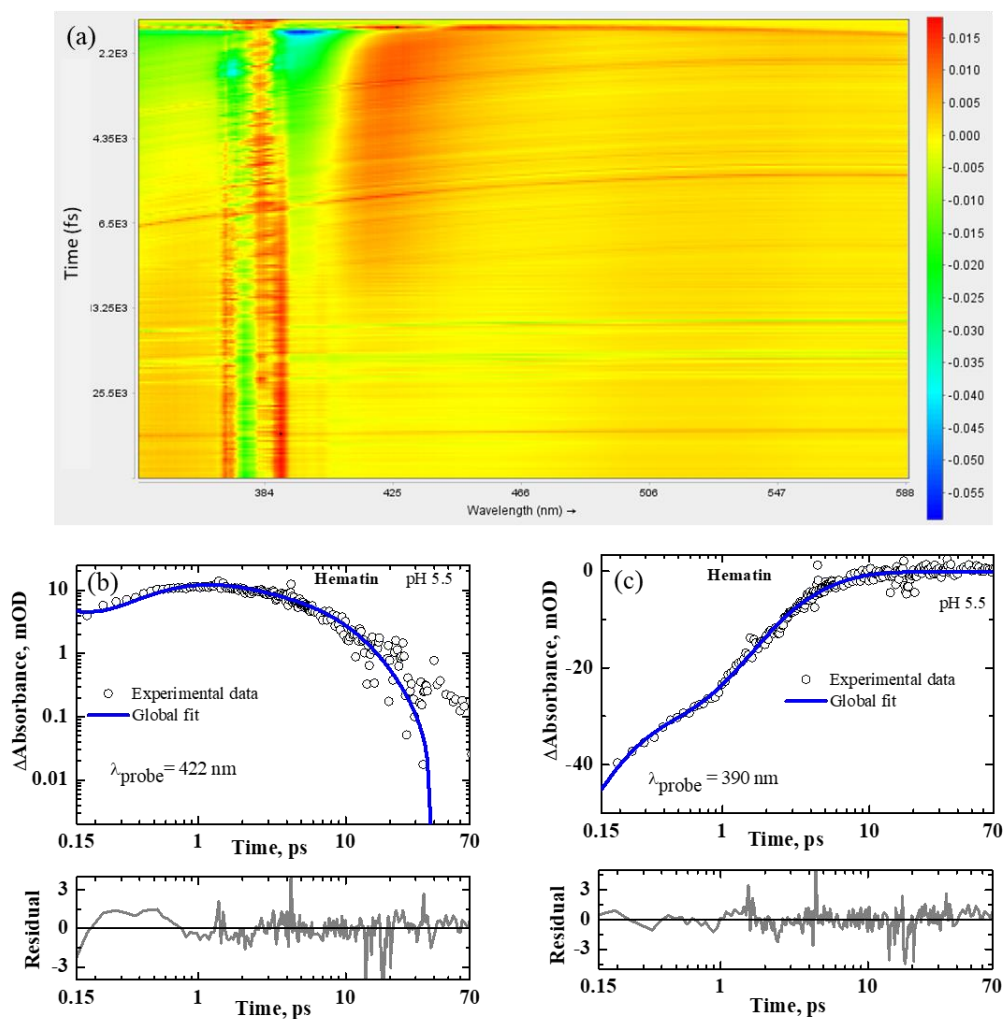


Figure 5.18 Heat map of FTAS of **Hematin** at pH 5.5 as a function of time delay (vertical) and probe wavelength (horizontal) in 70 ps time window upon excitation at 385 nm (a). The time profile at ESA maximum (b) and GSB maximum (c) (open circles) along with four-exponential fit (solid line) and residual (ash coloured solid line, lower panel), obtained from global analysis.

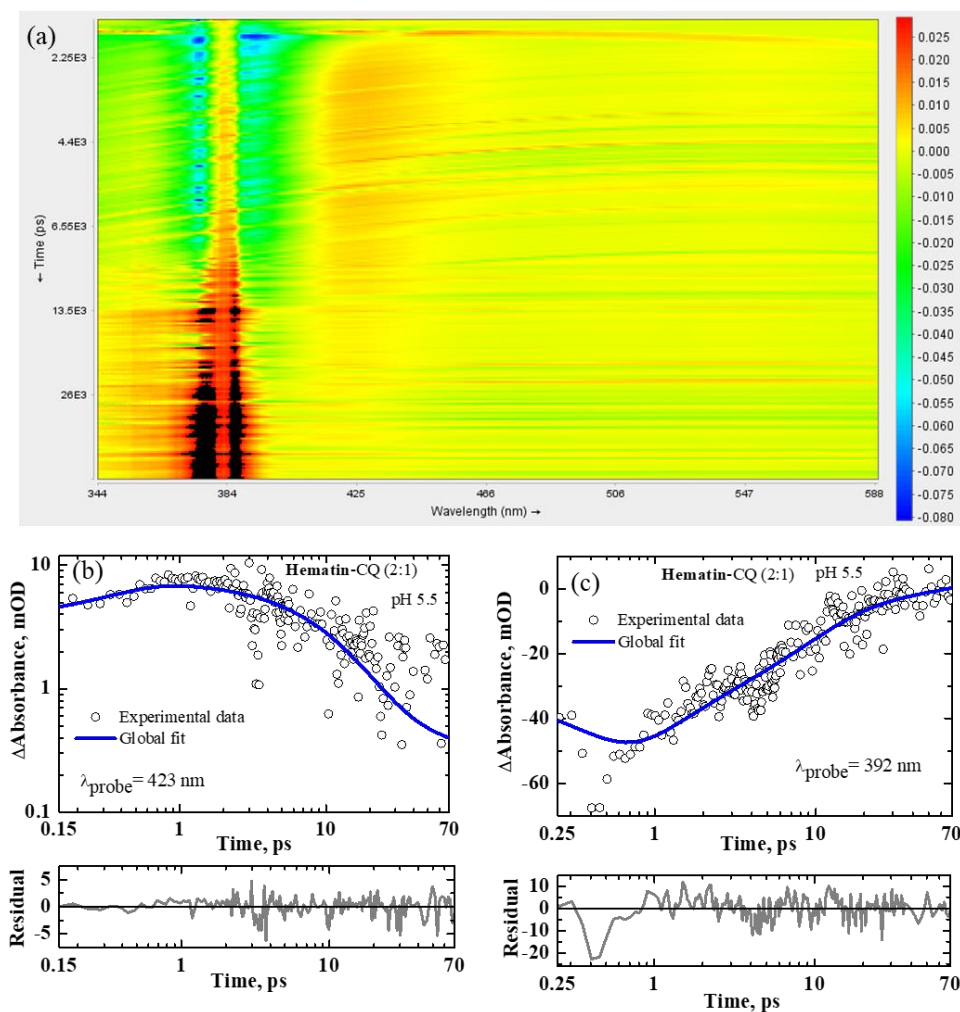


Figure 5.19 Heat map of FTAS of **Hematin-CQ** at pH 5.5 as a function of time delay (vertical) and probe wavelength (horizontal) in 70 ps time window upon excitation at 385 nm (a). The time profile at ESA maximum (b) and GSB maximum (c) (open circles) along with four-exponential fit (solid line) and residual (ash coloured solid line, lower panel). obtained from global analysis.

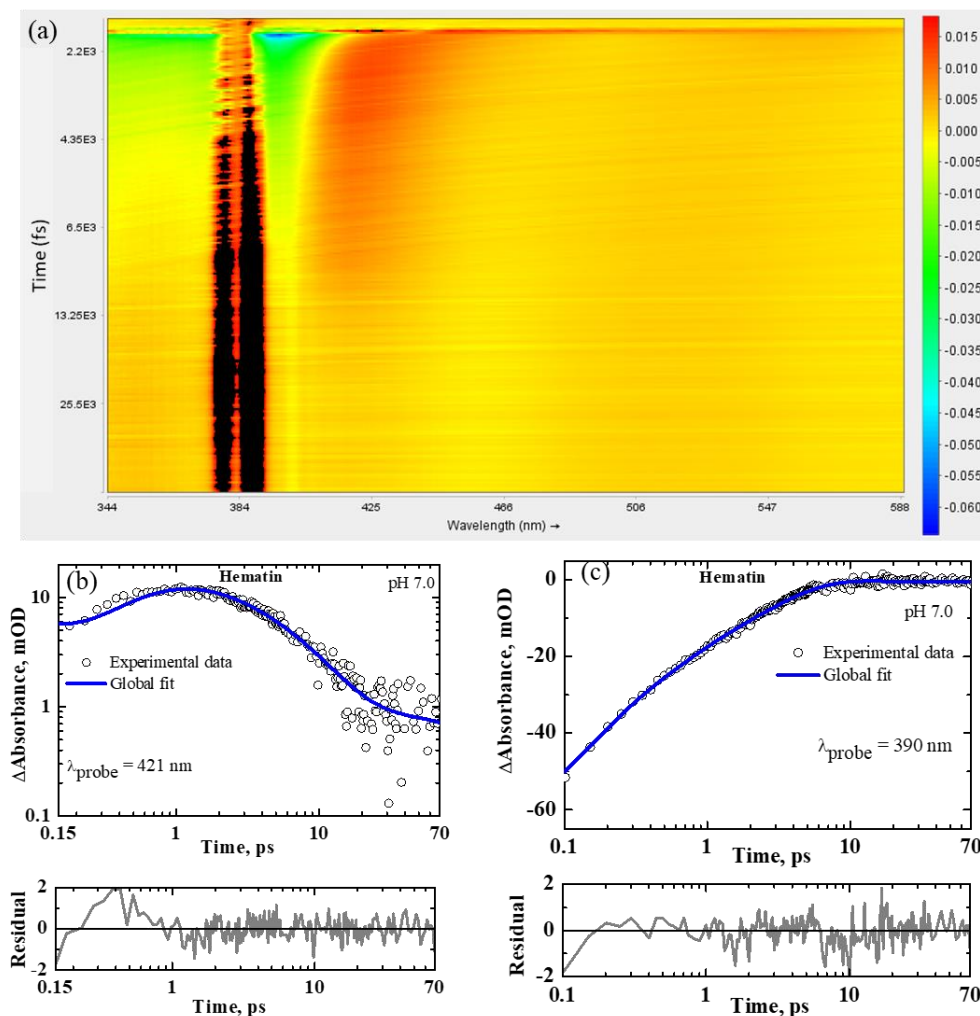


Figure 5.20 Heat map of FTAS of **Hematin** at pH 7.0 as a function of time delay (vertical) and probe wavelength (horizontal) in 70 ps time window upon excitation at 385 nm (a). The time profile at ESA maximum (b) and GSB maximum (c) (open circles) along with four-exponential fit (solid line) and residual (ash coloured solid line, lower panel). obtained from global analysis.

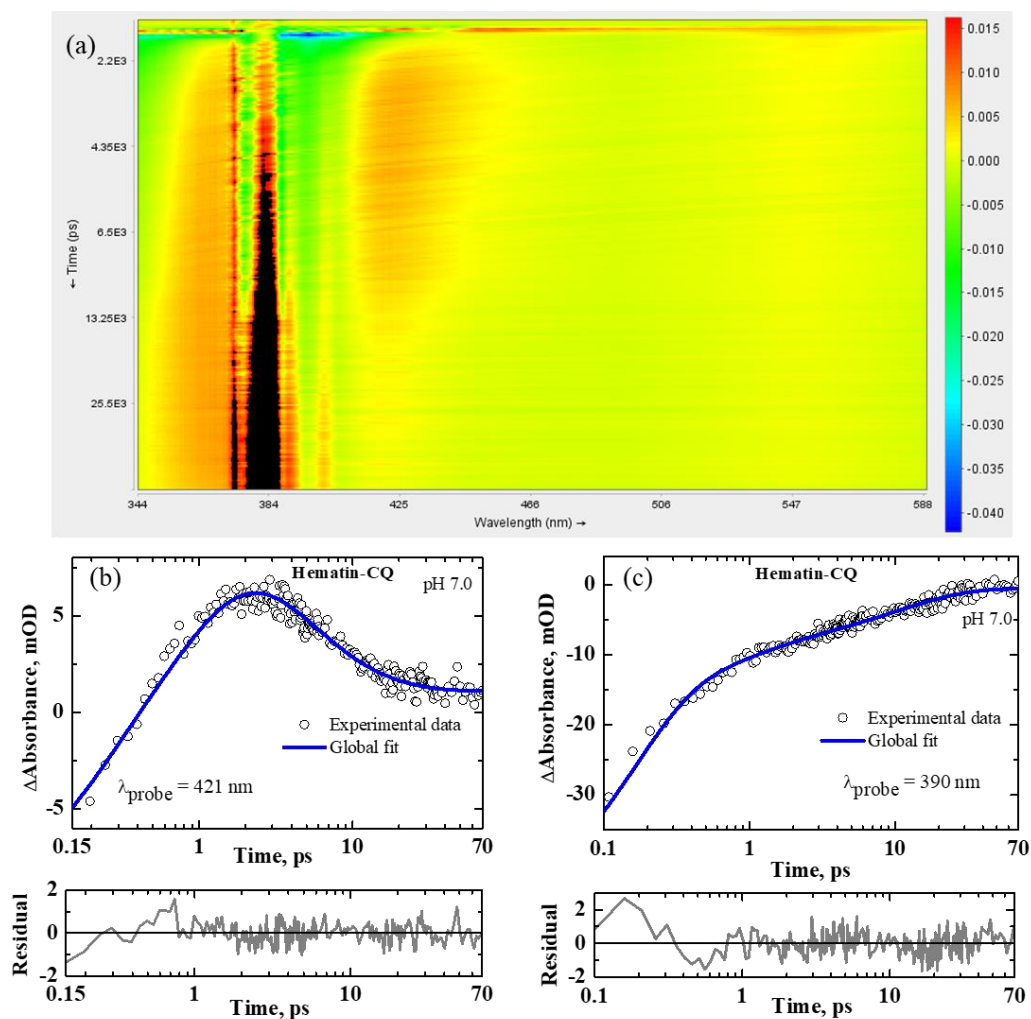


Figure 5.21 Heat map of FTAS of **Hematin-CQ** at pH 7.0 as a function of time delay (vertical) and probe wavelength (horizontal) in 70 ps time window upon excitation at 385 nm (a). The time profile at ESA maximum (b) and GSB maximum (c) (open circles) along with four-exponential fit (solid line) and residual (ash coloured solid line, lower panel). obtained from global analysis.

Table 5.1 Time constants obtained by global analysis using for **Hematin** and **Hematin**–drug complexes at 385 nm excitation.

Sample	Hematin	Hematin–CQ (2:1)	Hematin–MFQ (2:1)
pH 5.5	$\tau_1 = 0.10 \pm 0.10$ ps	$\tau_1 = 1.00 \pm 0.05$ ps	$\tau_1 = 0.13 \pm 0.10$ ps
	$\tau_2 = 0.48 \pm 0.12$ ps	$\tau_2 = 3.20 \pm 0.50$ ps	$\tau_2 = 0.61 \pm 0.50$ ps
	$\tau_3 = 2.80 \pm 0.50$ ps	$\tau_3 = 8.02 \pm 0.20$ ps	$\tau_3 = 2.54 \pm 0.30$ ps
	$\tau_4 = 5.92 \pm 1.20$ ps	$\tau_4 = 45.58 \pm 1.10$ ps	$\tau_4 = 6.58 \pm 1.20$ ps
pH 7.0	$\tau_1 = 0.11 \pm 0.10$ ps	$\tau_1 = 0.15 \pm 0.2$ ps	$\tau_1 = 0.12 \pm 0.04$ ps
	$\tau_2 = 0.42 \pm 0.03$ ps	$\tau_2 = 0.82 \pm 0.05$ ps	$\tau_2 = 0.51 \pm 0.03$ ps
	$\tau_3 = 2.60 \pm 0.25$ ps	$\tau_3 = 4.14 \pm 0.50$ ps	$\tau_3 = 2.74 \pm 0.20$ ps
	$\tau_4 = 6.50 \pm 1.00$ ps	$\tau_4 = 12.90 \pm 1.00$ ps	$\tau_4 = 8.79 \pm 1.10$ ps

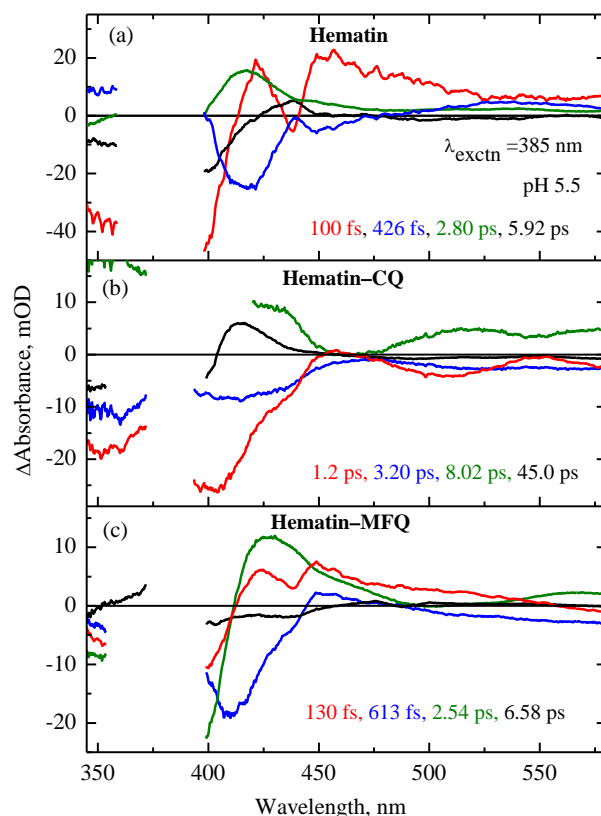


Figure 5.22 DAS of **Hematin** (a), **Hematin-CQ** and **Hematin-MFQ** at pH 5.5 obtained from global analysis.

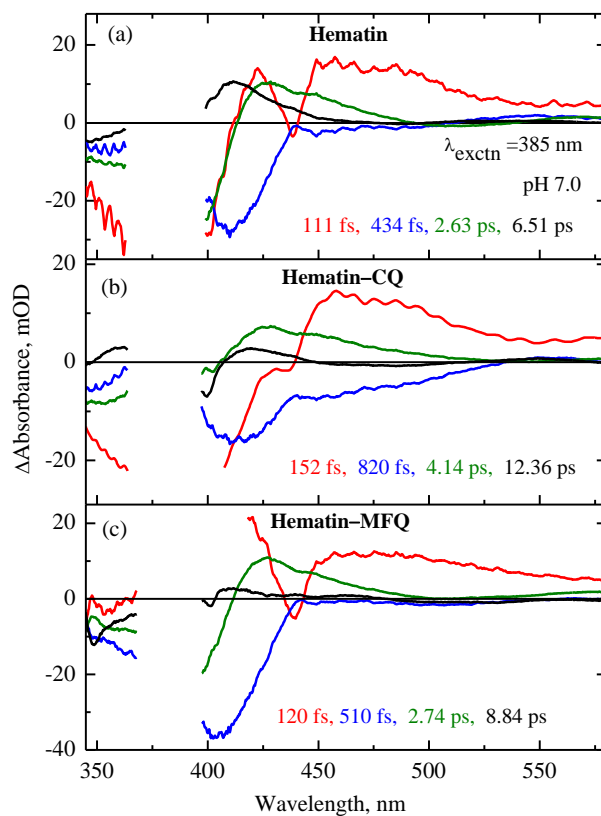


Figure 5.23 DAS of **Hematin** (a), **Hematin-CQ** and **Hematin-MFQ** at pH 7.0 obtained from global analysis.

5.3.3.2 Signature of Vibrational Cooling Dynamics

The excited–state relaxation dynamics of **Hematin**, after the ultrafast excitation follow the similar relaxation pathway observed in **Hemin–Cl** (chapter 2). The relaxation dynamics comprised of the sequential steps of LMCT, d–d transition of Fe atom and vibrational relaxation.^{55–58} The shifting of the ESA band of **Hematin** towards the blue region along with narrowing of the spectral width upon increasing the delay time in the picosecond range⁵⁸ indicates the occurrence of vibrational cooling dynamics in the transient absorption spectra. Alternatively, the possibility of ground state recovery by back electron transfer (MLCT) was calculated by determining the ratio between the areas of the complete Soret band region of the stationary and transient absorption spectra (**Table 5.2**). It is observed that $\sim 50 \pm 5\%$ of excited molecules of **Hematin** at pH 5.5 and 7.0 decay to the hot electronic ground state directly, indicating the strong signature of vibrational relaxation in the excited–state dynamics. Whereas in the case of **Hematin–CQ** complex, the ground state recovery ($\sim 37 \pm 5\%$) is less than that of **Hematin** reflecting that the ground state is recovering preferably through the involvement of a different pathway along with vibrational cooling. In the case of **Hematin–MFQ** complex, the recovery ratio is similar to that of **Hematin** in both the pH.

5.3.3.3 Involvement of Multiple Electronic Spin States

As in the case of heme model compounds, signature of the involvement of multiple electronic spin state of the iron atom in the relaxation dynamics of **Hematin** and **Hematin**–drug complexes are observed. The appearance of a new peak at around 525 nm after ~ 400 fs in the Q–band region in the transient absorption spectra reflects the involvement of a ferrous iron in the relaxation dynamics (**Figure 5.26** and **5.27**).⁵⁸ The transient absorption spectra at the Q–band region with doublet features having peaks at ~ 525 and 560 nm resemble the ground–state absorption spectra of the low spin ferrous form

of **Hemin** (Figure 5.26). Hence the involvement of different electronic spin states along with the vibrational cooling dynamics is proposed in the excited-state relaxation dynamics of **Hematin**. The detailed discussion of the four time constants for **Hematin** and **Hematin**–drug complexes based on spectral evolution and literature^{55-56, 58-60} are given below.

$\tau_1 \sim \text{LMCT}$: The time constant τ_1 , ~ 100 fs is assigned to the LMCT process as it is supported by the observation of the broad peak around 660 nm consistent with the formation of a porphyrin cation in the transient absorption spectra of **Hematin** and **Hematin**–drug complexes (Figure 5.28).⁶¹⁻⁶² However this time constant might also be due to the IC from S_2 to S_1 state impeding the ultrafast LMCT transition. Though the time constant is within the IRF of our femtosecond pump-probe spectroscopy (< 120 fs), it could be possible to deconvolute from the femtosecond transient absorption data by global analysis.

$\tau_2 \sim \text{MLCT}$: τ_2 could be attributed to the lifetime of back electron transfer from metal to porphyrin as the porphyrin cation formed by LMCT is stable enough and electron can be transferred back to refilling the porphyrin HOMO from the metal orbital.^{59, 63} In addition, the DAS of τ_2 is similar to the singlet absorption spectra of the metallo–porphyrins⁶⁴⁻⁶⁵ and porphyrin cations.^{62, 66}

τ_3 and $\tau_4 \sim (S = 1/2 \text{ and } 3/2)$: The appearance of double peaks (~ 525 and 560) in the Q–band region after the 400 fs time delay in the transient absorption spectra for **Hematin**, **Hematin**–CQ and **Hematin**–MFQ (Figure 5.26 and 5.27) illustrates the spectral resemblance between the transient absorption spectra of **Hematin** at 1 ps and the steady–state absorption spectra of the low spin ferrous form of **Hemin**–Cl in the Q–band region. Hence, it reflects the similar electronic distribution on the heme macrocycle, particularly the population of the Fe orbitals where the d_π orbitals are stabilized leading to

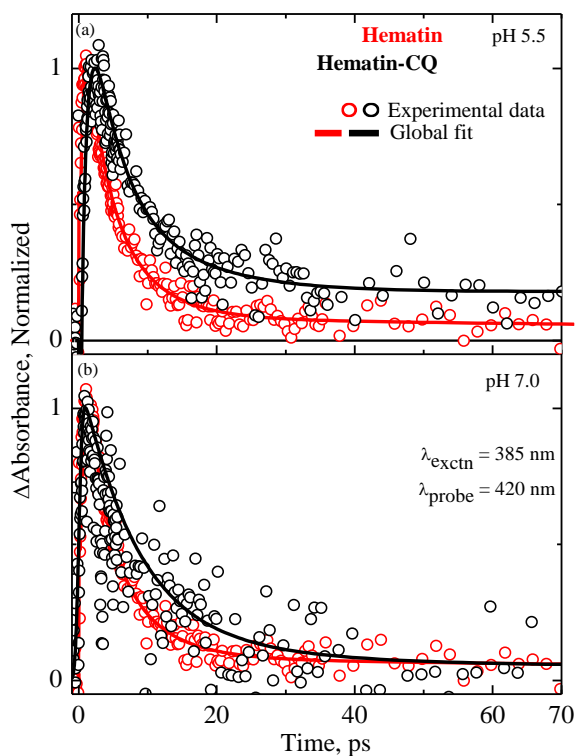


Figure 5.24 The time profile of **Hematin** and **Hematin–CQ** complex at pH 5.5 (a) and 7.0 (b) probed at 420 nm (open circles) along with four-exponential fit curve obtained from global analysis (solid line).

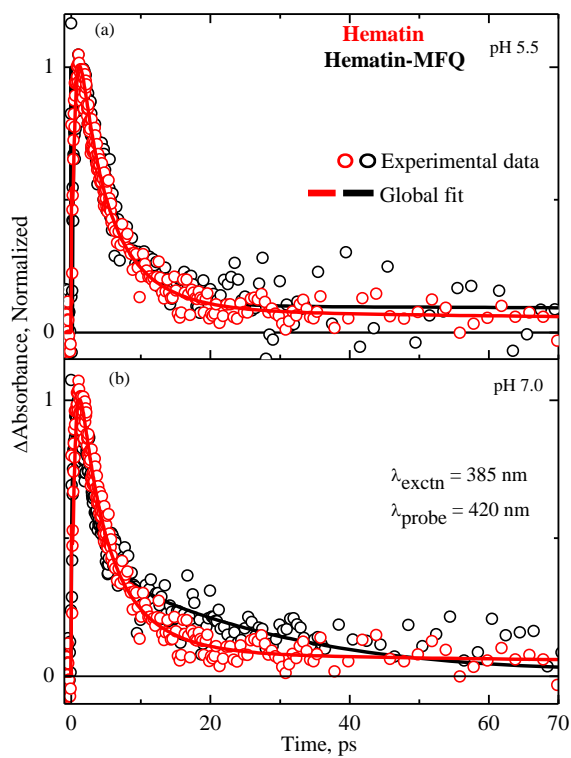


Figure 5.25 The time profile of **Hematin** and **Hematin–MFQ** complex at pH 5.5 (a) and 7.0 (b) probed at 420 nm (open circles) along with four-exponential fit curve obtained from global analysis (solid line).

Table 5.2 The calculation details for the ground state recovery for the **Hematin** and **Hematin**–drug complexes at different pH.

Compound	pH	λ_{exctn}	Ground state absorption spectra		Transient absorption spectral time	Excited–state absorption spectra		Ratio of absolute area
			Wavelength range (nm)	Absolute area		Wavelength range (nm)	Absolute area	
Hematin	5.5	385	307 – 433	89.22	250 fs	349– 417	159.77	55.84 %
	7.0	385	307 – 432	87.52	250 fs	357– 416	161.25	54.27 %
Hematin–CQ	5.5	385	293 – 435	110.29	350 fs	354– 418	297.35	37.09 %
	7.0	385	290 – 451	115.00	350 fs	362 – 423	364.28	31.57 %
Hematin–MFQ	5.5	385	300 – 445	88.15	350 fs	360 – 425	153.25	57.52 %
	7.0	385	290– 442	81.18	300 fs	362 – 423	163.26	49.72 %

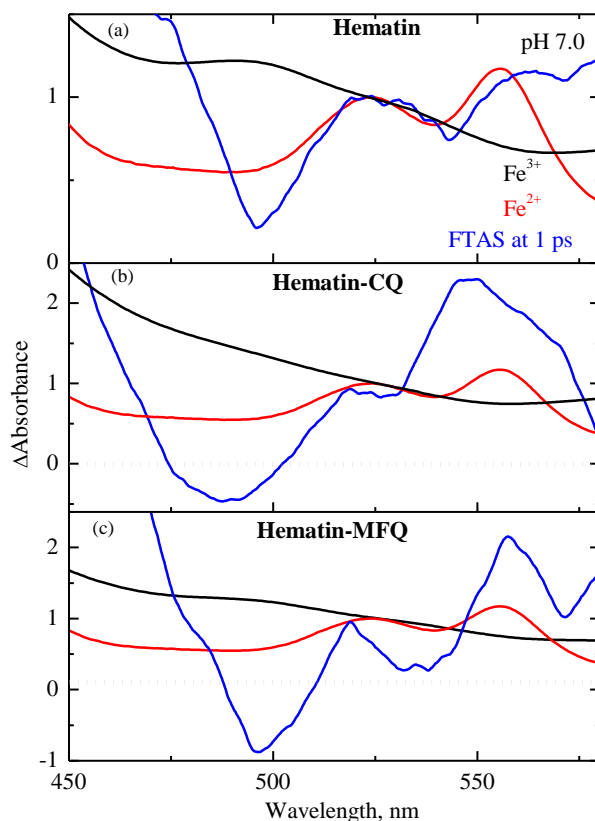


Figure 5.26 Comparison of the stationary absorption spectra and FTAS in the enlarged region of the Q band at 1 ps in the ferric form of **Hematin** (a), **Hematin-CQ** (b) and **Hematin-MFQ** (c) at pH 7.0 with absorption spectra of ferrous **Hemin** (red).

the low spin state. Thus, the time constant τ_3 is attributed to the state where the iron is in the low spin state ($S = 1/2$) having four electrons in the d_π orbitals. The ground state will be recovered by passing through the intermediate quartet spin state ($S = 3/2$) to the high spin ground state ($S = 5/2$). Hence, the time constant, τ_4 , is assigned to the intermediate spin state, where the iron would be in the spin state of ($S = 3/2$).

5.3.3.4 Dynamics at Different pH

When compared to the **Hematin** alone, the increase of all the relaxation time constants of **Hematin-CQ** at pH 5.5 is significant than at pH 7.0. Such increase of the time constants indicates that the drug stabilizes the energy level of both the d_z^2 and d_π orbitals leading to the stabilization of intermediate or low spin states (**Scheme 5. 1**).⁵⁸ The reduction of ground state recovery of the **Hematin-CQ** complex by the vibrational cooling (37 %) also reflects that the relaxation dynamics is predominantly controlled by the involvement of

different electronic spin states. In addition it is possible that the hydrogen bonding interaction between the tertiary amino group in the side chain of the quinoline and the heme propionate group could stabilize the **Hematin–CQ** complex.⁶⁷

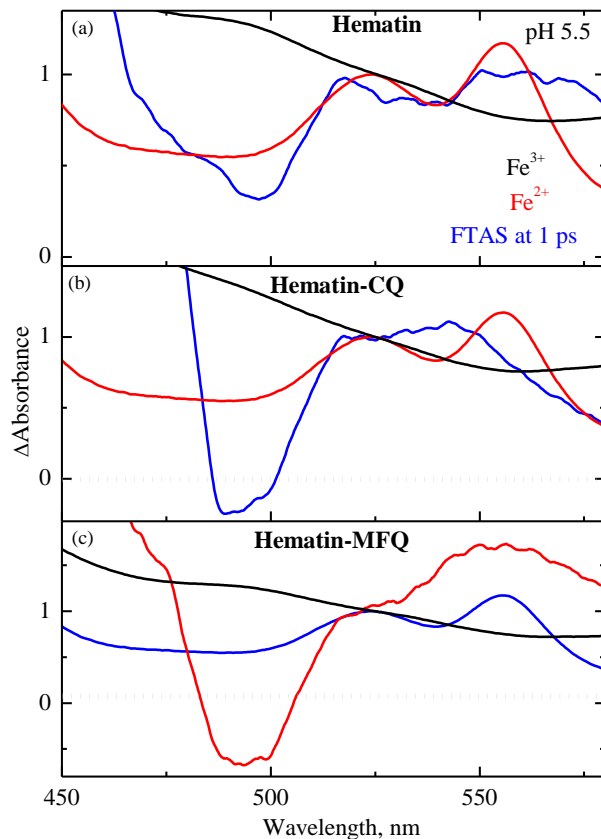


Figure 5.27 Comparison of the steady–state absorption spectra and FTAS in the enlarged region of the Q band at 1 ps in the ferric form of **Hematin** (a), **Hematin–CQ** (b) and **Hematin–MFQ** (c) at pH 5.5 with absorption spectra of ferrous **Hemin** (red).

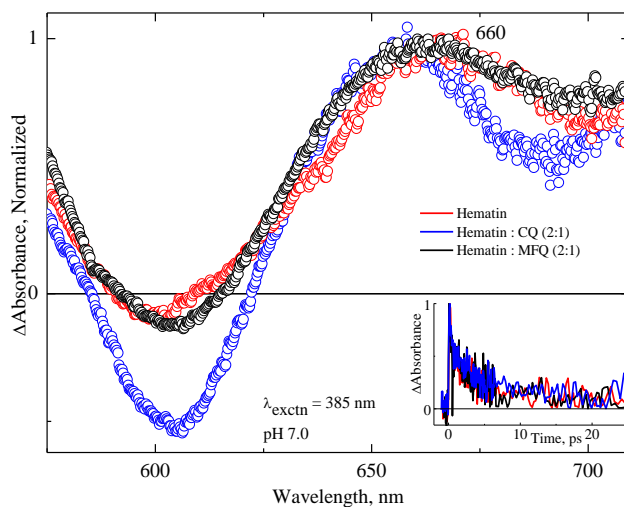
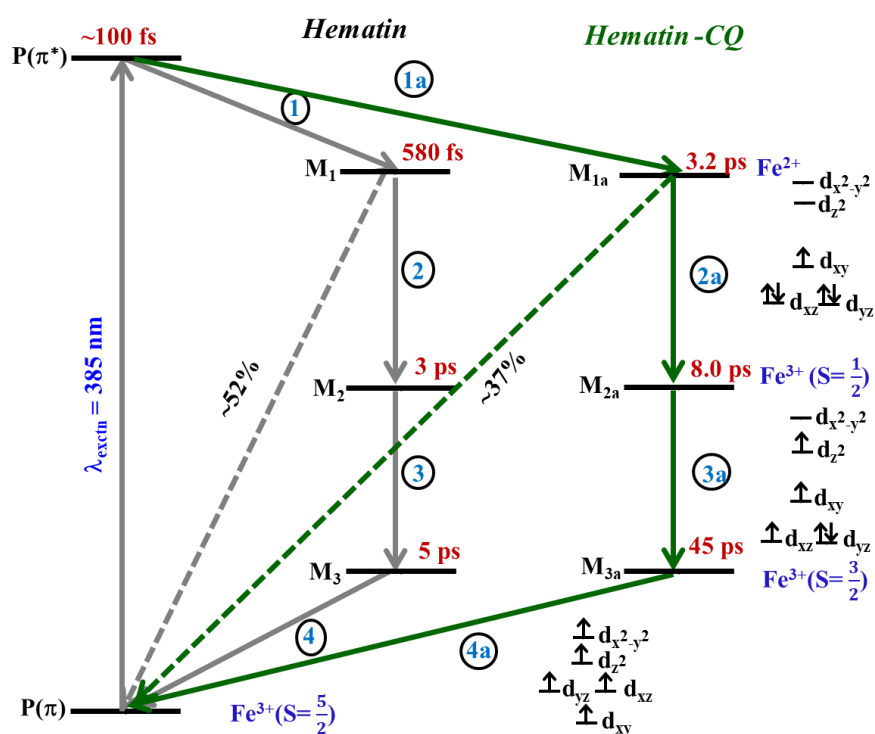


Figure 5.28 FTAS of **Hematin** (red), **Hematin–CQ** and **Hematin–MFQ** in the longer wavelength region measured at 1 ps after the photo–excitation.

However, the relaxation time constants of **Hematin**–MFQ complex are similar to that of **Hematin** (Table 5.1) reflecting the formation of weak complex between MFQ and **Hematin**. The excited–state relaxation dynamics of **Hematin** and with antimalarial drugs involving vibrational cooling and multi–spin electronics states are given in the Scheme 5.1.



Scheme 5.1 Proposed mechanism for excited–state relaxation dynamics of **Hematin** and **Hematin**–CQ complex involving different electronic spin states of iron atom.

5.4 Conclusion

The femtosecond pump–probe spectroscopy was used to investigate the interaction dynamics of with CQ and MFQ at pH 5.5 and pH 7.0. In both pH, **Hematin** forms ground state complex with CQ and MFQ. The transient absorption spectra of **Hematin** and **Hematin**–drug complexes reveal evidence of the involvement of both vibrational relaxation and intermediate electronic spin states in the excited–state relaxation dynamics

similar to the heme model compounds. In the case of **Hematin–CQ** complex the relaxation dynamics is predominantly through the different electronic spin states, whereas in the case of **Hematin–MFQ**, the relaxation dynamics are similar to that of **Hematin**. The observation of longer time constant in **Hematin–CQ** reveals that π – π dimer of **Hematin** forms more stabilized complex with **CQ** compared to **MFQ**. The formation of such complex could prevent the **Hematin** crystallization leading to the formation of hemozoin. The understanding of **Hematin**–drug interactions will enable the design of new antimalarial drugs.

5.5 Materials and Methods

Hematin, **CQ** and **MFQ** were purchased from Sigma Aldrich and used without further purification. Buffers were prepared containing 20 mM acetate (pH 5.5) and phosphate (pH 7.0) with 50 mM NaNO₃ in 40% methanol–water (vol/vol). The pH of the buffers was measured using a FiveEasyPlus pH meter (Calgon Scientific) equipped with a glass electrode and adjusted using either nitric acid or NaOH to avoid coordinating chloride ions. Stock solutions of **Hematin** were prepared in 50 mM NaOH.

The concentration of **Hematin** used for measuring the transient absorption spectra was 200 μ M. The integrity of the sample is tested by measuring the absorption spectra of the sample before and after the experiments and found to be no significant changes in the absorption spectra.

5.6 References

1. White, N. J.; Pukrittayakamee, S.; Hien, T. T.; Faiz, M. A.; Mokuolu, O. A.; Dondorp, A. M., *The Lancet* **2014**, 383 (9918), 723-735.
2. Laishram, D. D.; Sutton, P. L.; Nanda, N.; Sharma, V. L.; Sobti, R. C.; Carlton, J. M.; Joshi, H., *Malar. J.* **2012**, 11 (1), 29.
3. Hill, A. V. S., *Philos. Trans. R Soc. Lond. B Biol. Sci.* **2011**, 366 (1579), 2806-2814.
4. Krugliak, M.; Zhang, J.; Ginsburg, H., *Mol. Biochem. Parasitol.* **2002**, 119 (2), 249-256.
5. Ali, M. E.; Oppeneer, P. M., *Chem. Eur. J* **2015**, 21 (23), 8544-8553.
6. Ketchum, M. A.; Olafson, K. N.; Petrova, E. V.; Rimer, J. D.; Vekilov, P. G., *J. Chem. Phys.* **2013**, 139 (12), 121911.
7. Pagola, S.; Stephens, P. W.; Bohle, D. S.; Kosar, A. D.; Madsen, S. K., *Nature* **2000**, 404 (6775), 307-310.
8. Liu, Z.; Miao, J.; Cui, L., *Future microbiol.* **2011**, 6 (11), 1351-1369.
9. Slater, A. F.; Swiggard, W. J.; Orton, B. R.; Flitter, W. D.; Goldberg, D. E.; Cerami, A.; Henderson, G. B., *Proc. Natl. Acad. Sci. U. S. A.* **1991**, 88 (2), 325-329.
10. Bohle, D. S.; Conklin, B. J.; Cox, D.; Madsen, S. K.; Paulson, S.; Stephens, P. W.; Yee, G. T., Structural and Spectroscopic Studies of β -Hematin (the Heme Coordination Polymer in Malaria Pigment). In *Inorganic and Organometallic Polymers II*, American Chemical Society: **1994**; 572, 497-515.
11. Bohle, D. S.; Dinnebier, R. E.; Madsen, S. K.; Stephens, P. W., *J. Biol. Chem.* **1997**, 272 (2), 713-716.
12. Dorn, A.; Stoffel, R.; Matile, H.; Bubendorf, A.; Ridley, R. G., *Nature* **1995**, 374 (6519), 269-271.
13. Bendrat, K.; Berger, B. J.; Cerami, A., *Nature* **1995**, 378 (6553), 138-139.

14. Egan, T. J., *J. Inorg. Biochem.* **2002**, *91* (1), 19-26.
15. Bohle, D. S.; Debrunner, P.; Jordan, P. A.; Madsen, S. K.; Schulz, C. E., *J. Am. Chem. Soc.* **1998**, *120* (32), 8255-8256.
16. Egan, T. J.; Combrinck, J. M.; Egan, J.; Hearne, G. R.; Marques, H. M.; Ntenti, S.; Sewell, B. T.; Smith, P. J.; Taylor, D.; van Schalkwyk, D. A.; Walden, J. C., *Biochem. J.* **2002**, *365* (Pt 2), 343-347.
17. Ridley, R. G., *Nature* **2003**, *424* (6951), 887-889.
18. Kyle, R. A.; Shampe, M. A., *Jama* **1974**, *229* (4), 462.
19. Gregson, A.; Plowe, C. V., *Pharmacol. Rev.* **2005**, *57* (1), 117.
20. Greenwood, D., *J. Antimicrob. Chemoth.* **1995**, *36* (5), 857-872.
21. Bruce-Chwatt, L. J., *Bull. World Health Organ.* **1962**, *27* (2), 287-290.
22. Basso, L. G. M.; Rodrigues, R. Z.; Naal, R. M. Z. G.; Costa-Filho, A. J., *Biochim. Biophys. Acta.* **2011**, *1808* (1), 55-64.
23. Sevene, E.; González, R.; Menéndez, C., *Expert. Opin. Pharmacother.* **2010**, *11* (8), 1277-1293.
24. Shack, J.; Clark, W. M., *J. Biol. Chem.* **1947**, *171* (1), 143-187.
25. Brown, S. B.; Jones, P.; Lantzke, I. R., *Nature* **1969**, *223* (5209), 960-961.
26. Brown, S. B.; Dean, T. C.; Jones, P., *Biochem. J.* **1970**, *117* (4), 733-739.
27. Blauer, G.; Zvilichovsky, B., *Arch. Biochem. Biophys.* **1968**, *127*, 749-755.
28. O'Keeffe, D. H.; Barlow, C. H.; Smythe, G. A.; Fuchsman, W. H.; Moss, T. H.; Lilienthal, H. R.; Caughey, W. S., *Bioinorg. Chem.* **1975**, *5* (2), 125-147.
29. Asher, C.; de Villiers, K. A.; Egan, T. J., *Inorg. Chem.* **2009**, *48* (16), 7994-8003.
30. de Villiers, K. A.; Kaschula, C. H.; Egan, T. J.; Marques, H. M., *J. Biol. Inorg. Chem.* **2007**, *12* (1), 101-117.

31. Kumar, S.; Guha, M.; Choubey, V.; Maity, P.; Bandyopadhyay, U., *Life Sci.* **2007**, *80* (9), 813-828.
32. Macomber, P. B.; Sprinz, H.; Tousimis, A. J., *Nature* **1967**, *214* (5091), 937-939.
33. Fitch, C. D., *Proc. Natl. Acad. Sci. U S A* **1969**, *64* (4), 1181-1187.
34. Slater, A. F. G.; Cerami, A., *Nature* **1992**, *355* (6356), 167-169.
35. Egan, T. J., *Drug Discov. Rev.* **2004**, *1* (1), 93-110.
36. Cohen, S. N.; Phifer, K. O.; Yielding, K. L., *Nature* **1964**, *202*, 805-806.
37. Sugioka, Y.; Suzuki, M., *Biochim. Biophys. Acta* **1991**, *1074* (1), 19-24.
38. Moreau, S.; Perly, B.; Biguet, J., *Biochimie* **1982**, *64* (11-12), 1015-1025.
39. Adams, P. A.; Berman, P. A.; Egan, T. J.; Marsh, P. J.; Silver, J., *J. Inorg. Biochem.* **1996**, *63* (1), 69-77.
40. Leed, A.; DuBay, K.; Ursos, L. M. B.; Sears, D.; de Dios, A. C.; Roepe, P. D., *Biochemistry* **2002**, *41* (32), 10245-10255.
41. de Dios, A. C.; Tycko, R.; Ursos, L. M. B.; Roepe, P. D., *J. Phys. Chem. A* **2003**, *107* (30), 5821-5825.
42. Chou, A. C.; Chevli, R.; Fitch, C. D., *Biochemistry* **1980**, *19* (8), 1543-1549.
43. de Villiers, K. A.; Marques, H. M.; Egan, T. J., *J. Inorg. Biochem.* **2008**, *102* (8), 1660-1667.
44. Olafson, K. N.; Nguyen, T. Q.; Rimer, J. D.; Vekilov, P. G., *Proc. Natl. Acad. Sci. U.S.A* **2017**, *114* (29), 7531.
45. Crespo, M. P.; Tilley, L.; Klonis, N., *J. Biol. Inorg. Chem.* **2010**, *15* (7), 1009-1022.
46. Chen, A.; Huang, K.-C.; Bopp, S.; Summers, R.; Dong, P.; Huang, Y.; Zong, C.; Wirth, D.; Cheng, J.-X., *J. Biomed. Opt.* **2019**, *25* (1), 014507.
47. Abshire, J. R.; Rowlands, C. J.; Ganesan, S. M.; So, P. T. C.; Niles, J. C., *Proc. Natl. Acad. Sci. U. S. A.* **2017**, *114* (11), E2068.

48. Hanna, D. A.; Harvey, R. M.; Martinez-Guzman, O.; Yuan, X.; Chandrasekharan, B.; Raju, G.; Outten, F. W.; Hamza, I.; Reddi, A. R., *Proc. Natl. Acad. Sci. U. S. A.* **2016**, *113* (27), 7539.
49. Moore, D. E.; Hemmens, V. J., *Photochem. Photobiol.* **1982**, *36* (1), 71-77.
50. Tønnesen, H. H.; Moore, D. E., *Int. J. Pharm.* **1991**, *70* (1), 95-101.
51. Pandey, A.; Bisht, H.; Babbarwal, V.; Srivastava, J.; Pandey, K.; Chauhan, V., *Biochem. J.* **2001**, *355*, 333-338.
52. Rosenberg, L. S.; Schulman, S. G., *J. Pharma. Sci.* **1978**, *67* (12), 1770-1772.
53. Viola, G.; Salvador, A.; Cecconet, L.; Basso, G.; Vedaldi, D.; Dall'Acqua, F.; Aloisi, G. G.; Amelia, M.; Barbafina, A.; Latterini, L.; Elisei, F., *Photochem. Photobiol.* **2007**, *83* (6), 1415-1427.
54. Snellenburg, J. J.; Laptinok, S.; Seger, R.; Mullen, K. M.; van Stokkum, I. H. M., *J. Stat. Softw.* **2012**, *49* (3), 22.
55. Marcelli, A.; Jelovica Badovinac, I.; Orlic, N.; Salvi, P. R.; Gellini, C., *Photochem. Photobiol. Sci.* **2013**, *12* (2), 348-355.
56. Ha-Thi, M.-H.; Shafizadeh, N.; Poisson, L.; Soep, B., *Phy. Chem. Chem. Phys.* **2010**, *12* (45), 14985-14993.
57. Rodriguez, J.; Kirmaier, C.; Holten, D., *J.Chem.Phys.* **1991**, *94* (9), 6020-6029.
58. Govind, C.; Karunakaran, V., *J. Phys. Chem. B* **2017**, *121* (14), 3111-3120.
59. Consani, C.; Auböck, G.; Bräm, O.; van Mourik, F.; Chergui, M., *J. Chem. Phys.* **2014**, *140* (2), 025103.
60. Franzen, S.; Kiger, L.; Poyart, C.; Martin, J.-L., *Biophys. J.* **2001**, *80* (5), 2372-2385.
61. Dolphin, D.; Felton, R. H., *Acc. Chem. Res.* **1974**, *7* (1), 26-32.

62. Fajer, J.; Borg, D. C.; Forman, A.; Dolphin, D.; Felton, R. H., *J. Am. Chem. Soc.* **1970**, *92* (11), 3451-3459.
63. Huszánk, R.; Lendvay, G.; Horváth, O., *J. Biol. Inorg. Chem.* **2007**, *12* (5), 681-690.
64. Rodriguez, J.; Kirmaier, C.; Holten, D., *J. Am. Chem. Soc.* **1989**, *111* (17), 6500-6506.
65. Zhang, X.; Wasinger, E. C.; Muresan, A. Z.; Attenkofer, K.; Jennings, G.; Lindsey, J. S.; Chen, L. X., *J. Phys. Chem. A* **2007**, *111* (46), 11736-11742.
66. Chang, C. K.; Hanson, L. K.; Richardson, P. F.; Young, R.; Fajer, J., *Proc. Natl. Acad. Sci. USA* **1981**, *78* (5), 2652-2656.
67. Asghari-Khiavi, M.; Vongsvivut, J.; Perepichka, I.; Mechler, A.; Wood, B. R.; McNaughton, D.; Bohle, D. S., *J. Inorg. Biochem.* **2011**, *105* (12), 1662-1669.

ABSTRACT

Name of the Student: **Mrs. Chinju Govind M. V.**
Faculty of Study: Chemical Sciences
AcSIR academic centre/CSIR Lab: CSIR-National
Institute for Interdisciplinary
Science and Technology (CSIR-NIIST)

Registration No.: 10CC14A39003
Year of Submission: 2020

Name of the Supervisor: Dr. V. Karunakaran

Title of the thesis: **Ultrafast electronic, vibrational and conformational relaxation dynamics of heme model compounds and proteins in various environments using femtosecond pump-probe spectroscopy.**

The electronic, vibrational and conformational changes of the protein due to redistribution of the excess energy generated by biological functions play an important role. These can be optically triggered by ultrafast pulsed lasers and probed by ultrafast spectroscopy. Here, the excited state relaxation dynamics of various heme model compounds, heme protein–**Cytochrome c (Cyt c)** with lipids and **Hematin** with antimalarial drugs are investigated using femtosecond pump-probe spectroscopy to correlate the relaxation dynamics with biological functions of the protein. An overview of biological functions and ultrafast dynamics of heme model compounds and heme proteins are included in the **Chapter 1**. **Chapter 2** involves a detailed discussion on the technical aspects of femtosecond pump-probe spectroscopy and analysis of transient absorption spectra and description of other experimental techniques used in this thesis.

In **Chapter 3**, the ultrafast excited state relaxation dynamics of various heme model compounds (**Hemin–Cl**, **Hemin–Br** and **Hemin–meso**) and **met-myoglobin** have been investigated by femtosecond pump-probe spectroscopy upon excitation at 380 nm to understand the influence of the axial ligands, peripheral substituents and the solvents on the excited state relaxation dynamics of the heme. An excited state deactivation pathway of heme model compounds comprising different electronic spin states of iron along with the vibrational cooling dynamics is proposed. This study revealed that the involvement of multiple iron spin states in the electronic relaxation dynamics of heme model compounds and **met–Mb** is an inherent feature of the heme *b* type.

The interaction dynamics of **Cyt c** with various phospholipids having different charges [**CL**: 2–, **POPG**: 1– and **POPC**: 0] are discussed in **Chapter 4** to understand the electronic, vibrational, and conformational changes of the protein in its partially unfolded state. The various degrees of partial unfolding are observed in **Cyt c** in the presence of liposomes from steady state and excited state optical spectroscopy. The decrease of efficiency of fluorescence resonance energy transfer (FRET) from tryptophan (Trp) to heme upon an increase of the partial unfolding of the proteins by liposomes revealed the Trp as a marker amino acid to reflect the dynamics of partial unfolding of the protein. In addition, the refolding of the protein after the addition of NaCl indicated the electrostatic interaction between **Cyt c** and liposomes rather than the hydrophobic interaction.

The interaction dynamics between **Hematin** and antimalarial drugs including chloroquine (**CQ**) and mefloquine (**MFQ**) have been investigated in pH 5.5 and 7.0 using steady state and time resolved absorption and emission spectroscopy in **Chapter 5**. In both pH, **Hematin** formed ground state complex with **CQ** and **MFQ**. The excited state relaxation pathway of **Hematin** in the presence of drugs comprise of both multiple electronic spin states and vibrational relaxation process. **Hematin–CQ** complex was more stabilized than **Hematin** by non-covalent interactions and thereby preventing the formation of hemozoin. The understanding of **Hematin**-drug interactions will enable the design of new antimalarial drugs to overcome the parasite resistance.

Details of the Publications Emanating from the Thesis Work

Published

1. **C. Govind**, V. Karunakaran*, “Ultrafast Relaxation Dynamics of Photoexcited Heme Model Compounds: Observation of Multiple Electronic Spin States and Vibrational Cooling”, *J. Phys. Chem. B.*, **2017**, 121, 3111-3120.
2. **C. Govind**, M. Paul, V. Karunakaran*, “Ultrafast Heme Relaxation Dynamics Probing the Unfolded States of Cytochrome c Induced by Liposomes: Effect of Charge of Phospholipids”, *J. Phys. Chem. B.*, **2020**, 124, 14, 2769-2777.

Manuscript under preparation

1. **C. Govind**, M. Paul, V. Karunakaran*, “Interaction Dynamics of Hematin with Antimalarial Drug: An Ultrafast Investigation” (To be submitted).

List of Publications from Other Related Works.

1. E. Orłowska, M. Babak, O. Dömötör, E. A. Enyedy, P. Rapta, M. Zalibera, L. Bučinský, M. Malček, **C. Govind**, V. Karunakaran, D. Luneau, D. Schaniel, W. H. Ang, V. B. Arion*, “NO releasing and anticancer properties of octahedral ruthenium- nitrosyl complexes with equatorial 1H-indazole ligands”, *Inorg. Chem.* **2018**, 57,10702-10717.
2. A. U. Neelambra, **C. Govind**, T.T. Devassia, G. M. Somashekharappa, V. Karunakaran*, “Direct Evidence of Solvent Polarity Governing the Intramolecular Charge and Energy Transfer: Ultrafast Relaxation Dynamics of Push-Pull Fluorene Derivative”, *Phys.Chem.Chem.Phys.*, **2019**, 21, 11087-11102.
3. K. Mahato, **C. Govind**, V. Karunakaran, S. Nandy, C. Sudakar, E. Prasad*, “Enhanced Charge Transport and Excited State Charge Transfer Dynamics in a Colloidal Mixture of CdTe and Graphene Quantum Dots”, *J. Phys. Chem. C.*, **2019**, 123, 33, 20512-20521.
4. I. Allison, H. Lim, A. Shukla, V. Ahmad, M. Hasan, K.Deshmukh, R. Wawrzinek, S. K. M. McGregor, J. K. Clegg, V. V. Divya, **C. Govind**, C. H. Suresh, V. Karunakaran, N. Unni, A. Ajayaghosh, E. B. Namdas*, S.-C. Lo*, “Solution Processable Deep-Red Phosphorescent Pt(II) Complex: Direct Conversion from Its Pt(IV) Species via a Base Promoted Reduction”, *ACS Appl. Electron. Mater.*, **2019**,1, 1304-1313.
5. G. Augustine, s. S. Raghavan, K. NumbiRamudu, S. Easwaramoorthi, G. Shanmugam, J. S. Murugaiyan, K. Gunasekaran, **C. Govind**, V. Karunakaran, N. Ayyadurai*, “Excited State Electronic Interconversion and Structural Transformation of Engineered Red Emitting Green Fluorescent Protein Mutant”, *J. Phys. Chem. B.*, **2019**, 123, 2316-2324.

6. G. Somashekharappa, **C. Govind**, K. P. Vijith, M. Paul, M. A. G. Namboothiry*, S. Das*, V. Karunakaran*, “Unsymmetrical Squaraine Dye-Based Organic Photodetectors Exhibiting Enhanced Near Infrared Sensitivity”, *J. Phys. Chem. C* **2020**, 124, 39, 21730–21739.
7. S. Paul, **C. Govind**, V.Karunakaran*, “Planarity of the Bridge Control the Efficiency of Intramolecular Singlet Fission Dynamics in Pentacene Dimers”, *J. Phys. Chem. B* **2020**, <https://doi.org/10.1021/acs.jpcc.0c08590>.
8. S.K.M. McGregor, **C. Govind**, M.K.R Wood, A. Shukla, H. Lim, R.J Lepage, E.H. Krenske, N.K.N. Unni, A. Ajayaghosh, V. Karunakaran, E.B. Namdas, and S. Lo, “Structural Integration of Carbazole and Tetraphenylethylene: Ultrafast Excited-State Relaxation Dynamics and Efficient Electroluminescence”. *Adv. Photonics Res.*,**2021**, <https://doi.org/10.1002/adpr.202000144>.

Posters Presented and Attended in Conferences

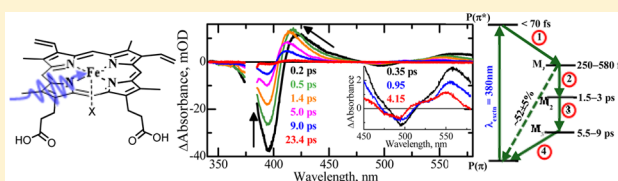
1. “Exploring the Ultrafast Relaxation Dynamics of the Heme in the Apoptosis Process: Interaction Dynamics of Cytochrome c with Different Liposomes”, *Faraday Discuss.*, **2018**, 207, 523-524.
Poster presented at “Faraday Discussion: Photoinduced Processes in Nucleic Acids and Proteins”, Royal Society of Chemistry (RSC), Thiruvananthapuram. 11-13, January **2018**.
2. Attended “International Conference on Ultrafast Spectroscopy (ICUS2020)”, IISER-Thiruvananthapuram, Thiruvananthapuram, 21-22, February **2020**.

Ultrafast Relaxation Dynamics of Photoexcited Heme Model Compounds: Observation of Multiple Electronic Spin States and Vibrational Cooling

Chinju Govind^{†,‡} and Venugopal Karunakaran^{*,†,‡} [†]Photosciences and Photonics Section, Chemical Sciences and Technology Division, CSIR-National Institute for Interdisciplinary Science and Technology, Thiruvananthapuram 695 019, Kerala India[‡]Academy of Scientific and Innovative Research (AcSIR), New Delhi 110 001, India

Supporting Information

ABSTRACT: Hemin is a unique model compound of heme proteins carrying out variable biological functions. Here, the excited state relaxation dynamics of heme model compounds in the ferric form are systematically investigated by changing the axial ligand (Cl/Br), the peripheral substituent (vinyl/ethyl-meso), and the solvent (methanol/DMSO) using femtosecond pump–probe spectroscopy upon excitation at 380 nm. The relaxation time constants of these model compounds are obtained by global analysis. Excited state deactivation pathway of the model compounds comprising the decay of the porphyrin excited state (S^*) to ligand to metal charge transfer state (LMCT, τ_1), back electron transfer from metal to ligand (MLCT, τ_2), and relaxation to the ground state through different electronic spin states of iron (τ_3 and τ_4) are proposed along with the vibrational cooling processes. This is based on the excited state absorption spectral evolution, similarities between the transient absorption spectra of the ferric form and steady state absorption spectra of the low-spin ferrous form, and the data analysis. The observation of an increase of all the relaxation time constants in DMSO compared to the methanol reflects the stabilization of intermediate states involved in the electronic relaxation. The transient absorption spectra of met-myoglobin are also measured for comparison. Thus, the transient absorption spectra of these model compounds reveal the involvement of multiple iron spin states in the electronic relaxation dynamics, which could be an alternative pathway to the ground state beside the vibrational cooling processes and associated with the inherent features of the heme *b* type.



1. INTRODUCTION

The ultrafast excited state relaxation dynamics of Iron metalloporphyrins^{1–7} have been investigated extensively, as they serve as a model system for heme proteins performing a broad range of biological functions including transport and storage of diatomic molecules such as CO, NO, and O₂, signaling, catalysis, and electron transfer.^{8–12} The reactivity of heme, the prosthetic group of heme proteins, can be modified by changing the axial ligands, peripheral substituents, oxidation states of the iron atom, and polar and nonpolar groups around the heme.^{13–16} It is well-known that various heme groups (viz., *a*, *b*, and *c*) are available in nature and categorized based on the peripheral substituents.^{13,17} The transient absorption spectra of various heme model compounds and heme proteins were investigated to understand the underlying mechanism in the relaxation dynamics of the heme.^{3,6,17–26} Based on the experimental evidence, two distinct models comprising of vibrationally excited (“hot”) electronic ground state^{6,19,21–27} and the multiple electronic intermediate excited state^{17,18,20,21,28–31} are proposed. Interestingly, the heme model compounds are simplest, ubiquitous, possess a rich diversity of chemical structures and reaction, and importantly do not undergo ligand photodissociation in the ferric form

which could impede the electronic and vibrational dynamics of the heme.^{21,32}

The femtosecond time-resolved transient absorption spectra of ferric Hemin were investigated in solution and gaseous states^{3,5} and the experimental details along with the assignment of the time constants are given in Table 1. It was reported that the excited heme relaxed to the ground state by internal conversion with the sub-picosecond time scale, and subsequently ground state was completely recovered through vibrational cooling with a time constant of ~ 5.5 ps.³ Soep et al.⁵ investigated the excited state relaxation dynamics of Hemin in the gas phase by femtosecond pump–probe spectroscopy with 90 fs time resolution. They found the two exponential components including the ultrafast initial decay on the order of 50 fs attributed to the charge transfer process from ligand to metal and a second relaxation time constant of 250 fs corresponding to the relaxation of the LMCT state to the ground state.

Received: February 13, 2017

Revised: March 22, 2017

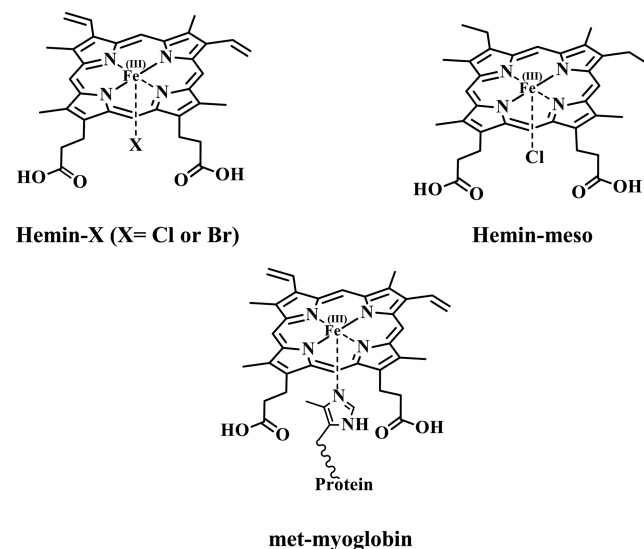
Published: March 22, 2017

Table 1. Details of Previous Studies and Assignments of Excited State Relaxation Dynamics of Hemin and met-Mb Using Femtosecond Time Resolved Pump–Probe Spectroscopy^{3,5,18,33}

no.	authors	λ_{excitn} (IRF) ^a	compounds	time constants	assignment
1	Marcelli et al. ³	400 and 500 nm (160 fs)	Hemin (Methanol)	$\tau_1 = 0.2$ ps $\tau_2 = 1.5$ ps $\tau_3 = 5.7$ ps	τ_1 = Ligand to metal charge transfer τ_2 = Iron d-d transition τ_3 = Vibrational relaxation
2	Soep et al. ⁵	396 nm (90 fs)	Hemin (Gas phase)	$\tau_1 = 50$ fs $\tau_2 = 0.25$ ps	τ_1 = Ligand to metal charge transfer τ_2 = Relaxation of the LMCT to ground state
3	Kitamura et al. ³³	400 nm (130 fs)	met-Mb (pH 7)	$\tau_1 = 70$ fs $\tau_2 = 0.54$ ps $\tau_3 = 4.1$ ps	τ_1 = Relaxation of S ₁ state τ_2 = Ligand to metal charge transfer τ_3 = Vibrational relaxation
4	Chergui et al. ¹⁸	400 nm (130 fs)	met-Mb (pH 7)	$\tau_1 = < 80$ fs $\tau_2 = 0.51$ ps $\tau_3 = 1.14$ ps $\tau_4 = 4.77$ ps	τ_1 = Ligand to metal charge transfer τ_2 = Back electron transfer τ_3 = Electronic decay of intermediate spin state ($S = \frac{1}{2}$) τ_4 = Electronic decay of intermediate spin state ($S = \frac{3}{2}$)

^a λ_{excitn} : excitation wavelength; IRF: Instrument Response Function.

In this paper, to understand the influence of the axial ligands, peripheral substituents and the solvents on the excited state relaxation dynamics of the heme, transient absorption spectra of various heme model compounds (Hemin-Cl, Hemin-Br, and Hemin-meso) were systematically measured in methanol (MeOH) and DMSO using femtosecond time-resolved pump–probe spectroscopy upon excitation at 380 nm. To the best of our knowledge, the transient absorption spectra of Hemin-Br and Hemin-meso have not been reported. As the solvent DMSO (0.28) possessing the similar value of dipolar solvation [$\Delta f(\epsilon, n)$] compared to the water (0.32),^{34–36} it could mimic the aqueous environment of the biological system. Figure 1 shows the chemical structures of various ferric heme

**Figure 1.** Chemical structures of heme model compounds and met-myoglobin.

model compounds used for the investigation. In order to corroborate the excited state relaxation dynamics of model compounds with met-myoglobin (met-Mb), which is an oxygen storage protein having heme *b* and high spin in nature,^{37,38} the transient absorption spectra of met-Mb in 0.1 M KPi buffer at pH 7 were also measured and compared. Here it is important to note that Chergui et. al recently observed the early relaxation dynamics of met-Mb which was controlled by spin state

crossover within the iron atom along with the generally accepted concept of vibrational cooling.¹⁸ The spectral and kinetic analysis of transient absorption spectra of heme model compounds reveals the involvement of multiple electronic spin states in the excited state relaxation dynamics and also the ground state recovery by the vibrational relaxation.

2. EXPERIMENTAL SECTION

2.1. Sample Preparation. Hemin-Cl, Hemin-Br, and Hemin-meso and dehydrated met-Mb were purchased from Frontier Scientific and Sigma-Aldrich, respectively, and used without further purification. The absorption spectra were measured with a Shimadzu UV-2600 UV/vis spectrophotometer coupled with Peltier thermostatic cell holders at various temperatures. In order to record the femtosecond transient absorption spectra, the absorbance of the samples was made to have between 0.4 and 0.6 at the pump wavelength (380 nm) in a 0.4 mm optical path length spinning sample cell, equivalent to a concentration of 60–100 μM . The ferrous compounds were prepared by the addition of sodium dithionite under argon atmosphere.

2.2. Femtosecond Transient Absorption Spectroscopy. The experimental details for the femtosecond transient absorption measurements have already been described elsewhere.³⁹ Briefly, it is a Ti:sapphire laser (Mai Tai HP, Spectra Physics, USA) centered at 800 nm having pulse width of <100 fs with 80 MHz repetition rate. The amplified laser was split into two in the ratio of 75:25%. The high energy beam was used to convert to the required wavelength (380 and 530 nm) for exciting the sample by using TOPAZ (Prime, Light Conversion). The white light continuum (340–1000 nm) was generated by focusing the part of amplified beam (200 mW) on a 1-mm-thick CaF₂ plate which split into two beams (sample and reference probe beams). The sample cell (0.4 mm path length) was refreshed by rotating in a constant speed. Finally, the white light continuum was focused into a 100 μm optical fiber coupled to imaging spectrometer after passing through the sample cell. The pump probe spectrophotometer (ExciPro) setup was purchased from CDP Systems Corp, Russia. Normally transient absorption spectra were obtained by averaging about 2000 excitation pulses for each spectral delay. All the measurements were carried out at the magic angle (54.7°). The time resolution of the pump–probe spectrometer is found to be about >120 fs.

3. RESULTS AND DISCUSSION

3.1. Stationary Absorption Spectra. The steady state absorption spectra of heme model compounds including the Hemin-Cl, Hemin-Br, and Hemin-meso in the ferric form were measured. All of these derivatives exhibit the characteristic features of penta-coordinated and high spin state.⁴⁰ Figure 2

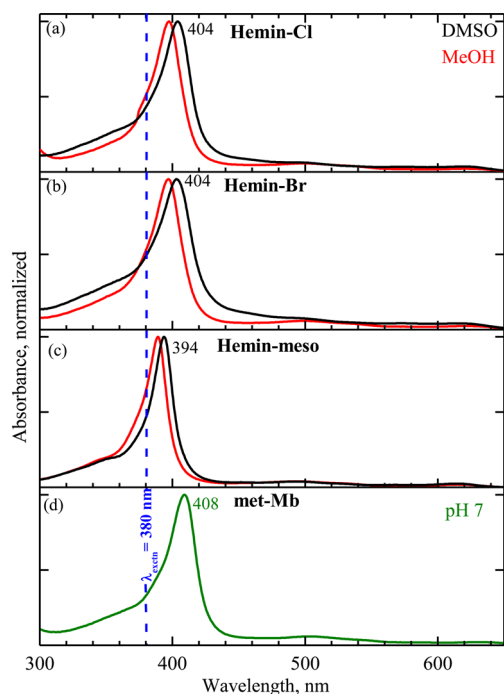


Figure 2. Absorption spectra of Hemin-Cl (a), Hemin-Br (b), and Hemin-meso (c) in MeOH (red) and DMSO (black). The absorption maxima of the heme model compounds in DMSO are given. The absorption spectra of met-Mb (d) in 0.1 M Kpi buffer at pH 7 is shown for comparison. The excitation wavelength ($\lambda_{\text{exctn}} = 380$ nm) used for transient absorption measurements is also shown in a dotted line (blue).

shows the absorption spectra of heme model compounds in MeOH and DMSO at room temperature. In Figure 2, the absorption spectrum of Hemin-Cl is dominated by Soret band appearing at 397 nm and Q bands around 500 and 623 nm due to the $\pi-\pi^*$ transition and consistent with previous literature.^{3,41} In the Hemin-Br, no significant changes in the absorption spectrum are observed in the Soret band region when compared to the Hemin-Cl, whereas in the case of Hemin-meso, the absorption spectra shifted toward the blue region (~ 389 nm) compared to Hemin-Cl reflecting that the saturation of the vinyl to ethyl group at the periphery minimized the electron withdrawing nature (or conjugation) of peripheral substituents.⁴² In DMSO where the axial ligand is still covalently associated,²⁸ all three model compounds showed red-shifted absorption maxima compared to the compounds in MeOH. The absorption spectrum of met-Mb in 0.1 M Kpi buffer at pH 7 is also shown for comparison in Figure 2.

The temperature-dependent absorption spectra of all the derivatives (20 to 50 °C in MeOH with an increment of 10 °C) and met-Mb were measured and shown in the Supporting Information as Figure S1. The purpose of measuring the temperature dependent absorption spectra is to correlate with the spectral shape obtained in the transient absorption spectra. Indeed, the differential absorption spectra obtained at temper-

ature ~ 40 °C (insets Figure.S1) show the similar characteristic features of transient absorption spectra at ~ 1 ps (Figure 3, vide

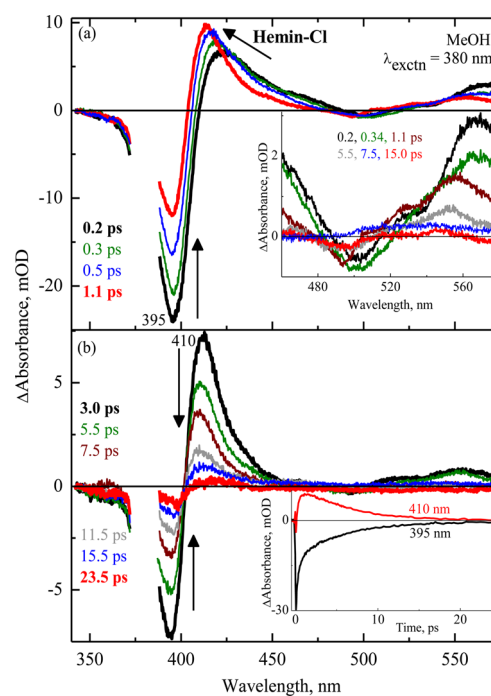


Figure 3. Femtosecond time-resolved transient absorption spectra of Hemin-Cl in MeOH obtained upon excitation at 380 nm. The different spectral time delays are given and the arrows show the spectral evolution. Inset: Transient absorption spectra at Q-band region (panel a) and kinetic decays obtained at the probe wavelengths of 395 and 410 nm (panel b).

infra), exhibiting positive and negative absorption at around the Soret band region due to the red-shift and broadening of absorption spectra at high temperatures. With an increase of temperature, the broadening of spectral bandwidth for Hemin-meso in MeOH is observed compared to met-Mb where no or little change of spectral bandwidth until 60 °C was seen.⁴³ This could be due to weakening of the extent of coupling between heme vibronic transitions and low-frequency motions in the model compounds at high temperatures.⁴⁴

3.2. Femtosecond Transient Absorption Spectra.

Figures 3 and 4 show the femtosecond time-resolved transient absorption spectra $\Delta A(\lambda, t)$ of the Hemin-Cl and -Br in MeOH obtained by exciting at 380 nm. In Figure 3 the spectral evolution of the Hemin-Cl at various time delays after the photoexcitation starting from 0.2 to 1.1 ps and 3.0 to 23.5 ps are shown in panel a and b, respectively. In the ultrafast transient absorption spectra, negative ΔA relates to the bleaching, due to the depopulation of the ground state, or stimulated emission from an excited state, whereas a positive ΔA initiates from the excited state absorption—photoinduced absorption of excited species. However, these spectral features typically overlap with each other. The earliest spectrum at 0.2 ps is dominated by a bleach band at ~ 395 nm and the excited state absorption at 415 to 470 nm and beyond 525 nm. In Figure 3a, when the spectral time increased to 0.5 ps, the decrease of the bleach band and an increase of excited state absorption along with a narrowing of spectral bandwidth and shifting toward blue region are observed. Figure 3b represents the transient absorption spectra at longer time delays where the

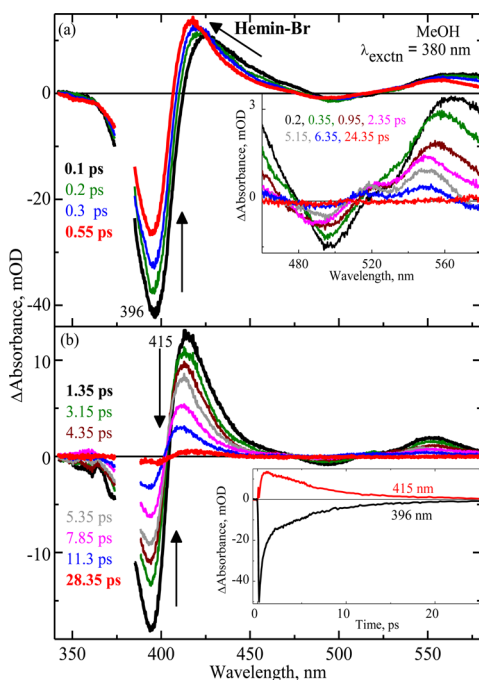


Figure 4. Femtosecond time-resolved transient absorption spectra of Hemin-Br in MeOH obtained upon excitation at 380 nm. The different spectral time delays are given and the arrows show the spectral evolution. Inset: Transient absorption spectra at Q-band region (panel a) and kinetic decays obtained at the probe wavelength of 396 and 415 nm (panel b).

overall spectral intensity decreased with time and recovered back to equilibrium on the spectral time scale of ~ 23.5 ps. The spectral evolution and shape of the transient absorption spectra of Hemin-Cl in MeOH are consistent with an earlier report.³ The inset in Figure 3a represents the enlarged spectral evolution starting from 460 to 580 nm at specific time intervals for clarity. Interestingly, it is observed that there is a peak formed at ~ 525 nm after the time delays of ~ 300 fs which persists longer than 8 ps.

The kinetic traces obtained at the excited state absorption (410 nm) and bleach (395 nm) maxima are shown as an inset in Figure 3b. The pattern of transient absorption spectra of Hemin-Br (Figure 4) in MeOH is similar to that of Hemin-Cl. In order to explore the influence of the excitation wavelength on the excited state dynamics, the transient absorption spectra of Hemin-Cl and -Br in MeOH were also measured upon excitation at 530 nm (Figures S2 and S3). The transient absorption spectra obtained by excitation at 380 nm shows a red shift and broadening in the excited state absorption spectra compared to 530 nm excitation. Due to the experimental limitation (excitation laser scattering at 530 nm), there is no access to observe the transient formation of the peak around 525 nm which could support the involvement of the electronic spin states (vide infra). In order to understand the effect of peripheral substituent on the excited state relaxation dynamics, for instance, replacement of vinyl by ethyl group leading to an increase in electron density on the porphyrin ring, the transient absorption spectra of Hemin-meso were measured in MeOH upon excitation at 380 nm. Figure 5 shows the transient absorption spectra of Hemin-meso in MeOH at different spectral time delays.

To get a better insight of chromophore–solvent interaction which influences the excited state relaxation dynamics of the

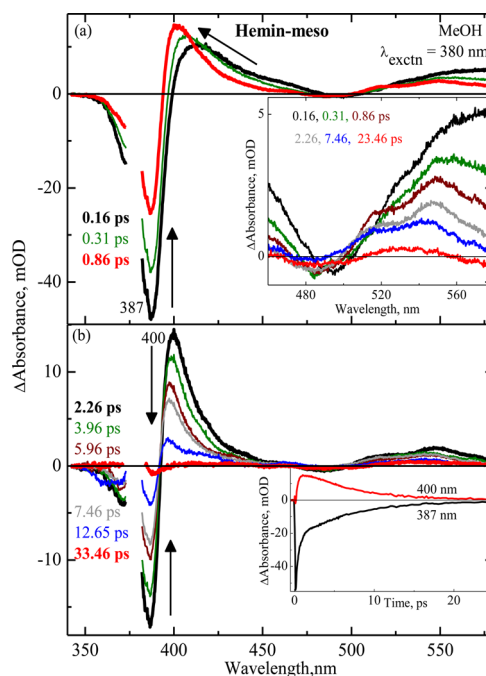


Figure 5. Femtosecond time-resolved transient absorption spectra of Hemin-meso in MeOH obtained upon excitation at 380 nm. The different spectral time delays are given in the insets and the arrows show the spectral evolution. Inset: Transient absorption spectra at Q-band region (panel a) and kinetic decays obtained at the probe wavelength of 400 and 387 nm (panel b).

heme, the transient absorption spectra of Hemin-Cl, -Br, and -meso in DMSO were also measured upon excitation 380 nm and are shown in Figures 6, S4, and S5, respectively. Though the pattern of spectral evolutions in DMSO is similar to that of MeOH, the relaxation dynamics is found to be stabilized in DMSO. Also, the presence of a long-lived species in all three

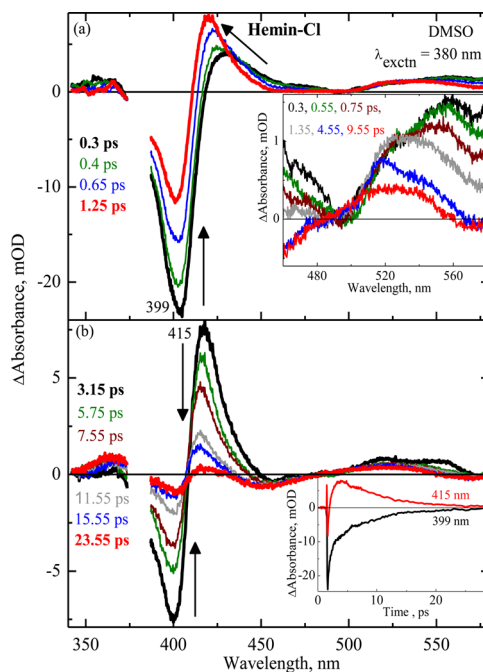


Figure 6. Femtosecond time-resolved transient absorption spectra of Hemin-Cl in DMSO obtained upon excitation at 380 nm.

heme model compounds is observed substantially in DMSO, which could be due to the formation of photoproducts.^{1,45} The amount of the long-lived components obtained in DMSO (Figure S6) is larger, and it is negligible in methanol. This could reflect that the compounds are more susceptible to form photoproducts in DMSO compared to the methanol upon laser excitation. To correlate the excited state dynamics of model compounds with the met-Mb where the heme is the prosthetic group, transient absorption spectra of met-Mb in 0.1 M Kpi buffer at pH 7 were measured upon excitation at 380 nm (Figure 7). The spectral evolution of the met-Mb at different

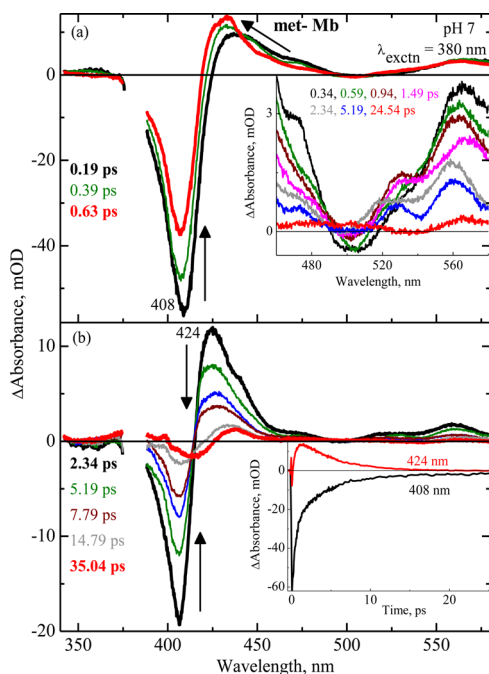


Figure 7. Femtosecond transient absorption spectra of met-Mb in 0.1 M Kpi buffer at pH 7 obtained upon excitation at 380 nm.

time delays shown in Figure 7 is rather similar to that of Hemin-Cl (Figure 3) in MeOH and the patterns are consistent with the literature.¹⁸ There is no contamination of MbO₂ in the met-Mb sample, which is confirmed by the absence of dual peaks in the Q-band region in the absorption spectra (Figure 2).

3.3. Spectral Analysis. The analysis of the femtosecond transient absorption spectra consisting of a three-dimensional data set including wavelength, time, and change in absorbance was performed with the global analysis program GLOTAR-AN.⁴⁶ In order to describe the excited state relaxation dynamics of model compounds completely, four exponential components

were optimally fitted to the transient absorption spectral data. The time constants obtained are shown in Table 2. Similarly, the transient absorption spectra of met-Mb were fitted with four exponentials globally and the resulted time constants are $\tau_1 \approx 70$ fs, $\tau_2 = 434 \pm 10$ fs, $\tau_3 = 1.09 \pm 0.06$ ps, and $\tau_4 = 4.34 \pm 0.07$ ps. These time constants are in good agreement with previous reports.^{18,33} The decay-associated spectra of these time constants for the model compounds in MeOH and DMSO are shown in Figure 8 and Figure S6, respectively. The decay-associated spectra obtained for the excitation at 380 nm exhibit common features of transient absorption spectra.

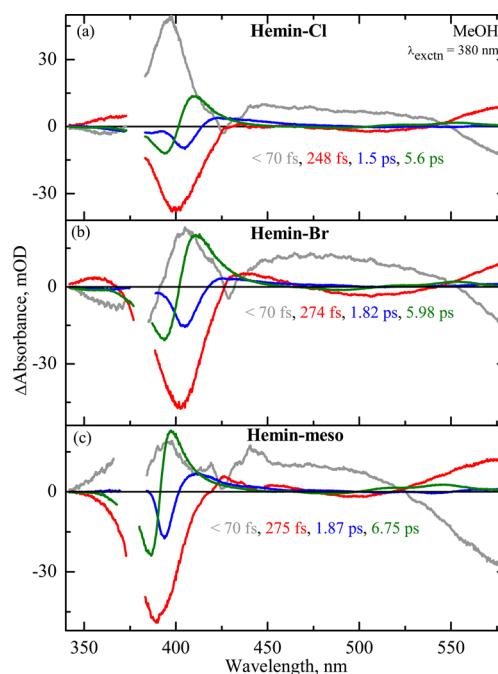


Figure 8. Decay associated spectra of heme model compounds in MeOH obtained from global analysis for 380 nm excitation.

3.3.1. Signature of Vibrational Cooling Dynamics. The generally accepted mechanism for the excited state relaxation dynamics of heme model compounds after the ultrafast excitation involved the sequential steps of ligand to metal charge transfer, iron d–d transition, and, importantly, the recovery of the ground state by vibrational relaxation.^{3,5,19,47} Indeed, the transient absorption spectra (Figures 3–7) of these model compounds exhibit that the excited state absorption spectra shift toward the blue region by narrowing the spectral width with the increase of spectral time in the picosecond range. This is a clear signature of the vibrational relaxation dynamics occurring in the system. We have calculated the

Table 2. Time Constants Obtained by Global Analysis Using Glotaran⁴⁶ for Heme Model Compounds at 380 nm Excitation

solvent	Hemin-Cl	Hemin-Br	Hemin-meso
Methanol	$\tau_1 < 70$ fs	$\tau_1 < 70$ fs	$\tau_1 < 70$ fs
	$\tau_2 = 248 \pm 10$ fs	$\tau_2 = 274 \pm 10$ fs	$\tau_2 = 275 \pm 15$ fs
	$\tau_3 = 1.50 \pm 0.05$ ps	$\tau_3 = 1.82 \pm 0.05$ ps	$\tau_3 = 1.87 \pm 0.06$ ps
	$\tau_4 = 5.60 \pm 0.06$ ps	$\tau_4 = 5.98 \pm 0.05$ ps	$\tau_4 = 6.75 \pm 0.07$ ps
DMSO	$\tau_1 < 70$ fs	$\tau_1 < 70$ fs	$\tau_1 < 70$ fs
	$\tau_2 = 296 \pm 10$ fs	$\tau_2 = 499 \pm 10$ fs	$\tau_2 = 580 \pm 20$ fs
	$\tau_3 = 2.02 \pm 0.05$ ps	$\tau_3 = 2.61 \pm 0.05$ ps	$\tau_3 = 2.95 \pm 0.06$ ps
	$\tau_4 = 6.58 \pm 0.06$ ps	$\tau_4 = 7.57 \pm 0.05$ ps	$\tau_4 = 9.22 \pm 0.08$ ps

amount of the ground state recovery occurring through back electron transfer (MLCT) by determining the ratio between the areas of the complete Soret band region of the static and transient absorption spectra (see Supporting Information, Table S1). It is found that $\sim 52 \pm 5\%$ of excited molecules directly relax to the hot electronic ground state reflecting the strong signature of vibrational relaxation in the excited state dynamics.¹⁸ (It is to be noted that the transition strength of the transient state Soret band is assumed to be the same as that of ground state.¹⁸) The spectral evolution of the excited state absorption of the compounds obtained by exciting at 380 nm compared to 530 nm excitation exhibits a red shift and broadening in the excited state absorption spectra (Figure S7). The time constants obtained for Hemin-Cl and Hemin-Br by using global analysis for the 530 nm excitation are given in Table S2 in the Supporting Information. Though $\sim 7500 \text{ cm}^{-1}$ additional energy is distributed over the large number of modes at 380 nm excitation, significant changes in the time constants are not observed at 380 nm excitation compared to 530 nm excitation. The increase of local heme temperature⁴⁸ to $\sim 880 \text{ K}$ by 380 nm excitation compared to 530 nm excitation ($\sim 750 \text{ K}$) is reflected in a red shift and broadening of the Soret band in the transient absorption spectra of 380 nm excitation. Though such a similar observation was also reported in different heme systems such as cytochrome c and met-myoglobin,¹⁸ it needs further investigation. In addition, the calculated amount of the direct ground state recovery for the 530 nm excitation is comparable to that of the 380 nm excitation ($\sim 50 \pm 10\%$) revealing the independence of pump energy.

3.3.2. Evidence of Multiple Electronic Spin States. In addition to the signature of the vibrational relaxation dynamics, the following spectral evolutions are observed in the transient absorption spectra of all the compounds. First, the appearance of a new peak around 525 nm after $\sim 300 \text{ fs}$ in the Q-band region of the transient absorption spectra of all the heme model compounds suggests the presence of a new electronic intermediate state in the fast relaxation dynamics. Second, the resemblance of the spectra at the Q-band region between the transient absorption spectra of the ferric form and ground state absorption spectra of the low spin ferrous form of heme model compounds indicates the involvement of low spin state of the central metal atom (Figure 9).^{18,49} Hence, the involvement of different electronic spin states in the excited state relaxation dynamics of model compounds is proposed along with the vibrational cooling processes.

Hence, the assignment of the resulting four time constants for the model compounds is described in detail based on the spectral evolution and literature as follows.^{3,5,18,31}

$\tau_1 \sim \text{LMCT}$. As the fluorescence lifetimes of the metalloporphyrins are shorter^{3,50} due to the electron transfer from the porphyrin macrocyclic ring to the metal iron atom, the time constant τ_1 , $< 70 \text{ fs}$ within our temporal resolution time, could be attributed to the ligand to metal charge transfer process. The ligand to metal charge transfer transition is supported by the observation of the broad peak around 630 nm consistent with the formation of a porphyrin cation in the transient absorption spectra of the model compounds (Figure 10).^{33,51,52} Alternatively, this time constant might also be due to the internal conversion from S_2 to S_1 state impeding the ultrafast ligand to metal charge transfer transition.

$\tau_2 \sim \text{MLCT}$. The decay-associated spectra of τ_2 possess the absorption maxima between 430 and 470 nm and longer than 550 nm, which is comparable to the singlet absorption spectra

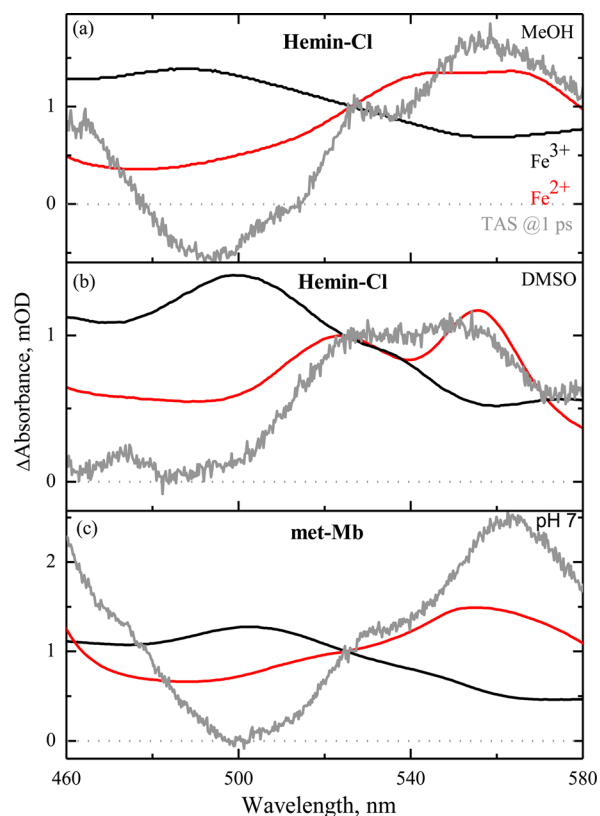


Figure 9. Steady state absorption spectra of ferric (black) and ferrous (red) forms of Hemin-Cl in MeOH (a) and DMSO (b) and met-Mb (c) in 0.1 M Kpi buffer at pH 7. Femtosecond transient absorption spectra (gray) recorded at 1 ps are also given for comparison. All the spectra are normalized at 525 nm for clarity.

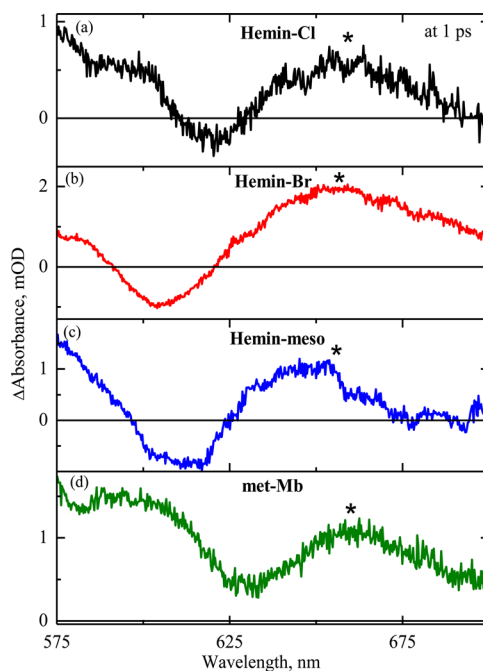


Figure 10. Transient absorption spectra of model compounds and met-Mb measured at 1 ps after the photoexcitation. The asterisk represents the absorption maximum of the porphyrin cation.

of the metallo-porphyrins^{20,53} and porphyrin cations.^{52,54} The transiently formed porphyrin cation (charge separated species)

by LMCT is stable enough and electron transferred to the metal orbital can be promoted back to refilling the porphyrin HOMO.^{18,55} Furthermore, this time constant is much faster compared to the generally observed vibrational cooling time constant in the range of picoseconds (~ 3 – 8 ps).^{26,56} Such a similar time constant was obtained for hemoglobin and attributed to the back electron transfer.³¹ Hence, the time constant obtained in the range of 248 to 580 fs could be correlated to the dynamics of the back electron transfer from the metal to porphyrin orbital.^{20,31}

τ_3 and $\tau_4 \sim (S = \frac{1}{2}$ and $\frac{3}{2}$). There is a formation of the peak at ~ 525 nm appearing as double peaks in the Q-band region after the 300 fs time delay in the transient absorption spectra for all the heme model compounds and met-Mb (Figures 3–7 and Figure S8). The spectral resemblance between the transient absorption spectra of Hemin-Cl at 1 ps and the steady state absorption spectra of the low spin ferrous form of Hemin-Cl in MeOH and DMSO in the Q-band region is shown in Figure 9. Furthermore, the transient water ligated 6C ferric met-Mb and 6C ferrous Mb showed similar spectral features around Q-band region at low temperature.⁴⁹ Hence, these resembling observations could reflect the similar electronic distribution on the heme macrocycle, particularly the population of the Fe orbitals where the $d\pi$ orbitals are stabilized leading to the low spin state. Thus, the time constant τ_3 is attributed to the state where the iron is in the low spin state ($S = \frac{1}{2}$) having four electrons in the $d\pi$ orbitals. Apparently, the relaxation dynamics will be completed by passing through the intermediate quartet spin state ($S = \frac{3}{2}$) to the high spin ground state ($S = \frac{5}{2}$). Hence, the time constant, τ_4 , is tentatively assigned to the intermediate spin state, where the iron would possess the spin state of ($S = \frac{3}{2}$).

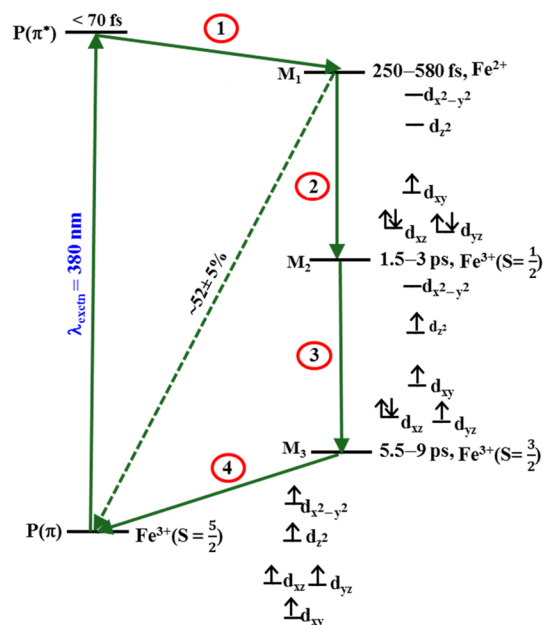
It is important to note that these assignments are corroborated with the earlier observation of the transient absorption spectra of met-Mb where the initial relaxation dynamic was found to have the different electronic spin state of the iron atom.¹⁸ The involvement of electronically excited intermediate state in the relaxation dynamics has also been reported in the literature for the model compounds as well as proteins.^{18,29,30} However, the involvement of different electronic spin states can be further characterized by using the femtosecond X-ray absorption spectroscopy⁵⁷ and femtosecond stimulated resonance Raman spectroscopy with the time resolution of 50 fs.²³

Thus, based on the spectral evolution, global analysis, and literature,^{3,5,18} the mechanism of excited state relaxation dynamics of heme model compounds comprising different electronic spin states is proposed and illustrated in Scheme 1.

3.4. Effect of Axial Ligands, Peripheral Substituents, and Solvents. Though the energy levels of Fe centered d-orbitals in the various heme model compounds could be different, the correlation of variation of time constants among the model compounds has been attempted. Here the time constants obtained for different heme model compounds in MeOH and DMSO are compared with respect to the Hemin-Cl in MeOH. Since the shortest time constant, τ_1 , obtained for different compounds is within our instrument response function (< 120 fs), no conclusion can be made by comparison.

3.4.1. Hemin-Br. The relaxation time constants, particularly, τ_3 and τ_4 obtained for Hemin-Br, are increased when compared to the Hemin-Cl. This could be due to the fact that the

Scheme 1. Proposed Mechanism for Excited State Relaxation Dynamics of Model Compounds Involving Different Electronic Spin States of Iron



replacement of ligand with weaker field strength (Cl > Br) could stabilize the energy level of both the d_z^2 and d_x orbitals, consequently leading to the intermediate or low spin states by dropping an electron from the $d_{x^2-y^2}$ orbital to one of the lowest d_x orbitals^{58–60} as shown in Scheme 1.

3.4.2. Hemin-meso. The relaxation time constants of Hemin-meso are longer when compared to Hemin-Cl. In the case of Hemin-meso, when the vinyl is replaced by the ethyl group, the lowering of conjugation in the periphery of the porphyrin ring would lead to the increase of electron density at the iron center. In addition, certain significant changes including the absence of the torsional conformers, the basicity of amide nitrogen atoms, and binding affinity of ligand to a central metal occur in the Hemin-meso.^{42,44} These changes could collectively lead to the increase of the time constants for the Hemin-meso compared to the Hemin-Cl.

3.4.3. DMSO. Interestingly, a systematic increase of all the relaxation time constants in DMSO is observed for all the compounds, compared to MeOH. This may be due to the increase of interaction between axial ligand and oxygen of the DMSO which altered the electron density of iron atom in the porphyrin leading to the stabilization of the relaxation pathway. Nevertheless, the slower time constants in DMSO by the less efficient energy dissipation due to the higher viscosity of DMSO⁶¹ may not be ruled out. Such stabilization of charge transfer dynamics, vibrational cooling, and different electronic spin states with the increase of solvent polarity and viscosity were already observed in different metallo-porphyrin derivatives.^{62–65}

4. CONCLUSION

The femtosecond pump–probe spectroscopy was used to investigate the effect of the axial ligand (Cl/Br), peripheral substituent (vinyl/ethyl-meso), and solvent (methanol/DMSO) on the excited state relaxation dynamics of the heme. Overall, the transient absorption spectra of the model compounds reveal evidence of the involvement of both

vibrational relaxation and intermediate electronic spin states in the excited state relaxation dynamics. For example, the signature of the vibrational cooling is reflected by the evolution of excited state absorption spectra as the narrowing of the spectral bandwidth and shifting toward the blue region with an increase of the spectral time in the picosecond range. Simultaneously the existence of multiple electronic spins states is observed by the appearance of the new peak at ~ 525 nm after ~ 300 fs and lasting for ~ 8 ps which leads to the spectral similarities between the transient absorption spectra of the ferric form and ground state absorption spectra of the low spin ferrous form of heme model compounds. Coincidentally the time constants proposed for the different electronic spin states can be correlated with the various stages of the vibrational cooling processes. As the spectral and kinetic analysis of transient absorption spectra of the model compounds showed similar characteristics to that of met-Mb, the involvement of multiple electronic spin states could be an alternative pathway to the ground state along with the vibrational relaxation process in the deactivation pathway of photoexcited heme model compounds and related to be an inherent feature of the heme *b* type.

■ ASSOCIATED CONTENT

📄 Supporting Information

The Supporting Information is available free of charge on the ACS Publications website at DOI: [10.1021/acs.jpcc.7b01416](https://doi.org/10.1021/acs.jpcc.7b01416).

Ground state absorption spectra of heme model compounds and met-Mb at different temperatures, the femtosecond transient absorption spectra of Hemin-Br and -meso in DMSO at 380 nm excitation, transient absorption spectra of Hemin-Cl and -Br in MeOH obtained by excitation at 530 nm and respective time constants, and normalized transient absorption spectra of the compounds in the Q-band region (PDF)

■ AUTHOR INFORMATION

Corresponding Author

*E-mail: k.venugopal@niist.res.in. Phone: 091-471-2515240.

ORCID

Venugopal Karunakaran: [0000-0001-8482-0900](https://orcid.org/0000-0001-8482-0900)

Notes

The authors declare no competing financial interest.

■ ACKNOWLEDGMENTS

C.G gratefully acknowledges UGC, New Delhi for her fellowship. V. K. acknowledges DST-Extra Mural Research Funding (EMR/2014/001116), Government of India, for financial support. The authors acknowledge DST Indo-European project (OISC-LARGECELL) for setting up femto-second pump–probe spectrometer.

■ REFERENCES

- (1) Rury, A. S.; Wiley, T. E.; Sension, R. J. Energy Cascades, Excited State Dynamics, and Photochemistry in Cob(III)alamins and Ferric Porphyrins. *Acc. Chem. Res.* **2015**, *48*, 860–867.
- (2) Rury, A. S.; Goodrich, L. E.; Galinato, M. G. I.; Lehnert, N.; Sension, R. J. Ligand Recruitment and Spin Transitions in the Solid-State Photochemistry of Fe(III)TPPCL. *J. Phys. Chem. A* **2012**, *116*, 8321–8333.
- (3) Marcelli, A.; Jelovica Badovinac, I.; Orlic, N.; Salvi, P. R.; Gellini, C. Excited-State Absorption and Ultrafast Relaxation Dynamics of

Protoporphyrin IX and Hemin. *Photochem. Photobiol. Sci.* **2013**, *12*, 348–355.

- (4) Moroni, L.; Gellini, C.; Salvi, P. R.; Marcelli, A.; Foggi, P. Excited States of Porphyrin Macrocycles. *J. Phys. Chem. A* **2008**, *112*, 11044–11051.

- (5) Ha-Thi, M.-H.; Shafizadeh, N.; Poisson, L.; Soep, B. First Observation in the Gas Phase of the Ultrafast Electronic Relaxation Pathways of the S₂ States of Heme and Hemin. *Phys. Chem. Chem. Phys.* **2010**, *12*, 14985–14993.

- (6) Challa, J. R.; Gunaratne, T. C.; Simpson, M. C. State Preparation and Excited Electronic and Vibrational Behavior in Hemes. *J. Phys. Chem. B* **2006**, *110*, 19956–19965.

- (7) Rury, A. S.; Sension, R. J. Broadband Ultrafast Transient Absorption of Iron (III) tetraphenylporphyrin Chloride in the Condensed phase. *Chem. Phys.* **2013**, *422*, 220–228.

- (8) Poulos, T. L. Heme Enzyme Structure and Function. *Chem. Rev.* **2014**, *114*, 3919–3962.

- (9) Kleingardner, J. G.; Bren, K. L. Biological Significance and Applications of Heme c Proteins and Peptides. *Acc. Chem. Res.* **2015**, *48*, 1845–1852.

- (10) Vos, M. H. Ultrafast Dynamics of Ligands within Heme Proteins. *Biochim. Biophys. Acta, Bioenerg.* **2008**, *1777*, 15–31.

- (11) Girvan, H. M.; Munro, A. W. Heme Sensor Proteins. *J. Biol. Chem.* **2013**, *288*, 13194–13203.

- (12) Kepp, K. P. Heme: from Quantum Spin Crossover to Oxygen Manager of Life. *Coord. Chem. Rev.* **2016**, *1* DOI: [10.1016/j.ccr.2016.08.008](https://doi.org/10.1016/j.ccr.2016.08.008).

- (13) Bowman, S. E. J.; Bren, K. L. The Chemistry and Biochemistry of Heme c: Functional Bases for Covalent Attachment. *Nat. Prod. Rep.* **2008**, *25*, 1118–1130.

- (14) Schneider, S.; Marles-Wright, J.; Sharp, K. H.; Paoli, M. Diversity and Conservation of Interactions for Binding Heme in b-type Heme Proteins. *Nat. Prod. Rep.* **2007**, *24*, 621–630.

- (15) Satoh, T.; Itoga, A.; Isogai, Y.; Kurihara, M.; Yamada, S.; Natori, M.; Suzuki, N.; Suruga, K.; Kawachi, R.; Arahira, M.; et al. Increasing the Conformational Stability by Replacement of Heme Axial Ligand in c-Type Cytochrome. *FEBS Lett.* **2002**, *531*, 543–547.

- (16) Paoli, M.; Marles-Wright, J.; Smith, A. Structure–Function Relationships in Heme-Proteins. *DNA Cell Biol.* **2002**, *21*, 271–280.

- (17) Walker, F. A.; Simonis, U. Iron Porphyrin Chemistry. In *Encyclopedia of Inorganic Chemistry*; John Wiley & Sons, Ltd, 2006.

- (18) Consani, C.; Auböck, G.; Bräm, O.; van Mourik, F.; Chergui, M. A Cascade Through Spin States in the Ultrafast Haem Relaxation of met-Myoglobin. *J. Chem. Phys.* **2014**, *140*, 025103.

- (19) Ye, X.; Demidov, A.; Rosca, F.; Wang, W.; Kumar, A.; Ionascu, D.; Zhu, L.; Barrick, D.; Wharton, D.; Champion, P. M. Investigations of Heme Protein Absorption Line Shapes, Vibrational Relaxation, and Resonance Raman Scattering on Ultrafast Time Scales. *J. Phys. Chem. A* **2003**, *107*, 8156–8165.

- (20) Rodriguez, J.; Kirmaier, C.; Holten, D. Optical Properties of Metalloporphyrin Excited States. *J. Am. Chem. Soc.* **1989**, *111*, 6500–6506.

- (21) Petrich, J. W.; Poyart, C.; Martin, J. L. Photophysics and Reactivity of Heme Proteins: A Femtosecond Absorption Study of Hemoglobin, Myoglobin, and Protoheme. *Biochemistry* **1988**, *27*, 4049–4060.

- (22) Baskin, J. S.; Yu, H.-Z.; Zewail, A. H. Ultrafast Dynamics of Porphyrins in the Condensed Phase: I. Free Base Tetraphenyl Porphyrin. *J. Phys. Chem. A* **2002**, *106*, 9837–9844.

- (23) Ferrante, C.; Pontecorvo, E.; Cerullo, G.; Vos, M. H.; Scopigno, T. Direct Observation of Subpicosecond Vibrational Dynamics in Photoexcited Myoglobin. *Nat. Chem.* **2016**, *8*, 1137–1143.

- (24) Karunakaran, V. Ultrafast Heme Dynamics of Ferric Cytochrome c in Different Environments: Electronic, Vibrational, and Conformational Relaxation. *ChemPhysChem* **2015**, *16*, 3974–3983.

- (25) Kholodenko, Y.; Volk, M.; Gooding, E.; Hochstrasser, R. M. Energy Dissipation and Relaxation Processes in Deoxy myoglobin After Photoexcitation in the Soret Region. *Chem. Phys.* **2000**, *259*, 71–87.

- (26) Zhang, Y.; Fujisaki, H.; Straub, J. E. Direct Evidence for Mode-Specific Vibrational Energy Relaxation from Quantum Time-Dependent Perturbation Theory. I. Five-Coordinate Ferrous Iron Porphyrin Model. *J. Chem. Phys.* **2009**, *130*, 025102.
- (27) Mizutani, Y.; Kitagawa, T. Direct Observation of Cooling of Heme Upon Photodissociation of Carbonmonoxy Myoglobin. *Science* **1997**, *278*, 443–446.
- (28) Atak, K.; Golnak, R.; Xiao, J.; Suljoti, E.; Pflüger, M.; Brandenburg, T.; Winter, B.; Aziz, E. F. Electronic Structure of Hemin in Solution Studied by Resonant X-ray Emission Spectroscopy and Electronic Structure Calculations. *J. Phys. Chem. B* **2014**, *118*, 9938–9943.
- (29) Helbing, J. Spin State Transitions Upon Visible and Infrared Excitation of Ferric MbN3. *Chem. Phys.* **2012**, *396*, 17–22.
- (30) Lim, M.; Jackson, T. A.; Anfinrud, P. A. Femtosecond Near-IR Absorbance Study of Photoexcited Myoglobin: Dynamics of Electronic and Thermal Relaxation. *J. Phys. Chem.* **1996**, *100*, 12043–12051.
- (31) Franzen, S.; Kiger, L.; Poyart, C.; Martin, J.-L. Heme Photolysis Occurs by Ultrafast Excited State Metal-to-Ring Charge Transfer. *Biophys. J.* **2001**, *80*, 2372–2385.
- (32) Cornelius, P. A.; Steele, A. W.; Chernoff, D. A.; Hochstrasser, R. M. Different Dissociation Pathways and Observation of an Excited Deoxy State in Picosecond Photolysis of Oxy- and Carboxymyoglobin. *Proc. Natl. Acad. Sci. U. S. A.* **1981**, *78*, 7526–7529.
- (33) Ishizaka, S.; Wada, T.; Kitamura, N. Femtosecond Transient Absorption Study on Relaxation Intermediates in Oxymyoglobin. *Photochem. Photobiol. Sci.* **2009**, *8*, 562–566.
- (34) Mataga, N.; Kaifu, Y.; Koizumi, M. Solvent Effects upon Fluorescence Spectra and the Dipolemoments of Excited Molecules. *Bull. Chem. Soc. Jpn.* **1956**, *29*, 465–470.
- (35) Lakowicz, J. R. *Principles of Fluorescence Spectroscopy*; Springer: New York, 2006; pp 208.
- (36) Weigel, A.; Dobryakov, A. L.; Veiga, M.; Pérez Lustres, J. L. Photoinduced Processes in Riboflavin: Superposition of $\pi\pi^*$ – $n\pi^*$ States by Vibronic Coupling, Transfer of Vibrational Coherence, and Population Dynamics Under Solvent Control. *J. Phys. Chem. A* **2008**, *112*, 12054–12065.
- (37) Cao, W.; Christian, J. F.; Champion, P. M.; Rosca, F.; Sage, J. T. Water Penetration and Binding to Ferric Myoglobin. *Biochemistry* **2001**, *40*, 5728–5737.
- (38) Evans, S. V.; Brayer, G. D. Horse Heart met-Myoglobin. A 2.8-Å Resolution Three-Dimensional Structure Determination. *J. Biol. Chem.* **1988**, *263*, 4263–4268.
- (39) Karunakaran, V.; Das, S. Direct Observation of Cascade of Photoinduced Ultrafast Intramolecular Charge Transfer Dynamics in Diphenyl Acetylene Derivatives: Via Solvation and Intramolecular Relaxation. *J. Phys. Chem. B* **2016**, *120*, 7016–7023.
- (40) Owens, J. W.; O'Connor, C. J. Comparison of the Electronic and Vibrational Spectra of Complexes of Protoporphyrin-IX, Hemeoctapeptide, and Heme Proteins. *Coord. Chem. Rev.* **1988**, *84*, 1–45.
- (41) Boffi, A.; Das, T. K.; della Longa, S.; Spagnuolo, C.; Rousseau, D. L. Pentacoordinate Hemin Derivatives in Sodium Dodecyl Sulfate Micelles: Model Systems for the Assignment of the Fifth Ligand in Ferric Heme Proteins. *Biophys. J.* **1999**, *77*, 1143–1149.
- (42) Caughey, W. S.; Ibers, J. A. Crystal and Molecular Structure of the Free Base Porphyrin, Protoporphyrin IX Dimethyl Ester. *J. Am. Chem. Soc.* **1977**, *99*, 6639–6645.
- (43) Chaijan, M.; Benjakul, S.; Visessanguan, W.; Faustman, C. Characterisation of Myoglobin From Sardine (*Sardinella gibbosa*) Dark Muscle. *Food Chem.* **2007**, *100*, 156–164.
- (44) Boffi, A.; Zamparelli, C.; Verzili, D.; Ilari, A.; Chiancone, E. Effect of the Vinyl–Globin Interactions on the Temperature-Dependent Broadening of the Soret Spectra: A Study with Horse Myoglobin and Scapharca Dimeric Hemoglobin Reconstituted with Unnatural 2,4-Heme Derivatives. *Arch. Biochem. Biophys.* **1997**, *340*, 43–51.
- (45) Consani, C.; Bräm, O.; van Mourik, F.; Cannizzo, A.; Chergui, M. Energy Transfer and Relaxation Mechanisms in Cytochrome c. *Chem. Phys.* **2012**, *396*, 108–115.
- (46) Snellenburg, J. J.; Liptonok, S.; Seger, R.; Mullen, K. M.; van Stokkum, I. H. M. Glotaran: A Java-Based Graphical User Interface for the R Package TIMP. *J. Stat. Softw.* **2012**, *49*, 22.
- (47) Rodriguez, J.; Kirmaier, C.; Holten, D. Time-resolved and Static Optical Properties of Vibrationally Excited Porphyrins. *J. Chem. Phys.* **1991**, *94*, 6020–6029.
- (48) Henry, E. R.; Eaton, W. A.; Hochstrasser, R. M. Molecular Dynamics Simulations of Cooling in Laser-Excited Heme Proteins. *Proc. Natl. Acad. Sci. U. S. A.* **1986**, *83*, 8982–8986.
- (49) Engler, N.; Ostermann, A.; Gassmann, A.; Lamb, D. C.; Prusakov, V. E.; Schott, J.; Schweitzer-Stenner, R.; Parak, F. G. Protein Dynamics in an Intermediate State of Myoglobin: Optical Absorption, Resonance Raman Spectroscopy, and X-Ray Structure Analysis. *Biophys. J.* **2000**, *78*, 2081–2092.
- (50) Berezin, M. Y.; Achilefu, S. Fluorescence Lifetime Measurements and Biological Imaging. *Chem. Rev.* **2010**, *110*, 2641–2684.
- (51) Dolphin, D.; Felton, R. H. Biochemical Significance of Porphyrin pi Cation Radicals. *Acc. Chem. Res.* **1974**, *7*, 26–32.
- (52) Fajer, J.; Borg, D. C.; Forman, A.; Dolphin, D.; Felton, R. H. pi-Cation Radicals and Dications of Metalloporphyrins. *J. Am. Chem. Soc.* **1970**, *92*, 3451–3459.
- (53) Zhang, X.; Wasinger, E. C.; Muresan, A. Z.; Attenkofer, K.; Jennings, G.; Lindsey, J. S.; Chen, L. X. Ultrafast Stimulated Emission and Structural Dynamics in Nickel Porphyrins. *J. Phys. Chem. A* **2007**, *111*, 11736–11742.
- (54) Chang, C. K.; Hanson, L. K.; Richardson, P. F.; Young, R.; Fajer, J. pi Cation Radicals of Ferrous and Free Base Isobacteriochlorins: Models for Siroheme and Sirohydrochlorin. *Proc. Natl. Acad. Sci. U. S. A.* **1981**, *78*, 2652–2656.
- (55) Huszánk, R.; Lendvay, G.; Horváth, O. Air-Stable, Heme-Like Water-Soluble Iron(II) Porphyrin: in Situ Preparation and Characterization. *JBIC, J. Biol. Inorg. Chem.* **2007**, *12*, 681–690.
- (56) Bu, L.; Straub, J. E. Simulating Vibrational Energy Flow in Proteins: Relaxation Rate and Mechanism for Heme Cooling in Cytochrome c. *J. Phys. Chem. B* **2003**, *107*, 12339–12345.
- (57) Shelby, M. L.; Lestrangle, P. J.; Jackson, N. E.; Haldrup, K.; Mara, M. W.; Stickrath, A. B.; Zhu, D.; Lemke, H. T.; Chollet, M.; Hoffman, B. M.; et al. Ultrafast Excited State Relaxation of a Metalloporphyrin Revealed by Femtosecond X-ray Absorption Spectroscopy. *J. Am. Chem. Soc.* **2016**, *138*, 8752–8764.
- (58) Sakai, T.; Ohgo, Y.; Hoshino, A.; Ikeue, T.; Saitoh, T.; Takahashi, M.; Nakamura, M. Electronic Structures of Five-Coordinate Iron(III) Porphyrin Complexes with Highly Ruffled Porphyrin Ring. *Inorg. Chem.* **2004**, *43*, 5034–5043.
- (59) Goff, H. M.; Shimomura, E. T.; Phillippi, M. A. Correlations of Axial Ligand Field Strength and Zero-Field Splittings in the Carbon-13 NMR Spectra of Five- and Six-Coordinate High-Spin Iron(III) Porphyrin Complexes. *Inorg. Chem.* **1983**, *22*, 66–71.
- (60) Ikezaki, A.; Nakamura, M. Effects of Solvents on the Electron Configurations of the Low-Spin Dicyano[meso-tetrakis(2,4,6-triethylphenyl)porphyrinato]iron(III) Complex: Importance of the C–H...N Weak Hydrogen Bonding. *Inorg. Chem.* **2002**, *41*, 2761–2768.
- (61) Liu, J.-Y.; Fan, W.-H.; Han, K.-L.; Deng, W.-Q.; Xu, D.-L.; Lou, N.-Q. Ultrafast Vibrational and Thermal Relaxation of Dye Molecules in Solutions. *J. Phys. Chem. A* **2003**, *107*, 10857–10861.
- (62) Yu, H. Z.; Baskin, J. S.; Steiger, B.; Wan, C. Z.; Anson, F. C.; Zewail, A. H. Femtosecond Dynamics of Metalloporphyrins: Electron Transfer and Energy Redistribution. *Chem. Phys. Lett.* **1998**, *293*, 1–8.
- (63) Dietzek, B.; Kiefer, W.; Hermann, G.; Popp, J.; Schmitt, M. Solvent Effects on the Excited-State Processes of Protochlorophyllide: A Femtosecond Time-Resolved Absorption Study. *J. Phys. Chem. B* **2006**, *110*, 4399–4406.
- (64) Liu, J.-Y.; Fan, W.-H.; Han, K.-L.; Deng, W.-Q.; Xu, D.-L.; Lou, N.-Q. Ultrafast Vibrational and Thermal Relaxation of Dye Molecules in Solutions. *J. Phys. Chem. A* **2003**, *107*, 10857–10861.

(65) Benniston, A. C.; Matousek, P.; McCulloch, I. E.; Parker, A. W.; Towrie, M. Detailed Picosecond Kerr-Gated Time-Resolved Resonance Raman Spectroscopy and Time-Resolved Emission Studies of Merocyanine 540 in Various Solvents. *J. Phys. Chem. A* **2003**, *107*, 4347–4353.

Ultrafast Heme Relaxation Dynamics Probing the Unfolded States of Cytochrome c Induced by Liposomes: Effect of Charge of Phospholipids

Chinju Govind, Megha Paul, and Venugopal Karunakaran*

Cite This: *J. Phys. Chem. B* 2020, 124, 2769–2777

Read Online

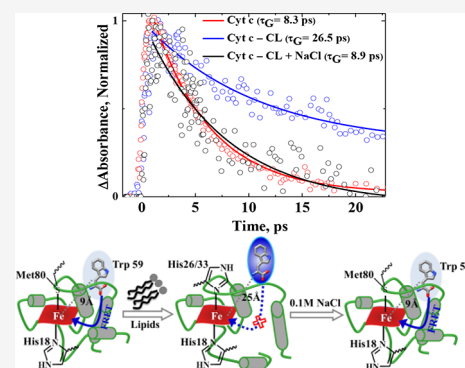
ACCESS |

Metrics & More

Article Recommendations

Supporting Information

ABSTRACT: The ubiquitous electron transfer heme protein, Cytochrome c (Cyt c) catalyzes the peroxidation of cardiolipin (CL) in the early stage of apoptosis, where Cyt c undergoes conformational changes leading to the partial unfolding of the protein. Here the interaction dynamics of Cyt c with liposomes having different charges [CL, -2 ; POPG (2-Oleoyl-1-palmitoyl-*sn*-glycero-3-phospho-rac-(1-glycerol) sodium salt), -1 ; and POPC (2-Oleoyl-1-palmitoyl-*sn*-glycero-3-phosphocholine), 0] leading to various degrees of partial unfolding is investigated with steady state optical spectroscopy and femtosecond time-resolved pump–probe spectroscopy. The signature of the partial unfolding of the protein was observed in the absorption, fluorescence, and CD spectra of Cyt c–liposome complexes with an increase of lipid/protein (L/P) ratio, and the protein was refolded by the addition of 0.1 M of NaCl. The femtosecond transient absorption spectra of the complexes were measured by selectively exciting the heme and tryptophan (Trp) at 385 and 280 nm, respectively. Though significant changes were not observed in the excited state relaxation dynamics of the heme in liposomes by exciting at 385 nm, the 280 nm excitation exhibited a systematic increase of the excited state relaxation dynamics leading to the increase of lifetime of Trp and global conformational relaxation dynamics with the increase of anionic charge of the lipids. This reveals the decrease of efficiency of fluorescence resonance energy transfer from Trp to heme due to the increase of distance between them upon increase of partial unfolding of the proteins by liposomes. Such observation exhibits the Trp as a marker amino acid to reflect the dynamics of partial unfolding of the protein rising from the change in the tertiary structure and axial ligand interaction of the heme proteins in liposomes. The relaxation dynamics of the complexes in the presence of salt are similar to that of the protein alone, reflecting that the refolding of the protein and the interactions are dominated by electrostatic interaction rather than the hydrophobic interaction.



1. INTRODUCTION

Cytochrome c (Cyt c), is an important electron transfer heme protein found in mitochondria.^{1–3} Over the past decade, intense research has been focused to understand the catalytic role and unfolding nature of Cyt c in the apoptosis process (programmed cell death)^{4–7} besides the protein being used as a suitable model for understanding the folding and unfolding processes of the heme proteins.^{8,9} This globular protein is six-coordinated and in low spin state containing a prosthetic heme group with His18 (proximal) and Met80 (distal) as axial ligands¹⁰ (Figure 1). Cyt c contains a single Trp residue (Trp59) that is supposed to specifically probe the structural and conformational perturbation during the unfolding process.¹¹ In the early stages of apoptosis, Cyt c acts as a catalyst for peroxidation of an anionic phospholipid, CL, where it undergoes conformational changes leading to partial unfolding once bound with CL.^{12–17}

The interaction dynamics of Cyt c with different lipids have been carried out using various spectroscopies including NMR, FRET, EPR, CD, absorption, resonance Raman, and flash

photolysis.^{18–23} Though various mechanisms including electrostatic and hydrophobic interactions and hydrogen bonding⁶ proposed for the Cyt c–liposome interaction, understanding of the interaction dynamics is not yet clear. The two binding sites were proposed for the interaction of Cyt c with liposomes, namely A and C sites. A site involves the electrostatic interaction via positively charged Lys72 and 73 and negatively charged phosphate group of lipids. However, the C site has the hydrophobic interaction through hydrogen bonding between Asn52 and protonated lipid phosphate group.^{24,25} A third binding L site was recently observed by the involvement of Lys22, Lys27, Lys87, and His33.²⁶

Received: December 27, 2019

Revised: March 14, 2020

Published: March 17, 2020



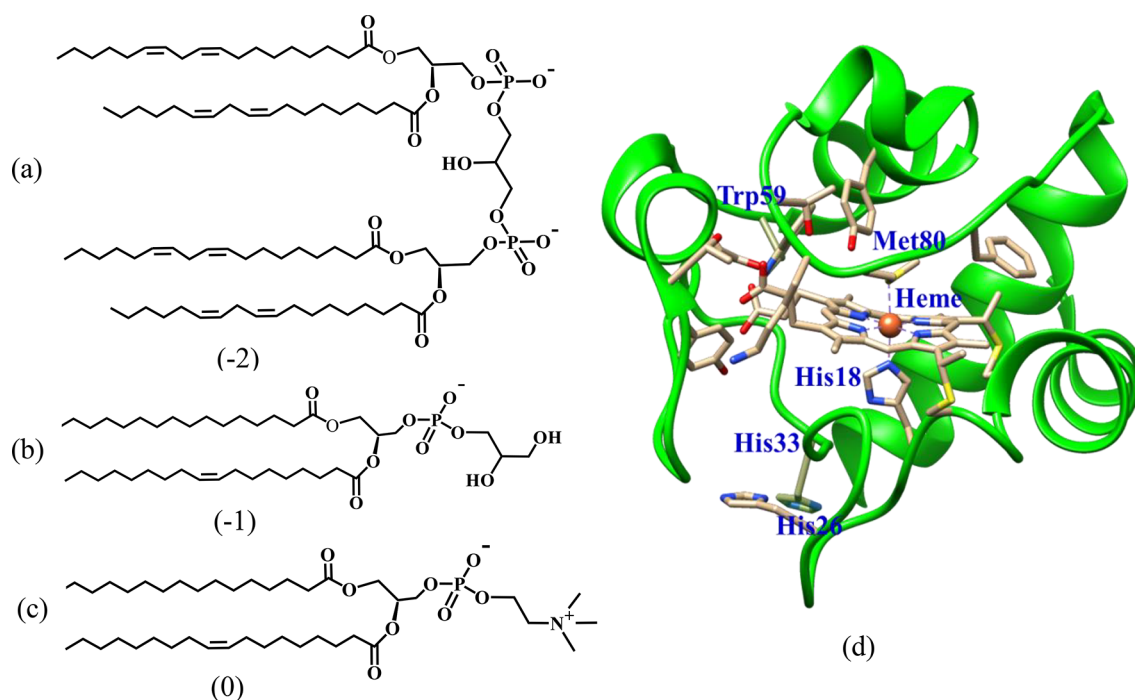


Figure 1. Chemical structures of CL (a), POPG (b), and POPC (c) and crystal structure of horse heart ferric Cyt c (d) from PDB: 1HRC.¹⁰ The charge of the lipids is also mentioned.

Hong et al.²⁷ reported the two distinct conformations including an extended and compact form for CL bound Cyt c using time-resolved FRET and found that their distribution was dependent on the CL content and protein coverage of the membrane surface. Schweitzer-Stenner et al.²⁸ investigated binding interaction of ferric Cyt c with liposomes composed of TOCL (20%) + DOPC (80%) using fluorescence and circular dichroism (CD) spectroscopy. The studies revealed the presence of two independent binding sites with different affinity yielding various degrees of unfolding of the protein eliminating the probability of significant protein insertion into the membrane. Upon interaction with CL,¹⁸ the Cyt c formed a misligated bis-His species (His18 and His26/His33) by the rupture of the His26···Pro44 hydrogen bond characterized by resonance Raman and EPR spectroscopies. The surfactant, sodium dodecyl sulfate, induced unfolding of Cyt c that occurred by one step cooperative processes with an activation barrier of 16.8 kJ/mol, and conformational structure of Cyt c persisted in an intermediate state.²⁹ Using picosecond flash photolysis system, Vos et al.²³ observed the multistep binding process of nitric oxide in ferric Cyt c–CL complex having a high value of escape fraction of NO and open nature of heme pocket in the complex

Here to understand the effect of the charges of liposomes on the electronic, vibrational, and conformational relaxation dynamics of Cyt c upon complexation with lipids having different charges, absorption, emission, CD, and femtosecond transient absorption spectra of the complexes were measured. Hence the Cyt c is systematically complexed with CL, POPG, and POPC having charges of -2 , -1 , and 0 , respectively. CL has a unique structure with four hydrophobic fatty acid tail and a hydrophilic phosphate headgroup carrying two negative charges.^{11,15} POPG is a phosphatidylglycerol having single negative charge with two acyl chains. However, POPC is a phosphatidylcholine and zwitterionic over a wide pH range as it possesses a quaternary ammonium group and a phosphate

moiety.³⁰ The chemical structures of different phospholipids are also shown in Figure 1. It is inferred that the transient absorption spectra obtained by excitation at 280 nm exhibited the excited state dynamics of Trp and changes of tertiary structure reflecting the conformational changes of the protein during partial unfolding of Cyt c upon complexation with liposomes.

2. EXPERIMENTAL SECTION

Horse heart Cyt c was obtained from Sigma-Aldrich. In order to completely remove any ferrous forms present in the protein solution, potassium ferricyanide was added to the sample and was then passed through a Sephadex G-25 column to remove any remaining oxidizing agents and impurities. POPG, POPC, bovine heart CL, and 4-(2-hydroxyethyl)-1-piperazineethanesulfonic acid (HEPES) were purchased from Sigma-Aldrich and used without further purification. The lipids were dissolved in a 2:1 chloroform/methanol mixture. The solvent was removed by drying under the nitrogen atmosphere until a uniform thin, dry lipid film was formed. The film was kept in a vacuum desiccator overnight. The lipid film was then rehydrated with 25 mM HEPES buffer (pH 7.4) to obtain the desired concentration.³¹ The solution was then sonicated in an ice bath for 2 h. The solution was centrifuged for 45 min at 13 000 rpm to remove all the impurities. The supernatant was then allowed to stabilize overnight. The Cyt c concentration was 10 μM for all steady state optical spectroscopy. Different Cyt c–liposome mixtures were prepared by varying the concentration of liposome.

The size distributions of liposomes having a concentration of 500 μM were measured using dynamic light scattering experiment. Particle radii were obtained from dynamic light scattering particle size analyzer (Zeta Nano-ZS, Ms. Malvern Instruments, U.K.). A 10 mm path-length quartz cuvette was used to collect the data at room temperature. Absorption spectra were recorded using UV-2600 UV–visible spectrophoto-

tometer (Shimadzu). CD spectra were measured with JASCO 810 spectrometer at room temperature. Steady-state fluorescence spectra were recorded with a FluoroLog-3 (Horiba) equipped with a 450W Xe arc lamp.

Femtosecond Transient Absorption Spectroscopy.

The instrumentation details for the femtosecond transient absorption measurements have been described elsewhere.³² It is a Ti:sapphire laser (MaiTai HP, Spectra Physics, U.S.A.) centered at 800 nm having 80 MHz repetition rate with a pulse width of <100 fs. The amplified laser was split into two and the high energy beam was used as the pump (385 and 280 nm) for exciting the sample by using TOPAS (Prime, Light Conversion). The other part of the amplified beam (200 mW) focused on a 1 mm thick CaF₂ plate to generate white light continuum (340–1000 nm) which further split into two beams (sample and reference probe beams). The sample cell (0.4 mm path length) was refreshed by rotating at a constant speed. Finally, the white light continuum was focused into a 100 μ m optical fiber coupled to imaging spectrometer after passing through the sample cell. The pump–probe spectrophotometer (ExciPro) setup was purchased from CDP Systems Corp, Russia. Normally transient absorption spectra were obtained by averaging about 2000 excitation pulses for each spectral delay. All the measurements were carried out at the magic angle (54.7°). All the transient absorption spectra obtained from the equipment is compensated for chirp of the white light by determining the time zero using coherent artifact observed in the solvent.³³ The time resolution of the pump–probe spectrometer is found to be about ≤ 120 fs. The concentration of Cyt c used for measuring the transient absorption spectra was 100 μ M. The integrity of the sample is tested by measuring the absorption spectra of the sample before and after the experiments and found to be no significant changes in the absorption spectra.

3. RESULTS AND DISCUSSION

3.1. Steady State Photophysical Characterization.

The steady state absorption spectra of Cyt c and Cyt c-liposomes obtained with various lipids including CL, POPG, and POPC at different L/P ratio are shown in Figure 2. DLS spectra of all liposomes (Figure S1 in Supporting Information) show the size distribution between 20 and 200 nm, indicating the formation of unilamellar vesicles in all the lipids.^{28,34} Cyt c in HEPES buffer shows a Soret absorption maximum at 409 nm and broad asymmetric Q-band near 530 nm. In the Cyt c in the CL and POPG liposomes complexes, the Soret band is shifted to 407 nm. The inset of Figure 2 shows the enlarged view of region near charge transfer band at 695 nm by normalizing the spectra at 640 nm. With an increase of the L/P ratio, there is a decrease of absorbance of peak around 695 nm, characteristic of metal-to-ligand charge transfer band, indicating the dissociation of Met80 from the heme consistent with previous reports.^{6,13,35,36} An appearance of a new band at ~ 620 nm in the higher L/P ratio was also observed and it could be due to the formation of ferric high-spin (HS) species.³⁷ The Cyt c–POPC complex does not show any significant changes in the absorption spectra as charge of POPC is neutral. As the mixture of CL and POPC could mimic the mitochondrial membrane, the complex of Cyt c with CL and POPC mixture (20:80%) was also prepared and its absorption spectra found to be similar to that of negatively charged liposomes. Interestingly by the addition of 0.1 M NaCl, the charge

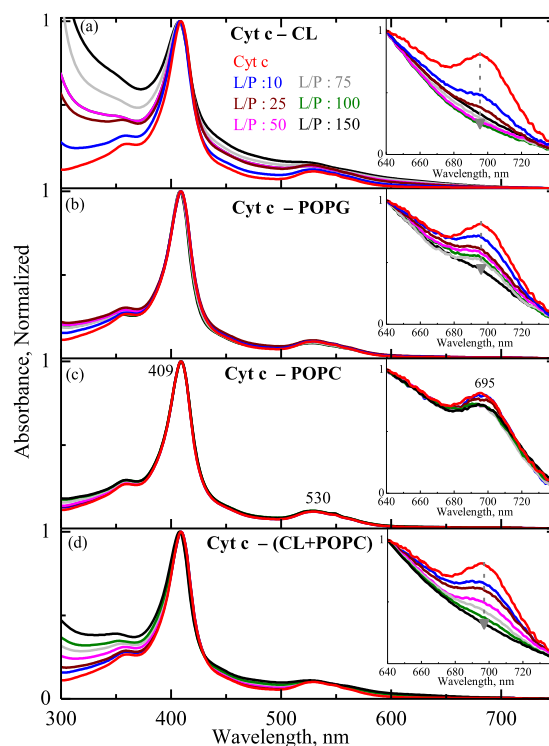


Figure 2. Steady state absorption spectra of Cyt c–CL (a), Cyt c–POPG (b), Cyt c–POPC (c), and Cyt c–(CL+POPC) (d) complexes at different L/P ratios in 25 mM HEPES buffer at pH 7.4. Insets show enlarged view of region near charge transfer band at 695 nm by normalizing the spectra at 640 nm. The arrow indicates the decrease of absorbance of the charge transfer band at 695 nm with increase of the L/P ratio.

transfer band at 695 nm reappeared back in the Cyt c–liposome complexes.

Figure 3 shows the fluorescence spectra of Cyt c–liposome complexes including CL, POPG, POPC, and CL+POPC at different L/P ratio obtained by exciting at 290 nm in room temperature. With increase of concentration of liposomes, a gradual increase of intensity at around 340 nm due to Trp emission indicated the occurrence of partial unfolding of Cyt c.^{38,39}

The increase of fluorescence intensity is attributed to the decrease of the fluorescence resonance energy transfer^{40,41} from the Trp to the heme as the distance between Trp and heme increased from ~ 10 Å to 25 Å^{29,41,42} upon increase of partial unfolding of the proteins by the liposomes. Cyt c–CL, –POPG, and –CL+POPC complexes showed higher emission intensity with an increase of liposome concentration when compared to POPC liposomes. In addition, the broad weak emission band at ~ 430 nm, attributed to P band²⁸ was observed with an increase of concentration of liposomes. To understand the significance of electrostatic interaction in Cyt c–liposome complex, fluorescence spectra of various Cyt c–liposome complexes was measured by the addition of 0.1 M NaCl. Insets of Figure 3 show the fluorescence spectra of Cyt c–liposome complexes having L/P ratio of 50 in 25 mM HEPES buffer with and without 0.1 M NaCl. It is observed that the emission peak at ~ 340 nm obtained for Cyt c–liposome complexes due to Trp is decreased in the presence of NaCl when compared to the complexes in the absence of NaCl.

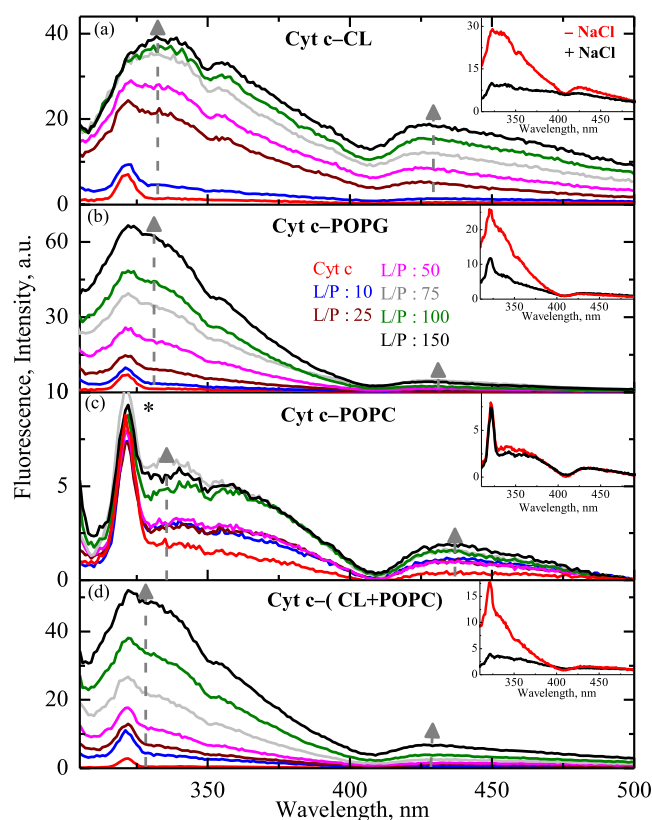


Figure 3. Fluorescence spectra of Cyt *c*-CL (a), Cyt *c*-POPG (b), Cyt *c*-POPC (c), and Cyt *c*-(CL+POPC) (d) complexes at different L/P ratio in 25 mM HEPES buffer at pH 7.4 obtained by exciting at 290 nm. Insets show the fluorescence spectra of complexes having L/P ratio of 50 with (black) and without NaCl (red). Asterisk (*) represents the characteristic O-H stretching frequency of water. The arrow indicates the increase of the fluorescence intensity with an increase of the L/P ratio.

The CD spectra of Cyt *c*-liposome complexes at different L/P ratio with and without NaCl were measured and shown in Figure 4 to understand the structural and conformational changes of Cyt *c* upon interaction with liposomes. The CD spectrum of the native protein displays a bisignate band—characteristic change of sign in the region of absorption maximum (~ 409 nm) due to the variation of absorption of right- and left-circularly polarized light (Cotton effect) arises from electronic and vibronic perturbations of the heme group in the protein.^{43,44} In addition, Cyt *c* exhibits three negative bands at ~ 285 , 330, and 371 nm. Weak positive band in the 450–520 nm region is attributed to charge transfer transition between porphyrin and heme iron.³⁶ The negative band around 417 nm is related to the presence of Met80 at the sixth coordination position of the heme.⁴⁵ The couplet gradually disappears and is replaced by a positive Cotton band with increase of L/P ratios for CL, CL+POPC, and POPG, reflecting a relaxation of the tertiary structure and axial ligand interactions of the heme in the protein. However, there is no significant changes in the CD spectra of Cyt *c*-POPC complex even at higher concentration [L/P: 150] indicating the weak interaction of neutral liposome with Cyt *c*. Upon addition of 0.1 M NaCl, the reappearance of the negative Cotton band at ~ 417 nm was observed as shown in the insets of Figure 4. The observation of a decrease of Trp emission intensity and reappearance of Cotton band in the presence of 0.1 M NaCl

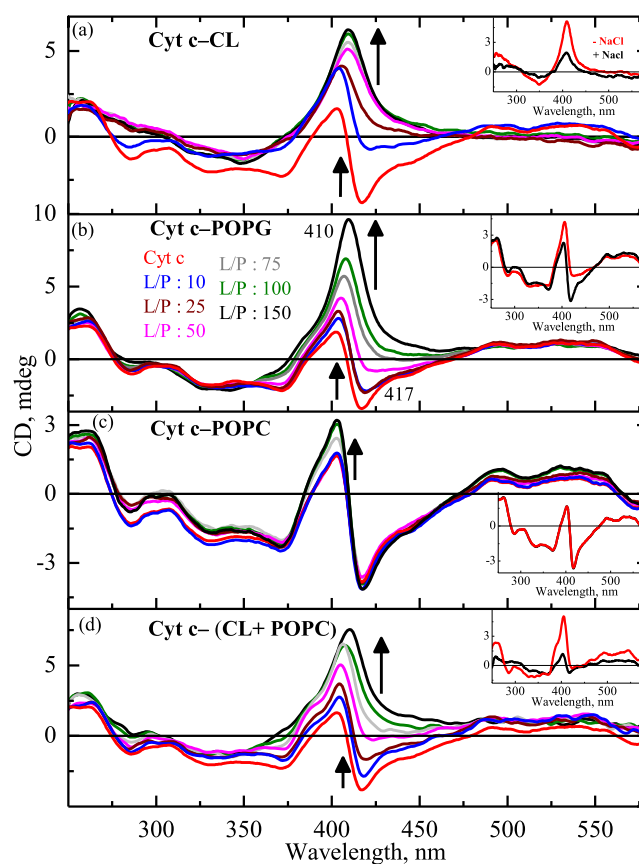


Figure 4. CD spectra of Cyt *c*-CL (a), Cyt *c*-POPG (b), Cyt *c*-POPC (c), and Cyt *c*-(CL+POPC) (d) complexes at different L/P ratios in 25 mM HEPES buffer (pH 7.4) at room temperature. Insets show the CD spectra of the complex having an L/P ratio of 50 with (black) and without 0.1 M NaCl (red).

suggests the existence of electrostatic interaction between Cyt *c* and liposomes. The refolding of the partially unfolded protein occurred by increasing the interaction between the Na^+ ions and anionic phospholipids by competing the interaction of the lipids with positive charge on the surface of the protein.

3.2. Femtosecond Time-Resolved Excited State Relaxation Dynamics. The excited state relaxation dynamics of heme in Cyt *c* complexed with various liposomes were investigated using femtosecond time-resolved pump–probe spectroscopy. The pump wavelength was chosen to specifically excite the heme and Trp in Cyt *c* at 385 and 280 nm, respectively. Figures 5, 6, S2, S3, and S4 show the femtosecond time-resolved transient absorption spectra $\Delta A(\lambda, t)$ of Cyt *c*-CL, Cyt *c*-POPG, Cyt *c*-POPC, Cyt *c*-(CL+POPC) complexes and Cyt *c*, obtained by exciting at 385 nm. In Figure 5 the spectral evolution of the Cyt *c*-CL complex at different delay time immediately after the photoexcitation starting from 200 fs to 1.0 ps and 2.0 to 13.0 ps are shown in panels a and b, respectively. In Figure 5a, the earliest spectrum at 200 fs exhibits a strong bleach band at ~ 408 nm and the excited state absorption at 375 and 419 nm. With increase of delay time, decrease of bleach band (408 nm), and an increase of excited state absorption (419 nm) along with a narrowing of spectral bandwidth and shifting toward blue region were observed until ~ 2.0 ps. In Figure 5b, the intensity of both bleach and excited-state absorption decreases with an increase of the delay time and attaining back to the equilibrium within

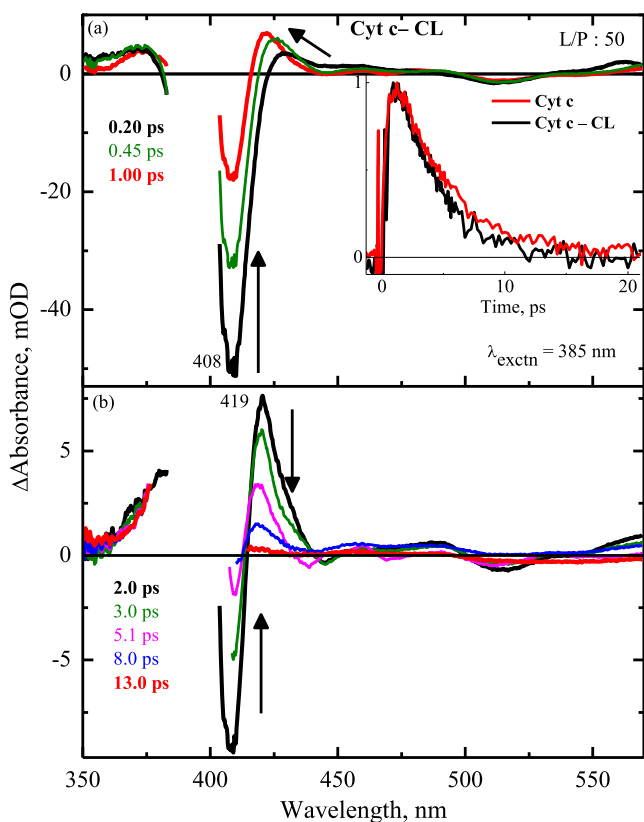


Figure 5. Femtosecond time-resolved transient absorption spectra of Cyt c–CL complex having L/P ratio of 50 in 25 mM HEPES buffer at pH 7.4 upon excitation at 385 nm. The different delay times are given and the arrows show the spectral evolution. Inset shows the transient decay profile of Cyt c and Cyt c–CL complex probed at 419 nm.

20 ps. The spectral features of transient absorption spectra of Cyt c–CL obtained by excitation at 385 nm are similar to that of native Cyt c (Figure S2). The transient decay of the Cyt c–CL complex probed at 419 nm is compared with that of the native Cyt c (inset) and there was found to be no significant changes in the dynamics. The transient absorption spectra of other complexes including Cyt c–POPG, –POPC, and –CL+POPC obtained by exciting at 385 nm are similar to that of Cyt c–CL.

Transient absorption spectra of Cyt c–CL, –POPG, –POPC, and –CL+POPC complexes obtained by exciting at 280 nm are shown in Figures 7, 8, S6, and S7, respectively. The selective excitation at 280 nm is used to probe the dynamics of Trp, heme, and tertiary structure associated with the partially unfolded form of the protein in the liposomes. It is to be noted that heme will be excited indirectly through the fluorescence resonance energy transfer by the excitation of Trp at 280 nm. This will lead to the change in the bleach of the Soret band and consecutive heme electronic and vibrational relaxation processes. Similar to the 385 nm excitation, in Figures 7 and 8 the decrease of the bleach band and an increase of excited state absorption along with a narrowing of spectral bandwidth and shifting toward blue region are observed until ~2.0 ps with increase of delay time. When compared to the 385 nm excitation, the excited state relaxation dynamics obtained upon excitation at 280 nm are longer having the time constant (τ_4) of ~14, 21, 22, and 26 ps for Cyt c–POPC, –POPG, –(CL+POPC), and –CL respectively (Table 1, *vide infra*). In order to understand the influence of electrostatic interaction in the

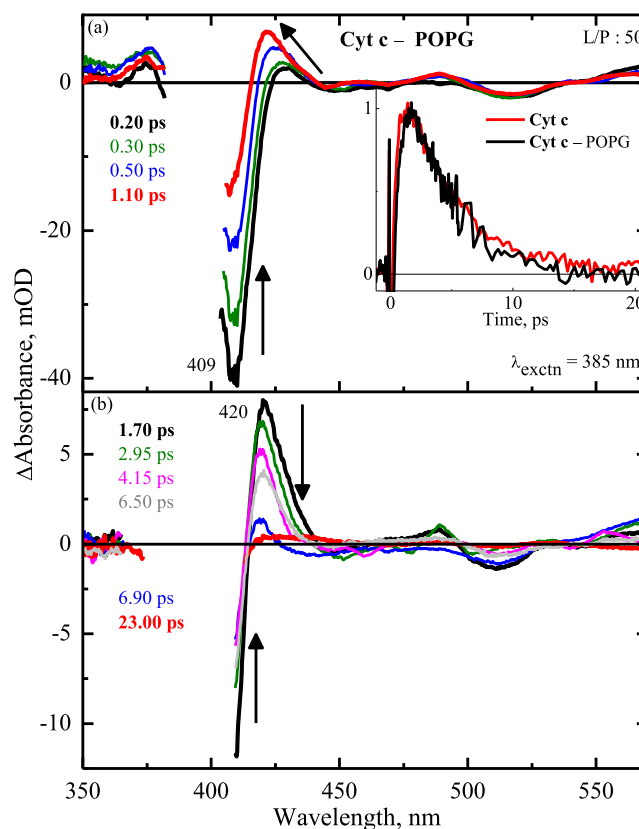


Figure 6. Femtosecond time-resolved transient absorption spectra of Cyt c–POPG complex having L/P ratio of 50 in 25 mM HEPES buffer at pH 7.4 upon excitation at 385 nm. Inset shows the transient decay profile of Cyt c and Cyt c–POPG complex probed at 419 nm.

excited state relaxation dynamics of protein–liposome complexes, transient absorption spectra of the complexes were measured in 0.1 M NaCl. The transient decay of protein–liposome complexes with and without 0.1 M NaCl monitored at 425 nm are shown (Figure 9) for comparison along with Cyt c. Interestingly by the addition of 0.1 M NaCl, the decay of the complexes obtained by exciting at 280 nm are similar to that of the native Cyt c.

Global analysis of the femtosecond transient absorption data was performed using the GLOTARAN program.⁴⁶ The optimal global exponential fit resulted four major time constants for all the measurements and the time constants are listed in Tables 1 and S1 for 280 and 385 nm excitation, respectively. The corresponding decay-associated spectra for these time constants are shown in Figures S10 and S11 for 385 and 280 nm excitation wavelengths, respectively. These spectra are similar to each other and showed the signature of excited-state absorption and a bleach band at the corresponding absorption maximum.

3.3. Effect of Excitation Wavelength. **3.3.1. Excitation at 385 nm.** In order to understand the relaxation dynamics of the heme in the liposomes, the time constants obtained for the heme in native form of Cyt c is discussed at first. The global analysis provided four exponential time constants for ferric Cyt c at pH 7.4: $\tau_1 = 148 \pm 50$ fs, $\tau_2 = 666 \pm 100$ fs, $\tau_3 = 3.72 \pm 0.30$ ps, and $\tau_4 = 10.11 \pm 1.0$ ps. These time constants are consistent with the previous reports^{9,47–49} of ferric Cyt c, within the experimental errors. It is known that in ferric Cyt c, the internal conversion (IC) occurs within hundreds of

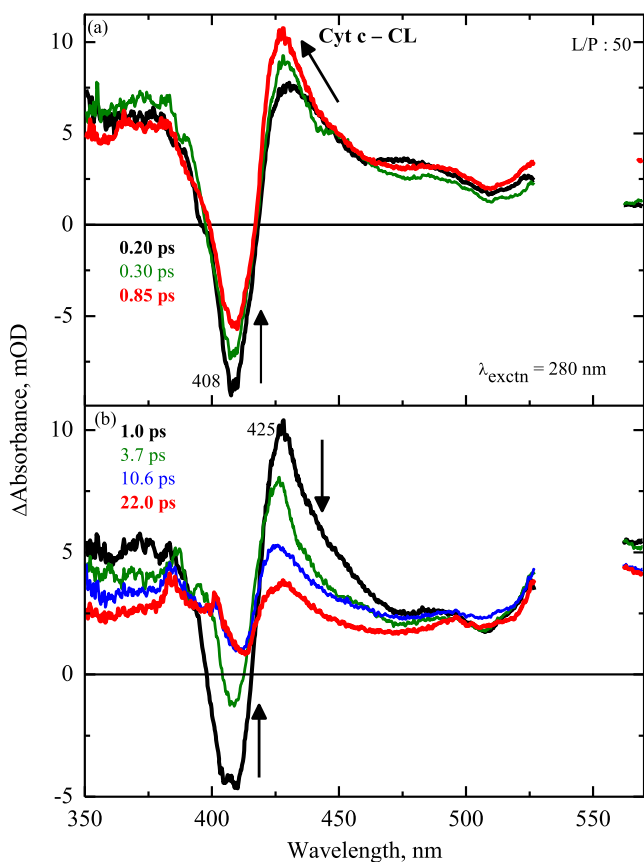


Figure 7. Femtosecond time-resolved transient absorption spectra of Cyt c-CL complex having L/P ratio of 50 in 25 mM HEPES buffer at pH 7.4 upon excitation at 280 nm.

femtoseconds.^{47,48} The decay-associated spectra of the τ_1 exhibited excited-state absorption and ground-state bleach at the corresponding absorption maximum. Hence, the time constant τ_1 is ascribed to an excited-state decay of the heme to the ground state. After the IC, the heme in the higher vibrational state of the ground state (hot) undergoes vibrational energy dissipation via multiple exponential pathways in the fast time scale. With an increase of the delay time, the shifting of the excited state absorption at 419 nm toward the blue region with narrowing of the spectral band confirms the occurrence of the vibrational relaxation having multiple exponential time constants.^{9,50} Therefore, the time constants τ_2 , τ_3 , and τ_4 are attributed to the various degrees of vibrational relaxation dynamics of the heme in the ground state. It is reported for the native protein that the fast and slow exponential components are due to the vibrational energy transfer via the coupling between heme and collective motions of the protein mainly through covalent bonds.⁵¹

The excited state relaxation dynamics of the heme in the liposomes (except POPC) upon excitation at 385 nm did not exhibit any significant changes when compared to that of native Cyt c reflecting heme environment still intact. This could be due to the fact that Met80 is replaced by either His33 or His26^{20,52} in the partially unfolded thermodynamic intermediate ground state. Similar relaxation behavior is supported by observing the comparable vibrational relaxation time constants for both the ferric and ferrous form of Cyt c.⁵¹

3.3.2. Excitation at 280 nm. In order to selectively excite the Trp which could probe the dynamics of Trp, heme, and

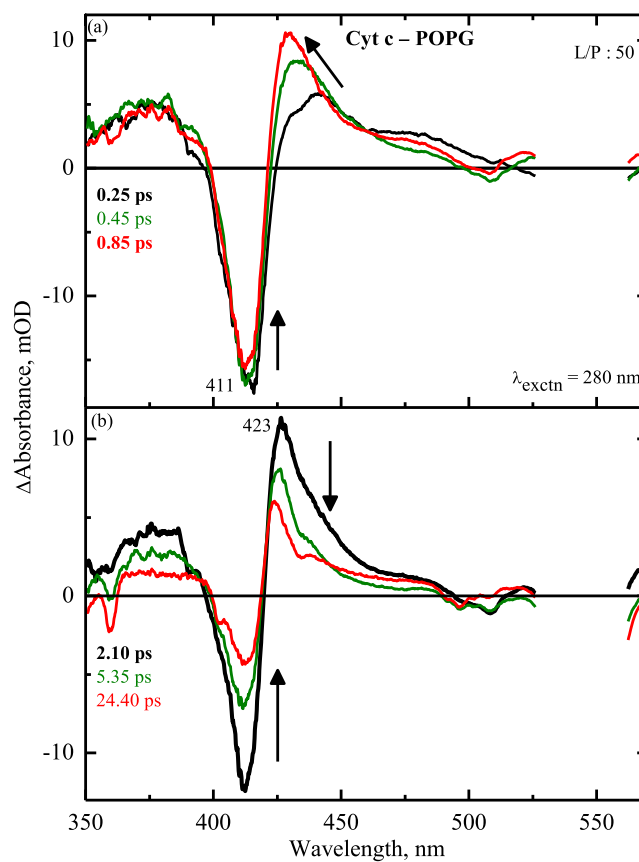
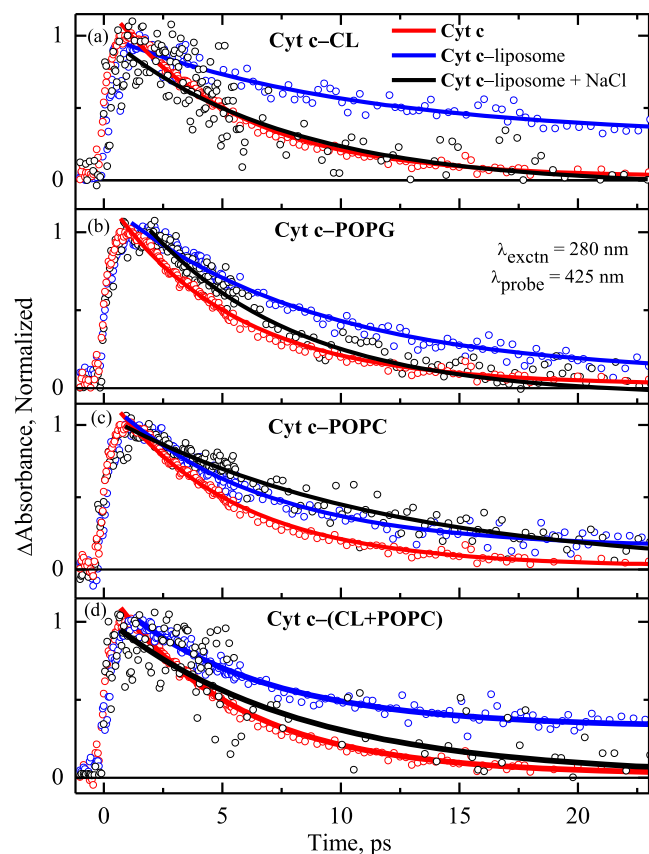


Figure 8. Femtosecond time-resolved transient absorption spectra of Cyt c-POPG complex having L/P ratio of 50 in 25 mM HEPES buffer at pH 7.4 upon excitation at 280 nm.

tertiary structures associated with the partially unfolded form of the protein in the liposome, the 280 nm excitation was used. The time constants obtained for ferric Cyt c upon excitation at 280 nm are $\tau_1 = 230 \pm 100$ fs, $\tau_2 = 840 \pm 120$ fs, $\tau_3 = 3.16 \pm 0.5$ ps, and $\tau_4 = 8.50 \pm 1.2$ ps. The exponential component τ_1 is ascribed to the excited state decay of heme, as in the case of 385 nm excitation. It is observed that the fluorescence intensity of the native protein is efficiently quenched by the fluorescence resonance energy transfer from the excited Trp to the porphyrin ring of the heme group.^{53,54} On the basis of the literature, the time constant of τ_2 is attributed to the excited-state lifetime of Trp⁴⁹ and τ_3 and τ_4 are assigned to vibrational relaxation time constants. From the Table 1, the rate of internal conversion (τ_1) of the heme in CL and POPG liposomes is observed to be increased reflecting the slowing down of electronic decay of the heme in the liposomes. Interestingly, when compared to the native Cyt c there is a systematic increase of the time constant of τ_2 to 0.98, 1.95, 2.01, and 2.35 ps for Cyt c-POPC, -POPG, -(CL+ POPC), and -CL complexes, respectively, with an increase of anionic charges of the liposomes. This reflects the regular extent of partial unfolding of the proteins leading to increase of distance between Trp and heme which reduces the resonance energy transfer from the Trp to heme. The increase of time constant τ_3 is also observed in the Cyt c-liposome complex when compared to native protein. Remarkably, the long-lived components τ_4 were observed for Cyt c-POPG, -(CL+ POPC), and -CL complexes with an increase of anionic charges in the liposomes reflecting the global conformational

Table 1. Time Constants Obtained by Global Analysis Using GLOTARAN⁴⁶ for Cyt c- Liposome Complex Having L/P Ratio of 50 for 280 nm Excitation

sample	Cyt c	Cyt c-CL	Cyt c-POPG	Cyt c-POPC	Cyt c-(CL+POPC)
absence of salt	$\tau_1 = 0.23 \pm 0.10$ ps	$\tau_1 = 0.38 \pm 0.15$ ps	$\tau_1 = 0.33 \pm 0.10$ ps	$\tau_1 = 0.29 \pm 0.10$ ps	$\tau_1 = 0.34 \pm 0.14$ ps
	$\tau_2 = 0.84 \pm 0.12$ ps	$\tau_2 = 2.35 \pm 0.50$ ps	$\tau_2 = 1.95 \pm 0.50$ ps	$\tau_2 = 0.98 \pm 0.10$ ps	$\tau_2 = 2.01 \pm 0.10$ ps
	$\tau_3 = 3.16 \pm 0.50$ ps	$\tau_3 = 5.49 \pm 0.20$ ps	$\tau_3 = 5.01 \pm 0.30$ ps	$\tau_3 = 3.91 \pm 0.15$ ps	$\tau_3 = 5.09 \pm 0.15$ ps
	$\tau_4 = 8.30 \pm 1.20$ ps	$\tau_4 = 26.50 \pm 1.10$ ps	$\tau_4 = 21.58 \pm 1.20$ ps	$\tau_4 = 14.00 \pm 1.50$ ps	$\tau_4 = 22.50 \pm 1.50$ ps
presence of salt	$\tau_1 = 0.21 \pm 0.10$ ps	$\tau_1 = 0.22 \pm 0.15$ ps	$\tau_1 = 0.28 \pm 0.14$ ps	$\tau_1 = 0.28 \pm 0.15$ ps	$\tau_1 = 0.20 \pm 0.13$ ps
	$\tau_2 = 0.80 \pm 0.13$ ps	$\tau_2 = 0.83 \pm 0.15$ ps	$\tau_2 = 0.87 \pm 0.13$ ps	$\tau_2 = 0.90 \pm 0.14$ ps	$\tau_2 = 0.80 \pm 0.14$ ps
	$\tau_3 = 3.20 \pm 0.50$ ps	$\tau_3 = 3.00 \pm 0.50$ ps	$\tau_3 = 3.07 \pm 0.20$ ps	$\tau_3 = 3.85 \pm 0.20$ ps	$\tau_3 = 3.20 \pm 0.50$ ps
	$\tau_4 = 8.50 \pm 1.20$ ps	$\tau_4 = 8.90 \pm 1.20$ ps	$\tau_4 = 8.79 \pm 1.20$ ps	$\tau_4 = 13.65 \pm 1.10$ ps	$\tau_4 = 8.60 \pm 2.00$ ps

**Figure 9.** Femtosecond transient decay of Cyt c-CL (a), Cyt c-POPG (b), Cyt c-POPC (c), and Cyt c-(CL+POPC) (d) liposomes having an L/P ratio of 50 with and without 0.1 M NaCl in 25 mM HEPES buffer at pH 7.4 probed at 425 nm.

change associated with the tertiary structure by unfolding of protein induced by liposomes. It is to be noted that the time constant τ_4 obtained for Cyt c-liposome complex is shorter compared to the longer time constant obtained for the completely unfolded protein induced by the addition of 4 M guanidine hydrochloride.⁹ This reflects the Cyt c in the complexes used in this study are partially unfolded and its conformational structures remained in an intermediate state between completely unfolded and native folded states.

In order to shed more light on the fluorescence resonance energy transfer process occurring from Trp to heme, the transient absorption spectra of Cyt c-CL complex have been measured upon excitation at 280 nm by varying the L/P ratio. The magnitude of the heme bleach probed at 409 nm with increase of L/P ratio is compared and shown in Figure S12. Interestingly when compared to the native protein, a

systematic decrease of magnitude of the heme bleach is observed with increase of L/P ratio. This reflects the occurrence of various degrees of unfolding leading to increased distance between heme and Trp. The transient absorption spectra of Cyt c-CL complexes with various L/P ratio were analyzed globally and resulting time constants are shown in Table S2. From Table S2, it is found that τ_2 , the excited-state lifetime of Trp⁴⁹ (corroborated to fluorescence resonance energy transfer time constant), is increased from ~ 840 fs for native protein to ~ 4.48 ps for the Cyt c-CL complex having the L/P ratio of 75. This confirms the decrease of efficiency of fluorescence resonance energy transfer as the distance between Trp and heme increased from ~ 10 to 25 \AA ^{29,41,42} upon increase of partial unfolding of the proteins by the liposomes.

The correlation between the increase of fluorescence intensity (Figure 3) with the increase of Trp's lifetime of various complexes having L/P ratio of 50 is shown in Figure S13. It is found that with the increase of anionic charge of phospholipids the magnitude of unfolding of the protein increases in the complexes.

3.4. Effect of Ionic Strength. In order to understand the effect of the ionic strength on the unfolding dynamics of the protein, femtosecond transient absorption spectra of complexes were measured by exciting at 280 nm by adding 0.1 M NaCl (Figures S8 and S9). The femtosecond time-resolved kinetic profiles of the protein and protein-liposome complexes probed at 425 nm are shown in Figure 9 with and without 0.1 M NaCl for comparison. The time constants obtained by exciting at 280 nm using global analysis for different liposomes in the presence of NaCl are also given in Table 1. It is interesting to note in the presence of 0.1 M NaCl that the dynamics are recovered back which is comparable to that of native Cyt c. It reflects the refolding of the partially unfolded protein in the Cyt c-CL, Cyt c-(CL+POPC), and Cyt c-POPG complexes in the presence of NaCl. In addition, it reveals that the charges of the phosphate group of lipids is essential in the Cyt c-liposome interaction and confirms the existence of the electrostatic nature of the interaction between Cyt c and negatively charged liposomes. However, in the case of the Cyt c-POPC complex the dynamics are not changed by adding NaCl, indicating the presence of weak hydrophobic interaction between POPC and Cyt c.

4. CONCLUSION

The interaction dynamics between Cyt c and liposomes were investigated using steady-state and time-resolved optical spectroscopy by systematically increasing the anionic charge in the liposome. The excited-state relaxation dynamics of heme in liposomes observed by exciting at 385 nm were found to be the same when compared to the native form reflecting the

heme environment stabilized by exchange of other ligands (His33/26).^{20,52} The femtosecond transient absorption spectra of the complexes obtained by exciting at 280 nm, where Trp selectively excited, showed regular increase of excited state relaxation dynamics due to a decrease of efficient fluorescence resonance energy transfer with an increase of anionic charge of the lipid. It is found that the extent of partial unfolding depends on the charges of the lipids and that the Trp acted as a probe to examine the dynamics of partial unfolding associated with the change in the tertiary structure and axial ligand interaction of the heme proteins in liposomes. The recovery of the relaxation dynamics of complexes are comparable to the native protein in the presence of 0.1 M NaCl and this suggests the importance of electrostatic interaction between Cyt c and liposomes.

■ ASSOCIATED CONTENT

SI Supporting Information

The Supporting Information is available free of charge at <https://pubs.acs.org/doi/10.1021/acs.jpbc.9b11957>.

Size distribution of CL, POPG, and POPC obtained from DLS experiment, femtosecond transient absorption spectra of Cyt c, Cyt c-POPC and Cyt c-(CL + POPC) without NaCl upon excitation at 385 nm, transient absorption spectra of Cyt c, Cyt c-POPC and Cyt c-(CL + POPC) without NaCl and Cyt c-POPG and Cyt c-POPC with NaCl, upon excitation at 280 nm, decay associated spectra of Cyt c and liposome complexes upon excitation at 385 and 280 nm (with and without NaCl), femtosecond transient absorption decay of Cyt c-CL complexes with different L/P ratio by excitation at 280 nm, correlation between the fluorescence intensity and lifetime of Trp for all the complexes having L/P ratio of 50, table of time constants of Cyt c-liposome complexes upon excitation at 385 nm, and time constants obtained by global analysis for Cyt c-CL complex having different L/P ratio upon excitation at 280 nm (PDF)

■ AUTHOR INFORMATION

Corresponding Author

Venugopal Karunakaran – Photosciences and Photonics Section, Chemical Sciences and Technology Division, CSIR-National Institute for Interdisciplinary Science and Technology, Thiruvananthapuram 695 019, Kerala, India; Academy of Scientific and Innovative Research (AcSIR), Ghaziabad 201002, India; orcid.org/0000-0001-8482-0900; Phone: 091-471-2515240; Email: k.venugopal@niist.res.in

Authors

Chinju Govind – Photosciences and Photonics Section, Chemical Sciences and Technology Division, CSIR-National Institute for Interdisciplinary Science and Technology, Thiruvananthapuram 695 019, Kerala, India; Academy of Scientific and Innovative Research (AcSIR), Ghaziabad 201002, India

Megha Paul – Photosciences and Photonics Section, Chemical Sciences and Technology Division, CSIR-National Institute for Interdisciplinary Science and Technology, Thiruvananthapuram 695 019, Kerala, India; Academy of Scientific and Innovative Research (AcSIR), Ghaziabad 201002, India

Complete contact information is available at: <https://pubs.acs.org/doi/10.1021/acs.jpbc.9b11957>

Notes

The authors declare no competing financial interest.

■ ACKNOWLEDGMENTS

C.G. and M.P. gratefully acknowledge the UGC, New Delhi for their fellowship. V.K. thankfully acknowledges Department of Biotechnology (DBT), Government of India for financial support (BT/PR24173/BRB/10/1604/2017). The authors thank Ms. S. Thomas for general help.

■ REFERENCES

- (1) Bren, K. L. Going with the Electron Flow: Heme Electronic Structure and Electron Transfer in Cytochrome C. *Isr. J. Chem.* **2016**, *56*, 693–704.
- (2) Alvarez-Paggi, D.; Hannibal, L.; Castro, M. A.; Oviedo-Rouco, S.; Demicheli, V.; Tórtora, V.; Tomasina, F.; Radi, R.; Murgida, D. H. Multifunctional Cytochrome C: Learning New Tricks from an Old Dog. *Chem. Rev.* **2017**, *117*, 13382–13460.
- (3) Kleingardner, J. G.; Bren, K. L. Biological Significance and Applications of Heme C Proteins and Peptides. *Acc. Chem. Res.* **2015**, *48*, 1845–1852.
- (4) Li, M.; Mandal, A.; Tyurin, V. A.; DeLucia, M.; Ahn, J.; Kagan, V. E.; van der Wel, P. C. A. Surface-Binding to Cardiolipin Nanodomains Triggers Cytochrome C Pro-Apoptotic Peroxidase Activity Via Localized Dynamics. *Structure* **2019**, *27*, 806–815.
- (5) Santucci, R.; Sinibaldi, F.; Cozza, P.; Polticelli, F.; Fiorucci, L. Cytochrome C: An Extreme Multifunctional Protein with a Key Role in Cell Fate. *Int. J. Biol. Macromol.* **2019**, *136*, 1237–1246.
- (6) Schweitzer-Stenner, R. Relating the Multi-Functionality of Cytochrome C to Membrane Binding and Structural Conversion. *Biophys. Rev.* **2018**, *10*, 1151–1185.
- (7) Kapetanaki, S. M.; Silkstone, G.; Husu, I.; Liebl, U.; Wilson, M. T.; Vos, M. H. Interaction of Carbon Monoxide with the Apoptosis-Inducing Cytochrome CΔCardiolipin Complex. *Biochemistry* **2009**, *48*, 1613–1619.
- (8) Chattopadhyay, K.; Mazumdar, S. Stabilization of Partially Folded States of Cytochrome C in Aqueous Surfactant: Effects of Ionic and Hydrophobic Interactions. *Biochemistry* **2003**, *42*, 14606–14613.
- (9) Karunakaran, V. Ultrafast Heme Dynamics of Ferric Cytochrome C in Different Environments: Electronic, Vibrational, and Conformational Relaxation. *ChemPhysChem* **2015**, *16*, 3974–3983.
- (10) Bushnell, G. W.; Louie, G. V.; Brayer, G. D. High-Resolution Three-Dimensional Structure of Horse Heart Cytochrome C. *J. Mol. Biol.* **1990**, *214*, 585–595.
- (11) Däum, G. Lipids of Mitochondria. *Biochim. Biophys. Acta, Rev. Biomembr.* **1985**, *822*, 1–42.
- (12) Hanske, J.; Toffey, J. R.; Morenz, A. M.; Bonilla, A. J.; Schiavoni, K. H.; Pletneva, E. V. Conformational Properties of Cardiolipin-Bound Cytochrome C. *Proc. Natl. Acad. Sci. U. S. A.* **2012**, *109*, 125–130.
- (13) Belikova, N. A.; Vladimirov, Y. A.; Osipov, A. N.; Kapralov, A. A.; Tyurin, V. A.; Potapovich, M. V.; Basova, L. V.; Peterson, J.; Kurnikov, I. V.; Kagan, V. E. Peroxidase Activity and Structural Transitions of Cytochrome C Bound to Cardiolipin-Containing Membranes. *Biochemistry* **2006**, *45*, 4998–5009.
- (14) Ow, Y.-L. P.; Green, D. R.; Hao, Z.; Mak, T. W. Cytochrome C: Functions Beyond Respiration. *Nat. Rev. Mol. Cell Biol.* **2008**, *9*, 532–542.
- (15) Osman, C.; Voelker, D. R.; Langer, T. Making Heads or Tails of Phospholipids in Mitochondria. *J. Cell Biol.* **2011**, *192*, 7–16.
- (16) Schlame, M.; Rua, D.; Greenberg, M. L. The Biosynthesis and Functional Role of Cardiolipin. *Prog. Lipid Res.* **2000**, *39*, 257–288.
- (17) Gonzalez, F.; Gottlieb, E. Cardiolipin: Setting the Beat of Apoptosis. *Apoptosis* **2007**, *12*, 877–885.
- (18) Milazzo, L.; Tognaccini, L.; Howes, B. D.; Sinibaldi, F.; Piro, M. C.; Fittipaldi, M.; Baratto, M. C.; Pogni, R.; Santucci, R.; Smulevich, G. Unravelling the Non-Native Low-Spin State of the

Cytochrome C–Cardiolipin Complex: Evidence of the Formation of a His-Ligated Species Only. *Biochemistry* **2017**, *56*, 1887–1898.

(19) Muenzner, J.; Pletneva, E. V. Structural Transformations of Cytochrome C Upon Interaction with Cardiolipin. *Chem. Phys. Lipids* **2014**, *179*, 57–63.

(20) Oellerich, S.; Lecomte, S.; Paternostre, M.; Heimburg, T.; Hildebrandt, P. Peripheral and Integral Binding of Cytochrome C to Phospholipids Vesicles. *J. Phys. Chem. B* **2004**, *108*, 3871–3878.

(21) Heimburg, T.; Marsh, D. Protein Surface-Distribution and Protein-Protein Interactions in the Binding of Peripheral Proteins to Charged Lipid Membranes. *Biophys. J.* **1995**, *68*, 536–546.

(22) Salamon, Z.; Tollin, G. Surface Plasmon Resonance Studies of Complex Formation between Cytochrome C and Bovine Cytochrome C Oxidase Incorporated into a Supported Planar Lipid Bilayer. I. Binding of Cytochrome C to Cardiolipin/Phosphatidylcholine Membranes in the Absence of Oxidase. *Biophys. J.* **1996**, *71*, 848–857.

(23) Silkstone, G.; Kapetanaki, S. M.; Husu, I.; Vos, M. H.; Wilson, M. T. Nitric Oxide Binding to the Cardiolipin Complex of Ferric Cytochrome C. *Biochemistry* **2012**, *51*, 6760–6766.

(24) Rytömaa, M.; Kinnunen, P. K. Evidence for Two Distinct Acidic Phospholipid-Binding Sites in Cytochrome C. *J. Biol. Chem.* **1994**, *269*, 1770–1774.

(25) Sinibaldi, F.; Milazzo, L.; Howes, B. D.; Piro, M. C.; Fiorucci, L.; Polticelli, F.; Ascenzi, P.; Coletta, M.; Smulevich, G.; Santucci, R. The Key Role Played by Charge in the Interaction of Cytochrome C with Cardiolipin. *JBIC, J. Biol. Inorg. Chem.* **2017**, *22*, 19–29.

(26) Kawai, C.; Prado, F. M.; Nunes, G. L. C.; Di Mascio, P.; Carmona-Ribeiro, A. M.; Nantes, I. L. Ph-Dependent Interaction of Cytochrome C with Mitochondrial Mimetic Membranes: The Role of an Array of Positively Charged Amino Acids. *J. Biol. Chem.* **2005**, *280*, 34709–34717.

(27) Hong, Y.; Muenzner, J.; Grimm, S. K.; Pletneva, E. V. Origin of the Conformational Heterogeneity of Cardiolipin-Bound Cytochrome C. *J. Am. Chem. Soc.* **2012**, *134*, 18713–18723.

(28) Pandiscia, L. A.; Schweitzer-Stenner, R. Coexistence of Native-Like and Non-Native Partially Unfolded Ferricytochrome C on the Surface of Cardiolipin-Containing Liposomes. *J. Phys. Chem. B* **2015**, *119*, 1334–1349.

(29) Das, T. K.; Mazumdar, S.; Mitra, S. Characterization of a Partially Unfolded Structure of Cytochrome C Induced by Sodium Dodecyl Sulphate and the Kinetics of Its Refolding. *Eur. J. Biochem.* **1998**, *254*, 662–670.

(30) Sathappa, M.; Alder, N. N. The Ionization Properties of Cardiolipin and Its Variants in Model Bilayers. *Biochim. Biophys. Acta, Biomembr.* **2016**, *1858*, 1362–1372.

(31) Muenzner, J.; Toffey, J. R.; Hong, Y.; Pletneva, E. V. Becoming a Peroxidase: Cardiolipin-Induced Unfolding of Cytochrome C. *J. Phys. Chem. B* **2013**, *117*, 12878–12886.

(32) Govind, C.; Karunakaran, V. Ultrafast Relaxation Dynamics of Photoexcited Heme Model Compounds: Observation of Multiple Electronic Spin States and Vibrational Cooling. *J. Phys. Chem. B* **2017**, *121*, 3111–3120.

(33) Megerle, U.; Pugliesi, I.; Schriever, C.; Sailer, C. F.; Riedle, E. Sub-50 fs Broadband Absorption Spectroscopy with Tunable Excitation: Putting the Analysis of Ultrafast Molecular Dynamics On solid Ground. *Appl. Phys. B: Lasers Opt.* **2009**, *96*, 215–231.

(34) Lin, C.-M.; Li, C.-S.; Sheng, Y.-J.; Wu, D. T.; Tsao, H.-K. Size-Dependent Properties of Small Unilamellar Vesicles Formed by Model Lipids. *Langmuir* **2012**, *28*, 689–700.

(35) Schejter, A.; George, P. The 695-M μ Band of Ferricytochrome C and Its Relationship to Protein Conformation*. *Biochemistry* **1964**, *3*, 1045–1049.

(36) Mugnol, K. C. U.; Ando, R. A.; Nagayasu, R. Y.; Faljoni-Alario, A.; Brochsztain, S.; Santos, P. S.; Nascimento, O. R.; Nantes, I. L. Spectroscopic, Structural, and Functional Characterization of the Alternative Low-Spin State of Horse Heart Cytochrome C. *Biophys. J.* **2008**, *94*, 4066–4077.

(37) Babul, J.; Stellwagen, E. Participation of the Protein Ligands in the Folding of Cytochrome C. *Biochemistry* **1972**, *11*, 1195–1200.

(38) Pandiscia, L. A.; Schweitzer-Stenner, R. Salt as a Catalyst in the Mitochondria: Returning Cytochrome C to Its Native State after It Misfolds on the Surface of Cardiolipin Containing Membranes. *Chem. Commun.* **2014**, *50*, 3674–3676.

(39) Sanghera, N.; Pinheiro, T. J. Unfolding and Refolding of Cytochrome C Driven by the Interaction with Lipid Micelles. *Protein Sci.* **2000**, *9*, 1194–1202.

(40) Bräm, O.; Consani, C.; Cannizzo, A.; Chergui, M. Femtosecond Uv Studies of the Electronic Relaxation Processes in Cytochrome C. *J. Phys. Chem. B* **2011**, *115*, 13723–13730.

(41) Lee, J. C.; Engman, K. C.; Tezcan, F. A.; Gray, H. B.; Winkler, J. R. Structural Features of Cytochrome C' Folding Intermediates Revealed by Fluorescence Energy-Transfer Kinetics. *Proc. Natl. Acad. Sci. U. S. A.* **2002**, *99*, 14778.

(42) Tsong, T. Y. The Trp-59 Fluorescence of Ferricytochrome C as a Sensitive Measure of the over-All Protein Conformation. *J. Biol. Chem.* **1974**, *249*, 1988–1990.

(43) Dragomir, I.; Hagarman, A.; Wallace, C.; Schweitzer-Stenner, R. Optical Band Splitting and Electronic Perturbations of the Heme Chromophore in Cytochrome C at Room Temperature Probed by Visible Electronic Circular Dichroism Spectroscopy. *Biophys. J.* **2007**, *92*, 989–998.

(44) Myer, Y. P. Conformation of Cytochromes. Iii. Effect of Urea, Temperature, Extrinsic Ligands, and Ph Variation on the Conformation of Horse Heart Ferricytochrome C. *Biochemistry* **1968**, *7*, 765–776.

(45) Santucci, R.; Ascoli, F. The Soret Circular Dichroism Spectrum as a Probe for the Heme Fe(II)-Met(80) Axial Bond in Horse Cytochrome C. *J. Inorg. Biochem.* **1997**, *68*, 211–4.

(46) Snellenburg, J. J.; Laptinok, S.; Seger, R.; Mullen, K. M.; van Stokkum, I. H. M. Glotaran: A Java-Based Graphical User Interface for the R Package Timp. *J. Stat. Softw.* **2012**, *49*, 22.

(47) Negrerie, M.; Cianetti, S.; Vos, M. H.; Martin, J.-L.; Kruglik, S. G. Ultrafast Heme Dynamics in Ferrous Versus Ferric Cytochrome C Studied by Time-Resolved Resonance Raman and Transient Absorption Spectroscopy. *J. Phys. Chem. B* **2006**, *110*, 12766–12781.

(48) Zang, C.; Stevens, J. A.; Link, J. J.; Guo, L.; Wang, L.; Zhong, D. Ultrafast Proteinquake Dynamics in Cytochrome C. *J. Am. Chem. Soc.* **2009**, *131*, 2846–2852.

(49) Consani, C.; Bräm, O.; van Mourik, F.; Cannizzo, A.; Chergui, M. Energy Transfer and Relaxation Mechanisms in Cytochrome C. *Chem. Phys.* **2012**, *396*, 108–115.

(50) Ye, X.; Demidov, A.; Rosca, F.; Wang, W.; Kumar, A.; Ionascu, D.; Zhu, L.; Barrick, D.; Wharton, D.; Champion, P. M. Investigations of Heme Protein Absorption Line Shapes, Vibrational Relaxation, and Resonance Raman Scattering on Ultrafast Time Scales. *J. Phys. Chem. A* **2003**, *107*, 8156–8165.

(51) Bu, L.; Straub, J. E. Simulating Vibrational Energy Flow in Proteins: Relaxation Rate and Mechanism for Heme Cooling in Cytochrome C. *J. Phys. Chem. B* **2003**, *107*, 12339–12345.

(52) Colon, W.; Wakem, L. P.; Sherman, F.; Roder, H. Identification of the Predominant Non-Native Histidine Ligand in Unfolded Cytochrome C. *Biochemistry* **1997**, *36*, 12535–41.

(53) Fisher, W. R.; Taniuchi, H.; Anfinsen, C. B. On the Role of Heme in the Formation of the Structure of Cytochrome C. *J. Biol. Chem.* **1973**, *248*, 3188–3195.

(54) Dickerson, R. E.; Takano, T.; Eisenberg, D.; Kallai, O. B.; Samson, L.; Cooper, A.; Margoliash, E. Ferricytochrome C: I. General Features of the Horse and Bonito Proteins at 2.8 Å Resolution. *J. Biol. Chem.* **1971**, *246*, 1511–1535.